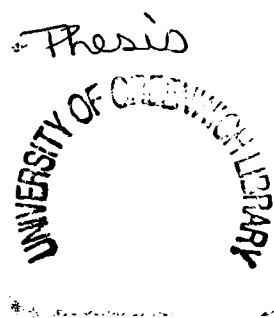


6082881

u6010842TP

**EXAMINATION OF HYDRATED AND  
ACCELERATED CARBONATED CEMENT-HEAVY  
METAL MIXTURES**

**QUANYUAN CHEN**



A thesis submitted in partial fulfilment of the requirements of  
the University of Greenwich  
for the Degree of Doctor of Philosophy

November 2003

## Abstract

Cement –based solidification/stabilisation (s/s) has been applied to the disposal of heavy metal bearing contaminated soil and wastes for approximately 50 years. This work studies the interactions of cement and heavy metals and provides further insight into encapsulation of heavy metals in cement matrices.

The pastes and suspensions of calcium oxide, calcium hydroxide, pure cement phases ( $C_3S$ ,  $C_3A$ ,  $C_4AF$ ,  $C_{12}A_7$  and  $CA$ ) and Portland cement with or without heavy metals ( $Zn^{2+}$ ,  $Pb^{2+}$ ,  $Cu^{2+}$  and  $Cr^{3+}$ ) were examined by a number of analytical techniques. These techniques were X-ray powder diffraction (XRD), solid state magic angle spinning/nuclear magnetic resonance (MAS/NMR), scanning electron microscopy (SEM), energy dispersive X-ray spectroscopy (EDS), differential thermal analysis (DTA) and thermogravimetry (TG). Thermodynamic modelling using a geochemical code, PHREEQC, and the edited database, was carried out to elucidate the chemical reactions occurring in cement/heavy metal systems.

Heavy metals acted as accelerators for hydration of  $CaO$ ,  $C_3S$  and Portland cement except that  $Zn^{2+}$  retarded the early-age hydration of  $C_3S$  and Portland cement. This work confirmed that the precipitation of portlandite was retarded due to the hydrolysis of heavy metals. Calcium ions resulting from the decomposition of cement phases combined with heavy metals to form calcium-heavy metal double hydroxides, including  $CaZn_2(OH)_6 \cdot 2H_2O$ ,  $Ca_2(OH)_4Cu(OH)_2 \cdot mH_2O$  and  $Ca_2Cr(OH)_7 \cdot 3H_2O$ .

The carbonation of  $C_3S$  and Portland cement resulted in the formation of calcium carbonate and the condensation of silicates from single tetrahedra to branching sites and three-dimensional frameworks (low Ca/Si ratio C-S-H gel). The polymerisation of C-S-H gel, and the polymorphism conversion and decomposition temperature of calcium carbonate were influenced by heavy metals. The incorporation of heavy metal cations in C-S-H gel is similar to that seen in glass. Heavy metals acted as network modifiers or network intermediates. In hydrated Portland cement pastes, aluminium was partitioned in ettringite or calcium carboaluminate. After carbonation, this work revealed that aluminium was in the tetrahedral form, forming mixed  $AlO_4/SiO_4$  branching or three-

dimensional networks. This thesis presents the new structural models for C-S-H gel and the chemical mechanisms of C<sub>3</sub>S reactions with water and carbon dioxide in the presence or absence of heavy metals.

In the absence of gypsum, the reaction products detected in the pastes of C<sub>3</sub>A, C<sub>4</sub>AF, C<sub>12</sub>A<sub>7</sub> and CA were gehlenite hydrate, calcium carboaluminate, C<sub>4</sub>AH<sub>x</sub> and hydrogarnet. Heavy metals, especially Zn<sup>2+</sup>, inhibited the formation of hydrogarnet and promoted the conversion of C-A-H to calcium carboaluminate and calcium carbonate.

In the presence of gypsum, the major hydration product of C<sub>3</sub>A was ettringite. During carbonation, CO<sub>3</sub><sup>2-</sup> substituted for SO<sub>4</sub><sup>2-</sup> and formed calcium carboaluminate, and eventually transformed into calcium carbonate and gibbsite. The conversion of metastable calcium carbonate polymorphs (aragonite and vaterite) to calcite through Ostwald ripening occurred very slowly in the carbonated pastes containing gypsum.

The reactivity of C<sub>3</sub>A, C<sub>12</sub>A<sub>7</sub>, CA and C<sub>4</sub>AF during carbonation was much lower than seen during hydration. Heavy metals influenced the rates and products of hydration or carbonation of C<sub>3</sub>A, C<sub>12</sub>A<sub>7</sub>, CA and C<sub>4</sub>AF and were completely incorporated in the reaction products of these phases.

Thermodynamic modelling confirmed that accelerated carbonation could be beneficially employed to cement-based s/s to improve its effectiveness. Calculations of solubility and equilibrium phase assemblage are consistent with the experimental examination obtained in this work.

**Key words:** cement, hydration, carbonation, heavy metal, solidification, stabilisation, modelling, C-S-H, C-A-H, portlandite, calcite, aragonite, vaterite, double hydroxide

## **Acknowledgements**

This work was carried out in the Centre for Contaminated land Remediation, School of Earth and Environmental Sciences, the University of Greenwich. I was supported by the school bursary, which enabled me to conduct this work.

I am indebted to my supervisors, Drs Colin D. Hills, from the University of Greenwich, and Mark Tyrer, from Imperial College of Science, Technology and Medicine, for their guidance and advice in the preparation of this thesis. Without their encouragement throughout my studentship, this thesis might never have emerged.

I wish to thank Drs P. Carey, I. Slipper, M. Derron, A. Brough, A. Mendham and D. Wray, and Mrs A. Raza for their technical supports. Drs. I. Slipper and G. Manby gave a lot of time to make detailed review and corrections of the manuscripts.

I have also appreciated the assistance and informative discussions offered by Drs. C. Macleod, K. Canning and D. Johnson.

I wish to acknowledge my gratitude to the authorities of Changsha Research Institute of Mining and Metallurgy for leaves of absence.

I would also like to mention those friends and colleagues who have freely give their support, often when it was needed most, especially M. Derron, M. Gilpin, S. Johnson, O. Shtepenکو and G.Lu.

My deepest gratitude goes to my family for their supports and continued help and sacrificing many precious hours that rightfully belonged to them.

## Nomenclature

A	alumina, $\text{Al}_2\text{O}_3$	
C	$\text{CaO}$	
F	$\text{Fe}_2\text{O}_3$	
H	$\text{H}_2\text{O}$	
S	silica, $\text{SiO}_2$	
M	$\text{MgO}$	
N	$\text{Na}_2\text{O}$	
<u>C</u>	$\text{CO}_3^{2-}$	
<u>S</u>	$\text{SO}_3$	
$\text{C}_3\text{S}$	tricalcium silicate, $\text{Ca}_3\text{SiO}_5$	
$\text{C}_2\text{S}$	dicalcium silicate, $\text{Ca}_2\text{SiO}_4$	
$\text{C}_3\text{A}$	tricalcium aluminate, $\text{Ca}_3\text{Al}_2\text{O}_6$	
$\text{C}_4\text{AF}$	ferrite, $\text{Ca}_2\text{AlFeO}_5$	
AFm	monosulphate, $\text{C}_4\text{A}\underline{\text{S}}\text{H}_{12}$	
AFt	ettringite, $\text{C}_3\text{A}\cdot 3\underline{\text{C}}\underline{\text{S}}\cdot \text{H}_{32}$	
CH	portlandite, $\text{Ca}(\text{OH})_2$	
C-S-H	calcium silicate hydrate gel of variable composition	
C-A-H	calcium aluminate hydrate gel	
$\text{C}_3\text{AH}_6$	hydrogarnet, $3\text{CaO}\cdot\text{Al}_2\text{O}_3\cdot 6\text{H}_2\text{O}$	
$\text{CAH}_{10}$	$\text{CaO}\cdot\text{Al}_2\text{O}_3\cdot 10\text{H}_2\text{O}$	
$\text{C}_2\text{AH}_8$	$2\text{CaO}\cdot\text{Al}_2\text{O}_3\cdot 8\text{H}_2\text{O}$	
$\text{C}_4\text{AH}_{13}$	$4\text{CaO}\cdot\text{Al}_2\text{O}_3\cdot 13\text{H}_2\text{O}$	
$\text{C}_4\text{AH}_{19}$	$4\text{CaO}\cdot\text{Al}_2\text{O}_3\cdot 19\text{H}_2\text{O}$	
$\text{C}_4\text{A}(\text{CARB})_{0.5}\text{H}_{12}$	$\text{C}_4\text{A}(\text{CaCO}_3)_{0.5}\text{H}_{12}$	$4\text{CaO}\cdot\text{Al}_2\text{O}_3\cdot 0.5\text{CO}_2\cdot 12\text{H}_2\text{O}$
$\text{C}_4\text{A}(\text{CARB})\text{H}_{11}$	$\text{C}_4\text{A}(\text{CaCO}_3)\text{H}_{11}$	$4\text{CaO}\cdot\text{Al}_2\text{O}_3\cdot \text{CO}_2\cdot 11\text{H}_2\text{O}$
XRD	X-ray Diffraction	
SEM	Scanning Electron Microscopy	
NMR	Nuclear Magnetic Resonance	
EDS	Energy Dispersive Spectroscopy	
DTA	Differential Thermal Analysis	
TG	Thermal Gravimetry	

# Contents

<b>Abstract</b>	I
<b>Acknowledgements</b>	III
<b>Nomenclature</b>	IV
<b>List of Figures</b>	XI
<b>List of Tables</b>	XVI
<b>Introduction</b>	1
1. Objectives of this research	2
2. Outline of this thesis	2
<b>Chapter 1 Literature review</b>	4
1.1 Waste disposal	4
1.2 Cements	5
1.2.1 Non-hydraulic cements	6
1.2.2 Hydraulic cements	7
1.2.2.1 Characteristics of pure cement phases	7
1.2.2.2 Portland cement	8
1.2.2.3 High alumina cement (HAC)	10
1.2.2.4 Calcium sulphoaluminate cement (CSAC)	11
1.2.2.5 Blended cements	12
1.3 Hydration of pure cement phases	13
1.3.1 Hydration of tricalcium silicate	13
1.3.2 Hydration of dicalcium silicate	16
1.3.3 Hydration of tricalcium aluminate	16
1.3.4 Hydration of calcium aluminoferrite	18
1.4 Hydration of Portland cement	18
1.5 Cement hydration products	20
1.5.1 Portlandite	21

1.5.2 Calcium silicate hydrate (C-S-H) gel	21
1.5.3 Ettringite and monosulphoaluminate	24
1.5.4 Minor phases	26
1.6 Carbonation of cement	27
1.6.1 Atmospheric carbonation (natural carbonation)	28
1.6.2 Accelerated carbonation (rapid carbonation)	29
1.6.3 Mechanisms of carbonation	29
1.7 Characteristics of cement carbonation products	30
1.7.1 Calcium carbonate	30
1.7.2 Silica gel	31
1.8 Chemistry of cement -based solidification/stabilisation	33
1.8.1 Interface phenomena	33
1.8.2 Effects of admixtures	35
1.8.3 Effects of carbonation	37
1.8.4 Factors affecting on cement -based s/s processes	38
1.8.4.1 Particle size	38
1.8.4.2 Free water content	39
1.8.4.3 Temperature	39
1.8.5 Mechanisms of heavy metal immobilisation	40
1.8.5.1 Sorption	40
1.8.5.2 Complexation	41
1.8.5.3 Diiodochy	41
1.8.5.4 Precipitation	41
1.8.5.5 Current views on heavy metal incorporation in cement pastes	42
1.9 The durability of concrete and cement -based s/s products	43
1.10 Characterisation of cement systems	44
1.11 Summary	46
<b>Chapter 2 Materials, procedures and experimental methods</b>	<b>48</b>
2.1 Background	48
2.2 Materials	48
2.2.1 Portland cement	49
2.2.2 Pure cement phases	49
2.2.3 Chemical reagents	49

2.3 Experimental procedures	49
2.3.1 Preparation of hydrated pastes	49
2.3.2 Carbonation experiments	50
2.3.2.1 Carbonation equipment and conditions	50
2.3.2.2 Procedure of accelerated carbonation	51
2.3.2.3 Carbonation of hydrated cement pastes	51
2.3.3 Suspensions	51
2.3.5 Carbonation of suspensions	52
2.4 X-ray powder diffraction (XRD)	52
2.5 Scanning electron microscopy and energy dispersive X-ray spectrometer	54
2.5.1 Principle of technique	54
2.5.2 Instrumentation and sample handling	55
2.6 Nuclear magnetic resonance (NMR)	56
2.6.1 Principle of technique	56
2.6.2 Instrumentation and sample preparation	59
2.7 Thermal analysis	60
2.7.1 Differential thermal analysis (DTA)	60
2.7.2 Thermogravimetry (TG)	61
2.7.3 Instrumentation and sample preparation	61
2.8 Summary	62

### **Chapter 3 Interactions of calcium oxide or calcium hydroxide with heavy metals in pastes and suspensions**

<b>heavy metals in pastes and suspensions</b>	64
3.1 Background	64
3.2 Experimental	66
3.3 Results and discussion	68
3.3.1 Crystalline phases in hydrated pastes	68
3.3.2 Crystalline phases in carbonated pastes	68
3.3.3 Phase development in calcium oxide or calcium hydroxide suspensions	69
3.3.3.1 Calcium hydroxide suspensions	70
3.3.3.2 Calcium oxide suspensions	73
3.3.4 Thermal analyses of calcium oxide pastes	80

3.3.4.1 Hydrated pastes	80
3.3.4.2 Carbonated pastes	86
3.4 Summary	91
<b>Chapter 4 Investigation of tricalcium silicate/heavy metal systems</b>	92
4.1 Background	92
4.2 Experimental	94
4.3 Results and discussion	96
4.3.1 Hydration	96
4.3.2 Accelerated carbonation	108
4.3.3 Silicate polymerisation in the hydrated or carbonated C <sub>3</sub> S pastes	116
4.3.4 Structural models of C-S-H gel	120
4.3.4.1 In the control hydrated C <sub>3</sub> S paste	122
4.3.4.2 In the control carbonated C <sub>3</sub> S paste	123
4.3.4.3 In the hydrated C <sub>3</sub> S pastes with heavy metals	124
4.3.4.4 In the carbonated C <sub>3</sub> S pastes with heavy metals	124
4.4 Summary	125
<b>Chapter 5 Investigation of aluminium -bearing phase/heavy metal systems</b>	128
5.1 Background	128
5.2 Experimental	130
5.3 Results and discussion	131
5.3.1 C <sub>3</sub> A in the absence of gypsum	131
5.3.1.1 Hydration	131
5.3.1.2 Accelerated carbonation	137
5.3.2 C <sub>3</sub> A in the presence of gypsum	143
5.3.2.1 Hydration	143
5.3.2.2 Accelerated carbonation	143
5.3.3 C <sub>12</sub> A <sub>7</sub> , CA and C <sub>4</sub> AF	148
5.3.3.1 Hydration	148
5.3.3.2 Accelerated carbonation	149

5.4. Further discussion—reactivity of phases containing aluminium	150
5.5 Summary	154

## **Chapter 6 Phase development in heavy metal -doped Portland cement**

### **pastes and suspensions** 156

6.1 Background	156
6.2 Experimental	158
6.3 Results and discussion	160
6.3.1 Hydration	160
6.3.2 Accelerated carbonation	170
6.3.3 Characterisation of C-S-H gel in Portland cement pastes	177
6.3.4 Additional discussion	185
6.4 Summary	186

## **Chapter 7 Morphology and microanalysis of heavy metal -doped**

### **Portland cement pastes** 188

7.1 Background	188
7.2 Experimental	189
7.3 Results and discussion	190
7.3.1 Anhydrous particles and reaction products of cement	190
7.3.2 Incorporation of heavy metals in the cement matrix	197
7.4 Summary	204

## **Chapter 8 Thermodynamic modelling of heavy metal -cement systems**

### **using PHREEQC** 205

8.1 Background	205
8.2 Databases	206
8.3 Geochemical modelling codes	206
8.4 Modelling strategy of this work	207
8.5 Results and discussion	208
8.5.1 pH values of cement suspensions	208
8.5.2 Thermodynamic modelling of phases in cement pastes	209

8.5.3 Thermodynamic modelling of heavy metal precipitates in cement systems	215
8.5.3.1 Hydrated cement systems	216
8.5.3.2 Carbonated cement systems	218
8.5.4 Solubility control compounds of heavy metals in cement systems	219
8.6 Shortcoming of thermodynamic modelling	222
8.7 Summary	224
<b>Chapter 9 General discussion</b>	<b>226</b>
9.1 Background	226
9.2 Interaction mechanisms of heavy metals and cement	227
9.2.1 Hydration of C <sub>3</sub> S and Portland cement	228
9.2.2 Carbonation of C <sub>3</sub> S and Portland cement	230
9.3 Heavy metal incorporation in cement matrices	232
9.4 Aspects relevant to the practical applications of accelerated carbonation	235
9.5 Major contributions of this work	236
9.6 Recommendations for the further work	237
<b>Chapter 10 Conclusions</b>	<b>239</b>
<b>References</b>	<b>243</b>
<b>Appendix A Syntheses of cement pure phases and heavy metal compounds</b>	<b>267</b>
<b>Appendix B Diffractograms of hydrated or carbonated pastes of C<sub>12</sub>A<sub>7</sub>, CA and C<sub>4</sub>AF</b>	<b>268</b>
<b>Appendix C Main aqueous databases and geochemical codes</b>	<b>280</b>
<b>Appendix D Glossary</b>	<b>284</b>

# List of Figures

## Chapter 1 Literature review

Fig. 1.1. Surface charge layer on hydrating  $C_3S$  grain

Fig. 1.2. Heat evolution profile from hydrating cement

Fig. 1.3. The micelle bridging model of silica gel

Fig. 1.4. The adsorption of water on the surface of silica gel

## Chapter 2 Material, procedure and experimental methods

Fig. 2.1. Schematic diagram of reaction chamber

Fig. 2.2. The XRD equipment used in this work

Fig. 2.3. SEM equipment used in this work

Fig. 2.4. Fourier transform NMR block diagram

Fig. 2.5. The Varian 300mHz NMR instrument used in this work

## Chapter 3 Interactions of calcium oxide or calcium hydroxide with heavy metals in pastes and suspensions

Fig. 3.1. Diffractograms of hydrated calcium oxide pastes aged one month

Fig. 3.2. Diffractograms of accelerated carbonated calcium oxide pastes aged one month

Fig. 3.3. Diffractograms of calcium hydroxide suspensions at the age of 14 days

Fig. 3.4. Diffractograms of carbonated calcium hydroxide suspensions at the age of 1 day

Fig. 3.5. Diffractograms of hydrated calcium oxide suspensions at the age of 1 month

Fig. 3.6. Diffractograms of hydrated calcium oxide suspensions at the age of 2 months

Fig. 3.7. Diffractograms of hydrated calcium oxide suspensions at the age of 3 months

Fig. 3.8. Diffractograms of carbonated calcium oxide suspensions at the age of 1 month

Fig. 3.9. Diffractograms of carbonated calcium oxide suspensions at the age of 3 months

Fig. 3.10. DTA curves of hydrated calcium oxide pastes

Fig. 3.11. TG curves of hydrated calcium oxide pastes

Fig. 3.12. DTA curves of the carbonated pastes of calcium oxide

Fig. 3.13. TG curves of the carbonated pastes of calcium oxide

## **Chapter 4 Investigation of tricalcium silicate/heavy metal systems**

Fig. 4.1. Diffractograms of one-month old hydrated C<sub>3</sub>S pastes

Fig. 4.2. XRD intensity of main phases in one-month old hydrated C<sub>3</sub>S pastes

Fig. 4.3. The pH of C<sub>3</sub>S suspensions

Fig. 4.4. Diffractograms of C<sub>3</sub>S suspensions at the age of 3 months

Fig. 4.5. Diffractograms of one-year old hydrated C<sub>3</sub>S pastes

Fig. 4.6. DTA curves of hydrated C<sub>3</sub>S pastes

Fig. 4.7. TG curves of hydrated C<sub>3</sub>S pastes

Fig. 4.8. The pH of C<sub>3</sub>S suspensions, 1 hour after carbonation

Fig. 4.9. The pH of C<sub>3</sub>S suspensions after 8 cycles of carbonation

Fig. 4.10. The pH of carbonated metal hydroxide suspensions

Fig. 4.11. Diffractograms of carbonated C<sub>3</sub>S suspensions at the age of 2 weeks

Fig. 4.12. Diffractograms of carbonated C<sub>3</sub>S suspensions at the age of 1 month

Fig. 4.13. Diffractograms of carbonated C<sub>3</sub>S pastes aged 1 month

Fig. 4.14. Diffractograms of carbonated C<sub>3</sub>S pastes aged 1 year

Fig. 4.15. DTA curves of carbonated C<sub>3</sub>S pastes

Fig. 4.16. TG curves of carbonated C<sub>3</sub>S pastes

Fig. 4.17. <sup>29</sup>Si NMR spectra of hydrated C<sub>3</sub>S pastes with or without heavy metals

Fig. 4.18. <sup>29</sup>Si NMR spectra of carbonated C<sub>3</sub>S pastes with or without heavy metals

Fig. 4.19. The incorporation model of heavy metal in calcium silicate hydrate gel

## **Chapter 5 Investigation of aluminium -bearing phase/heavy metal systems**

- Fig. 5.1. Diffractograms of hydrated  $C_3A$  pastes aged 28-days
- Fig. 5.2. Diffractograms of hydrated  $C_3A$  pastes aged 1 year
- Fig. 5.3. The main phases in 28-day old hydrated  $C_3A$  pastes
- Fig. 5.4. The main phases in hydrated  $C_3A$  pastes at one year
- Fig. 5.5. Diffractograms of the hydrated  $C_3A$  suspensions at the age of 1 month
- Fig. 5.6. Diffractograms of carbonated  $C_3A$  pastes at 28-days
- Fig. 5.7. Phase detected in the accelerated carbonated  $C_3A$  pastes
- Fig. 5.8. Diffractograms of carbonated  $C_3A$  aged 1 year
- Fig. 5.9. Diffractograms of carbonated  $C_3A$  suspensions at different times
- Fig. 5.10. Diffractograms of carbonated  $C_3A$  suspension and paste at 3 months of age
- Fig. 5.11. Diffractograms of hydrated 28-day old  $C_3A$  pastes in the presence of gypsum
- Fig. 5.12. Diffractograms of hydrated 1 year old  $C_3A$  pastes in the presence of gypsum
- Fig. 5.13. Diffractograms of carbonated  $C_3A$  pastes aged 1 month with gypsum
- Fig. 5.14. XRD patterns of accelerated carbonation of  $C_3A$  aged 1 year with gypsum
- Fig. 5.15. The pH of pure cement phase suspensions, 1 hour after carbonation
- Fig. 5.16. The pH of pure cement phase suspensions after 8 cycles of carbonation

## **Chapter 6 Phase development in heavy metal -doped Portland cement pastes and suspensions**

- Fig. 6.1. Diffractograms for hydrated cement pastes aged one month
- Fig. 6.2. Diffractograms of hydrated cement suspensions at the age of three months
- Fig. 6.3. pH values of cement suspensions with time
- Fig. 6.4. Diffractograms of hydrated Portland cement pastes aged one year
- Fig. 6.5. DTA curves of hydrated cement pastes
- Fig. 6.6. TG curves of hydrated cement pastes
- Fig. 6.7. Suspension pH for different carbonation cycles

Fig.6.8. The pH of cement suspensions as function of time following the 8<sup>th</sup> cycle of carbonation

Fig. 6.9. Suspension pH of carbonated metal hydroxide

Fig. 6.10. Diffractograms of carbonated cement suspensions

Fig. 6.11. Diffractograms of carbonated pastes aged one month

Fig. 6.12. Diffractograms of carbonated cement pastes aged one year

Fig. 6.13. XRD patterns of carbonation of 28-day old hydrated cement pastes

Fig. 6.14. DTA curves of carbonated cement pastes

Fig. 6.15. TG curves of carbonated cement pastes

Fig. 6.16. <sup>27</sup>Al NMR spectra of hydrated cement pastes

Fig. 6.17. <sup>29</sup>Si NMR spectra of carbonated cement pastes

Fig. 6.18. <sup>27</sup>Al NMR spectra of carbonated cement pastes

Fig. 6.19. <sup>29</sup>Si NMR spectra of carbonated cement pastes

## **Chapter 7 Morphology and microanalysis of heavy metal -doped Portland cement pastes**

Fig. 7.1. SEM images of fracture surface of hydrated cement pastes

Fig. 7.2. SEM images of fracture surface of carbonated cement pastes

Fig. 7.3. Atom ratio plots of Al/S versus Si/S in the hydrated cement pastes

Fig. 7.4. Atom ratio plots of Al/S versus Si/S in the carbonated cement pastes

Fig.7.5. Atom ratio plots of chromium with cement components in the Cr<sup>3+</sup>-doped hydrated cement paste

Fig.7.6. Atom ratio plots of lead with cement components in the Pb<sup>2+</sup>-doped hydrated paste

Fig.7.7. Atom ratio plots of copper with cement components in the Cu<sup>2+</sup>-doped hydrated cement paste

Fig.7.8. Atom ratio plots of zinc with cement components in the Zn<sup>2+</sup>-doped hydrated cement paste

Fig.7.9. Atom ratio plots of chromium with cement components in the Cr<sup>3+</sup>-doped carbonated cement paste

Fig.7.10. Atom ratio plots of lead with cement components in the  $\text{Cu}^{2+}$ -doped carbonated cement paste

Fig.7.11. Atom ratio plots of copper with cement components in the  $\text{Pb}^{2+}$ -doped carbonated cement paste

## **Chapter 8 Thermodynamic modelling of heavy metal-cement systems using PHREEQC**

Fig. 8.1. The equilibrium pH of hydration products of calcium silicate

Fig. 8.2. The modelled aqueous solubility of copper compounds with pH

Fig. 8.3. The modelled aqueous solubility of lead compounds with pH

Fig. 8.4. The modelled aqueous solubility of zinc compounds with pH

## **Appendix B Diffractograms of pastes of $\text{C}_{12}\text{A}_7$ , CA and $\text{C}_4\text{AF}$**

Fig. 1. Diffractograms of  $\text{C}_{12}\text{A}_7$  hydration aged 28-days

Fig. 2. Diffractograms of  $\text{C}_{12}\text{A}_7$  hydration aged one year

Fig. 3. Diffractograms of carbonated  $\text{C}_{12}\text{A}_7$  pastes at 28-days

Fig. 4. Diffractograms of carbonated  $\text{C}_{12}\text{A}_7$  pastes at one year

Fig. 5. Diffractograms of CA hydration aged 28-days

Fig. 6. Diffractograms of CA hydration aged one year

Fig. 7. Diffractograms showing carbonated CA at 28-days

Fig. 8. Diffractograms showing carbonated CA at one year

Fig. 9. Diffractograms of  $\text{C}_4\text{AF}$  hydration aged 28-days

Fig. 10. Diffractograms of  $\text{C}_4\text{AF}$  hydration aged one year

Fig. 11. Diffractograms showing carbonated  $\text{C}_4\text{AF}$  at 28-days

Fig. 12. Diffractograms showing carbonated  $\text{C}_4\text{AF}$  at one year

# List of Tables

## Chapter 1 Literature Review

Table 1-1. Hydration products of Portland cement

Table 1-2. Reactions for the accelerated carbonation of cement

## Chapter 2 Experimental Material, Methods and Procedures

Table 2-1. The compositions of Portland cement

## Chapter 3 Interactions of calcium oxide or calcium hydroxide with heavy metals in pastes and suspensions

Table 3-1. Nucleation time with supersaturation number

Table 3-2. Phases in calcium hydroxide suspensions

Table 3-3. Phases in carbonated calcium hydroxide suspensions

Table 3-4. The phase development in calcium oxide suspensions

Table 3-5. Phases identified by XRD for carbonated calcium oxide suspensions

Table 3-6. Thermal analysis results of hydrated calcium oxide pastes

Table 3-7. Thermal analysis results of carbonated pastes of calcium oxide

## Chapter 4 Investigation of tricalcium silicate/heavy metal systems

Table 4-1. The phase development in hydrated  $C_3S$  suspensions

Table 4-2. Thermal analysis results of hydrated  $C_3S$  pastes

Table 4-3. The evaluation of average Ca/Si ratio in C-S-H gel derived from thermal analysis results

Table 4-4. The phase development in carbonated  $C_3S$  suspensions

Table 4-5. Thermal analysis results of carbonated C<sub>3</sub>S pastes

Table 4-6. <sup>29</sup>Si NMR data of hydrated C<sub>3</sub>S pastes

Table 4-7. <sup>29</sup>Si NMR spectra data of carbonated C<sub>3</sub>S pastes

Table 4-8. Phases of C<sub>3</sub>S pastes

## **Chapter 5 Investigation of aluminium-bearing phase/heavy metal systems**

Table 5-1. Phases detected in the hydrated C<sub>3</sub>A pastes in the absence of gypsum

Table 5-2. Phase development in hydrated C<sub>3</sub>A suspensions

Table 5-3. The major phases detected by XRD in the carbonate C<sub>3</sub>A pastes

Table 5-4. Phase development in the carbonated C<sub>3</sub>A suspensions

Table 5-5. A comparison of pure cement phases containing aluminium

Table 5-6. The pH of pure cement phase suspensions

## **Chapter 6 Phase development in heavy metal -doped Portland cement pastes and suspensions**

Table 6-1. Phase development in hydrated Portland cement suspensions

Table 6-2. TG results of hydrated cement pastes

Table 6-3 TG results of carbonated cement pastes

Table 6-4. <sup>27</sup>Al NMR data of raw cement and hydrated cement pastes

Table 6-5. <sup>29</sup>Si NMR data of hydrated Portland cement pastes

Table 6-6. The chemical shift of aluminium associated with silicon

Table 6-7. <sup>29</sup>Si NMR data of carbonated cement pastes

## **Chapter 7 Morphology and microanalysis of heavy metal-doped Portland cement pastes**

Table 7-1. The compositions of some residuals of hydrated cement pastes

Table 7-2. The compositions of C-S-H gel in different brightness around the clinker of cement

Table 7-3. The compositions of C-S-H gel in the control hydrated cement paste

Table 7-4. The Compositions of C-S-H in the carbonated cement pastes

Table 7-5. Average compositions of microanalyses of the hydrated cement pastes

Table 7-6. Average compositions of microanalyses of the carbonated cement pastes

Table 7-7. The correlation coefficients of atom ratio in the hydrated pastes

Table 7-8. The correlation coefficients of atom ratio in the carbonated pastes

## **Chapter 8 Thermodynamic modelling of heavy metal-cement systems using PHREEQC**

Table 8-1. The suspension pH of cement pure phases and cement

Table 8-2. The pH of hydrated and carbonated cement suspensions with heavy metals

Table 8-3. The decomposition of cement phases and precipitates

Table 8-4. The major phases of carbonated cement

Table 8-5. The calculated aqueous solution compositions of major reaction products of cement

Table 8-6. The comparison of calculated solubility of C-S-H, portlandite and calcite at different pH values

Table 8-7. The aqueous solution compositions of cement phase assemblages

Table 8-8. Modelling heavy metal compounds in hydrated cement pastes

Table 8-9. Simulation of heavy metal compounds precipitating in hydrated cement pastes

Table 8-10. Modelling heavy metal compounds in carbonated cement pastes

Table 8-11. Simulation of heavy metal compounds precipitating in carbonated cement pastes

Table 8-12. The phase assemblage in the calculations of aqueous solubility of heavy metal compounds

Table 8-13. Comparison of the modelled aqueous solubility of heavy metals compounds in cement pastes

Table 8-14. The prediction of heavy metal releases from hydrated or carbonated cement pastes

## **Chapter 9 General Discussion**

Table 9-1. The solubility and suspension pH of metal compounds

Table 9-2. The solubility products of metal hydroxides on the surface of silica and bulk solution

## Introduction

Industrial activities in the production of materials and chemicals give rise to very large quantities of wastes each year. The use of toxic, mutagenic and carcinogenic heavy metals such as Pb, Zn, Cu and Cr has resulted in the contamination of soils and waters, which pose a serious threat to human and animal health (Glasser, 1997; Wiles, 1987; Bozkurt *et al.*, 2000).

Solidification/stabilisation (s/s) of heavy metal bearing sludge, industrial residues and contaminated soil is an attractive technology to reduce their toxicity and facilitate handling prior to landfill (Conner, 1990; Alunno and Medici, 1995; Conner and Hoeffner, 1998). The selection of binders and operating parameters depends upon an understanding of the chemistry of the waste stream to be treated in order to ensure that certain toxic metals are immobilised effectively (Klich *et al.*, 1990; 1999). Hydraulic and pozzolanic cementitious materials are flexible binders currently available for the immobilisation of toxic metals (Arafat and Hebatpuria, 1999; Cannell *et al.*, 2000).

The hydration products of cement are unstable on exposure to the atmosphere and will undergo alteration with time, partly due to carbonation (Walton *et al.*, 1995; 1997). These changes can affect the kinetics of penetration of aggressive agents into the solidified waste forms and kinetics of release of chemicals into the environment (Cartledge *et al.*, 1990). Currently, accelerated carbonation technology has been adopted to induce setting and strength development, and improve the effectiveness of cement-based s/s, where cement hydration is significantly retarded (Lange *et al.*, 1996; Hills *et al.*, 2003).

The interactions of cement and heavy metals in cement-based s/s are not yet fully understood despite extensive research (Stephan *et al.*, 1999; Murat and Sorrentino, 1996). To minimise the release of contaminants into the environment, there is an urgent need to understand the phase development, phase characteristics, waste-binder interactions and mechanisms of contaminant fixation during cement-based s/s processes (Berger *et al.*, 1972; Klich *et al.*, 1999; Johannesson and Utgenannt, 2001).

## **1. Objectives of this research**

The objectives of this research were:

- to investigate the reaction products formed during the hydration of cement in the presence of heavy metals ( $\text{Zn}^{2+}$ ,  $\text{Pb}^{2+}$ ,  $\text{Cu}^{2+}$  and  $\text{Cr}^{3+}$ ) and to determine the changes induced by heavy metal ions on these products;
- to characterise the carbonation products of pure cement phases and Portland cement with or without heavy metals;
- to examine hydrated and carbonated cement pastes with regard to the immobilisation mechanisms of heavy metals;
- to elucidate the interactions of heavy metals with cement using thermodynamic modelling with a geochemical code.

The outcome of these studies is expected to be used to extend existing s/s techniques and take measures to prolong the life of solidified wastes. In addition, this work is also important to the field of cement and concrete science and contributes to the effects of carbonation on the performance of cementitious materials.

## **2. Outline of this thesis**

To achieve the above objectives, cement pastes and suspensions doped with heavy metals were investigated with XRD, DTA/TG,  $^{29}\text{Si}$  and  $^{27}\text{Al}$  MAS/NMR, SEM/EDS techniques and thermodynamic modelling. Cementitious materials used in this work were calcium oxide, calcium hydroxide, pure cement phases ( $\text{C}_3\text{S}$ ,  $\text{C}_3\text{A}$ ,  $\text{C}_4\text{AF}$ ,  $\text{C}_{12}\text{A}_7$  and  $\text{CA}$ ), and Portland cement. Heavy metals were nitrate salts of  $\text{Zn}^{2+}$ ,  $\text{Pb}^{2+}$ ,  $\text{Cu}^{2+}$  and  $\text{Cr}^{3+}$ . The followings briefly describe the contents of each chapter.

**Chapter 1:** provides a review of the literature pertinent to waste treatment, the state of the art of cement-based s/s technology, the chemistry of cement and the interactions of cement with admixtures including heavy metals.

**Chapter 2:** describes the materials used, the preparation of cement pastes and suspensions, carbonation procedures and methodology of phase characterisation.

**Chapter 3:** describes the interactions of heavy metals with calcium oxide and calcium hydroxide in suspensions and pastes during carbonation and hydration processes.

**Chapter 4:** the pastes and aqueous suspensions of tricalcium silicate doped with heavy metals were examined at different ages by XRD, DTA/TG and  $^{29}\text{Si}$  MAS/NMR techniques. The effects of heavy metals on reactions of  $\text{C}_3\text{S}$  in pastes and suspensions were studied.

**Chapter 5:** presents the reaction products of  $\text{C}_3\text{A}$ ,  $\text{C}_4\text{AF}$ ,  $\text{C}_{12}\text{A}_7$  and CA pastes and suspensions with or without heavy metals. The reactivity and changes induced by the presence of heavy metals on the reaction products of these phases are discussed.

**Chapter 6:** hydrated and carbonated pastes and suspensions of Portland cement in the presence of heavy metals were characterised using XRD, DTA/TG, and  $^{29}\text{Si}$  and  $^{27}\text{Al}$  solid state magic angle spinning/nuclear magnetic resonance (NMR) techniques. The reaction products for different systems were examined and compared.

**Chapter 7:** presents the morphology and composition of reaction products in hydrated and carbonated Portland cement pastes doped with heavy metals. The statistical analyses of micro-analytical data were used to identify chemical associations between heavy metal and cement components.

**Chapter 8:** describes the thermodynamic modelling methods, computer programming codes, databases and the modelling strategy used. This chapter also presents the thermodynamic modelling results of likely aqueous reaction processes between cement and heavy metals using a geochemical code, PHREEQC.

**Chapter 9:** summarises the interaction mechanisms of heavy metals and cement, the chemical mechanisms of heavy metal fixation, original contributions of this thesis to science and the recommendations for further work.

**Chapter 10:** presents the conclusions of this work.

# Chapter 1

## Literature review

### *1.1 Waste disposal*

The most common methods for waste treatment are physical and chemical separation, thermal treatment (incineration), solidification/stabilisation (s/s) and bioremediation (Conner, 1990, Hills, 1992; Hills *et al.*, 2003). Every method has its limitations, for example, many pollutants in contaminated soil, industrial effluents and residuals are resistant to biological degradation and may exert significant toxicity towards the mixed microbial communities within biological treatment systems, reducing the efficiency (Harrison and de Mora, 1996). Thermal treatment (incineration) and separation of wastes could result in the emission of toxic substances into the environment in treatment processes. In addition, the products from these processes often need further treatment (Caldewell and Cote, 1990; Hudales, 1994).

Solidification/stabilisation technology is recognised as one of most effective management techniques to reduce the mobility of the toxic waste element, making the waste acceptable for landfill (Lo, 1996). Cement-based s/s has been widely used in the treatment of industrial residues and contaminated soil for about 50 years (Alunno and Medici, 1995). This technique generally involves mixing wastes or contaminated soils with binders (Arafat and Hebatpuria, 1999; Lo *et al.*, 2000). It may be undertaken as an in-situ process or ex-situ process. The latter variation of the process is usually undertaken within the confines of site before replacement and compaction of the material.

Since the Control of Pollution Act of 1974 was introduced in the UK, there has been a steady increase in use of landfill disposal for soil and waste (Akhter *et al.*, 1997). The Landfill Directive sets operational guidelines for landfill practice and requires pre-treatment of a range of wastes prior to landfill (Environmental data service, 2003). The Directive 1999/31/EC includes a number of stringent measures aimed at increasing the level of environment protection, and will be adopted in the UK and European Union in

July 2004. As a consequence of this it is anticipated that s/s technology will become more commonly used as a waste management strategy (Hills *et al.*, 2003).

Organic binders rely on refined materials such as asphalt, polyethylene, resins, epoxies, urea formaldehyde, polyesters and potentially organophilic clays (Lo, 1996; Jun *et al.*, 1997; Soundarajan *et al.*, 1990). The employment of an organic binder, however, may not be environmentally desirable or cost-effective. The application of organic encapsulation, therefore, tends to be limited to particularly hazardous materials, such as nuclear wastes (Banfill and Saunders, 1986).

The most popular binders of solidification/stabilisation are often based on Portland cement, calcium aluminate cement, modified cement, slag cement, Portland cement plus fly ash or kiln dust or calcium oxide (Hudales, 1994; Redmond *et al.*, 2002a; 2002b). Cement-based stabilisation/solidification methods tend to cost less than other treatments such as vitrification and organic encapsulation (Albino *et al.*, 1996; Shimaoka and Hanashima, 1996; Soundarajan *et al.*, 1990). The development of cement-based s/s remediation technology relies on the formation of stable reaction products capable of binding waste components and providing the solidified product with strength and dimensional stability (Stegemann and Cote, 1990).

Despite the widespread use of cement-based s/s, work that has been published on the mechanisms that take place between the cementing media and waste components and the durability so far lacks consistency and comparison (Glasser, 1997). In addition, there is no convincing short term testing procedure, which can predict longer term properties and stability of solidified/stabilised wastes in different environments at present (Tyrer, 1994). It is necessary to limit potential waste/binder interactions, understand the mechanisms of waste immobilisation and improve the effectiveness of this waste management technique.

## ***1.2 Cements***

Cement is well known as an ideal material for treating contaminated land and the other wastes, where it is expected to endure aggressive environments and at same time

maintain a high level of performance. Two main classes of cements are defined: non-hydraulic cements and hydraulic cements.

### 1.2.1 Non-hydraulic cements

Non-hydraulic cements such as calcium oxide, calcium hydroxide and gypsum deteriorate rapidly in moist or wet environment due to high solubility (Komilis and Han, 1999). Calcium oxide or calcium hydroxide is most widely used alkali, and global production is believed to be over 200 million tonnes per annum (Oates and Joseph, 1998). Calcium oxide has been used in enormous quantities in the drying, modification and stabilisation of clay soils to yield a product with more desirable geotechnical properties than the original clay (Holt and Freer, 1996; Komilis and Han, 1999).

Hydroxide ions have a retarding effect on CaO hydration due to the common ion effect. It is recognised that the slaking of calcium oxide and the dissolution of calcium hydroxide are both controlled by the diffusion of calcium or hydroxide ions away from the surface of calcium oxide (Ritchie and Xu, 1990, Giles *et al.*, 1993; Xu *et al.*, 1997).

Impurities or admixtures influence the slaking process of calcium oxide, including slaking rate and the polymorphism, habit, morphology and particle size of products. For example, Boynton (1980) reported a doubling in the rate of CaO slaking in the presence of 1-3 % chloride, while the presence of 0.1-3 % sulphates and carbonates decreases the CaO hydration rate. Xu *et al.* (1998) has examined the slaking of CaO in solutions containing various concentrations of Na<sub>2</sub>CO<sub>3</sub>. They inferred that the retarding effect of CO<sub>3</sub><sup>2-</sup> on the CaO slaking may be due to the presence of a calcium carbonate coating on the CaO particles.

Conducting the CaO hydration in the presence of additional salt can affect the particle size of Ca(OH)<sub>2</sub>. Slaking CaO in the presence of a solution containing Na<sub>2</sub>SO<sub>4</sub> gives Ca(OH)<sub>2</sub> crystals as hexagonal plates with a side of 5-20 microns, while slaking in the presence of NaCl or NaOH gives Ca(OH)<sub>2</sub> crystals with a side of 2-5 microns, which is only slightly larger than the size of the crystals formed in the absence of added salts (Glasson, 1961; Boynton, 1980).

## 1.2.2 Hydraulic cements

Hydraulic cements are silicate or aluminate powders that react with water to generate hard and solid matrices, which continue to increase in compressive strength even when the matrices are placed in excess water (Hill and Sharp, 2002). Within this category are Portland cement, high alumina cements (HAC) and calcium sulpho-aluminate cements (CSA) and various blend cements (Spence and Cook, 1983).

### 1.2.2.1 Characteristics of pure cement phases

Tricalcium silicate,  $C_3S$  or  $Ca_3SiO_5$ , is pseudo trigonal/triclinic and a solid solution of CaO in dicalcium silicate proposing the formula  $Ca_2(SiO_4(CaO))$ . It is suggested that in  $C_3S$  the layers of orthosilicate  $C_2S$  are parted by layers rich in CaO (Lea, 1970; Tyrer, 1990; Taylor, 1997).

Dicalcium silicate,  $C_2S$  or  $\beta-Ca_2SiO_4$ , is a complex material containing point defects, which undergoes inversions on cooling, resulting in an accumulation of strain in the lattice which induces multiple twinning. Five polymorphs of this mineral are recognised of which the  $\beta$ -(orthorhombic) is the stable form at room temperature (Taylor, 1997).

Tricalcium aluminate,  $C_3A$  or  $Ca_3Al_2O_6$ , is the only cement compound not to show polymorphic transformations with temperature. The  $C_3A$  phase is very reactive (Atkins and Macphee, 1991).

Calcium mono-aluminate, CA or  $CaAl_2O_4$ , is the principal hydraulic mineral present in calcium alumina cements (CACs). Its hydration contributes to the high early strength of CACs. Calcium mono-aluminate is a monoclinic, pseudo-hexagonal phase and resembles the structure of  $\beta$ -tridymite, with an infinite three-dimensional framework of  $AlO_4$  tetrahedra sharing corners. The large ionic radius of the  $Ca^{2+}$  distorts the tridymite network and a section of the calcium atoms has irregular co-ordination polyhedra with oxygen (Shimaoka and Hanashima, 1996). Under the optical microscope CA appears as irregular colourless grains.

Dodecacalcium hepta-aluminate,  $C_{12}A_7$  or  $Ca_{12}Al_{14}O_{33}$ —mayenite, is composed of  $Ca^{2+}$  ions with irregular six-fold co-ordination with oxygen, which has an incomplete framework of corner-sharing  $AlO_4$  tetrahedra that has the empirical composition  $Al_7O_{16}^{11-}$ . In each unit formula one of the  $O^{2-}$  ions is distributed between twelve sites, which is thought to increase two of the  $AlO_4$  groups to  $AlO_5$ . The calcium ions in mayenite have a highly balanced shell of oxygen atoms, which are roughly distributed on the surface of a hemisphere. These co-ordinating hemispheres occur in pairs along the axes of crystal symmetry, in which the planar faces are defined by vacancies amongst the twelve-fold positions (Taylor, 1997). Mayenite is the most reactive of all calcium aluminate species occurring in HACs, and will hydrate very rapidly in contrast to CA. Due to this fact the amount of mayenite contained in calcium aluminate is very carefully regulated by manufacturers.

Alumino-ferrite phase,  $C_4AF$ ,  $Ca_2(Fe_{1-x}Al_x)_2O_5$ , where  $0 < X < 0.7$ , is orthorhombic. It is a solid solution between  $C_6AF_2$  and  $C_6A_2F$  (Taylor, 1997).

### **1.2.2.2 Portland cement**

The oldest man-made hydraulic cement is Portland cement. Portland cement consists of a complex mixture of phases that are produced from the raw materials by chemical reaction and crystallisation during calcination and subsequent clinker cooling (Chandra, 1997). Cements of this class are typically manufactured from a mixture of calcareous and argillaceous materials in a rotary kiln, which is usually about 30-100m long, inclined at an angle, and is rotated slowly. This is operated under oxidising conditions at a high temperature. Fuel is blown into the kiln so that the temperature increases towards the exit.

The raw materials are fed into the flue gas for pre-heating, and then travel down the kiln towards the hot zone. As the raw meal passes through the kiln it undergoes chemical, mineralogical and morphological changes. At first, limestone decomposes to calcium oxide and carbon dioxide. Then particles begin to sinter and form into irregular lumps known as clinker. At the highest temperature ( $1450^\circ C$ ) the clinker begins to fuse and new phases of cement form. This stage is marked by diffusion. To aid this process, fluxes are

used, notably aluminium and iron oxides, although their effect on the final clinker composition has to be carefully controlled (Berner, 1992; Bennett, 1992). The clinker is mixed with 3-5 percent of gypsum and finely ground to make the cement (Clark and Brown, 1999; Damidot and Glasser, 1992).

Portland cement is a heterogeneous mixture of four main compounds with the following composition: 50-70% alite, 20-30% belite, 5-12% aluminate, 5-12% ferrite and 3-5% gypsum (Tyrrer, 1990; Chandra, 1997).

- Alite: tricalcium silicate ( $\text{Ca}_3\text{SiO}_5$ ) containing  $\text{Mg}^{2+}$ ,  $\text{Al}^{3+}$ ,  $\text{Fe}^{3+}$  and other ions, may appear as sub-hexagonal (pseudomorphic remnants of high temperature trigonal) structure. It reacts readily with water to produce calcium silicate hydrate gel (C-S-H) and portlandite ( $\text{Ca}(\text{OH})_2$ ). Alite is considered to be the most significant constituent phase with respect to strength development up to 28 days.
- Belite: substituted dicalcium silicate ( $\text{Ca}_2\text{SiO}_4$ ), is normally present as the polymorph, which may be stabilised by impurities in the lattice, for example, the monoclinic symmetry of the  $\alpha$ - form has been found in Portland cement. The grains of belite are darker and more rounded than those of alite, and often distinctively yellow in transmitted light. Its reaction with water to form C-S-H gel and portlandite is relatively slow compared with that of alite and so it contributes little to early strength development, however, after one year the compressive strengths of alite and belite are comparable.
- The aluminate phase is tricalcium aluminate ( $\text{Ca}_3\text{Al}_2\text{O}_6$ ) which is substantially modified in structure and composition by the incorporation of ions, particularly,  $\text{Si}^{4+}$ ,  $\text{Fe}^{3+}$ ,  $\text{Na}^+$  and  $\text{K}^+$ . It constitutes 5–10% of a Portland cement clinker. Group I metal substitution (for calcium) causes changes in symmetry from the essentially cubic lattice. Five compositional polymorphs have been identified. In practice, Fe, Mg, Si, Ti, Na, and K can constitute as much as 10% by weight in this phase. Lea (1970) estimates the probable iron content in this phase at around 4.1% by weight (as  $\text{Fe}_2\text{O}_3$ ). Aluminate reacts rapidly with water and may cause undesirably rapid setting in the absence of a set-controlling agent such as gypsum (Tyrrer, 1990; Zhang and Odler, 1996).

- The ferrite phase, tetracalcium aluminoferrite ( $\text{Ca}_2\text{AlFeO}_5$ ), significantly modified by the incorporation of  $\text{Si}^{4+}$ ,  $\text{Fe}^{3+}$ ,  $\text{Na}^+$  and  $\text{K}^+$  ions and variable Al/Fe ratio, constitutes 5–15% of a Portland cement clinker. Its reactivity with water is variable. This mineral contains the bulk of the metals, especially Mg, Ti, Mn and Cr. MgO and  $\text{SiO}_2$  substitute for  $(\text{Al}, \text{Fe})_2\text{O}_3$  up to about 10 mole percent.

It is possible to predict, by calculation, the phase make-up of a given Portland cement clinker by use of the Bogue equation. This calculation relies on data obtained by totalling the elemental analyses of all of the raw materials and expressing these as oxides (Lea, 1970).

### 1.2.2.3 High alumina cements (HACs)

High alumina cement (HAC) was patented in 1908 by Lafarge to fill the need for cement that was resistant to sulphate attack. High alumina cements are mostly manufactured by fusion, i.e. melting, at high temperatures ranging from 1000–1600°C, although different methods exist, for example, a sintering process (Lea, 1970).

The feed stock is limestone and bauxite. This material is coarsely crushed rather than ground to form the raw meal. The large particles then leave a porous structure through which the hot gases from combustion can permeate. The raw meal is placed in a reverberatory furnace that is heated by a strong coal or oil flame. The crushed feed stock melts, is tapped off into moulds and is sprayed with water to give the correct rate of cooling. The cold blocks of clinker (called pigs) are then stockpiled in the open until ground. During the manufacture of HAC, the  $\text{SiO}_2$  content of the raw materials is carefully controlled. Excessive  $\text{SiO}_2$  leads to the formation of the very slowly hydrating phase such as akermanite and gehlenite ( $\text{C}_2\text{AS}$ ). The cost of the low silica bauxite and other raw materials, or treatment to try to reduce the levels of silica contaminants, adds to the intrinsically high cost of HAC manufacture (Chen and Wu, 2000).

The main advantage of HAC cements are their high reactivity, high early strength generation, and resistance to sulphate attack compared with Portland cements. They can attain the same strength at 24 hours that would be expected from Portland cement after

28 days. The increased activity is attributed to their mineral compositions. The main strength contribution is made from the CA phases, by precipitation of the crystalline hydrate  $CAH_{10}$ . It has been observed that set HAC acts as an accelerator for unhydrated HAC (Taylor, 1997). The set HAC presumably acts as a seed site for the further bulk precipitation of  $CAH_{10}$ . The post hydration conversion of the initial product  $CAH_{10}$  to  $C_3AH_6 + Al(OH)_3$  leads to a rapid increase in porosity and a consequent decrease in compressive strength (De Ceukelairre and Van Nieuwenburg, 1993; Osborne, 1999).

The hydration reactions of the minerals  $C_{12}A_7$ , CA and  $C_3A$  are considerably exothermic (about 400kJ/kg). The rapid evolution of heat as the cement hydrates causes the temperature of the concrete to increase; this renders HAC suitable for use at subzero temperatures.

#### **1.2.2.4 Calcium Sulpho-Aluminate Cement (CSAC)**

Calcium sulphoaluminate cement (CSAC) has been used in China and Japan to build bridges and buildings in much the same way as Portland cement is used in Europe (Zhang and Odler, 1996). A feature of the commercially available CSA cements, which have a reported composition of 55-75%  $C_4A_3$  and 15-25%  $\alpha$ - $C_2S$ , is the presence of high amounts of silicate phases in the cement.

Calcium sulphoaluminates are manufactured under oxidising conditions, using a rotary calcining kiln, from limestone, bauxite and gypsum. The production of CSAC utilises bauxite with high silica content. The level of silica is far greater than HAC manufacture can tolerate. This ability has been attributed to the behaviour of contaminant silica in the presence of high amounts of sulphate.

In the presence of high levels of sulphate and/or magnesium the cement preferentially forms  $C_2S$  phases, rather than  $C_3S$ . This can be observed in a commercially available Chinese CSA. It has been demonstrated that the high sulphate levels directs the contaminating  $SiO_2$  to form  $C_2S$  rather than either  $C_3S$  or low reactivity aluminate phases such as  $C_2AS$  even in the presence of excess calcium oxide (Zhang *et al.*, 1993; 2000).

### 1.2.2.5 Blended Cements

Cements have usually been blended with some form of reactive additives such as pulverised fly ash (PFA)- a coal combustion product; blast furnace slag (BFS), from iron making, and condensed silica fume (CSF, with 86-95% SiO<sub>2</sub>, glassy SiO<sub>2</sub> particles of ≈100 nm diameter) from the ferrosilicon industry to make concrete (Taylor, 1997; Tyrer, 1994; 2001; De Ceukelaire and Van Nieuwenburg, 1993).

PFA arises as a dust in chimney stacks above coal-burning power station furnaces and has widely variable compositions depending on furnace operating conditions and coal source. Particle sizes of PFA may be fine with 50% < 10 μm or coarse with 50% < 40 μm (Hudales, 1994; Shimaoka and Hanashirma, 1996). Particles are generally spherical (formed by rapid cooling from a melt) and may be hollow (*cenospheres*) with or without spheres inside (*plerospheres*), which are largely glassy (85 - 90%) with small crystallites of mullite (A<sub>3</sub>S<sub>2</sub>) and quartz (Arafat and Hebatpuria, 1999; Lo, 1996; Tyrer and Yunus, 1995).

Different forms of slag product are produced depending on the method used to cool the molten slag in metallurgical industry. These products include air-cooled blast furnace slag (ACBFS), expanded or foamed slag, pelletized slag, and granulated blast furnace slag.

**Air-cooled blast furnace slag:** If the liquid slag is poured into beds and slowly cooled under ambient conditions, a crystalline structure is formed, and a hard, lump slag is produced, which can subsequently be crushed and screened.

Crushed ACBFS is angular, roughly cubical, and has textures ranging from rough, vesicular (porous) surfaces to glassy (smooth) surfaces with conchoidal fractures. There can be, however, considerable variability in the physical properties of blast furnace slag, depending on the iron production process (Redmond *et al.*, 2002a). ACBFS has been used as an aggregate in Portland cement concrete, asphalt concrete, concrete, asphalt and road bases.

**Expanded or foamed blast furnace slag:** If the molten slag is cooled and solidified by adding controlled quantities of water, air, or steam, the process of cooling and solidification can be accelerated, increasing the cellular nature of the slag and producing

a lightweight expanded or foamed product. Foamed slag is distinguishable from air-cooled blast furnace slag by its relatively high porosity and low bulk density.

**Pelletized blast furnace slag:** If the molten slag is cooled and solidified with water and air quenched in a spinning drum, pellets, rather than a solid mass, can be produced. By controlling the process, the pellets can be made more crystalline, which is beneficial for aggregate use, or more vitrified (glassy), which is more desirable in cementitious applications (Rixom *et al.*, 1986; Alunno *et al.*, 1995). Pelletized blast furnace slag has been used as lightweight aggregate and for cement manufacture.

**Granulated blast furnace slag:** If the molten slag is cooled and solidified by rapid water quenching to a glassy state, little or no crystallization occurs. This process results in the formation of sand size (or frit-like) fragments, usually with some friable clinkerlike material (Shimaoka and Hanashima, 1996).

Blast furnace slag consists primarily of silicates, aluminosilicates, and calcium-alumina-silicates (Macphee *et al.*, 1989). Granulated blast furnace slag has been used as a raw material for cement production and as an aggregate and insulating material and granulated slags have also been used as sand blasting shot materials (Berner, 1992; Xu and Viehland, 1996). When crushed or milled to very fine cement-sized particles, ground granulated blast furnace slag (GGBFS) has cementitious properties, which make a suitable partial replacement for or additive to Portland cement (Conner and Lear, 1991; Glasser, 1992; 1997).

Reactivity of blend cements, in all cases, depends on glass content, particle size, composition (nature of impurities) and external influences such as temperature, humidity and hydrating liquid composition (Williams *et al.*, 2002). The chemical reactions between blend cement and water is slow, but it is greatly enhanced by the presence of calcium hydroxide, alkalis, water glass and gypsum.

Blend cements have economical advantages and good durability compared to Portland cement. They are resistant to carbonation and chemical attack. The suitability of slag or other materials for a particular application depends on its reactivity, cost, availability and its influence on the properties of the resulting concrete (Redmond *et al.*, 2002a; 2002b).

### ***1.3 Hydration of pure cement phases***

#### **1.3.1 Hydration of tricalcium silicate**

Tricalcium silicate reacts rapidly with water to produce a gelatinous mass of calcium silicate hydrate gel. The core of the mineral grains may continue a slow reaction over a period of several years. The original orthosilicate ions ( $\text{SiO}_4$  tetrahedra) present in the lattice are converted to disilicate ions ( $\text{SiO}_7^{6-}$ ) and subsequently into higher polymeric forms. The layer of first hydrate so formed prevents further rapid reaction and is thought to be responsible for the onset of the 'dormant' period. During this period, supersaturation of the solution with respect to calcium hydroxide occurs up to the nucleation of portlandite crystals. Two models have been developed to explain the hydration of cement (Taylor, 1990; 1997; Salhan *et al.*, 2003), which are discussed below:

- The gel model: when cement is in contact with water, a membrane of C-S-H gel is formed on the surface of cement grains, which permits the inward flow of water molecules. An osmotic pressure differential on the membrane causes the membrane to rupture periodically and re-form by extruding concentrated silicate solution. As a result, an excess of portlandite will accumulate on the fluid side of membrane. This model has been demonstrated to be useful in explaining the retardation of setting of cement in the presence of heavy metal waste. The observed retarding effect is due to the formation of insoluble gelatinous hydroxyl compounds of metals in an alkaline medium.
- The crystal model: when cement is in contact with water, calcium silicate minerals dissociate into charged silicate and calcium ions. These charged silicate ions then concentrate as a thin layer on the surface of cement grains to retard the interaction of the cement surface and water. The nucleation and growth of hexagonal crystals of calcium hydroxide fill up the spaces and cavities between the cement grains. Meanwhile, particles of C-S-H precipitate out of water onto the silicate-rich layer on the cement grains and gradually form needles or spines. Eventually needles from different cement grains come into contact with each other to form sheets of tobermorite (Taylor, 1990; 1997).

Skalny and Young (1980) proposed another mechanism for the early stage of hydration. They consider the initial dissolution to be incongruent and that calcium and hydroxyl move rapidly into solution leaving the surface layers rich in silica. In doing so the surface layer adopts a negative zeta potential which strongly adsorbs calcium ions to it as shown in Fig. 1-1. They suggested that this adsorbed layer and its correspondingly low silicate concentration account for the lack of immediate hydration products seen on the surface.

Taylor (1986; 1993) proposed that there is no diffusion of water molecules through either the inner or outer product layers and suggested that hydrogen ions are transferred from one oxygen atom to another until they reach the  $C_3S$  surface. He proposed that a narrow zone exists as an interface where atomic rearrangements convert  $C_3S$  into C-S-H gel. As this zone moves into the hydrating grain, calcium and silicate ions move through the product and into the surrounding liquid to be precipitated ultimately in the outer product layers or (for calcium) as portlandite. Taylor (1993) suggested that the migration of silicon is by a series of movements through the faces of the tetrahedra, from sites initially filled to those initially empty. He similarly proposed this as a mechanism for the change of silicate anion type both during and after C-S-H formation.

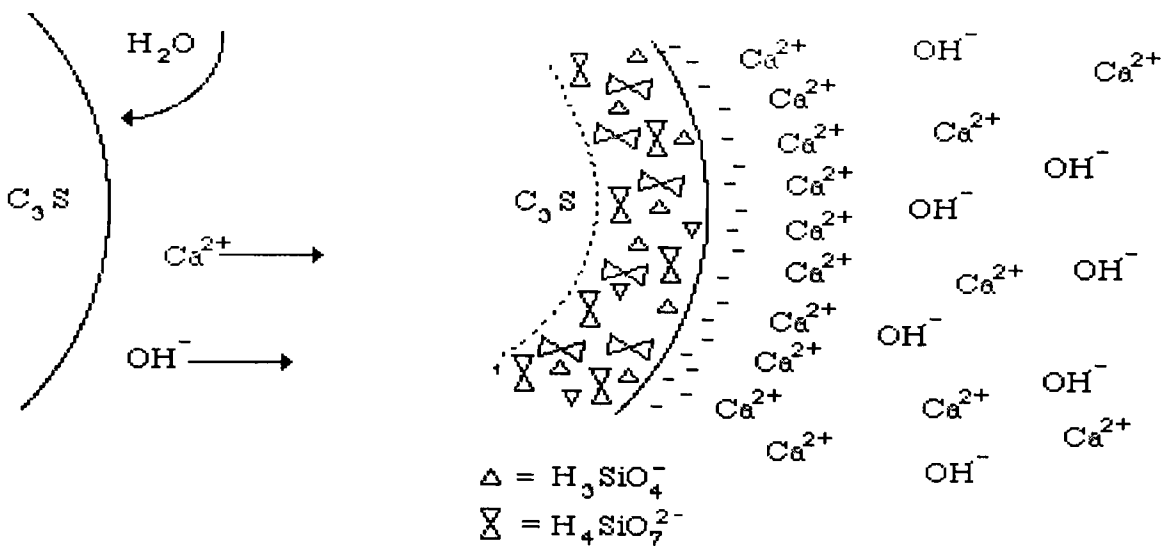


Fig. 1-1. Surface charge layer on hydrating  $C_3S$  grain (After Skalny and Young, 1980)

There is little disagreement, however, that this mineral reacts in at least four stages (Taylor, 1997), as revealed by conduction calorimetry, and that the overall chemistry of hydration can be summarized thus:



In conclusion, the hydration mechanisms for tricalcium silicate are not fully understood but the models proposed so far are not mutually exclusive (Bozkurt *et al.*, 2000).

### 1.3.2 Hydration of dicalcium silicate

This mineral reacts slowly to produce the same reaction products as  $C_3S$  but only results in approximately one third of the portlandite produced. This mineral does make a significant contribution to the late strength if hydration is allowed to continue. Overall the hydration is around twenty times slower than for  $C_3S$  and the reaction can be summarised as:

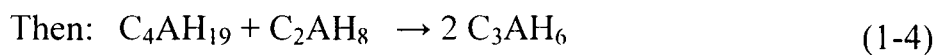


The mechanism of hydration is thought to be similar to that for  $C_3S$  although the morphology of its hydrates is more variable. During fracture,  $C_2S$  hydrate may be completely separated from the anhydrous core, a phenomenon rarely seen in  $C_3S$  (McConnell, 1955, Sun *et al.*, 1999). Relatively little work has been done on the hydration chemistry of  $C_2S$ , which is perhaps not surprising given the relatively minor contribution to early strength afforded by this phase (Chimenos *et al.*, 2000).

### 1.3.3 Hydration of tricalcium aluminate

$C_3A$  is the most reactive towards water and its rapid dominance of the rheological properties of cement paste requires the intergrinding of gypsum to control immediate hydration. The reaction of  $C_3A$  with water gives the initial formation of a gel hydrate which increases in crystallinity to form hexagonal hydrates of the composition  $C_2AH_8$  and  $C_4AH_{19}$ . The  $C_4AH_{19}$  loses bound water at R.H. < 88% to become  $C_4AH_{13}$ . The

hexagonal hydrates ( $C_xAH_y$ ) formed initially are converted to icosahedra of the cubic hydrate  $C_3AH_6$  (hydrogarnet). These hydrates are thought to have a structure consisting of sheets of  $Ca_2Al(OH)_6^+$  with  $Al(OH)_4^-$  or  $OH^-$  in the interlayer region, which balance the net positive charge of the layer, together with water. The hydration can be summarised as follows:



The conversion from the metastable hexagonal form to the stable cubic form is accompanied by a volume change that may have detrimental effects if it occurs in a loaded structure. In cements with a high  $C_3A$  content, the heat of hydration is normally sufficient to ensure conversion occurs quickly (before setting) from nucleated crystals of the cubic  $C_3AH_6$ . This ensures the continued growth of cubic hydrates even at temperatures that would not otherwise ensure complete conversion. In the presence of calcium hydroxide the formation of  $C_4AH_{19}$  (or  $C_4AH_{13}$ ) is favoured, the hydration rate is generally slower and the conversion to  $C_3AH_6$  is inhibited.

The hydration of tricalcium silicate in the presence of sulphate follows a different route. Assuming that an adequate supply of sulphate ions is available, the first hydrate to form is ettringite (AFt) producing a membrane around the hydrating grain which impedes the diffusion of ions from the solution to the un-reacted  $C_3A$ , again resulting in a dormant period. This reaction will continue slowly by the repeated rupture and fresh reaction of this coating until the surrounding solution is depleted in both calcium and sulphate ions. An osmotic mechanism has also been proposed for the end of the dormant period in this mineral. Eventually, the stage is reached where formation of further ettringite is not stoichiometrically favoured and a second, related mineral begins to precipitate as calcium monosulphoaluminate hydrate ('monosulphate' or AFm-sulphate). Associated with this precipitation, is the gradual transformation of ettringite to monosulphate by reaction with the pore solution. Solid solution (particularly of  $Al^{3+}$  for  $Fe^{3+}$ ) is common in these minerals to produce two phases of variable composition. AFt is the phase formed during the hydration of Portland cement at temperatures below about  $40^\circ C$  (the 't' indicates tri-sulphate although substitution for other anions is thought to occur). Morphologically,

this phase is present as prismatic and/or acicular crystals of hexagonal cross section. Similarly the AFm phase is thought to derive from pure monosulphate with partial substitution of  $\text{Al}^{3+}$  for  $\text{Fe}^{3+}$  and sulphate for other ions. These phases dissolve in pure water to re-precipitate as calcium hydroxide, gypsum and alumina gel. Tashiro *et al.* (1977; 1979) have studied the effects of heavy metal oxides such as  $\text{Cr}_2\text{O}_3$ ,  $\text{PbO}$  and  $\text{ZnO}$  as well as  $\text{Cu}(\text{OH})_2$  on the formation of ettringite and properties of cement mortar.

#### **1.3.4 Hydration of calcium aluminoferrite**

Essentially, the hydration products of this mineral are similar to those of  $\text{C}_3\text{A}$ , but forming much more slowly and with substantial substitution of  $\text{Fe}^{3+}$  for  $\text{Al}^{3+}$ . If the unhydrated composition is considered to be  $x\text{C}_2\text{A}(1-x)\text{C}_2\text{F}$ , then reactivity of the phase increases with  $x$  (Tamas *et al.*, 1992). Assuming, as is the case in Portland cement hydration, calcium hydroxide is available, then hexagonal hydrates of the form  $\text{C}_4(\text{A}, \text{F})\text{H}_{13}$  and  $\text{C}_2(\text{A}, \text{F})\text{H}_8$  precipitate. Hydrogarnets are formed when pastes are cured at high temperature. Like  $\text{C}_3\text{A}$ , aluminoferrite reacts with sulphates to produce ettringite and related phases, which ultimately convert to monosulphate. Thus, it is reasonable to expect some competition for the available sulphate to occur between this phase and  $\text{C}_3\text{A}$ . Rogers and Aldridge (1977) examined the hydration of  $\text{C}_2\text{F}$  and reported that this composition yields  $\text{C}_4\text{FH}_{13}$ , initially forming as  $\text{C}_4\text{FH}_{19}$  and converting to  $\text{C}_4\text{FH}_6$  within a day. This product is metastable and ultimately decomposes to calcium hydroxide and haematite.

#### **1.4 Hydration of Portland cement**

Hydration of Portland cement can be considered as essentially those reactions described above with relatively little interaction between the separate hydrating phases. The existence of silico-aluminates in the hydration products of Portland cement, which is evidence for some reaction between the individual phases, has been well documented (Taylor, 1997; Tashiro and Oba, 1979; 1980).

Jennings and Pratt (1978) and Jennings *et al.* (1981) discussed the hydration of  $C_3A$  and  $C_3S$  in the presence of gypsum. They suggested that a membrane with a composition approaching AFt replaces the initial C-S-H as aluminium becomes available in solution and that the chemistry of this membrane changes with time. They proposed that this membrane continues to grow during hydration (as it does not rely on soluble silicates) to envelop adjacent particles thus forming agglomerations and contributing to the 'set' in the early stages of hydration.

The hydration of Portland cement is a sequence of overlapping chemical reactions between clinker compounds, calcium sulphate and water, leading to continuous cement paste stiffening and hardening. As shown by a broad knowledge base derived from extensive cement hydration studies, the formation of hydration products and the development of microstructural features dependent on solution processes, interfacial reactions and, ultimately, solid-state reactions (Macphee *et al.*, 1989). Namely, the hydration of cement proceeds through three successive reactions:

- dissolution of phases,
- precipitation of calcium silicate hydrate (C-S-H), ettringite (AFt) and portlandite,
- interaction of hydration products

On the first contact of cement with water, the phases of cement dissolve and are hydrated immediately. Calcium and silica pass rapidly into solution, due to the small grain size and the metastable nature of cement phases, a supersaturated solution of lime hydrate being initially formed. After a certain time the colloid solution coagulates, forming a typical hydrogel, which causes the cement grains to cohere.

The rate of reaction of cement with water is varied and is dependent on, for example, the phase composition, temperature and presence of accelerators or retarding agents. Impure alite and belite phases present in Portland cement react faster than the pure phases. Hydration of cement was strongly influenced by the additional components such as gypsum, which can alter the setting time and products of hydration. Other factors such as the particle shape and particle size distribution also influence the reactivity of the cement

(Ortego *et al.*, 1989; Ortego and Barroeta, 1991). It has been proposed that hydration of cement can be divided into five stages (Taylor, 1990), as shown in Fig. 1-2:

- initial period (0-15 minutes): including surface wetting, dissolution of cement phases and nucleation and growth of hexagonal crystals of  $\text{Ca}(\text{OH})_2$ , which occur homogeneously from the solution phase, or heterogeneously at a solid-solution interface. Admixtures influence the nucleation of portlandite and ettringite.
- induction period (15min–4 hours): ettringite needle growth. C-S-H gel precipitates out of water onto the silicate-rich layer on the cement grain and gradually form needles or spines.
- acceleration period (4-8 hours): disruption of the hydrate protective layer by transformation of the hydrates or osmotic pressure effect, growth of C-S-H to form sheets and that of portlandite (CH) rapidly. The admixtures may influence the formation and properties (strength, structure, permeability) of the protective hydrate layer (NocunWczelik, 1997).
- deceleration and hardening period (8-24 hours), and
- curing period (1-28 days).

The hydration rate is characterised by the diffusion-controlled reaction. The depth of hydration for the different clinker minerals (in grain sizes between 30-50 micrometers) is 3-15 micrometers after 6 months.

In conclusion, the hydration of Portland cement can be considered as a set of complimentary reactions producing C-S-H gel, Portlandite, ettringite and a solid solution series of calcium aluminoferrite hydrates.

### **1.5 Cement hydration products**

According to Taylor (1990), the proportions of products of hydrated Portland cement approximately are: 20-25%  $\text{Ca}(\text{OH})_2$ , 60-70% C-S-H and 5-15% other phases (including

ettringite and unhydrated grains). Products of cement hydration are summarised in Table 1-1.

### 1.5.1 Portlandite

Portlandite is calcium hydroxide mineral,  $\text{Ca}(\text{OH})_2$ . Although the majority of portlandite is formed during the curing of concrete, it does occur in nature as soft, typically white masses. Occasional crystals may be found.

Portlandite is a bonding agent in cement and concrete and an undesirable phase in concrete, because it precipitates as platelets near aggregates (Oates and Joseph, 1998). The result is a porous paste/aggregate interface that increases concrete permeability and reduces compressive strength. Portlandite is also subject to acid attack and carbonation.

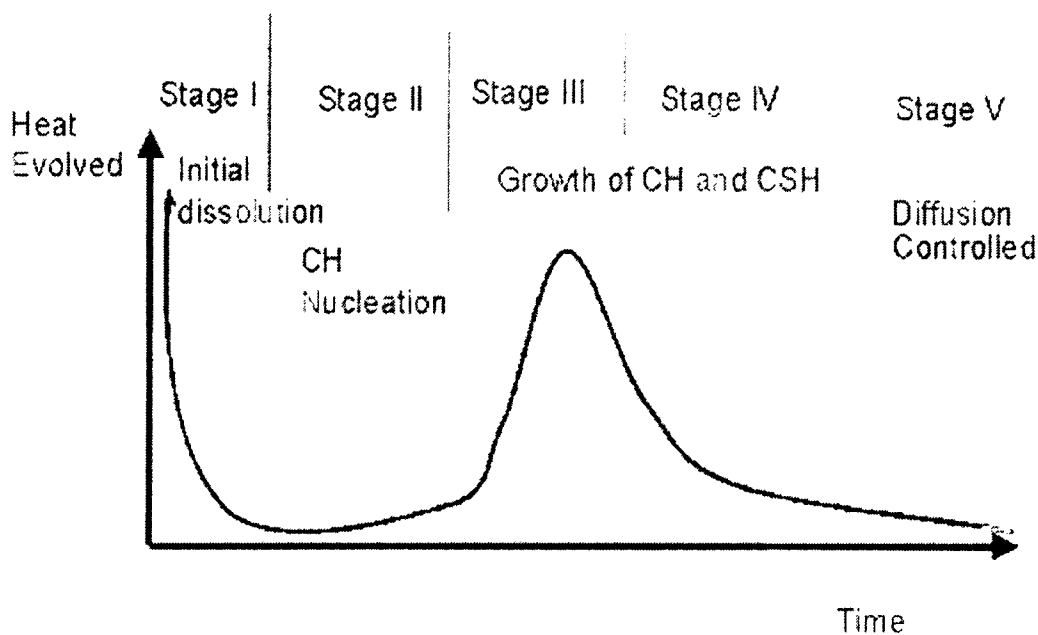


Fig. 1-2. Heat evolution profile from hydrating cement

### 1.5.2 Calcium silicate hydrate (C-S-H) gel

In nature, three kinds of calcium silicate hydrates are tobermorite, jennite and afwillite (Komarneni *et al.*, 1987). Crystalline tobermorite has long chains and cross linked, with included water being structural. 1.4 nm tobermorite ( $\text{C}_5\text{S}_6\text{H}_9$ ) has layer structure, bonding

together by surface forces with occasional strong ionic-covalent bonds linking adjacent particles. Loss of half the structural water allows shrinkage of interlayer space in 1.4 nm tobermorite, to give 1.1nm variety (Viehland *et al.*, 1996; 1997). Jennite ( $C_9S_6H_{11}$ ) has single layer structure with a higher Ca/Si ratio, bonding through solid–solid contacts. The chains of jennite are short and no cross linkages. Xonotlite is similar to tobermorite but with less disorder, in which cross-linkages between adjacent dreierketten make for stronger interlayer bonding. Afwillite is somewhat different from the other phases because the tetrahedra are isolated from one another.

Table 1-1. Hydration products of Portland cement

Component	Products	Hydration water	$\Delta H$ , J/g
$C_3S$	C-S-H, CH	0.24	-517
$C_2S$	C-S-H, CH	0.21	-262
$C_3A$	Hydrogarnet, C-A-H	0.29	-900
$C_4AF$	$C_6AFH_{12}$	0.37	-418
$CaSO_4$	$CaSO_4 \cdot 2H_2O$	0.26	-200
$CaSO_4 \cdot 0.5H_2O$	$CaSO_4 \cdot 2H_2O$	0.19	-104
CaO	CH	0.32	-1166
Portland cement	C-S-H, CH Monosulphate, Ettringite	0.3	-500

The structures of all the calcium silicate hydrates have many features in common. They are characterised by sheet-like structures with  $Ca(OH)_2$  layers, sandwiched by silicates tetrahedra. The silicate tetrahedra form chains. Silicate chains tend to adopt lengths of 2, 5, 8 and so on (tetrahedra termed dimer, pentamer, octamer, *etc*). Further variation is provided by the interlayer spaces, which are occupied by  $Ca^{2+}$  and  $OH^-$  anions and  $H_2O$  molecules, whose presence affect the already weak bonding between adjacent sheets. The mode of stacking provides a further mechanism for differences in structure.

The C-S-H gel is a mixture of poorly crystallised particles with different morphologies and chemical compositions that are not sharply defined by their stoichiometric

composition (Atkins and Macphee, 1991; Atkins *et al.*, 1992). Gel water occupies invariably about 25% of the gel volume (corresponding to about 15% of weight of cement). The C-S-H gel fills in all the capillary space and provides a bond between the original cement grains, which appear to be joined at the contact surfaces. C-S-H gel in the solid paste of Portland cement contains the bulk of micro-porosity. These gel pores give the hydrated paste a high surface area and largely control the sorption properties of cement pastes (Gougar *et al.*, 1996).

The average C/S ratio for C-S-H in Portland cement is 1.75 (Bennett, 1992; Zhang *et al.*, 2000). C-S-H gel may contain the silica, alumina and ferrite oxide, with lime hydrate surrounding a more or less continuous system of irregular gel pores, which may be dry, or partially or completely filled with water (Taylor, 1990; 1993; Andersen *et al.*, 2003).

Richardson and Groves (1993) suggested species detected by X-ray analyses in a substituted C-S-H, such as  $\text{OH}^-$ ,  $\text{SO}_4^{2-}$ , and  $\text{CO}_3^{2-}$ , can be accounted for by considering intimate mixing with other hydration phases of cement. Aluminium, Fe and Mg can also be present in the C-S-H. Some metals are immobilised by sorption or co-precipitation onto C-S-H. Metals such as  $\text{Ni}^{2+}$  and  $\text{Co}^{2+}$  can substitute at the C-S-H surface, probably for  $\text{Ca}^{2+}$ , and the Richardson-Groves model describes the waste immobilisation by C-S-H (Richardson and Groves, 1993; 1997; Richardson, 1999; 2000; Richardson *et al.*, 2002).

Since C-S-H is essentially amorphous, direct determination of the solid structure is not possible and inferences about structure must be made from indirect measurements (Taylor, 1990; Escalante-Garcia *et al.*, 1999; Faucon *et al.*, 1997). Early ideas favoured the concept of a disordered layer structure based primarily on structural analogies with related calcium silicate hydrates as deduced from poorly defined X-ray diffraction patterns. Structural regularity may be, however, almost entirely absent (Taylor, 1997). Furthermore, models based on non-layer structures have been proposed and the matter must be considered to be unresolved (Grutzeck *et al.*, 1999; Harris *et al.*, 2002).

NMR studies show that during hydration (Taylor, 1990; Cong and Kirpatrick, 1996),  $\text{SiO}_4$  groups in the clinker phases change to dimer ( $\text{Si}_2\text{O}_7$ ), some of which eventually react to form larger species collectively termed 'polymer'. This polymer consists of single chains or rings (mostly pentamer and octamer), but not more complex species such as double chain or clusters. The average chain length increases with age of cement, but

dimer still makes up approximately 40% of the chains after 20-30 years (Taylor, 1997; Kirkpatrick, *et al.*, 1997).

According to packing arrangements, there are two types of calcium silicate hydrate (C-S-H) gel: C-S-H(1) (tobermorite-like) and C-S-H(2) (jennite-like).

There are two density forms of C-S-H, namely HD and LD C-S-H, which form as inner product (within original cement grain boundaries) and outer products (in pore space) respectively. The ratio of HD C-S-H and LD C-S-H is influenced by cement compositions, additives, and conditions of hydration and curing. There is no obvious difference in composition between HD C-S-H and LD C-S-H (Jennings, 2000; Jeffrey, 1996; Juenger and Jennings, 2001; Jun *et al.*, 1997). It has reported that there are four types of C-S-H according to their morphology in concrete (Taylor, 1990):

- fibrous (type 1),
- reticular network (type 2),
- equate grain morphology (type 3),
- inner product morphology (type 4).

Type 1 is prominent at early stages of hydration. Type 2 is generally also found in early hydration products, whereas Type 3 and type 4 are both fairly massive and seem to appear only in older pastes.

Together with portlandite, C-S-H provides for a high pH environment and buffering capacity. If portlandite is removed selectively, for example, by carbonation, C-S-H gel will be decalcified and the pH of the cement paste will be affected (Glasser, 1992; Taylor, 1993; Goto *et al.*, 1995).

### **1.5.3 Ettringite and monosulfoaluminate**

The other important products of cement hydration are ettringite (AFt) and monosulfoaluminate (AFm). Ettringite is one of the main components of expansive,

shrinkage-resistant, rapid hardening, high early strength and low energy cements (Gougar *et al.*, 1996). Ettringite appears as a hydrate phase of Portland cement in the first stage of hydration. Moore and Taylor (1968; 1970) observed that the ettringite tends to be in the form of stubby, prismatic crystals closed to the aluminate surface while also forming away from these surfaces. Ettringite will change into monosulfoaluminate after a period of time at high temperature, or when sulphate in the cement is used up in hydration products. The average content of ettringite in modern Portlandite cement may have increased as more sulphate is added in order to control set time of clinkers and to improve early strengths (Glasser, 1997; Famy and Taylor, 2001).

The AFt and AFm phase are chemically and mineralogically complex. Their structure is very sensitive to the cement composition as well as to chemical changes induced by the reaction of cement solids–pore water system with its service environment. Damidot and Glasser (1992; 1993) reviewed the chemistry and mineralogy of ettringite formation. The authors assembled thermodynamic data for relevant solids and calculated equilibrium in the CaO-Al<sub>2</sub>O<sub>3</sub>-SO<sub>3</sub>-H<sub>2</sub>O system and compared with experimental results.

In AFt and AFm, columns of Ca<sub>6</sub>(Al(OH)<sub>6</sub>.24H<sub>2</sub>O are lines of Al(OH)<sub>6</sub><sup>3-</sup> octahedrally bonded with 3Ca<sup>2+</sup> ions. Water molecules complete the co-ordination number of calcium. Sulphates are intercolumnar and can occur in four different positions. Three of these positions are occupied by sulphates and remaining by two water molecules (Moore and Taylor, 1968; 1970). The layer structure of AFt and AFm incorporates variable amounts of water as well as anionic compounds including hydroxide and silicate (Gougar *et al.*, 1996).

An examination of ettringite minerals provides evidence of compositional change at the Ca<sup>2+</sup>, Al<sup>3+</sup>, SO<sub>4</sub><sup>2-</sup> and OH<sup>-</sup> sites. For example, half of the sulfate content of AFm and AFt can be substituted by anions such as OH<sup>-</sup>, Cl<sup>-</sup>, CO<sub>3</sub><sup>2-</sup> and SiO<sub>4</sub><sup>4-</sup>. Aluminium can be replaced by the tetravalent cation (Si<sup>4+</sup>). The maintenance of charge balance is accomplished by the substitutions described even though stoichiometry has been sacrificed (Gougar *et al.*, 1996; Glasser *et al.*, 1999).

#### 1.5.4 Minor phases

All C-A-H phases in cement pastes or concrete are thermodynamically metastable with respect to a mixture of  $C_3AH_6$  and  $AH_3$ , so mixtures with latter two solids are frequently encountered. Hydrogarnet  $C_3AH_6$  (strictly hydrogrossular) forms a solid solution series with grossular ( $C_3AS_3$ ), andradite ( $C_3FS_3$ ) and hydroandradite ( $C_3FH_6$ ) but with miscibility gaps at atmospheric pressure and temperature.

Calcium aluminate hydrates: A range of hexagonal hydrates commonly associated with high alumina cements, but also forming as minor components in Portland cement:  $C_2AH_8$ ,  $C_4AH_{13}$  and  $C_4AH_{19}$

Gehlenite hydrate,  $C_2ASH_8$ , is often found in slag cements. It is believed that hydrated gehlenite is a transitional phase which reacts with calcium hydroxide to produce more hydrogarnet. Earlier work by Sersale (1983) noted that hydrated gehlenite is not present after a year's hydration and only one phase per sample - either hydrogarnet or hydrated gehlenite is observed (Kulik and Kersten, 2001; Kwan *et al.*, 1996).

Anion substitution may partially stabilise C-A-H phases. In the presence of gypsum, C-A-H will react to become AFt or AFm. In the presence of calcium chloride, Kuzel's salt ( $C_3A0.5CaCl_20.5CaSO_4.10H_2O$ ) or Friedel's ( $C_3ACaCl_2.12H_2O$ ) salt may form (Taylor, 1990; Glasser, 1992; 1997; 1999). In the presence of an alkali, some phases such as U-phase ( $C_4A_{0.9}(SO_4)_{1.1}N_{0.5}H_{16}$ ) will form.

Hydrotalcite,  $M_4AH_{10}$ , is the dominant sink for magnesium in cements, although it is a minor phase. It forms sub-hexagonal platelets of very low solubility ( $\sim 10^{-10}$  mol.dm<sup>-3</sup>).

Zeolite P, with the approximate component,  $CaOAl_2O_32SiO_2.4H_2O$ , is similar to natural mineral gismondine. It has been shown to develop spontaneously in appropriate cement at  $>40^\circ C$  (Atkins *et al.*, 1992; Atkins and Bennett, 1992). It is a stable phase and can uptake toxic metals such as U and Pb. Initial curing of cement paste at elevated temperatures will catalyse its formation. Once formed it is predicted to be thermodynamically stable on cooling. The structure of zeolite P or gismondine consists of three-dimensional framework of  $SiO_4$  and  $Al_2O_3$  tetrahedra. The tetrahedra are cross-linked by the sharing of oxygen atoms. The resulting framework comprises eight member

ring channels that pervade the entire mineral structure. Calcium occupies the channel to give charge balance. Water molecules are also accommodated in this channel.

In cement pastes or concrete, Al-hydroxide phases have gibbsite, bayerite, nordstrandite ( $\text{Al}(\text{OH})_3$ ), boehmite ( $\text{AlOOH}$ ) and diaspore  $\alpha\text{-AlOOH}$  (Taylor, 1990; Lea, 1970). Al-sulfates have sabasaluminate  $\text{Al}_4(\text{OH})_{10}(\text{SO}_4)\cdot 5\text{H}_2\text{O}$ , saluminate  $\text{Al}_2(\text{OH})_4(\text{SO}_4)\cdot 7\text{H}_2\text{O}$ , julbanite  $\text{Al}(\text{OH})\text{SO}_4\cdot 5\text{H}_2\text{O}$  and alunogen  $\text{Al}_2(\text{SO}_4)_3\cdot 17\text{H}_2\text{O}$  (Deer *et al.*, 1982).

The structure of gibbsite is closely related to the structure of brucite,  $\text{Mg}(\text{OH})_2$ . The different symmetry of gibbsite and brucite is due to the different way that the layers are stacked (Deer *et al.*, 1982). The basic structure forms stacked sheets of linked octahedrons of aluminium hydroxide. The octahedra are composed of aluminium ions with a +3 charge bonded to six octahedrally coordinated hydroxides with a -1 charge. Each of the hydroxides is bonded to only two aluminium ions. The lack of a charge on the gibbsite sheets means that there is no charge to retain ions between the sheets and act as a "glue" to keep the sheets together (Perkins, 1998). The sheets are only held together by weak residual charge bonds.

### ***1.6 Carbonation of Cement***

Carbonation of cement involves the reaction of the solid hydrated material with the carbon dioxide (as  $\text{H}_2\text{CO}_3$ ,  $\text{HCO}_3^-$  &  $\text{CO}_3^{2-}$ ) to form minerals such as calcium carbonate, aluminium hydroxide and iron hydroxide and gelatinous silica. The carbonation of hydrated cement can be divided into four simple stages (Valls and Vazquez, 2000; Abderlaxig *et al.*, 1999; Nonat, 1997). They are:

- diffusion and hydration of carbon dioxide;
- decomposition or dissolution of cement phases/hydration products and release of calcium and silicate ions;
- formation of calcite and modified silica gel, and
- equilibrium of calcite and pure silica gel.

During carbonation, residual cement grains undergo hydration due to the formation of water, leading to a further gain in strength and further carbonation process under atmospheric conditions (Slegers and Rouxhet, 1976). It is known that carbonation is a rapid reaction and calcium hydroxide on the surface of cement paste is carbonated within seconds. According to Ngala and Page (1997), for less accessible inner phases, the reaction needs a relatively long time to occur, depending on the diffusion of carbon dioxide and water or other aqueous species.

Cement carbonation can be divided into natural carbonation (under atmospheric condition) and accelerated carbonation. Carbon dioxide gas, supercritical CO<sub>2</sub> (SCCO<sub>2</sub>) and carbonates (carbonates of ammonium, sodium and potassium) can be used as carbon source. Carbonation can also occur as the direct result of attack by acidic groundwater or from surface water (Asavapisit *et al.*, 1997; Berger and Banwart, 2000).

### **1.6.1 Atmospheric Carbonation (natural carbonation)**

Atmospheric carbonation or natural carbonation is usually a slow process due to the low concentration of carbon dioxide in the atmosphere. Atmospheric carbonation results in C-S-H decalcification, initially by lowering of its Ca/Si ratio, and ultimately by conversion into a highly porous and hydrous form of silica gel, in addition to portlandite transferring into calcium carbonate (Johannesson and Utgenannt, 2001). Ettringite and other phases will change into calcium carbonate, gypsum and gibbsite during carbonation (Young *et al.*, 1974; Goto *et al.*, 1995).

The carbonation rate is controlled by the diffusion of carbon dioxide, depending on a concentration gradient of carbon dioxide. It has been suggested that the depth of carbonation of cement paste can be predicted using Fick's first law (Goto *et al.*, 1995). Due to the low carbonation rate under normal atmospheric conditions, even after years of atmospheric exposure, the penetration depth of carbonation into a dense material or concrete could be very limited (Papadakis *et al.*, 1989; 1991). Many authors found different models to predict the depth of carbonation of concrete at natural carbonation conditions (Papadakis *et al.*, 1991; Jeffrey, 1996).

### **1.6.2 Accelerated Carbonation (rapid carbonation)**

Rapid carbonation or accelerated carbonation can be achieved by increasing the supply of carbon dioxide, i.e. increasing the concentration or partial pressure of carbon dioxide (Neville 1995; De Ceukelaire, 1993). Accelerated carbonation can provide information about the expected longer-term carbonation of a material (Loo *et al.*, 1994; Papadakis *et al.*, 1991) and simulate deleterious environmental alteration of cement stabilised hazardous wastes (Walton *et al.*, 1995; 1997). In addition, accelerated carbonation has also been used in order to achieve beneficial effects such as increasing strength of concrete (Isoo *et al.*, 2000, Young *et al.*, 1974) and reducing the release of heavy metals in solidified waste (Lange *et al.*, 1996; Sweeney *et al.*, 1998).

### **1.6.3 Mechanisms of carbonation**

There are many concept models for the atmospheric carbonation (natural carbonation) of hydrated cement (Saetta *et al.*, 1993, 1995; Papadakis *et al.*, 1989, 1991). Maries (1992) put forward the reaction scheme involved in carbonation of cement (Table 1-2).

Kinetics studies of the accelerated carbonation procedure by monitoring the volume of gas consumed as a function of time show that the reaction has a short induction period, which corresponds to steps 1-4 in Table 1-2, and then proceeds rapidly (Berger *et al.*, 1972; Bukowski and Berger, 1979). Generally speaking, the surface carbonation of cement and concrete only takes 30 or 40 minutes (Isoo *et al.*, 2000; Goodbrake *et al.*, 1979). Further carbonation reactions continue slowly (Bozkurt *et al.*, 2000; Bonen and Sarkar, 1995).

The presence of water is essential to carbonation (Harrison *et al.*, 1996). The solvation of carbon dioxide is governed by Henry's law, which shows that the rate of dissolution of a gas is proportional to the area of the interface and the relative partial pressures of the gas on either side. The hydration of CO<sub>2</sub>, a process requiring a matter of minutes to effect, is the kinetic control reaction (Stumm and Morgan, 1970; Nugent *et al.*, 1997). The subsequent ionisation of carbonic acid is effectively instantaneous. Once ionised the

carbonate ions can react with calcium ions from the calcium silicate or hydroxide to precipitate calcium carbonate.

The products of carbonation are more voluminous than hydration products or anhydrous clinker of cement (Papadakis *et al.*, 1989). Carbonation causes a reduction in porosity and permeability of concrete, which reduces the diffusion of CO<sub>2</sub> and blocks the further carbonation. Goodbrake *et al.* (1979) have shown that the rate of diffusion of calcium out of the mineral structure limits the formation of calcite. The limited carbonation of aluminosilicates is believed to be caused by the early formation of a surface layer of calcium carbonate which impedes the further dissolution of the mineral. This was discussed by Goto *et al.* (1995), Saetta *et al.* (1995) and Smith *et al.* (1997).

Table 1-2. Reactions for the accelerated carbonation of cement (after Maries, 1992)

Step	Process	Species involved
1	Diffusion	CO <sub>2</sub> in air
2	Permeation	CO <sub>2</sub> in concrete
3	Solvation	CO <sub>2(g)</sub> → CO <sub>2(aq)</sub>
4	Hydration	CO <sub>2(aq)</sub> → H <sub>2</sub> CO <sub>3</sub>
5	Ionisation	H <sub>2</sub> CO <sub>3</sub> ↔ H <sup>+</sup> / HCO <sub>3</sub> <sup>-</sup> / CO <sub>3</sub> <sup>2-</sup>
6	Dissolution	C <sub>3</sub> S, C-S-H
7	Nucleation	CaCO <sub>3</sub> , C-S-H
8	Precipitation	CaCO <sub>3</sub> , C-S-H

## 1.7 Characteristics of cement carbonation products

### 1.7.1 Calcium carbonate

There are no less than three polymorphs of CaCO<sub>3</sub>. Aragonite and vaterite are polymorphs with calcite, meaning they all have the same chemistry, but with different crystal structures and symmetries (Deer, *et al.*, 1982; Taylor, 1990). Aragonite is orthorhombic, vaterite is hexagonal and calcite is trigonal. Aragonite's more compact structure is composed of triangular carbonate ion groups (CO<sub>3</sub>), with a carbon at the centre of the triangle and the three oxygen atoms at each corner. Unlike in calcite, the carbonate ions in aragonite do not lie in a single plane pointing in the same direction.

Instead they lie in two planes that point in opposite directions; destroying the trigonal symmetry (Deer, *et al.*, 1982; Perkins, 1998). Aragonite has an orthorhombic symmetry instead of calcite's "higher" trigonal symmetry. Vaterite has a hexagonal symmetry .

Calcite is one of the most common minerals on the face of the Earth, comprising about 4% by weight of the Earth's crust and is formed in many different geological environments (Perkins, 1998). Calcite can form rocks of considerable mass and constitutes a significant part of all three major rock classification types. It forms oolitic, fossiliferous and massive limestone in sedimentary environments and even serves as a cement of sandstone and shale (Deer, *et al.*, 1982).

Aragonite is a common mineral, but is vastly exceeded by calcite, which is the more stable mineral at most temperatures and pressures and in most environments. It is stable at higher pressures, but not at higher temperatures so that in order to keep aragonite stable with increasing temperature, the pressure must also increase. As aragonite is unstable at normal surface temperatures and pressures, it will over time convert to calcite (Deer, *et al.*, 1982). Vaterite on the other hand is rarely seen in the nature (Perkins, 1998).

### **1.7.2 Silica gel**

Silica gel is an amorphous, porous form of polysilicic acid. It is a coherent, rigid three-dimensional network of contiguous particles of colloidal silica. When the micelles (discrete silicate acid units) collide,  $\equiv\text{SiOH}$  groups on the surface condense to form Si-O-Si, thus growing together because of differences in solubility of silica (Fig. 1-3). The necks joining the micelles increase in diameter until the difference in solubility becomes too small to cause measurable changes. Thus a simplified view of the structure of silica gel is a random three-dimensional network of linked micelles (Iler, 1982).

It is now generally accepted that the surface silicon atoms tend to have a complete tetrahedral configuration and that in an aqueous medium their free valence becomes saturated with hydroxyl groups, forming silanol groups (Iler, 1982). Silanol groups in turn, may condense to form siloxane bridges ( $=\text{Si-O-Si}=\text{}$ ). Therefore, the surface

composition of silica gel is made up of physically adsorbed water, chemically bound water, and silicon dioxide (Fig. 1-4).

The gelling process has been characterised as a colloidal aggregation leading to ramified aggregate morphologies. These parameters influence the formation of bonds between particles by influencing the properties of the particles. For instance a change in pH influences the charge of the particle surface. Charged surfaces repel and consequently the interaction between particles is affected. Similarly, other parameters affect the aggregation process at the molecular level, leading to a complex reaction system that is intrinsically chaotic.

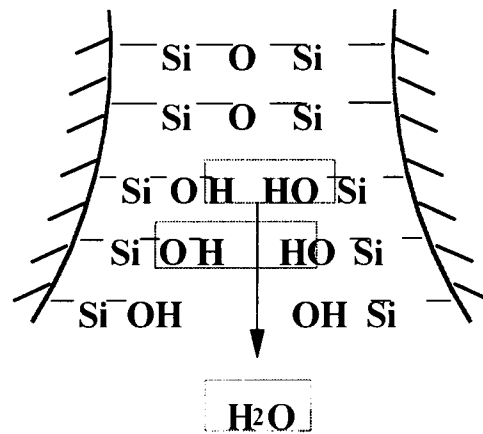


Fig. 1-3. The micelle bridging model of silica gel (after Iler, 1982)

The fresh gel morphology is weak and cannot survive harsh treatment like drying. Capillary forces destroy the vulnerable links between particles and lead to the production of a dense amorphous product rather than a porous gel with a high surface area. After gelation, ageing processes become dominant. These processes can reinforce the weak gel structure by additional bond formation inside the backbone or by addition of silica particles from the solution to the backbone. In the latter case this silica is often generated by dissolving silica from lower density regions of the aggregate, in a process called Ostwald ripening.

## Silica Gel Surface

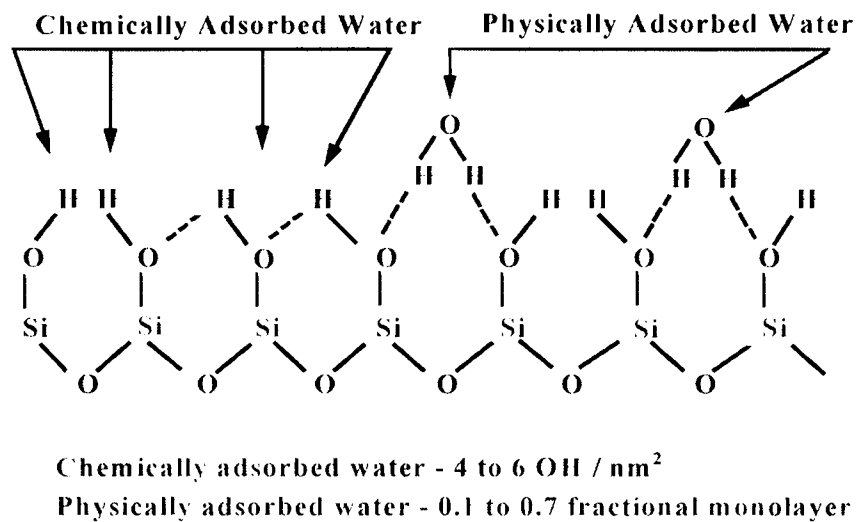


Fig. 1-4. The adsorption of water on the surface of silica gel (after Iler, 1982)

Ageing processes can be studied with small angle scattering of X-rays (SAXS) or neutrons (SANS) (Speiser *et al.*, 2000). Both techniques provide information concerning the mass density distribution of aggregates at different length scales and changes resulting from aggregate growth or ageing. The interpretation of scattering data, however, is not a straightforward process. Computer simulation is a valuable tool in studying the effect of changes in different process parameters on both the aggregation and ageing processes in colloidal systems. The combination of experimental and simulation investigation gives an insight into the effect of process parameters on the chemistry of silica gel.

### 1.8 Chemistry of cement-based solidification/stabilisation

#### 1.8.1 Interface phenomena

As described previously, the overall process of cement hydration or carbonation includes a combination of solution processes, interfacial phenomena and solid-state reaction. The complexity of cement-based s/s process results from the variability of wastes, the combined effects of solution equilibrium and kinetic process coupled with the surface and near-surface of cement phases (Abderlaxig *et al.*, 1999).

Some substances added in cement pastes exhibit an affinity towards the cement particles or cement hydration products by adsorption (electrostatic force, hydrogen-bonding interaction, chemical bonding, and hydrophobic forces). The adsorption of any species onto a surface is dependent on its surface properties, especially the surface charge. In literature (Stumm and Morgan, 1970; Yousuf and Mollah, 1995), three different types of surface charge are recognised:

- Permanent structural charge due to lattice imperfections or site vacancy at the solid surface or isomorphic substitution within the lattice. For example, trivalent cations may substitute for  $\text{Si}^{4+}$  or divalent cations for  $\text{Al}^{3+}$  or  $\text{Ti}^{4+}$  for  $\text{Fe}^{3+}$ .
- Coordinative surface charge due to the chemical reaction involving the surface functional groups. This type of surface charge is dependent on the degree of ionisation and pH.
- Charge due to inner-sphere complexes. The adsorption of specifically adsorbed ions on the surface greatly modifies the surface properties and results in surface charge. For example, the adsorption of some metal ions such as  $\text{Fe}^{3+}$  and  $\text{Mn}^{2+}$  onto the cement particle surface may increase the binding capacity and affinity for toxic metals (Sauman, 1971; Slegers and Rouxhet, 1976).

A number of models for adsorption processes have been developed to clearly understand the intrinsic mechanism involved in s/s processes (Yousuf and Mollah, 1995), for instance, the bi-layer model, the triple layer model and the charge dispersal model. In cement-based s/s systems, the Ca ions from initial hydration form a tightly bound bi-layer with the negatively charged C-S-H surface. And then the heavy metal hydroxyl or superplasticizer anions immediately surround the bi-layer to constitute a tri-layer, which inhibits further hydration (Yousuf and Mollah, 1995). In the charge dispersal model,  $\text{Ca}^{2+}$  ions surround the negatively charged C-S-H surface and preferentially adsorb to form a layer of positive charge; the dispersion of other complex ions surrounds the surface.

Adsorption of some substances on the surface of cement phases will inhibit homogeneous nucleation or heterogeneous nucleation and growth of hydration products and in some cases enhance silicate polymerisation (Smith *et al.*, 1997). Adsorbed compounds will also alter the surface properties of the cement particle and thus its

interaction with the solution as well as with other cement particles. For example, the adsorption of organic substance onto the surface of cement particles induces repulsive interactions between neighbouring particles, increasing dispersion and inhibiting nucleation and growth of the hydration products. Some organic compounds can, however, act as flocculating agents, preventing the dispersion of cement grains (Biddappa *et al.*, 1981). The presence of phenols, coal or lignite can cause problems with setting, curing, and strength of the end products (Abderlaixg *et al.*, 1999).

### 1.8.2 Effects of admixtures

Chemical admixtures, often found by trial and error, have been classified according to the specific function they perform, typically, water reduction, set retardation or acceleration, fluidification, air entrainment, corrosion inhibition, shrinkage control and freeze-thaw resistance (Taylor, 1997). In cement-based s/s, the most important admixtures are gypsum, calcium chloride, sodium carbonate, calcium carbonate and calcium hydroxide. In fact, carbon dioxide and wastes can be referred as special chemical admixtures (Kinniburgh *et al.*, 1976).

Calcium oxide or calcium hydroxide is certainly one of the most important factors determining the thermodynamic, kinetic, morphological and structural features of C-S-H formation. It also has effects on coagulation and rigidification processes. So the calcium hydroxide consuming process such as carbonation or the displacement of solubility equilibrium of portlandite (e. g. changes of temperature, addition of calcium salts or alkalis) might change the characteristics of C-S-H formation (Nonat, 1997).

Other alkali compounds, in general, accelerate the rate of early hydration of Portland cement and give high early compressive strength, although the final strengths are lower than those of the low alkali cement. In the presence of alkaline, some phases such as U-phase ( $C_4A_{0.9}S_{11}N_{0.5}H_{16}$ ) will form and may cause deleterious effects (Kantro, 1975). In particular U-phase formation was found to cause expansion (Taylor, 1997).

Because of the high reactivity of calcium aluminate and the undesirable properties of some products formed (e. g. hexagonal C-A-H), the aluminate hydration reaction is

carried out in the presence of sulphate ions. The latter provide control of the reaction rate through the formation of mixed aluminate sulphate products namely ettringite and monosulfoaluminate. Calcium sulphate used is usually gypsum ( $\text{CaSO}_4 \cdot 2\text{H}_2\text{O}$ ) or its analogues such as bassanite ( $\text{CaSO}_4 \cdot 0.5\text{H}_2\text{O}$ ) and anhydrous phases including anhydrousite  $\text{CaSO}_4$  and its polymorphic forms  $\alpha$ - and  $\gamma$ - $\text{CaSO}_4$ . They are added to the clinker as an admixture used to control the nature and properties of the aluminate hydration products and play a crucial role in cement hydration. Destructive expansion from reaction with sulphates can occur if the latter are present in excessive proportion in cement (Taylor, 1997).

Depending on the applications, accelerative additives such as calcium chloride (Valls and Vazquez, 2000) can be used. Calcium chloride can reduce the initial set from 3 hours to 1 hour and double the 1 day compressive strength, although final strength may be reduced (Taylor, 1990). In the presence of calcium chloride, Kuzel's salt ( $\text{C}_3\text{A}0.5\text{CaCl}_20.5\text{CaSO}_4 \cdot 10\text{H}_2\text{O}$ ), Friedel's salt ( $\text{C}_3\text{ACaCl}_2 \cdot 12\text{H}_2\text{O}$ ) will form (Taylor, 1997).

The effects of some organic substances (e.g. organic acids, polymers) and activated carbon have been studied by Abderlaxig *et al.* (1999). Organic matter may interfere with the bonding of waste materials with cement binders and decrease unconfined compressive strength and short-term or long-term durability. Organics can influence the interactions between anhydrous clinkers and cement hydration products with heavy metal (Rixom and Mailvaganam, 1986; Alunno and Medici, 1995).

Waste/Portland cement blends are found to be naturally prone to either increased levels of atmospheric carbonation, poisoning of normal hydration reactions or both (Conner 1990; Hills *et al.*, 1994). The effects of heavy metals on the hydration of cement will be discussed in Section 1.8.5. McWhinney *et al.* (1990) have studied the solidification of metal ion pollutants, namely Ba, Cr, Pb, Cd and Hg, in cement and noted that high carbonation has a feature common to all doped cements. The extent of carbonate formation was greater for the zinc, cadmium and mercury-doped cements.

Despite considerable research, the mechanisms by which the accelerating and retarding effects of admixtures are achieved are not fully understood (Rixom and Mailvaganam, 1986; Alunno and Medici, 1995; Hills and Pollard, 1997). This is partially due to the

wide choices of experimental conditions available, including varying cement compositions, type and dosage of admixtures used, which are too complicated to predict from composition (Hills *et al.*, 1994). The influence of the same species can be different, depending on the concentration and environment (Hills and Sollars, 1995).

### 1.8.3 Effects of carbonation

The effects of carbonation on the cement-based *s/s* process, there is disagreement in the literature. Carbon dioxide attack is probably the most common form of environmental attack to concrete. Carbonation lowers matrix pH due to the reaction between dissolved CO<sub>2</sub> and the phases in the paste and consumes Ca(OH)<sub>2</sub> and C-S-H. Degradation of such principal binding phase can lead to strength loss. There are, however, reports that accelerated carbonation increases the compressive strength of concrete (Dias, 2000, Lange *et al.*, 1997).

A more immediate concern is the loss of high pH in the vicinity of steel reinforcement. A pH of greater than about 10.5 is thought to preserve a passive film on the steel, protecting it from corrosion. Loss of pH therefore increases the corrosion risk (Berger *et al.*, 1972; Dweck and Buchler, 2000; Dweck *et al.*, 2001; 1003).

As described earlier, the incorporation of metals results in a decrease of the Ca(OH)<sub>2</sub> content of the cement paste and increases its vulnerability to carbonation and resistance against acidic corrosion. This has been discussed by Bonen and Sarkar (1995) and Chen and Wu (2000).

In cement-based *s/s* practices, carbonation has been shown to alter the rate at which some hazardous components leach from industrial wastes and Portland cement solidified/stabilised waste streams (Smith *et al.*, 1997; Walton *et al.*, 1997). Carbonation of cement results in a slightly increased strength and reduced permeability that would be a desirable attribute for a matrix used to confine toxic wastes (Lange *et al.*, 1997). The pore solution in contact with the fully carbonated cement paste will have a pH of 10.4-8.6 (Stumm and Morgan, 1970). Carbonation neutralises the alkaline nature of the

hydrated cement paste and reduces the solubility of some metals, which are very important in protecting the environment.

Sweeney *et al.* (1998) studied the accelerated carbonation of Portland cement and used it to s/s of heavy metal bearing wastes. The leachate Cr concentrations of non-carbonated samples were generally higher than that of their carbonated analogues, although the magnitude of Cr concentrations was the lowest of all the detectable metals. They also reported that Cu leachate concentrations were similar for both carbonated and non-carbonated samples. Carbonated samples demonstrated higher concentrations of Zn at low acid addition and similar concentrations at higher acid additions compared with non-carbonated samples.

Walton *et al.* (1997) conducted dynamic leaching tests using pure water and 0.5N acetic acid, and found that metals such as calcium, cadmium, lead and cobalt had higher leaching rates from carbonated waste forms compared with non-carbonated analogues. They showed that accelerated carbonation of mature cement s/s products could be detrimental. The inference from this work is that with time atmospheric carbonation can degrade the properties of Portland cement-based s/s products placed within the environment.

#### **1.8.4 Factors affecting cement-based s/s processes**

##### **1.8.4.1 Particle size**

Particle size and shape of cement grain affect the properties of solid products, determine whether rate of setting and influence the diffusion of soluble, hazardous constituents from the interior of large particles into the inter-particle space after solidification. The effect of fineness on the rate of hardening of Portland cement is, of course, due to the fact that the larger the surface area available for hydration, the more cement gel will formed at early ages, and the higher the initial strength developed by cement (Glasser, 1992). It should be noted that the fineness of cement is not more important than chemical composition when considering the ultimate strength of Portland cement. Waste particles less than 0.074mm can delay setting and hardening of cement.

#### **1.8.4.2 Free water content**

Free water is chemically unbound water and can react with anhydrous clinkers of cement in the system. The free water content affects the rate and degree of cement hydration and results in a layer of free-standing water on the surface of a solidified product. It also reduces strength and increases permeability of the final product. Evaporation of free water from surface of s/s product will inhibit or stop cement hydration and carbonation.

There is optimum moisture at which carbonation will occur, for example, concrete exposed to rain shows lower carbonation rates than those sheltered from rain (Sauman, 1971). Salhan *et al.* (2003) stated that an environment with 50-70% humidity is the most favourable to carbonation of cement. A water/solid ratio used in the accelerated carbonation process has been found to be very important (Lange *et al.*, 1996).

The solid content of waste affects both the setting and hardening of cement, and physical properties of the products of cement reaction. Glasser (1997) claimed that binders have the limited capacity of fixing wastes.

#### **1.8.4.3 Temperature**

Temperature, curing time and service environment affect the performances of cement and concrete (Escalante-Garcia and Sharp, 1998a; 1998b; 1999). Temperature can affect the hydration or carbonation degree of cement, reaction rates and products of cement. For example, thaumasite forms at 5°C, and AFt converts to AFm above 50°C (Taylor, 1997). Temperature influences the transport of species in concrete and causes expansion or shrinkage of concrete. If the temperature exceeds 60-70°C serious loss of durability can occur (Kiellsen, 1996). This could be partly due to increased micro-cracking, but a deleterious effect known as delayed ettringite formation can also occur.

The role of temperature in the accelerated carbonation process is not clear. Maries (1992) reported that low temperature has retarding effect on the onset of CO<sub>2</sub> uptake. Once initiated, however, total gas uptake and rate appear to be independent of temperature. The carbonation reaction is exothermic and can therefore strongly influence the temperature within a sample. The temperature within a sample undergoing carbonation is also likely

to have other influences upon the progress of the reaction, because the solubility of calcium carbonate decreases at elevated temperatures (Morse and Mackenzie 1990; Dias, 2000) and diffusion rates in water and gases are temperature dependent.

### **1.8.5 Mechanisms of heavy metal immobilisation**

In order to improve and extend solidification/stabilisation process of wastes containing heavy metals, research has been carried out to elucidate the effects on cement reactions and the mechanisms involved in the fixation of heavy metals in cement matrices. According to Thomas *et al.* (1981), metals may undergo hydrolysis, lowering pH of the paste, and retarding the normal hydration of cement (Conner, 1990). The retardation is attributed to the precipitation of insoluble metal colloidal gels on cement grain surfaces (Cartledge *et al.*, 1990). According to Tseng (1988) and Hong and Glasser (2002), possible immobilisation mechanisms of wastes can be through:

- physical and chemical adsorption,
- chemical reaction/chemical incorporation (ion exchange, surface complexation, precipitation, diadochy), and
- micro-encapsulation

#### **1.8.5.1 Sorption**

Sorption can be divided into physical adsorption and chemical adsorption (the word sorption is used as a general term and does not differentiate between chemical and physical processes) (Griffin and Shimp, 1976; Puls and Bohn, 1988). Physical adsorption phenomena occur when contaminants in the solution (the aqueous phase or the pore water) are attracted to the surfaces of particles because of the unsatisfied charges of the particles (Cheng and Bishop, 1992). Chemical adsorption refers to high affinity and specific adsorption, which generally occurs through covalent bonding (Wang and Vipulanandan, 2000). Selective adsorption of heavy metals is termed affinity or selectivity, and this varies with the minerals (Banfill and Saunders, 1986).

Heavy metal immobilisation in cement-based materials can also be through physical containment (Brady and Weil, 1996). Komarneni *et al.* (1988) confirmed that heavy metal wastes can also be physically isolated by portlandite (CH) in the pore space.

### **1.8.5.2 Complexation**

Complexation occurs when a metallic cation reacts with an anion that functions as an inorganic ligand. Metal ions with this ability include the transition metals and alkaline earth metals. Inorganic ligands able to complex with heavy metal ions include  $\text{OH}^-$ ,  $\text{Cl}^-$ ,  $\text{SO}_4^{2-}$ ,  $\text{CO}_3^{2-}$ ,  $\text{PO}_3^{3-}$  and  $\text{CN}^-$ . The complexes formed between inorganic ligands and metal ions are usually weaker than those formed with organic ligands. With increasing pH, the stability of metal complexes are thought to increase because of the increased ionisation of the functional groups and the resulting increased attraction for the cation retained in the complex (Biddappa *et al.*, 1981; Elliott *et al.*, 1986; Benjamin and Leckie, 1981).

### **1.8.5.3 Diodochy**

When one element substitutes for another of similar size and the same charge in a crystal lattice is known as diodochy. An example of this is zinc or magnesium for calcium in calcite. It was suggested that these metal ions could substitute for surface  $\text{Ca}^{2+}$ , but the extent of such substitution could not be evaluated (Komarneni *et al.*, 1988; Kulik and Kersten, 2001). Viehland *et al.* (1993) have shown that almost all calcium in tobermorite ( $\text{C}_5\text{S}_6\text{H}_5$ ) and xonotlite ( $\text{C}_5\text{S}_5\text{H}$ ) (natural crystalline phases of calcium silicate hydrate) can be replaced with heavy metals.

### **1.8.5.4 Precipitation**

In most cases the dominant fixation mechanism for metals in cement-based system is through the chemical precipitation of low solubility species (James *et al.*, 1996). Some metals may co-precipitate with other phases forming solid solutions. Metals can be precipitated as hydroxides, carbonates, sulphates and silicates (Trussel and Spence, 2000;

Hills *et al.*, 1994). Hydroxide precipitation occurs when the pH of a solution of dissolved metal ions is raised to some optimum level for a specific metal. The optimum pH is different for each metal and, for different valence states of a single metal (Hughes, 1976). Carbonate precipitation sometime has an advantage over hydroxide precipitation when metal carbonates are less soluble than corresponding hydroxides (Cocke *et al.*, 1989; Conner and Hoeffner, 1998).

#### **1.8.5.5 Current views on heavy metal incorporation in cement pastes**

As phases associated with heavy metals in cement-based s/s systems are too small (nano-scale) or non-crystalline mixtures of varying composition and water content and very difficult to characterise structurally, there are many contradictory speculations about the fixation mechanisms of heavy metals. The major hypotheses are summarised as follows.

Heavy metals are often described as hydrated metal ions associated with C-S-H gel or silica gel (Conner, 1990). Bonen and Sarkar (1995) indicated, however, that heavy metals are not incorporated into the C-S-H structure, rather the heavy metal compounds are physically encapsulated by C-S-H.

It is suggested that nickel and cadmium are converted into hydroxides, whereas mercury may remain in its original oxide form and be incorporated into matrices of cement concrete (Bonen and Sarkar 1995).

Copper is thought to be presented as  $\text{CuCO}_3$ ,  $\text{Cu}_3(\text{OH})_2(\text{CO}_3)_2$ ,  $\text{Cu}_2(\text{OH})_2\text{CO}_3$  and  $\text{Cu}_4\text{SO}_4(\text{OH})_6$  (Li *et al.*, 2001). Cu can also substitute for Ca in C-S-H or ettringite (Lin *et al.*, 1993; 1997).

$\text{Zn}^{2+}$  formed hydroxides or carbonates and were deposited on calcium silicate minerals (Komarneni *et al.*, 1988; Komilis *et al.*, 1999). Calcium hydroxide can also act with the zinc hydroxide to form  $\text{CaZn}_2(\text{OH})_6 \cdot 2\text{H}_2\text{O}$ , but the mechanism by which this action take place is not clear (Poon *et al.*, 1985; 1986; Jeffrey, 1996).

Richardson (1993) postulated that  $\text{Pb}^{2+}$  is bound with silica in Portland cement pastes. Thomas *et al.* (1981) and Ortego *et al.* (1989) suggested that replacement of silica is

questionable and existence as hydrated metal oxides is more likely. Analyses by thermogravimetric techniques, Fourier transformed infrared spectroscopy (Cocke *et al.*, 1989), X-ray photoelectron spectroscopy and  $^{29}\text{Si}$  nuclear magnetic resonance studies supported this view (Frey *et al.*, 1990).

Chromium can be chemically incorporated into all of the cement hydration products primarily substituting for both calcium and silica in C-S-H or Al in C-A-H and ettringite (Poellmann *et al.*, 1993). Ivey *et al.* (1990) and Lin *et al.* (1997) found that  $\text{Cr}^{3+}$  appeared to substitute for  $\text{Si}^{4+}$  in C-S-H.  $\text{Cr}^{3+}$  could be also bound into the silica matrix itself as  $\text{Cr}(\text{OH})_3 \cdot \text{SiO}_2$  (McWhinney *et al.*, 1990).  $\text{Cr}^{3+}$  associates solely with regions of high calcium content in the form of calcium-chromium crystalline precipitates and that the retention of chromium is not associated directly with C-S-H formation (Omotoso *et al.*, 1998; Abderlaxig *et al.*, 1999). Other phases such as ettringite ( $\text{M}^2_3\text{M}^{3+}(\text{OH})_6 \cdot 12\text{H}_2\text{O} \cdot \text{X}_3 \cdot n\text{H}_2\text{O}$ , have also shown potential for immobilising Cr ions. Substitution can occur for  $\text{Cr}^{3+}$  at  $\text{M}^{3+}$  site and  $\text{CrO}_4^{2-}$  for  $\text{SO}_4^{2-}$  in the  $\text{X}^{2-}$  site (Rinehart *et al.*, 1997). Chromium could also be entrapped in calcium aluminate silicate crystals or the compound  $\text{Ca}_2\text{Cr}_2\text{O}_5 \cdot 6\text{H}_2\text{O}$  could be present according to Valls and Vazquez (2000) and Abderlaxig *et al.* (1999).

### ***1.9 The durability of concrete and cement-based s/s products***

Cement-based solidified and stabilised wastes are vulnerable to the same physical and chemical degradation processes as concrete and other cement-based materials. The vulnerability of treated wastes to chemical and physical attack depends to large extent on factors such as permeability, chemical and mineralogical composition, and microstructure of the cement paste, as well as the cement and waste aggregates (Ortego and Barroeta, 1991). Aggressive solutions attack cement-based materials, causing secondary mineralization and ultimately may decompose concrete or treated waste (Osborne, 1999; Papadakis *et al.*, 1989; 1991; Park and Batchelor, 1999). Cement and concrete exposed to air will suffer attacks from carbon dioxide, sulphate, chloride, water and the degradation products of organic substances, causing expansion, cracking, spalling and strength loss (Malmstrom *et al.*, 2000; Matsuyama and Young, 2000).

The chemical process such as further hydration, carbonation, delayed ettringite formation, AFt--AFm conversion, formation of thaumasite and hydrogarnets and chemical attack would result in the change of porosity and volume and other performance of cement concrete (Taylor, 1990). For an up-to-date review of the durability of s/s waste form, the reader is directed to the draft of Environment Agency Guideline on [www.casst.co.uk](http://www.casst.co.uk). Portland cement based concrete structures and Portland cement- based s/s products suffer from a durability problem summarised as follows, in addition to carbonation.

- Sulphate attack: give rise to expansion via the reaction between monosulphate ( $4\text{CaO}\cdot\text{Al}_2\text{O}_3\cdot\text{SO}_3\cdot 12\text{H}_2\text{O}$ ) and  $\text{SO}_4^{2-}$  in the presence of aqueous  $\text{Ca}^{2+}$  to give ettringite. The conversion from the high-density phase to the low density one can cause expansion and cracking. The cracking opens up new connected porosity that accelerates the transport of sulphate into the cement paste and the deterioration of the paste (Taylor, 2001).
- Alkali-Aggregate Reaction (AAR): Generally, flints, opals, cherts and strained quartz have a high degree of reactivity in concrete. The reaction is driven by the high pH value of pore fluid and the reactive silica, giving rise to a sodium silicate gel product that contains only a small amount of calcium (Wang and Scrivener, 2003; Chimenos *et al.*, 2000). The gel imbibes water causing swelling and this gives rise to expansion cracks in affected concrete and the solidified product.

### ***1.10 Characterisation of cement systems***

There are many test methods applied to the solidified product evaluation. Physical evaluation methods, such as measurements of bulk density, porosity and moisture content, are used to determine the engineering properties and the volume change factor for a solidification process (Isenburg and Moore, 1992). This is an important cost consideration and may potentially be correlated with other properties of environmental concern (Breysse and Gerard, 1997).

Chemical evaluation methods, including leaching, extraction and measurement of acid neutralisation capacity, address the solubility and reactivity of contaminants when exposed to different reagents and environment and effect of solidification/stabilisation (Brindle *et al.*, 1987; Stegemann and Cote, 1990). Chemical evaluation can also give useful information on the binder in stabilising heavy metals (Byfors *et al.*, 1986; Mckinley *et al.*, 2001; Cheeseman *et al.*, 1993).

Leaching tests are widely used as indicators of matrix performance (Hebatpuria and Arafat, 1999a; 1999b). A number of new leaching test procedures have been introduced into Europe, which can found on [www. cassst.co.uk](http://www.cassst.co.uk).

The overall release of soluble species contained in a porous cement block in contact with water is result of a complex and coupled phenomenon. Water transfers in the porous medium up to aqueous saturation. Dissolution of species in the pore water according to local chemical conditions and transport of species in the leaching solution may occur. According to Roy *et al.* (1999), accelerated leaching tests characteristically used are:

- elevated temperatures,
- high specific surface areas perhaps achieved by crushing or grinding the matrix, and
- acidification and renewal of leachant.

The evaluation of the long-term performance of stabilised processes requires modelling, depending on the environmental level of exposure corresponding to the considered scenario. Problems arise initially because of the inadequate database relevant to cement that is necessary to support calculations. Most researchers consider that the mass transfer during leaching can be globally described by an apparent diffusion mechanism (Van Herck and Vandecasteele, 2001; Wang and Huang, 1994). Most models only take into account Fick's diffusion law. More recently, models accounting for more than one effect, for example, diffusion and chemical reaction or mass transfer at the interface have been proposed (Van Herck and Vandecasteele, 2001; Tessier, 1979).

Since the 1970s, thermogravimetry and derivative thermogravimetry have also been used in the characterisation of reaction products of cement phases. Thermogravimetry and

derivative thermogravimetry are more accurate methods than differential thermal analysis for a complete characterisation of the hydrated pastes of Portland cement (Dweck and Buchler, 2000; Dweck *et al.*, 2001; 2003).

The analytical techniques, such as XRD, X-ray photoelectron spectroscopy, SEM/EDS, TEM, Auger electron spectroscopy, ion scattering spectroscopy, Fourier transform infrared and solid state magic angle spinning/nuclear magnetic resonance have been used to characterise the reaction products of cement, leading to better understanding of chemical mechanisms and product structures (Cocke *et al.*, 1989; Lin *et al.*, 1997). The interfering effects of Zn, Cr, Cu on cement based s/s have been extensively studied using techniques such as Fourier transform infrared spectrum (FTIR), magic angle spinning/nuclear magnetic resonance (MAS-NMR), X-ray diffraction (XRD) and scanning electron microscopy (SEM) (Ortego *et al.*, 1989; McWhinney and Cocke, 1993). It is reported that the high spatial resolution of transmission electron microscopy (TEM) coupled with X-ray microanalysis on the nano-scale may make TEM a better tool than SEM for probing the location of metal ions in solidified waste forms (Brough *et al.*, 1996; Gatty *et al.*, 2001). As each characterisation methods with its set of limitations generally can not delineate complex heterogeneous systems, a group of carefully selected characterisation tools is needed (McWhinney *et al.* 1990a; 1990b; Lin *et al.*, 1997; Mollah *et al.*, 1995; 1998).

### ***1.11 Summary***

Cement-based stabilisation and solidification (s/s) technology is an attractive option for the treatment of wastes to reduce their toxicity, facilitate handling prior to landfill disposal and reduce the release of the contaminants into the environment. It has been used for the remediation of contaminated soils and treatment of sewage sludge and industrial wastes, which contain heavy metals in various forms. As cement hydration may be retarded by wastes, accelerated carbonation technology has been adopted to overcome these deleterious waste-binder interactions, which is capable of inducing setting and strength development where cement hydration is significantly retarded.

The reactions of pure cement phases and cements with water and carbon dioxide have been extensively investigated and the considerable divergences of opinion have been discussed. The reaction rates and products vary and depend on, for example, the phase composition, temperature, carbon dioxide concentration, water/solid ratio, particle shape and size, and presence of accelerators or retarding agents.

Most research conducted on solidified and stabilised wastes has been acquired through chemical, physical and leaching testing of treated wastes, typically during treatability studies and technology demonstrations. It is noted that the results of treatability studies and small-scale applications alone are not a guarantee of the effectiveness of s/s in the longer term, particularly as there are no reliable data on performance available. Therefore, understanding the cement-based s/s process at molecular level is very important to the development of this technology.

Heavy metals often alter the course of cement hydration reactions and the properties of concrete and solidified products. They may influence the formation and properties (structure and permeability) of the protective hydrated layer, and further influence the nucleation and growth of reaction products. They may also enter the gel and modify the crystal growth by substitution in the lattice of the hydrates. The possible interaction of wastes or admixtures with cement can be 1) physical and chemical adsorption, 2) chemical reaction/chemical incorporation (ion exchange, surface complexation, precipitation, diadochy) and 3) micro-encapsulation.

As reaction products associated with heavy metals in cement pastes are often nano-scale and non-crystalline mixtures of varying composition and water content, they are very difficult to characterise structurally. The mechanisms of cement reactions, especially in the presence of heavy metals, are not yet fully understood. The literature review relevant to cement hydration, cement carbonation and cement -based s/s technology has highlighted several areas of potential for further investigations, for example, the phase development of cement pastes in the presence of heavy metals, reactions of heavy metals with cement, the dissolution/precipitation of various phases, and interactions of aqueous species with anhydrous cement phases. These are keys to the understanding and improvement of effectiveness of cement -based s/s process. The immobilisation mechanisms of heavy metals in cement pastes are worthy of attention and study further.

## Chapter 2

### Materials, procedures and experimental methods

#### *2.1 Background*

As mentioned in the last chapter, cement-based s/s is applied to the disposal of wastes containing heavy metals and remediation of contaminated soil by heavy metals. Despite extensive research, the interactions of cement and heavy metals are not fully understood.

For the interests of improving the effectiveness of cement-based s/s technology, this work aimed to examine the interactions of cement with heavy metals at a fundamental level. As the reactions among cement phases, water, carbon dioxide and heavy metals are very complex, a variety of experimentation and analytical approaches were employed to examine various systems, including pastes and suspensions of pure cement phases and Portland cement with or without heavy metal ions.

Compounds associated with heavy metals in cement-based s/s systems may be nanoscale and the existence of non-crystalline mixtures of varying composition and water content make it difficult to characterise these materials structurally. The analysis techniques used in this work included differential thermal analysis (DTA) and thermogravimetry (TG), X-ray powder diffraction (XRD), scanning electron microscope (SEM/EDS) and solid state magic angle spinning/nuclear magnetic resonance (MAS/NMR).

This chapter addresses the details of the experimental programmes, materials, principles and instrumentation of characterisation techniques.

#### *2.2 Materials*

In this work, calcium oxide, calcium hydroxide, pure cement phases ( $C_3S$ ,  $C_3A$ ,  $C_4AF$ ,  $C_{12}A_7$  and  $CA$ ), Portland cement, and heavy metal nitrates were chosen as starting materials for various studies. The detailed examinations of literature found that heavy metals such as Cu, Cr, Pb and Zn cause serious problems to environment. These heavy metals have distinctive effects on the hydration and carbonation of cement.

### 2.2.1 Portland cement

Portland cement was supplied by Blue Circle Ltd. England. Calculated Bogue composition of cement is alite 56%, belite 20%, aluminat 9% and ferrite 7%. The oxide compositions of Portland cement are shown in Table 2-1.

Table 2-1. The compositions of Portland cement

Composition	SiO <sub>2</sub>	Fe <sub>2</sub> O <sub>3</sub>	CaO	MgO	Na <sub>2</sub> O	K <sub>2</sub> O	Al <sub>2</sub> O <sub>3</sub>	SO <sub>3</sub>
Content (%)	21.69	3.00	64.2	1.35	0.18	0.65	1.65	3.2

### 2.2.2 Pure cement phases

The pure phases of cement used in this study were made at Imperial College of Science, Technology and Medicine. Pure phases were synthesised from CaCO<sub>3</sub>, SiO<sub>2</sub> and Al<sub>2</sub>O<sub>3</sub> (Aldrich Chemical Company, 98% purity). The pure cement phases were synthesised followed Berger *et al.* (1972) and Aktins *et al.* (1992), summarised in Appendix 1. Calcium oxide, calcium hydroxide, sodium carbonate and sodium silicate (AR grade) were also used for various studies in this work.

### 2.2.3 Chemical reagents

The procedure involved preparing solutions of Cu, Cr, Pb and Zn ions were used from their respective standard reagent grade metal nitrates salts (BCD Ltd, purity 98%). Nitrate salts were chosen because of their high solubility in aqueous solution and because nitrate anion has little effect on the hydration and carbonation of cement (Thomas *et al.*, 1981). Each metal salt, Cu(NO<sub>3</sub>)<sub>2</sub>.3H<sub>2</sub>O, Zn(NO<sub>3</sub>)<sub>2</sub>.6H<sub>2</sub>O, Cr(NO<sub>3</sub>)<sub>3</sub>.9H<sub>2</sub>O and Pb(NO<sub>3</sub>)<sub>2</sub>, was dissolved in de-ionised water at concentrations of 1%, 2.5%, 5% , 10% and 15% w/w (by heavy metal ion weight, assuming ideal stoichiometry).

## 2.3 Experimental procedures

### 2.3.1 Preparation of hydrated pastes

In the preparation of hydrated pastes containing metal salts, 3g of calcium oxide, pure cement phase or Portland cement was mixed with the 10 (w/w) % solution of heavy

metal nitrate at a solid/liquid ratio of 10:4. For the control samples, calcium oxide, cement or pure cement phase was added to de-ionised water at the same solid/water ratio. These samples were kept in the sealed containers for examination at different times by XRD, DTA/TG and NMR techniques.

## **2.3.2 Carbonation experiments**

### **2.3.2.1 Carbonation equipment and conditions**

Carbonation was achieved in a sealed reaction chamber (Fig. 2-1), into which samples were placed under controlled conditions for fixed periods of time. After reaction the chamber was vented and the samples were removed for evaluation.

A comparison of the differing results from previous studies of accelerated carbonation shows that the most suitable reaction condition was a pure CO<sub>2</sub> atmosphere with a pressure of 0.2-0.5MPa. The previous trials (e.g. see Johnson *et al.*, 2001) showed that at a pressure of 0.3MPa, the rate and total consumption of carbon dioxide gas were repeatable for a range of materials. In order to limit the number of variables in the experimental design this value was then fixed throughout the investigative program. The regulator on the carbon dioxide cylinder was used to fix the pressure and this was checked with the gauge on the chamber.

As relative humidity influenced the carbonation process, a saturated sodium chloride solution was used to maintain a fixed value (50%) for this variable. The carbonation reaction is exothermic, and it is unrealistic to fix the temperature within samples when undergoing accelerated carbonation. The temperature in the laboratory remained constant at 17±2°C. The carbonation experiments were carried out in the following way.

The samples were placed into the chamber and the lid was then sealed in place and the chamber pressurised. After purging the reaction vessel of air (three times), the exit valve to the chamber was closed; however, the entry valve remained open to maintain a constant pressure of 0.3MPa as CO<sub>2</sub> as gas was consumed by the carbonation reaction. After the allotted reaction period the chamber was vented and the samples were removed for further investigation. All samples were stored in individual labelled zip-lock plastic bags to prevent contact with the atmosphere and cross contamination.

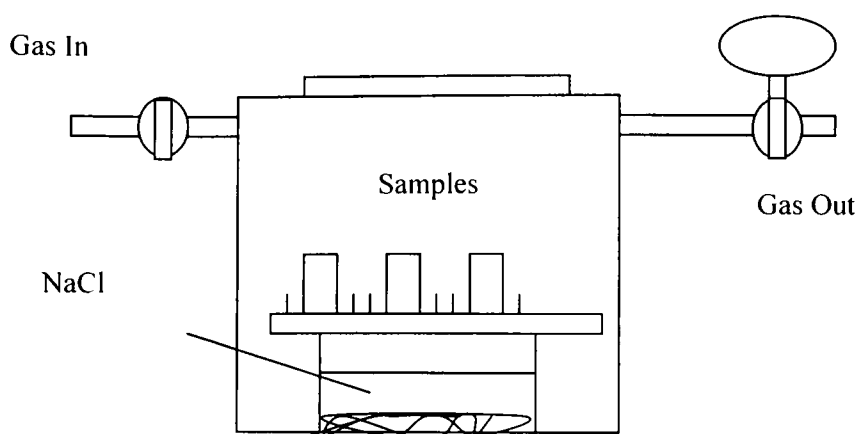


Fig. 2-1. Schematic diagram of the reaction chamber ( $\text{\O}300\text{mm}$ ,  $150\text{mm}$  high, after Johnson *et al.*, 2001)

### 2.3.2.2 Procedure of accelerated carbonation

Accelerated carbonation of cement and pure cement phases involved samples prepared at the same time and under the same conditions as for the hydration studies prior to exposure to  $100\%$   $\text{CO}_2$  for  $30\text{min}$  in the reaction chamber. Once samples were removed they were ground to less than  $0.03\text{mm}$  with a pestle and mortar prior to placement back in the reaction chamber and exposure to  $\text{CO}_2$ . This procedure was repeated 8 cycles to effect full carbonation, which is a finding of this research. The carbonated samples were kept in the sealed containers for examination at different times by XRD, DTA/TG and NMR techniques.

### 2.3.2.3 Carbonation of hydrated cement pastes

One month old hydrated cement pastes were ground to  $<0.03\text{ mm}$  with a pestle and mortar and mixed with water at a solid/liquid (S/L) ratio  $10:2$  prior to exposure to carbon dioxide in carbonation chamber for  $30\text{ minutes}$ . Full carbonation was effected with 5 cycles with the same procedure described above.

### 2.3.3 Suspensions

In the cement pastes, amorphous structure of heavy compounds tends to form, possibly because the nucleation and aggregation occur too fast and species lack sufficient mobility

to undergo proper orientation and alignment before bonding into a structure. As amorphous phases containing heavy metals in cement pastes are very difficult to characterise, in this work, to create the favourable conditions for heavy metal compounds crystallising, the suspensions of calcium oxide, cement and pure cement phases with or without heavy metals were used.

In order to study the hydration of calcium silicate, calcium aluminate phases, ferrite and Portland cement, the pH values of their suspensions with or without heavy metals were measured. Heavy metal nitrate solutions with concentrations of 0% and 5% w/w (metal) were mixed with ground calcium oxide, calcium hydroxide, pure cement phases or Portland cement at a solid/liquid ratio of 1:10. The suspensions were placed in sealed containers and agitated, and the pH was measured (Philips DW9418 pH meter) at regular intervals. The reaction products in all suspensions at different times were examined by XRD and thermal analysis techniques.

#### **2.3.4 Carbonation of suspensions**

In order to investigate the carbonation of calcium oxide, pure cement phases and Portland cement, the pH values of their suspensions with or without heavy metals were measured at different stages of carbonation. The conditions for preparing suspensions for carbonation were the exactly same as those for hydration studies. To effect carbonation, suspensions were placed in the carbonation chamber at 0.3MPa for 40 minute intervals prior to the measurement of pH. This cycle of exposure to CO<sub>2</sub> followed by measuring pH was repeated until the stable pH values were obtained. The reaction products in all suspensions at different times were examined by XRD and thermal analysis techniques.

#### **2.4 X-ray powder diffraction (XRD)**

X-ray powder diffractometry (XRD) is one of the most useful methods for exploring the structure of matter. The specimen is bombarded by a monochromatic, parallel beam of X-rays, and reflects X-rays, which are recorded by a counter. The signals from the counter are analysed by a computer. In principle XRD measurements come down to measuring distances between planes with plane x-ray waves. When Bragg condition:  $n\lambda = 2d \sin(\theta)$  is satisfied, a peak will be measured (Cullity, 1978). XRD is widely used in the

identification of the constituents of mixtures of crystalline phases such as minerals and alloys, as an adjunct to chemical analysis; for measurements of the lattice parameters of crystal structures. X-ray diffraction has been used to examine crystal structure of cements and the products of hydration and carbonation of cement since 1938 (Taylor, 1990).

In this study, a Siemens Kristalloflex-810 X-ray generator and microprocessor controlled D-500 Diffractometer system (Fig. 2-2) using crystal monochromated characteristic  $\text{CuK}(\alpha)$  radiation and LA 100 recorder (40KV, 40mA) were employed to analyse the crystalline compounds formed such as calcium hydrate and calcium carbonate, and to monitor any changes in cement phases such as alite, belite, aluminate and ferrite.

The finely ground samples ( $<50\mu\text{m}$ ) were examined between  $5\text{-}40^\circ 2\theta$  at scanning rate of  $1^\circ 2\theta$  per minute. The diffractograms were obtained with Diffplus and analysed using Bruker/AXS EVA software and were compared with the international powder data file (ICDD-JCPDS) for the purpose of phase identification (International centre for diffraction data, PDF-2 database, 2003).



Fig. 2-2. The XRD equipment used in this work

## ***2.5 Scanning electron microscopy and energy-dispersive X-ray spectrometer***

### **2.5.1 Principle of technique**

Scanning electron microscopy (SEM), accompanied by X-ray analysis, is considered a relatively rapid approach to surface analysis. It is often used to survey surface analytical problems before proceeding to techniques that are more surface-sensitive and more specialised. The SEM images provide useful information on microstructure and its relationship to physical and chemical properties of the matrix.

The scanning electron microscope produces and measures signals resulting from the electron beam/specimen interaction. Electrons are generated by passing a high voltage through a tungsten wire filament at top of microscope and then travel down the main column and are concentrated by series of electromagnetic lenses to form a finely focussed beam. High-resolution images of surface topography, with excellent depth of field are produced using a highly-focused, scanning (primary) electron beam. The primary electrons enter a surface with energy of 0.5-30KeV. The signals from the electron beam/specimen interaction are collected and processed. Common signals collected include secondary electrons, back scattered electrons and characteristic X-rays.

Secondary electrons, which result from the inelastic scattering of the incoming electrons, are for imaging surface topography. The intensity of these secondary electrons is largely governed by the surface topography of the sample. An image of the sample surface can thus be constructed by measuring secondary electron intensity as a function of the position of the scanning primary electron beam.

In addition to low energy secondary electrons, backscattered electrons and X-rays are also generated by primary electron bombardment. Back-scattered electrons (BE), which have been scattered and have higher energy than secondary electrons, are for highlighting compositional differences. The intensity of backscattered electrons can be correlated to the atomic number of the element within the sampling volume. The higher the mean atomic number is, the higher the intensity of its BE signal is. Hence, some qualitative elemental information can be obtained.

The resolution of BE images is lower than secondary electron images, but the back-scattered electron imaging is an ideal technique for distinguishing phases in a microstructure when using flat, polished specimens. Portland cement pastes appear as

contrasting light and dark areas that are related to the chemical composition of features within any field. Images analysis systems can differentiate 256 grey levels ranging from dark to bright depending on the mean atomic number of cement phases, for example, anhydrous cement phases are bright, C-S-H gel is grey, whereas pores are black (Famy and Taylor, 2001; Famy *et al.*, 2002a; 2002b).

It is worth pointing out that the condition of operation for SEM requires a high vacuum and this is known to alter the morphology of some cement hydration products, particular for C-S-H. In addition, salts may be precipitated at surface of specimens as moisture is lost to vacuum. It should therefore be appreciated that the microstructures observed may have been modified.

The analysis of characteristic X-rays emitted from the sample gives more quantitative elemental information. Since cementitious materials are highly complex and inhomogeneous, a number of images are required to adequately characterise them. Scrivener *et al.* (1999) reported that 12 images are needed to get within 95% of accuracy.

### **2.5.2 Instrumentation and sample handling**

In this work, JEOL JSM-840 (Fig. 2-3) and JSM-640 equipped with an energy dispersive X-ray analyser (LINK ANINCA, LINK ISIS 300) was used with an accelerating voltage being 15kV.

Micro-structural observations and EDS microanalyses were made on 6 month-old hydrated or carbonated cement pastes with or without heavy metals. It is not only because other ages of pastes are well documented, for example, 3 days, and 28 days (e.g. Hills, 1992), but also because 6-month old pastes are more stable for the interest of thermodynamic studies.

As cementitious materials are non-conductive, fracture specimens were gold coated for high quality images. For energy disperse X-ray analysis, polished specimens were mounted on stubs using two-part epoxy resin and their edges were coated with a carbon to ensure a good electrical contact. The target area was about 0.001mm diameter and enabled a semi-quantitative analysis to be obtained.



Fig. 2-3. SEM equipment used in this work

In this work more than 80 images were used to ensure a desirable degree of accuracy. The totals are lower than 100%, which is attributed to water and carbon dioxide contents, since hydrogen cannot be detected and carbon was not calculated. Micro-porosity could lower the totals due to the retardation of incident electrons by fields resulting from internal charging on the surfaces of pores. For the convenience of comparison, the most data were normalised. In most cases of this study, the microanalysis results were plotted as atom ratios and not as percentages of individual elements to eliminate the effects of micro porosity, carbon dioxide and water content of C-S-H gel.

The interpretation of the data is not straightforward because most microanalyses are of mixture of many phases (Harrison *et al.*, 1996; Famy *et al.*, 2002a; 2002b). In this study, the microanalysis data were analysed with statistical methods to provide information on the compositions of residual clinkers, products of hydration and carbonation in the cement pastes and heavy metal incorporation.

## **2. 6 Nuclear magnetic resonance (NMR)**

### **2.6.1 Principle of technique**

Nuclear Magnetic Resonance spectroscopy is a powerful and theoretically complex analytical tool (Engelhardt and Michel 1987). The chemical environment of specific nuclei is deduced from information obtained about the nuclei. Subatomic particles

(electrons, protons and neutrons) can be imagined as spinning on their axes. In many atoms (such as  $^{12}\text{C}$ ) these spins are paired against each other, such that the nucleus of the atom has no overall spin. However, in some atoms (such as  $^1\text{H}$  and  $^{13}\text{C}$ ) the nucleus does possess an overall spin.

The overall spin,  $I$ , is important. Quantum mechanics tells us that a nucleus of spin  $I$  will have  $2I + 1$  possible orientations. For example, a nucleus with spin  $1/2$  will have 2 possible orientations. In the absence of an external magnetic field, these orientations are of equal energy. If a magnetic field is applied, then the energy levels split. It is possible to excite these nuclei into the higher level with electromagnetic radiation. The frequency of radiation needed is determined by the difference in energy between the energy levels. If energy is absorbed by the nucleus, then the angle of precession will change. For a nucleus of spin  $1/2$ , absorption of radiation "flips" the magnetic moment so that it opposes the applied field (the higher energy state).

It is important to realise that only a small proportion of "target" nuclei are in the lower energy of state and can absorb radiation. There is the possibility that by exciting these nuclei, the population of the higher and lower energy levels will become equal. If this occurs, then there will be no further absorption of radiation and the spin system is saturated. The possibility of saturation means that we must be aware of the relaxation processes that return nuclei to the lower energy of state. If the relaxation rate is fast, then saturation is reduced. If the relaxation rate is too fast, line-broadening in the resultant NMR spectrum is observed.

The magnetic field at the nucleus is not equal to the applied magnetic field; electrons around the nucleus shield it from the applied field. The difference between the applied magnetic field and the field at the nucleus is termed the nuclear shielding. Consider the s-electrons in a molecule. They have spherical symmetry and circulate in the applied field, producing a magnetic field that opposes the applied field. This means that the applied field strength must be increased for the nucleus to absorb at its transition frequency. This upfield shift is also termed diamagnetic shift. Electrons in p-orbitals have no spherical symmetry. They produce comparatively large magnetic fields at the nucleus, which give a low field shift. This "deshielding" is termed paramagnetic shift.

Chemical shift is defined as nuclear shielding/applied magnetic field. Chemical shift is a function of the nucleus and its environment. It is measured relative to a reference compound. For  $^1\text{H}$  NMR and  $^{29}\text{Si}$ , the reference is usually tetramethylsilane,  $\text{Si}(\text{CH}_3)_4$ .

Nuclear magnetic resonance (NMR) spectroscopy is based upon the measurement of absorption of electromagnetic radiation in the radio-frequency region of roughly 4-600MHz. The excitation pulses are produced by crystal-controlled continuous oscillator and pass into a pulsar switch and power amplifier, and then transmitter coil and receiver coil (sample placed). The signals are digitised and collected in a computer for frequency analysis by a Fourier transform program (Fig. 2-4).

Solid state magic angle spinning/nuclear magnetic resonance (MAS/NMR) can be effective in revealing the structure of calcium silicate gel in the hydration and carbonation of cement. Lippmaa *et al.* (1980; 1982) have shown that the solid state high resolution  $^{29}\text{Si}$  NMR is an efficient method for the structural investigation of solid silicates and aluminosilicates. NMR has also been helpful in gaining an insight into the structure of cement hydration phases and mechanisms of cement-based solidification/stabilisation. It has been successfully applied to the characterisation of Portland cement (Lin *et al.*, 1997; Phair *et al.*, 2004).

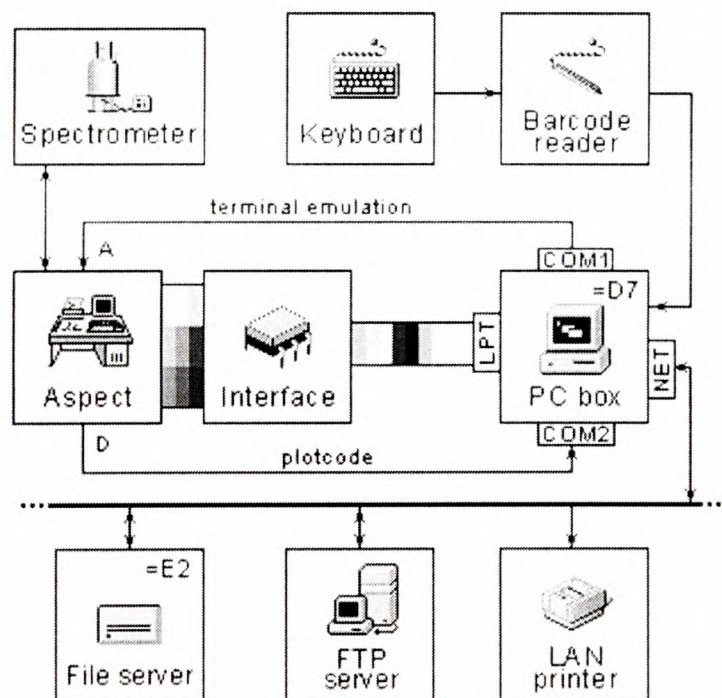


Fig. 2-4. Fourier transform NMR block diagram

The  $^{29}\text{Si}$  chemical shifts display a regular dependence upon the degree of condensation of silica-oxygen tetrahedral. The total range of  $^{29}\text{Si}$  shifts in silicates (about 50ppm) can be divided into well separated ranges for mono-silicates Q0 (-66 to 74ppm from TMS), di-silicates and chain end groups Q1 (-77 to -82 ppm), chain middle groups Q2 (-85 to -89 ppm), chain branching sites Q3 (-90 to -100 ppm) and the three dimensional cross-linked framework Q4 (-103 to -115 ppm). Q0 stands for isolated tetrahedra, i.e. without neighbouring Si atom ( $\text{Si}(\text{OH})_4$ ), Q1 one shared O/OH with neighbouring tetrahedra, Q2 two shared, Q3 cross linking and Q4 totally interlocking framework ( $\text{Si}(\text{SiO})_4$ ).

### 2.6.2 Instrumentation and sample preparation

The curing time of all samples was 1 year after hydration or after accelerated carbonation. To avoid the broad resonance, spinning the sample at the angle of  $54.7^\circ$  to the direction of the spectrometer magnetic field was used to acquire the silicon and aluminium data.

In this work,  $^{29}\text{Si}$  solid state NMR spectra were recorded on a Varian Infinity Plus-300 spectrometer equipped with a 7.1T magnet (Fig. 2-5). The large round cylinder on the left is the liquid helium-cooled magnet. The sample is placed in a small glass tube and dropped into this magnet. The computer screen can be seen just to the right of and partially behind the magnet; the box to the far right houses the source of the radio frequency radiation.

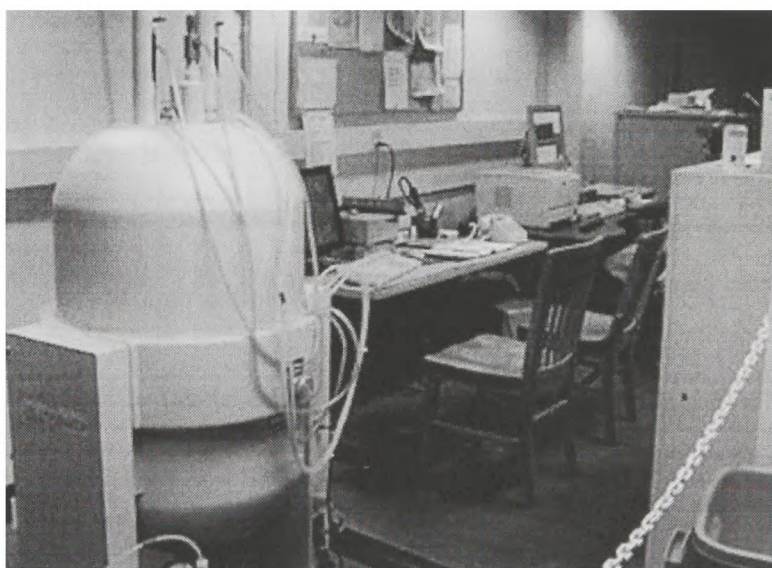


Fig. 2-5. The Varian 300MHz NMR instrument used in this work

The resonance frequency for  $^{29}\text{Si}$  was 59.49 MHz. To narrow the peaks of NMR all samples were spun at 4 KHz. The NMR experiments were operated at relaxation T1 30s pulse with a relaxation delay of 10s for  $\text{C}_3\text{S}$  and at relaxation T1 2s pulse with a relaxation delay of 2s for Portland cement.  $^{29}\text{Si}$  chemical shifts were reported related to tetramethylsilane (TMS).

$^{27}\text{Al}$  solid-state NMR spectra were recorded on a JEOL-JNM ECP 300 FT spectrometer equipped with a 6mm SH30T6/HS solid state probe and a 7.05T magnet in which the resonance frequency for  $^{27}\text{Al}$  was 78.31MHz. Since the  $^{27}\text{Al}$  nucleus is highly sensitive and relaxes quickly and allows spectra to be accumulated in relatively short times,  $^{27}\text{Al}$  spectra were acquired with short (1 $\mu\text{s}$ ) pulses and a relaxation delay of 2s in order to minimise intensity distortion arising from quadrupolar effects. Aluminium NMR data were reported to the nearest 1ppm, and referenced with respect to aluminium nitrate. Samples were packed into 6mm o. d. zirconium oxide rotors and spinning speed was 6KHz to narrow the NMR peaks.

## **2.7 Thermal analysis**

Thermal analysis is made up of various techniques for studying the thermal behaviour of materials. When a material is heated or cooled, its structure and chemical composition undergo changes: fusion, melting, crystallization, oxidation, decomposition, reaction, transition, expansion and sintering. To measure these transformations the variation in different parameters is followed up as a function of the temperature.

Thermal analyses include a group of techniques, in which a property of the sample is monitored against time or temperature, while the temperature of the sample in a specified atmosphere is programmed. The programme may involve heating or cooling at a fixed rate of temperature change, or holding the temperature constant, or any sequence of these (Dweck and Buchler, 2000; Dweck *et al.*, 2001; 2003).

### **2.7.1 Differential thermal analysis (DTA)**

Differential thermal analysis is a technique measuring the difference in temperature between a sample and a reference (a thermally inert material) as a function of the time or the temperature, when they undergo temperature scanning in a controlled atmosphere.

The DTA method enables any transformation to be detected for all the categories of materials. Differential thermal measurements have been used for studies of thermal behaviour of inorganic substances such as silicates, ferrite, oxides and glasses. Information is provided about such processes as fusion, adsorption, absorption, dehydration, crystallisation, vaporisation, polymerisation and solid chemical reaction.

According to Taylor (1997), three major endothermic reactions occur during the heating of the cementitious materials: release of the evaporable and part of the adsorbed water at 110°C approximately; and portlandite dehydration between 420-500°C and decomposition of the carbonate phases at 600-850°C.

### **2.7.2 Thermogravimetry (TG)**

Thermogravimetry is a technique measuring the variation in mass of a sample when it undergoes temperature scanning in a controlled atmosphere. This variation in mass can be either a loss of mass (vapour emission) or a gain of mass (gas fixation). Thermogravimetric methods are largely limited to studies of the decomposition, oxidation, vaporisation and desorption from the sample.

### **2.7.3 Instrumentation and sample preparation**

High-temperature simultaneous thermal analysis (STA) techniques comprise both differential thermal analysis (DTA) and thermogravimetry (TG). In this work, a Stanton Redcroft STA 780 Simultaneous Thermal Analyser was used to carry out DTA/TG analyses. It was designed to give simultaneous thermogravimetric (TG) records (i.e. weight versus temperature) and differential thermal analysis (DTA) curves (i.e.  $\Delta T$ -t curves, where  $\Delta T$  is the temperature difference between the sample and reference material alumina). The instrument consists of: 1) a sensitive analytical balance, 2) a furnace, 3) a purge gas system for providing an inert atmosphere, and 4) a microcomputer for instrument control and data acquisition and display.

The Stanton Redcroft STA operates in a manner similar to a differential scanning calorimeter (DSC). Two sample crucibles are heated or cooled at a precisely controlled rate in a controlled environment. One crucible contains a standard with a known thermal response; the unknown is placed in the second crucible. Differences in the thermal

behaviour of the two materials, caused by differences in specific heat, occurrence of an exothermic or endothermic reaction and a phase change, result in a temperature difference between the two crucibles.

Temperature differences, measured with a Pt vs. Pt-10Rh differential thermocouple, permit properties of the unknown to be determined relative to that of the standard. Simultaneously, any change in mass of the specimen during a heating cycle can be measured with a micro-balance as a function of temperature.

The control thermocouple out of Pt-Pt/Rh with a 20% Rh-Pt wire diameter 0.1mm was used. The tip of thermocouple was accurately positioned against the alumina tube and winding of furnace.

Samples (20 mg) were ground with an agate mortar and pestle to less than 50 microns and loosely packed in the crucible, which is 5.8mm in diameter and 4 mm high and made from rhodium-platinum (Pt<sub>87</sub>-Ph<sub>13</sub>). Samples were examined at a heating rate of 10°C/min under flowing nitrogen (40cm<sup>3</sup>/min) from 20°C to 1100°C for C<sub>3</sub>S samples or 30-900°C for other samples.

The calcium hydroxide and calcium carbonate contents were determined from the following equation:

$$CH(\%) = WL_{CH}(\%) MW_{CH} / MW_H$$

$$CC(\%) = WL_{CC}(\%) MW_{CC} / MW_C$$

Where CH(%) and CC(%) are the content of Ca(OH)<sub>2</sub> and CaCO<sub>3</sub>, WL<sub>CH</sub>(%) and WL<sub>CC</sub>(%) are the weight loss occurred during the decomposition of portlandite and calcium carbonate, MW<sub>CH</sub>, MW<sub>H</sub>, MW<sub>C</sub> and MW<sub>CC</sub> are the molar weight of portlandite, water, carbon dioxide and calcium carbonate. The mass loss percentages of pure calcium hydroxide and calcite are 24% and 44%, respectively.

## **2.8 Summary**

The materials under examination included calcium oxide, calcium hydroxide, C<sub>3</sub>S, C<sub>3</sub>A, C<sub>4</sub>AF, C<sub>12</sub>A<sub>7</sub> and CA, and Portland cement mixed with solutions of heavy metal nitrates. As the reaction products of cement in the presence of heavy metals are difficult to characterise and each analytical technique has its pros and cons for such complex

systems, analytical techniques should be used in a combined manner. This chapter presents the information on various experimental systems (pastes and suspensions) and a group of carefully selected characterisation tools.

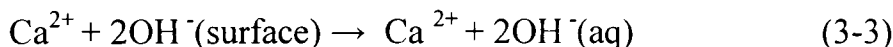
## Chapter 3

### Interactions of calcium oxide or calcium hydroxide with heavy metals in pastes and suspensions

#### 3.1 Background

Calcium oxide (CaO) and calcium hydroxide (Ca(OH)<sub>2</sub>) are relatively simple cementitious materials in comparison to Portland cement and pozzolanic materials. They are widely used in wastewater treatments as precipitants or coagulants. In addition, calcium oxide or calcium hydroxide is used in the modification and stabilisation of clay soils to yield a product with more desirable geotechnical properties than the original clay (Holt and Freer, 1996). In these applications the interaction of calcium oxide and heavy metals is often encountered, but the exact interaction mechanism is still unresolved, despite extensive studies.

As for the hydration mechanism, Giles *et al.* (1993) reported that, from a kinetic standpoint, hydration of CaO in water or caustic solutions proceeds according to:



From the above equations, it can be seen that hydroxide ions have a retarding effect on CaO hydration due to the common ion effect.

It is recognised that the slaking of calcium oxide and the dissolution of calcium hydroxide are both controlled by diffusion of calcium or hydroxide ions away from the calcium surface (Ritchie and Xu, 1990, Giles *et al.*, 1993). The diffusion of other ions in the solution towards the surface of calcium oxide is also found to influence the slaking process of calcium oxide. For example, the reaction of calcium oxide with aluminium ions is initially controlled by diffusion of aluminium ions to the calcium oxide surface,

and the calcium oxide is coated with a film of calcium aluminates before it is consumed, blocking further reactions (Xu *et al.*, 1997; 1998).

Impurities or admixtures influence the slaking process including slaking rate, and polymorphism, habit, morphology and particle size of hydration products. For example, slaking of CaO in the presence of Na<sub>2</sub>SO<sub>4</sub> gives Ca(OH)<sub>2</sub> crystals as hexagonal plates with a size of 5-20 microns, while slaking in the presence of NaCl or NaOH gives Ca(OH)<sub>2</sub> crystals with a size of 2-5 microns, which is only slightly larger than the size of the crystals formed in the control condition, i.e. in the absence of admixtures (Ritchie and Xu, 1990; Giles *et al.*, 1993).

The hydration temperature of calcium oxide can affect the morphology, solubility and specific surface area of Ca(OH)<sub>2</sub>. The surface specific area increases with an increase in the slaking temperature (Glasson, 1961). Solubility of calcium oxide or calcium hydroxide decreases with increasing temperature. These properties are important to the precipitation and sorption of heavy metals.

Boynton (1980) observed a doubling rate of CaO slaking in the presence of 1-3% chloride, while the presence of 0.1-3% sulphates or carbonates decreases the CaO hydration rate. Xu *et al.* (1998) examined the slaking of CaO in solutions containing various concentrations of Na<sub>2</sub>CO<sub>3</sub>. Calcium oxide hydration proceeds rapidly at a low Na<sub>2</sub>CO<sub>3</sub> solution (1g/l). However, the slaking rate drops off sharply at higher Na<sub>2</sub>CO<sub>3</sub> concentrations (5-11g/l), possibly due to the formation of a protective CaCO<sub>3</sub> coat, as dissolved calcium ions react with CO<sub>3</sub><sup>2-</sup> and precipitate on the Ca(OH)<sub>2</sub>/CaO surface. The retarding effect of CO<sub>3</sub><sup>2-</sup> on the CaO slaking may also be due to the presence of a calcium carbonate coating on the CaO particles.

The carbonation product of calcium oxide or calcium hydroxide is calcium carbonate. As mentioned in Chapter 1, the polymorphs of calcium carbonate include calcite, aragonite (orthorhombic) and vaterite (hexagonal). Polymorphs of calcium carbonate are determined by the crystallisation conditions such as the supersaturation, temperature, reagent concentrations, pH values and residence time in a reactor (Kitamura *et al.*, 2002).

The crystallisation kinetics and processes of calcium carbonate, including crystal nucleation and growth, were studied due to extensive industrial interests by Kitamura *et*

*al.* (2002) and Kang *et al.* (2003). The crystal growth of calcium carbonate is controlled by a second-order law or power law, in which a surface-integration is the rate-limiting step. Kitamura *et al.* (2002) and Kang *et al.* (2003) found that a rhombohedral crystal of calcium carbonate is favoured when saturation number (SN,  $IAP/K_{sp}$ , IAP represents Ion Activity Product) is slightly above 1, while a spindle-like crystal is predominantly produced when  $1 < SN < 5$ , and a needle-like crystal appeared when  $SN > 6$ .

This chapter examines the hydration of calcium oxide in the presence or absence of heavy metals. The interactions of calcium oxide and heavy metals, as well as reaction products in pastes and suspensions, were characterised by XRD, DTA/TG techniques. The use of calcium hydroxide is aimed to simplify the interpretation of experimental results.

This chapter also describes the effects of Cr, Cu, Pb and Zn on the carbonation of calcium oxide or calcium hydroxide. The carbonation experiments were conducted with pastes and suspensions of calcium oxide or calcium hydroxide doped with heavy metals. This study focuses on the characterisation of compounds associated with heavy metals and the conversion of calcium carbonate polymorphs.

## ***3.2 Experimental***

### **3.2.1 Materials**

Calcium oxide, calcium hydroxide and nitrate salts of copper, lead, zinc and chromium were A. R. chemicals (Aldrich Chemical Company or BCD Ltd, 98% purity).

### **3.2.2 Methods**

#### **3.2.2.1 Hydration**

In the preparation of hydrated pastes, 3g of calcium oxide or calcium hydroxide was mixed with the 10 % w/w solutions of heavy metal nitrates or de-ionised water at a solid/liquid ratio of 10:4. These samples were kept in the sealed containers for examination at 1 day, 2 weeks, 1 month and 3 months of age.

### **3.2.2.2 Accelerated carbonation**

Fresh pastes of calcium oxide were prepared under the same conditions as hydrated pastes and placed in a carbonation chamber and exposed to 100% CO<sub>2</sub> (constant pressure 0.3MPa). The carbonation-grinding cycle (see Chapter 2) was repeated up to 8 times at the laboratory ambient temperature of 17°C. Following carbonation, the samples were placed in a carbon dioxide bag until examination at the same ages as hydrated pastes. The pastes of calcium hydroxide were prepared, carbonated and examined in the same conditions and procedure as above.

### **3.2.2.3 Suspension studies**

Suspensions of calcium hydroxide used under this study were prepared using calcium oxide and calcium hydroxide with 0% or 5% heavy metal solutions at a solid/liquid ratio of 1:10. Reaction products were examined at 2 weeks, 1 month and 3 months after hydration or carbonation (see chapter 2).

### **3.2.3 X-ray powder diffraction (XRD)**

A Siemens D500 diffractometer and Kristalloflex 810 generator (CuK-alpha radiation, 40KV, 40mA) were used to identify the crystalline products present in the pastes or suspensions both before and after carbonation. The finely ground samples (<30µm) were examined between 5-40 degrees 2θ at a scanning rate of 1° 2θ per minute. The diffractograms were obtained with Diffplus and analysed using Bruker/AXS EVA software.

### **3.2.4 Thermal analysis (DTA/TG)**

In this work, a Stanton Redcroft STA 780 Simultaneous Thermal Analyser was used to conduct DTA/TG analyses. Samples (20 mg) were ground with agate mortar and pestle to less than 50 microns and were packed in the crucible, which is 5.8mm diameter and 4 mm

high and made from rhodium-platinum ( $\text{Pt}_{87}\text{-Rh}_{13}$ ). Samples were examined at a heating rate of  $10^\circ\text{C}/\text{min}$  under flowing nitrogen ( $40\text{cm}^3/\text{min}$ ) from  $30\text{-}900^\circ\text{C}$ .

### **3.3 Results and discussion**

#### **3.3.1 Crystalline phases in hydrated pastes**

In the one month old hydrated pastes of calcium oxide doped with heavy metals (Cr, Cu, Pb, Zn), phases such as portlandite,  $\text{Pb}(\text{OH})_2$  and double hydroxide of calcium and copper ( $2\text{Ca}(\text{OH})_2\cdot 4\text{Cu}(\text{OH})_2\cdot \text{H}_2\text{O}$ ), were detected by powder X-ray diffraction, as shown in Fig.3-1. Although the samples were sealed in the screw top bottles, a noticeable amount of carbonation still occurred. As a result, a small amount of calcite was detectable by XRD. It is worthy to mention that the diffractograms of calcium hydroxide pastes with or without heavy metal show almost the same patterns as hydrated calcium oxide pastes.

#### **3.3.2 Crystalline phases in carbonated pastes**

In the carbonated pastes of calcium oxide with heavy metals, at one month, only calcite was detected by XRD (Fig. 3-2). It is noted, however, that in the control sample, portlandite was detectable. Therefore, heavy metals appeared to promote the accelerated carbonation of calcium oxide. The acceleration effect could be attributed to the lower pH resulting from heavy metal ion hydrolysis or be caused by heavy metal adsorption on the surface of calcium oxide, which changed the surface properties such as solubility of surface reaction products and favoured the carbonation reactions of calcium oxide.

In the Cu -doped carbonated paste of calcium oxide, vaterite was detectable, differing from other pastes. Copper clearly influenced the conversion of  $\text{CaCO}_3$  polymorphs.

Compared the diffractograms of accelerated carbonated pastes of calcium oxide ( $\text{CaO}$ ) with those of accelerated carbonated pastes of calcium hydroxide ( $\text{Ca}(\text{OH})_2$ ), there were no notable differences.

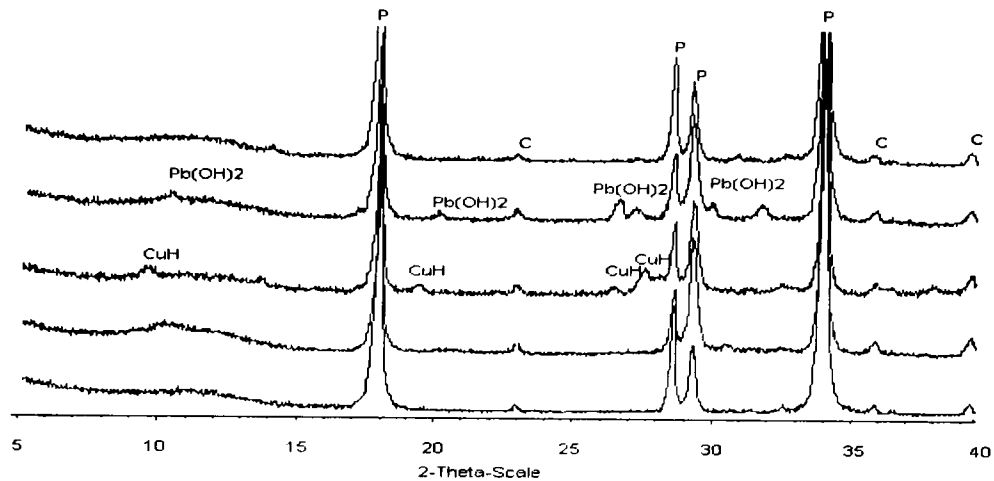


Fig. 3-1. Diffractograms of hydrated calcium oxide pastes aged one month (From bottom to top are control, Cr, Cu, Pb and Zn -doped pastes, Legend: C = calcite, P = portlandite, CuH =  $2\text{Ca}(\text{OH})_2 \cdot 4\text{Cu}(\text{OH})_2 \cdot \text{H}_2\text{O}$ )

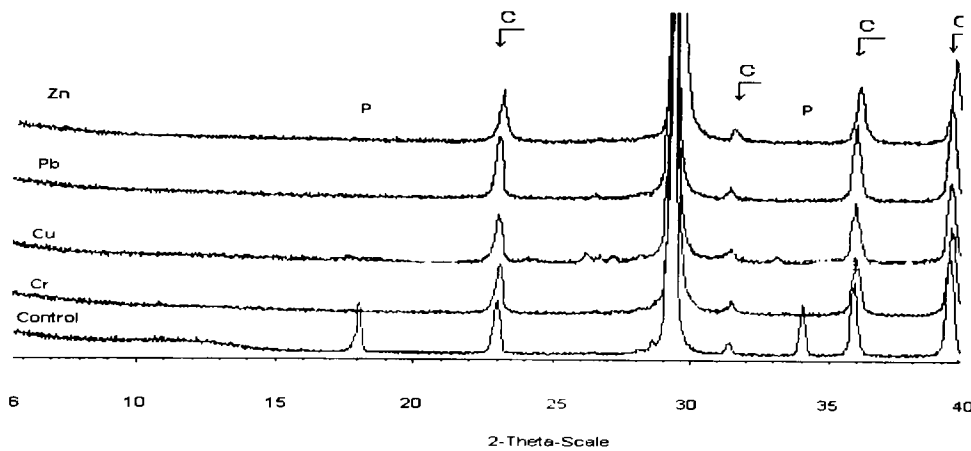


Fig. 3-2. Diffractograms of carbonated calcium oxide pastes aged one month (From bottom to top are control, Cr, Cu, Pb and Zn -doped pastes, Legend: C = calcite, P = portlandite)

### 3.3.3 Phase development in calcium oxide or calcium hydroxide suspensions

According to crystallisation theory, any crystallisation process can be considered to comprise three basic steps: 1) preparation of supersaturation, 2) formation of crystal nuclei, and 3) growth and agglomeration of the crystal (Mullin, 1972). Ideally,

crystallisation would consist of a strictly controlled step-wise procedure. In fact, the nucleation and growth of crystals occur simultaneously in solution. During ageing, processes such as agglomeration and Ostwald ripening occur.

Estimated nucleation times at different supersaturation numbers (IAP/K<sub>sp</sub>) are presented in Table 3-1, according to Mullin (1972). In the calcium oxide or calcium hydroxide pastes containing heavy metals, amorphous structures of heavy metal compounds tend to form, possibly because the nucleation and aggregation occur quickly due to very high supersaturation, and heavy metals have insufficient mobility or time to undergo proper orientation and alignment. In order to create a favourable environment for the crystallisation of heavy metal compounds, the suspensions in the presence of heavy metals were used and examined with different reaction times.

Table3-1. Nucleation time with supersaturation number (after Mullin, 1972)

Supersaturation number	Nucleation time
1.0	$\infty$
2.0	$10^{62}$ year
3.0	$10^3$ year
4.0	0.1s
5.0	$10^{-13}$ s

### 3.3.3.1 Calcium hydroxide suspensions

#### Hydration

The crystalline phases of calcium hydroxide suspensions with or without heavy metals at an age of 2 weeks are shown in Fig. 3-3. It was found that there was no apparent difference between diffractograms of the various samples at different ages (1 day to 3 months). All crystalline phases (Table 3-2) formed in the suspensions were very stable. However, Yousuf *et al.* (1995) reported that  $\text{CaZn}_2(\text{OH})_6 \cdot 2\text{H}_2\text{O}$  only persisted two weeks, as they failed to find the evidence of  $\text{CaZn}_2(\text{OH})_6 \cdot 2\text{H}_2\text{O}$  in the cement pastes containing zinc.

## Accelerated carbonation

The diffractograms of carbonated suspensions of calcium hydroxide with heavy metals at the age of 1 day are shown in Fig. 3-4. It is noted that heavy metals promoted effects the carbonation of calcium hydroxide, according to the peak intensities of portlandite at  $18^\circ$ , and  $34^\circ 2\theta$ , and calcite (main peak at  $29.5^\circ 2\theta$ ). With increasing time, the heavy metal compounds, including double hydroxides and  $\text{PbCO}_3$  disappeared (see Table 3-3), indicating that:

- The double hydroxides of heavy metal and calcium were not very stable in the lower pH solution due to carbonation.
- Calcium carbonate formed in the carbonation process had a very strong binding capacity for heavy metals.

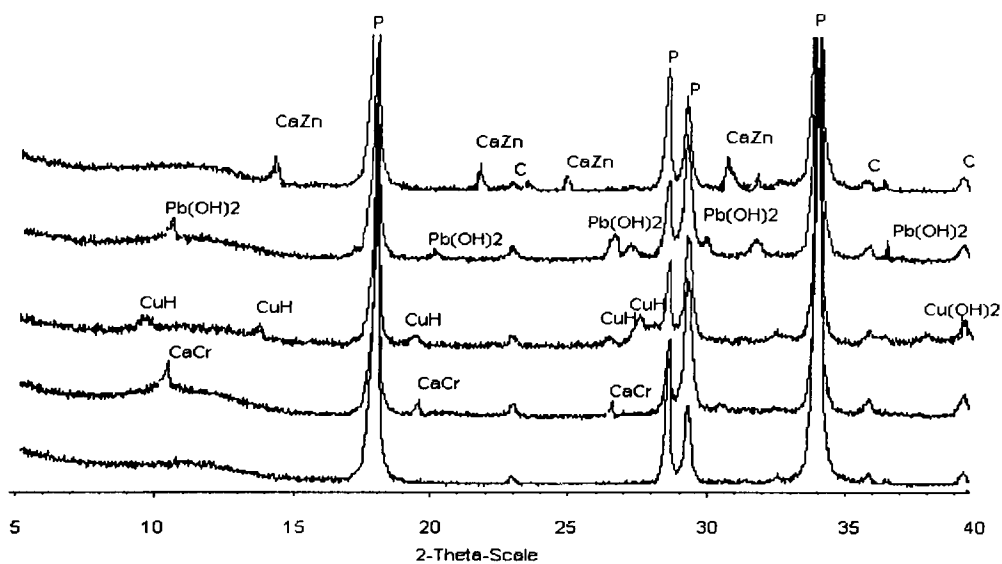


Fig. 3-3. Diffractograms of calcium hydroxide suspensions at the age of 14 days (From bottom to top are control, Cr, Cu, Pb and Zn -doped suspensions, Legend: C = calcite, P = portlandite,  $\text{CuH} = 2\text{Ca}(\text{OH})_2\text{Cu}(\text{OH})_2 \cdot \text{H}_2\text{O}$ ,  $\text{CaZn} = \text{CaZn}_2(\text{OH})_6 \cdot 2\text{H}_2\text{O}$ ,  $\text{CaCr} = \text{Ca}_2\text{Cr}(\text{OH})_7 \cdot 3\text{H}_2\text{O}$ )

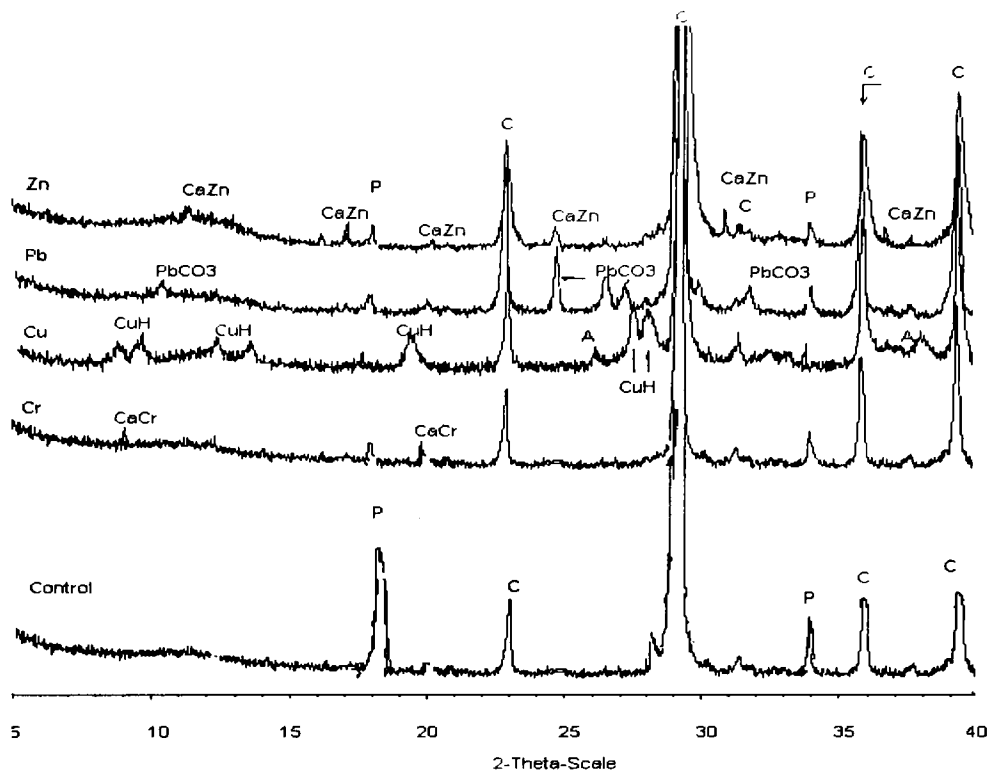


Fig. 3-4. Diffractograms of carbonated calcium hydroxide suspensions at the age of 1 day (From bottom to top are control, Cr, Cu, Pb and Zn -doped suspensions, Legend: C = calcite, P = portlandite, CuH =  $2\text{Ca}(\text{OH})_2\cdot 4\text{Cu}(\text{OH})_2\cdot \text{H}_2\text{O}$ , CaZn =  $\text{CaZn}_2(\text{OH})_6\cdot 2\text{H}_2\text{O}$ , CaCr =  $\text{Ca}_2\text{Cr}(\text{OH})_7\cdot 3\text{H}_2\text{O}$ )

Table 3-2. Phases in calcium hydroxide suspensions

Samples	Phases identified by XRD (1 –90 days)
Control	Portlandite
Cr	Portlandite, $\text{Ca}_2\text{Cr}(\text{OH})_7\cdot 3\text{H}_2\text{O}$
Cu	Portlandite, $2\text{Ca}(\text{OH})_2\cdot 4\text{Cu}(\text{OH})_2\cdot \text{H}_2\text{O}$ , $\text{Cu}(\text{OH})_2$
Pb	Portlandite, $\text{Pb}(\text{OH})_2$
Zn	Portlandite, $\text{CaZn}_2(\text{OH})_6\cdot 2\text{H}_2\text{O}$

Table 3-3. Phases in carbonated calcium hydroxide suspensions

Sample	Phases identified by XRD	
	1-14 days	30-90 days
Contr.	Portlandite, Calcite	Calcite
Cr	Portlandite, $\text{Ca}_2\text{Cr}(\text{OH})_7 \cdot 3\text{H}_2\text{O}$ , Calcite	Calcite
Cu	Portlandite, $2\text{Ca}(\text{OH})_2 \cdot 4\text{Cu}(\text{OH})_2 \cdot \text{H}_2\text{O}$ , Calcite, Aragonite	Calcite
Pb	Portlandite, Calcite, $\text{PbCO}_3$	Calcite
Zn	Portlandite, Calcite, $\text{CaZn}_2(\text{OH})_6 \cdot 2\text{H}_2\text{O}$	Calcite, Vaterite

### 3.3.3.2 Calcium oxide suspensions

#### Hydration

The crystalline phases formed in the suspensions of calcium oxide with or without heavy metals are shown in Table 3-4. For a period of up to two weeks, portlandite was absent in the Cr-, Zn- and Cu-doped calcium oxide suspensions due to low pH values (around 12) derived from hydrolyses of Cr, Zn and Cu ions. In the control suspension of calcium oxide, however, portlandite precipitated very quickly. There were no reflection peaks of CaO in the control suspension and heavy metal-doped suspensions. This indicates that Cr, Zn and Cu did not retard the hydration of calcium oxide, even though Cr, Zn and Cu inhibited the precipitation of portlandite. This interesting phenomenon will be investigated and discussed further with DTA/TG techniques latter in this chapter.

Figs. 3-5, 3-6 and 3-7 present the diffractograms of hydrated calcium oxide suspensions with heavy metals at the age of 1 month, 2 months and 3 months, respectively. The reflection peaks corresponding to  $\text{Ca}_2(\text{OH})_4\text{Cu}(\text{OH})_2 \cdot m\text{H}_2\text{O}$  and  $\text{Ca}_3\text{Cr}_2(\text{OH})_{12}$  disappeared after 2 months.

It was also observed that the intensities of portlandite in the heavy metal -doped suspensions of calcium oxide were much weaker than those in the control suspension in the ages of 1 month, 2 months and 3 months of hydration.

When calcium oxide suspensions were compared with calcium hydroxide suspensions described earlier, the following major differences observed were due to the slow slaking process of calcium oxide.

- Some calcium-heavy metal hydroxides,  $\text{Ca}_2(\text{OH})_4\text{xCu}(\text{OH})_2\cdot\text{mH}_2\text{O}$  and  $\text{Ca}_3\text{Cr}_2(\text{OH})_{12}$ , which depend on pH of the solution, were formed in the calcium oxide suspensions rather than in the calcium hydroxide suspensions.
- From the initial hydration of calcium oxide, heavy metal hydroxides such as  $\text{Pb}(\text{OH})_2$ ,  $\text{Cu}(\text{OH})_2$ ,  $\text{Zn}(\text{OH})_2$  precipitated and can be present at least for three months of age. In calcium hydroxide suspensions, the pH was 12.4 (supersaturated solution of calcium hydroxide) and heavy metal hydroxides, except for  $\text{Pb}(\text{OH})_2$ , did not form.

Table 3-4. The phase development in calcium oxide suspensions

Suspe nsion	Phases identified by XRD		
	14 days	28 days	90 days
Contr.	Portlandite	Portlandite	Portlandite
Cr	$\text{Ca}_3\text{Cr}_2(\text{OH})_{12}$ , $\text{Ca}_2\text{Cr}(\text{OH})_7\cdot 3\text{H}_2\text{O}$ , CrOOH	Portlandite, $\text{Ca}_3\text{Cr}_2(\text{OH})_{12}$ , $\text{Ca}_2\text{Cr}(\text{OH})_7\cdot 3\text{H}_2\text{O}$	Portlandite, $\text{Ca}_2\text{Cr}(\text{OH})_7\cdot 3\text{H}_2\text{O}$
Cu	$2\text{Ca}(\text{OH})_2\cdot 4\text{Cu}(\text{OH})_2\cdot \text{H}_2\text{O}$ , $\text{Cu}(\text{OH})_2$ , $\text{Ca}_2(\text{OH})_4\text{xCu}(\text{OH})_2\cdot \text{mH}_2\text{O}$	Portlandite, $\text{Ca}_2(\text{OH})_4\text{xCu}(\text{OH})_2\cdot \text{mH}_2\text{O}$ , $\text{Cu}(\text{OH})_2$ , $2\text{Ca}(\text{OH})_2\cdot 4\text{Cu}(\text{OH})_2\cdot \text{H}_2\text{O}$	Portlandite, $2\text{Ca}(\text{OH})_2\cdot 4\text{Cu}(\text{OH})_2\cdot \text{H}_2\text{O}$ , $\text{Cu}(\text{OH})_2$
Pb	Portlandite, $\text{Pb}(\text{OH})_2$	Portlandite, $\text{Pb}(\text{OH})_2$	Portlandite, $\text{Pb}(\text{OH})_2$
Zn	$\text{CaZn}_2(\text{OH})_6\cdot 2\text{H}_2\text{O}$ , $\text{Zn}(\text{OH})_2$	Portlandite, $\text{CaZn}_2(\text{OH})_6\cdot 2\text{H}_2\text{O}$ , $\text{Zn}(\text{OH})_2$	Portlandite, $\text{CaZn}_2(\text{OH})_6\cdot 2\text{H}_2\text{O}$ , $\text{Zn}(\text{OH})_2$

Note:  $\text{Ca}_2(\text{OH})_4\text{xCu}(\text{OH})_2\cdot \text{mH}_2\text{O}$  (d-space 0.769, 0.395, 0.336, 0.319, 0.313 nm)

In calcium hydroxide suspensions and calcium oxide suspensions, the layered double hydroxides,  $2\text{Ca}(\text{OH})_2\cdot 4\text{Cu}(\text{OH})_2\cdot \text{H}_2\text{O}$ ,  $\text{Zn}_2(\text{OH})_6\cdot 2\text{H}_2\text{O}$  and  $\text{Ca}_2\text{Cr}(\text{OH})_7\cdot 3\text{H}_2\text{O}$  were identified and were stable in common.

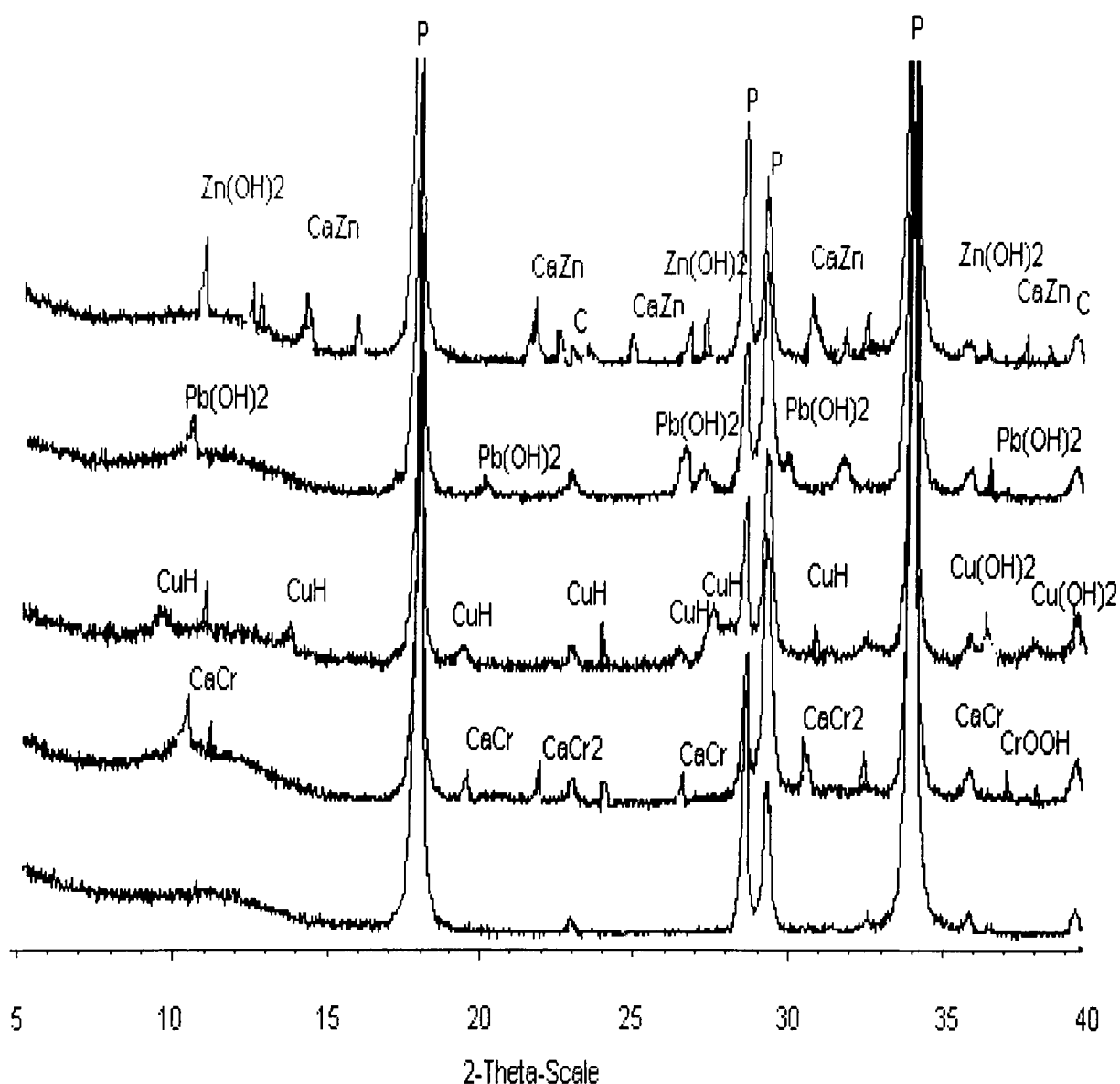


Fig. 3-5. Diffractograms of hydrated calcium oxide suspensions at the age of 1 month (From bottom to top are control, Cr, Cu, Pb and Zn -doped suspensions, Legend: C = calcite, P = portlandite, Pbh =  $\text{Pb}(\text{OH})_2$ , CuH =  $2\text{Ca}(\text{OH})_2\cdot 4\text{Cu}(\text{OH})_2\cdot \text{H}_2\text{O}$ , CaCu =  $\text{Ca}_2(\text{OH})_4\cdot x\text{Cu}(\text{OH})_2\cdot m\text{H}_2\text{O}$ , Cuh =  $\text{Cu}(\text{OH})_2$ , CaZn =  $\text{CaZn}_2(\text{OH})_6\cdot 2\text{H}_2\text{O}$ , Znh =  $\text{Zn}(\text{OH})_2$ , CaCr =  $\text{Ca}_2\text{Cr}(\text{OH})_7\cdot 3\text{H}_2\text{O}$ , CaCr2 =  $\text{Ca}_3\text{Cr}_2(\text{OH})_{12}$ )

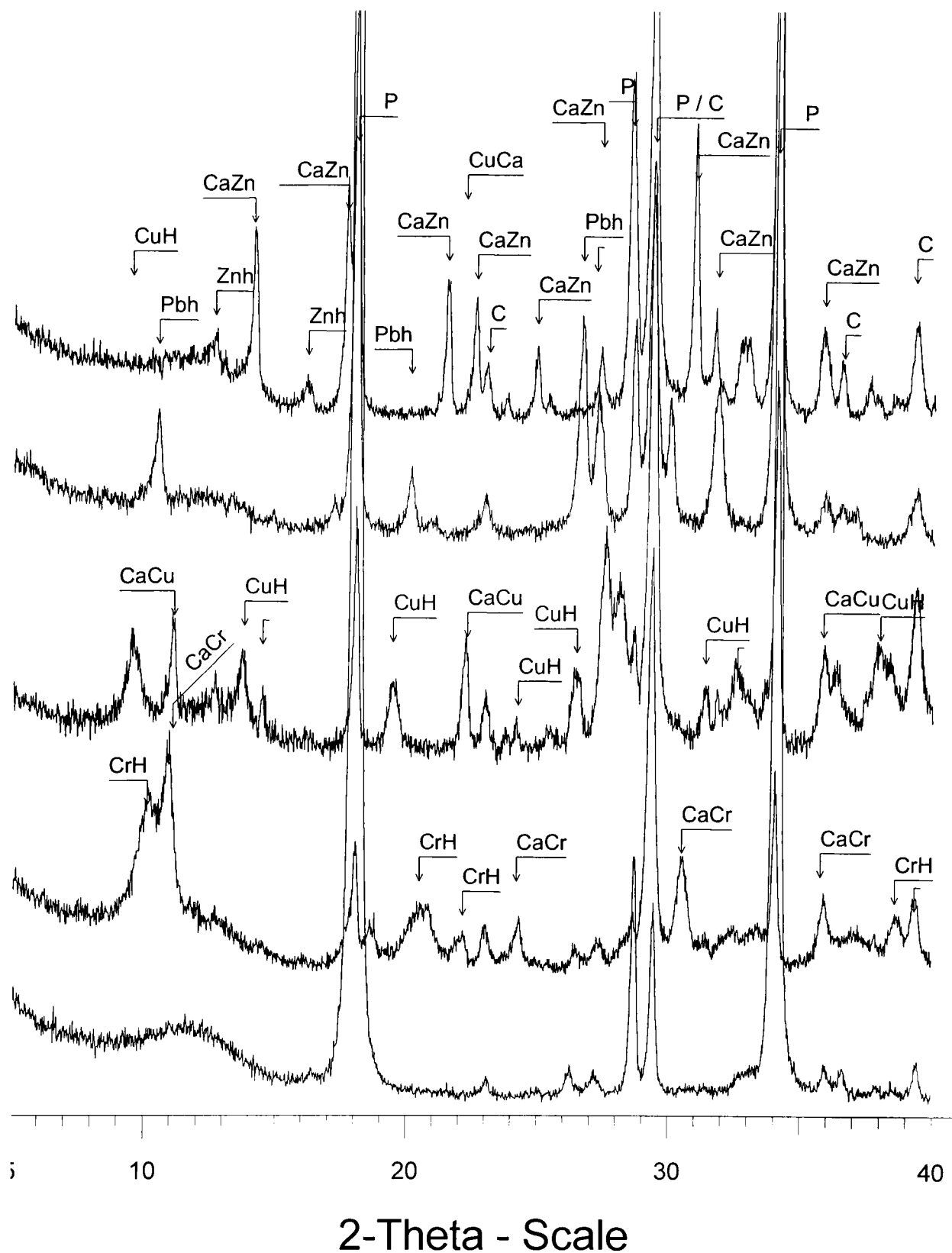


Fig. 3-6. Diffractograms of hydrated calcium oxide suspensions at the age of 2 months (From bottom to top are control, Cr, Cu, Pb and Zn -doped suspensions, Legend: C = calcite, P = portlandite, Pbh =  $\text{Pb}(\text{OH})_2$ , CuH =  $2\text{Ca}(\text{OH})_2\text{Cu}(\text{OH})_2 \cdot \text{H}_2\text{O}$ , CaCu =  $\text{Ca}_2(\text{OH})_4\text{Cu}(\text{OH})_2 \cdot m\text{H}_2\text{O}$ , Cuh =  $\text{Cu}(\text{OH})_2$ , CaZn =  $\text{CaZn}_2(\text{OH})_6 \cdot 2\text{H}_2\text{O}$ , Znh =  $\text{Zn}(\text{OH})_2$ , CaCr =  $\text{Ca}_2\text{Cr}(\text{OH})_7 \cdot 3\text{H}_2\text{O}$ , CrH =  $\text{Ca}_3\text{Cr}_2(\text{OH})_{12}$ )

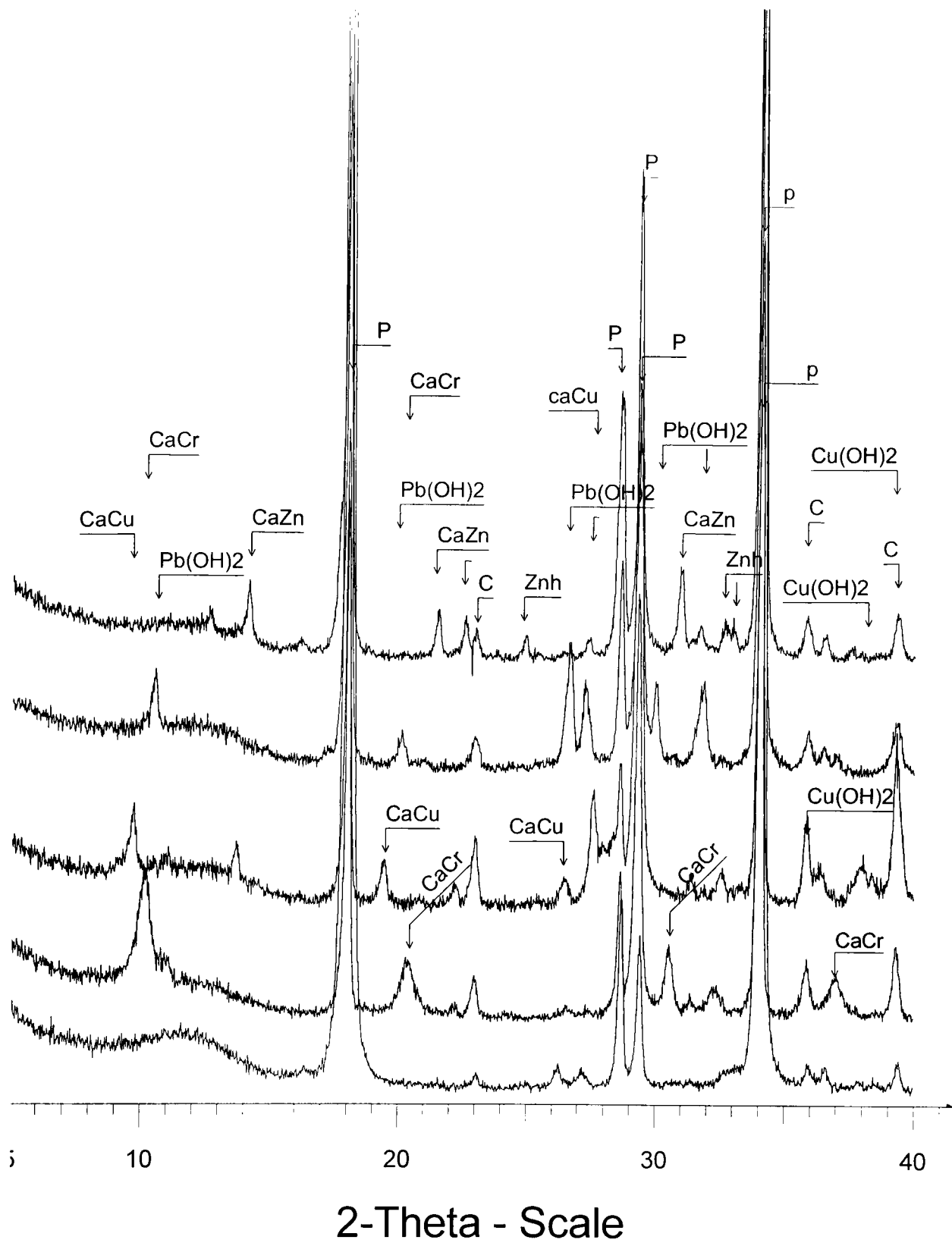


Fig. 3-7. Diffractograms of hydrated calcium oxide suspensions at the age of 3 months (From bottom to top are control, Cr, Cu, Pb and Zn -doped suspensions, Legend: C = calcite, P = portlandite, CaCu =  $2\text{Ca}(\text{OH})_2 \cdot 4\text{Cu}(\text{OH})_2 \cdot \text{H}_2\text{O}$ , CaZn =  $\text{CaZn}_2(\text{OH})_6 \cdot 2\text{H}_2\text{O}$ , Znh =  $\text{Zn}(\text{OH})_2$ , CaCr =  $\text{Ca}_2\text{Cr}(\text{OH})_7 \cdot 3\text{H}_2\text{O}$ )

## Carbonation

The diffractograms from accelerated carbonated calcium oxide suspensions in the presence or absence of heavy metals at the age of 1 month and 3 months are presented in Figs.3-8 and 3-9, respectively. The crystalline phases detected by XRD are summarised in Table 3-5.

It is noted that  $\text{Pb}(\text{OH})_2$  and  $\text{CrOOH}$  were detectable in the early stage during carbonation of calcium oxide. This was attributed to the ability of these compounds to precipitate in pH5-6. As carbonation proceeded, these hydroxides disappeared. In the carbonated Pb-doped suspension of calcium oxide, cerrusite ( $\text{PbCO}_3$ ) was also detected by XRD. It is worth pointing out that double hydroxides, for example,  $\text{CaZn}_2(\text{OH})_6 \cdot 2\text{H}_2\text{O}$  and  $2\text{Ca}(\text{OH})_2 \cdot 4\text{Cu}(\text{OH})_2 \cdot \text{H}_2\text{O}$ , were detectable in the carbonated suspensions of calcium oxide even three months after carbonation, differing from carbonated suspensions of calcium hydroxide.

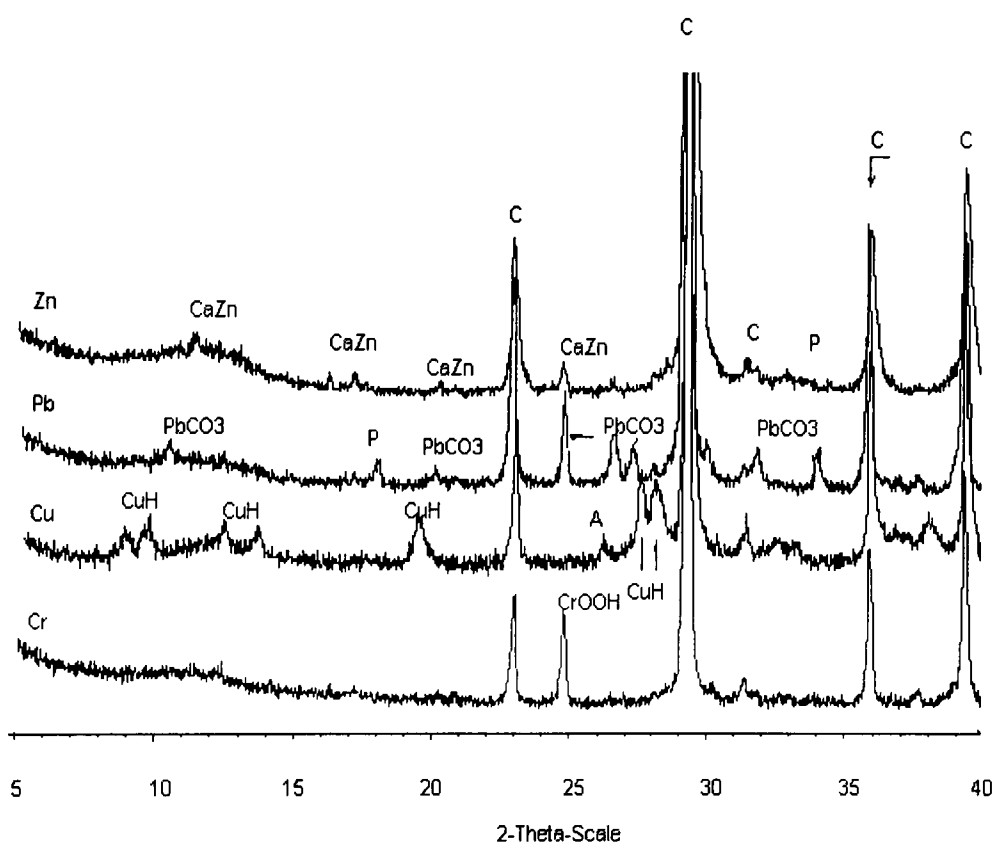


Fig. 3-8. Diffractograms of carbonated calcium oxide suspensions at the age of 1 month (From bottom to top are Cr, Cu, Pb and Zn -doped suspensions, Legend: C = calcite, A = aragonite,  $\text{CaZn} = \text{CaZn}_2(\text{OH})_6 \cdot 2\text{H}_2\text{O}$ ,  $\text{CuH} = 2\text{Ca}(\text{OH})_2 \cdot 4\text{Cu}(\text{OH})_2 \cdot \text{H}_2\text{O}$ )

In the control carbonated suspension of calcium oxide, calcite was the only phase formed at any stage of carbonation. An examination of the carbonated suspensions doped with heavy metals, however, indicated that heavy metals had influenced the polymorphism of calcium carbonate. According to Ostwald's rule, the structure with the highest entropy will develop first and then transform to more stable crystalline phases successively. Taylor (1997) claimed that aragonite should form first and then change into calcite with vaterite as an intermediate. This work demonstrated that heavy metals influenced the conversion rate of calcium carbonate polymorphs. Comparison of suspensions and pastes indicates that water also affected the stability of metastable calcium carbonate.

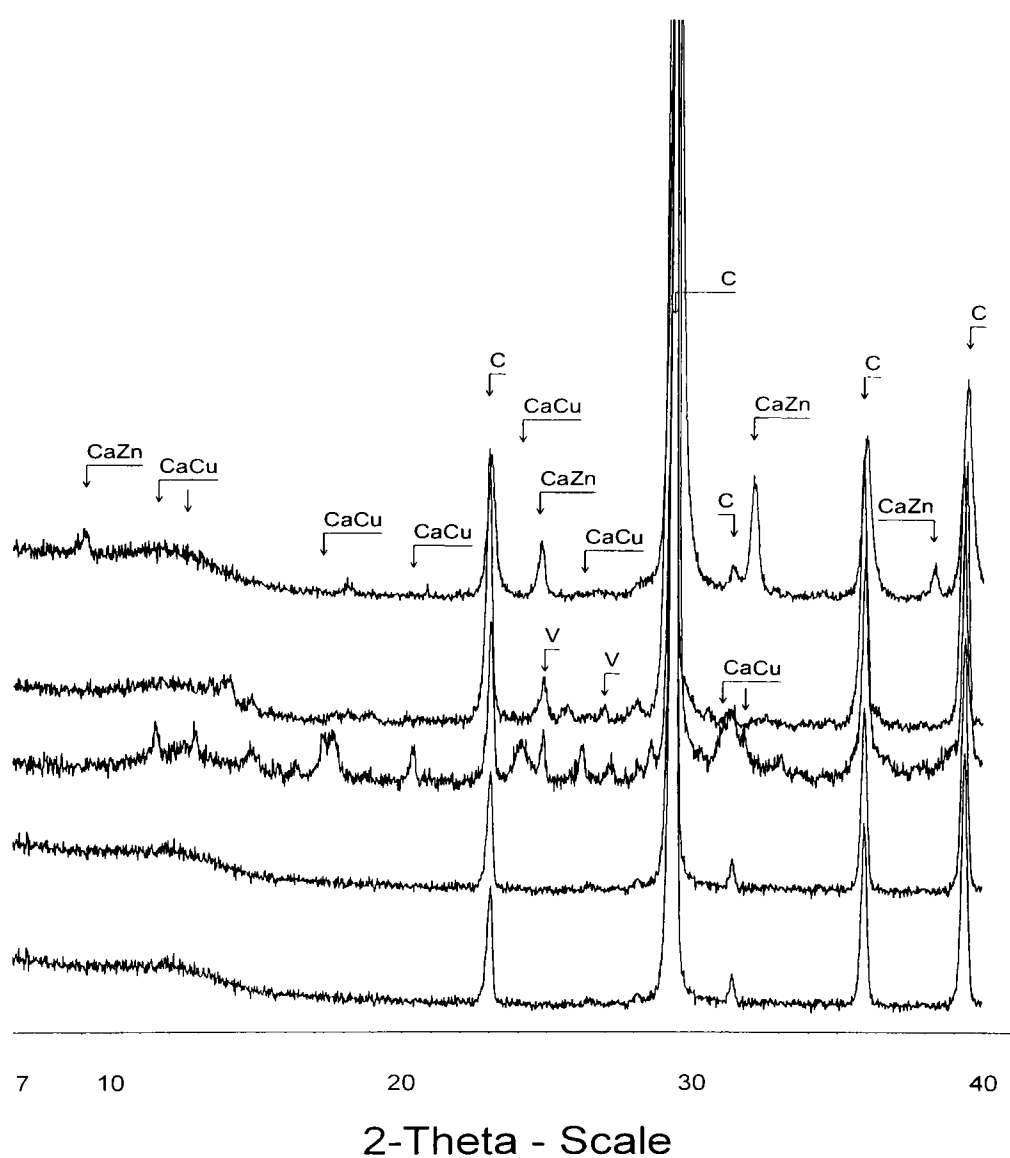


Fig. 3-9. Diffractograms of carbonation calcium oxide suspensions at the age of 3 months (From bottom to top are control, Cr, Cu, Pb and Zn -doped suspensions, Legend: C = calcite, V = vaterite,  $PbCO_3$ ,  $CaZn = CaZn_2(OH)_6 \cdot 2H_2O$ ,  $CuCa = 2Ca(OH)_2 \cdot 4Cu(OH)_2 \cdot H_2O$ )

Table 3-5. Phases identified by XRD for carbonated calcium oxide suspensions

Samp	Phases identified by XRD		
	14 days	28 days	3 months
le			
Contr	Calcite	Calcite	Calcite
Cr	Calcite, CrOOH, Ca <sub>2</sub> Cr(OH) <sub>7</sub> .3H <sub>2</sub> O	Calcite, CrOOH	Calcite
Cu	Calcite, Aragonite, 2Ca(OH) <sub>2</sub> 4Cu(OH) <sub>2</sub> H <sub>2</sub> O	Calcite, Aragonite, 2Ca(OH) <sub>2</sub> 4Cu(OH) <sub>2</sub> H <sub>2</sub> O	Calcite, Vaterite 2Ca(OH) <sub>2</sub> 4Cu(OH) <sub>2</sub> H <sub>2</sub> O
Pb	Calcite, Vaterite, PbCO <sub>3</sub> , Portlandite, Pb(OH) <sub>2</sub>	Calcite, Vaterite, PbCO <sub>3</sub>	Calcite, Vaterite, PbCO <sub>3</sub>
Zn	Calcite, Vaterite, CaZn <sub>2</sub> (OH) <sub>6</sub> .2H <sub>2</sub> O	Calcite, CaZn <sub>2</sub> (OH) <sub>6</sub> .2H <sub>2</sub> O	Calcite, CaZn <sub>2</sub> (OH) <sub>6</sub> .2H <sub>2</sub> O

### 3.3.4 Thermal analyses of calcium oxide pastes

A comparison of diffractograms from suspensions and pastes of calcium oxide indicates that amorphous compounds of heavy metals could form in the pastes. To confirm this hypothesis and to characterise the reaction products in the pastes further, thermal analysis was employed.

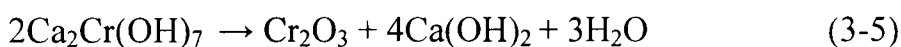
#### 3.3.4.1 Hydrated pastes

The DTA curves of hydrated calcium oxide aged 1 month with or without heavy metals are presented in Fig. 3-10. The simultaneous TG curves are shown in Fig. 3-11. Generally speaking, each endothermic peak can find its corresponding mass loss step in this work. For the convenience of comparison, Table 3-6 summarises the mass loss at three major temperature ranges.

For the control paste, an endothermic peak for portlandite dehydroxylation at 420-500°C and an endotherm of calcite decomposition at 680-750°C were recognised. Correspondingly, two steps of mass loss in the TG curve can be seen. The presence of

calcite is consistent with XRD examination and can be attributed to the carbonation process during the sample preparation and storage. According to the mass loss and the formulae given in Chapter 2, it is estimated that in the control paste the portlandite content and calcite content were 61.7% and 27.1%, respectively. TG results indicate that there was very little free water (0.4%) and anhydrous calcium oxide (around 10%) in the control hydrated paste of calcium oxide.

In the hydrated paste of calcium oxide doped with chromium, there were five major endothermic peaks in the DTA curves and five notable mass loss steps, which were located at 100-120°C, 280-310°C, 350-430°C, 450-500°C and 650-800°C, respectively. The first endothermic peak can be attributed to the evaporation of water, for example, the structural water in the double hydroxide ( $\text{Ca}_2\text{Cr}(\text{OH})_7 \cdot 3\text{H}_2\text{O}$ ). The second peak could be due to the dehydroxylation of the double hydroxide of calcium and chromium:  $\text{Ca}_2\text{Cr}(\text{OH})_7 \cdot 3\text{H}_2\text{O}$  and  $\text{Ca}_3\text{Cr}_2(\text{OH})_{12}$ , which corresponds to the second mass loss. The mass change at the temperature range of 250-600°C is complex and corresponds to three peaks associated with the dehydroxylation of the double hydroxide of calcium and chromium such as  $\text{Ca}_3\text{Cr}_2(\text{OH})_{12}$ ,  $\text{Ca}_2\text{Cr}(\text{OH})_7 \cdot 3\text{H}_2\text{O}$  and portlandite. According to the thermal analysis results, the decomposition of double hydroxide of calcium and chromium can occur in three successive reactions:



From the endothermic peak occurring in the DTA curve, the decomposition temperature of portlandite was 380-450°C. The portlandite content in the Cr -doped paste was estimated at 38.3% by mass, which was much lower than portlandite content in the control hydrated paste of calcium oxide. The last mass change corresponded to the fifth endothermic peak at 650-800°C and was assigned to the decomposition of calcium carbonate. According to the formulae given in Chapter 2, the calculated calcium carbonate content of the Cr-doped paste was 44.1% by mass, which was much higher than that of the control paste, indicating that the presence of chromium promoted the natural carbonation of calcium oxide. It is noteworthy to indicate that thermal analysis results

agreed with the conclusions obtained by examinations of XRD peak intensities of portlandite and calcite.

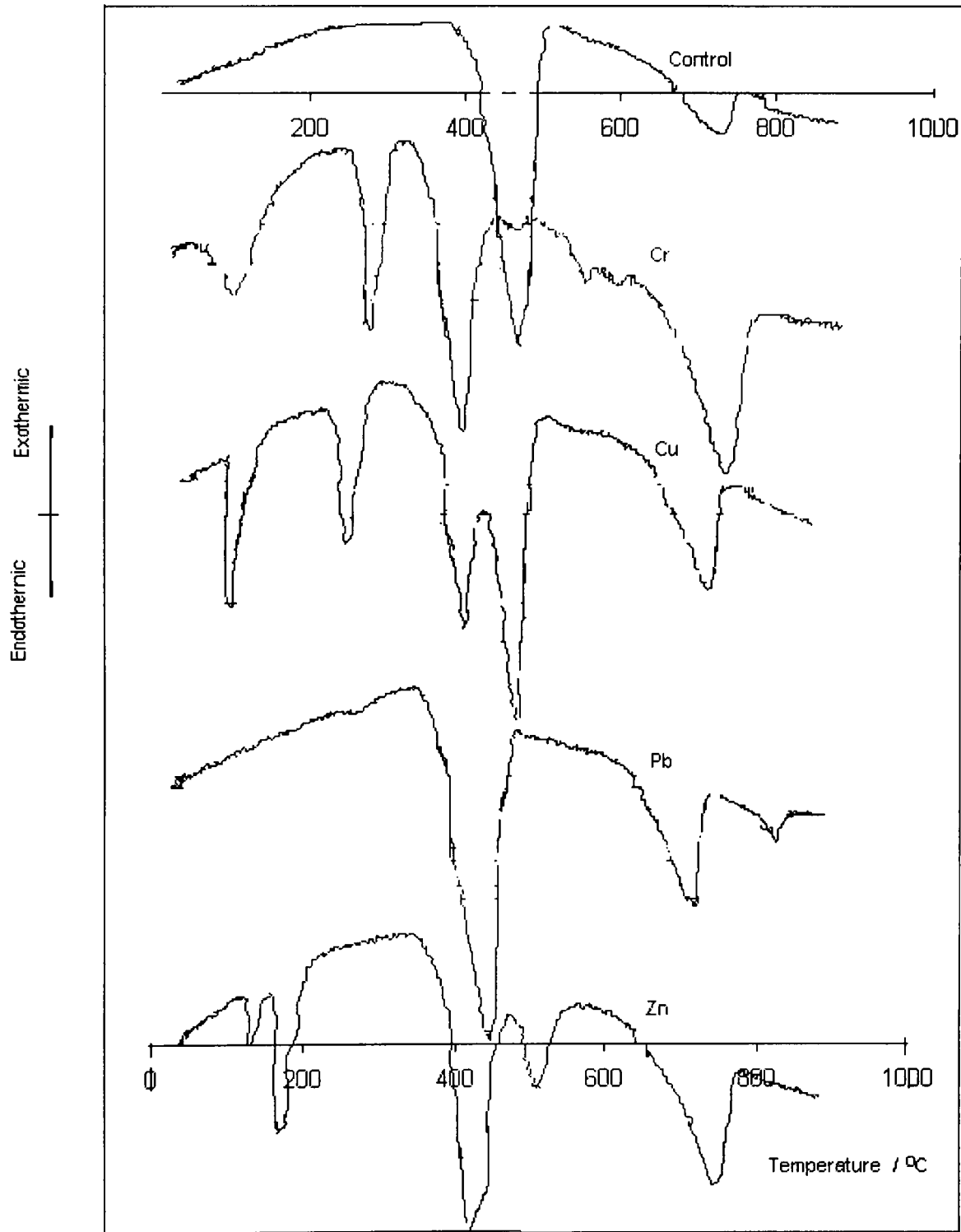


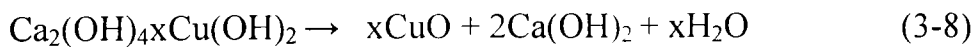
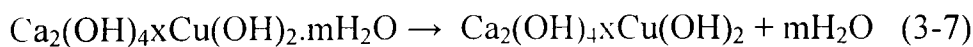
Fig. 3-10. DTA curves of hydrated pastes of calcium oxide

Table 3-6. Thermal analysis results of hydrated calcium oxide pastes (mass loss at indicated temperature, %)

Samples	Control	Cr	Cu	Pb	Zn
20-250°C	0.4	5	5.1	2.3	7.7
250-600°C	14.8	17.2	26.2	16.1	18.8
600-1100°C	11.9	19.4	12.1	12.3	11.5
Total mass loss	30.7	41.6	43.4	30.7	38.0
Ca(OH) <sub>2</sub> content	61.7	38.3	36.7	53.8	40.4
CaCO <sub>3</sub> content	27.1	44.1	37.5	25.45	25.5

The hydrated Cu-doped paste of calcium oxide exhibited five endothermic peaks and four major mass loss steps. Compared with the Cr-doped paste, Cu-doped paste gave more distinctive mass loss steps and the third step, which occurred in the Cu -doped paste had a much narrower range of temperature (400-500°C instead of 450-600°C).

The first endothermic peaks present in the Cu -doped paste can be attributed to a loss of chemically and physically bound water. The double endothermic peaks at 200-400°C were due to the decomposition of double hydroxides of copper and calcium:  $2\text{Ca}(\text{OH})_2\cdot 4\text{Cu}(\text{OH})_2\cdot \text{H}_2\text{O}$  and  $\text{Ca}_2(\text{OH})_4\cdot x\text{Cu}(\text{OH})_2\cdot m\text{H}_2\text{O}$ . From the thermal analysis results, we postulated that the decomposition of double hydroxide of calcium and copper can occur according to three step reactions:



In the Cu -doped paste, the strong endothermic peak at around 450°C and the corresponding mass loss step can be attributed to dehydroxylation of portlandite. The portlandite content in the Cu -doped paste was 36.7%. The last endothermic peak and corresponding mass loss was due to the decomposition of calcium carbonate. It is noted that Cu ions lowered the decomposition temperature of calcium carbonate, indicating that Cu ions decreased the stability of calcium carbonate possibly due to Cu ion sorption or

incorporation into the crystal lattice of calcium carbonate. The calculated calcium carbonate content due to natural carbonation during sample storage and preparation was 37.5%.

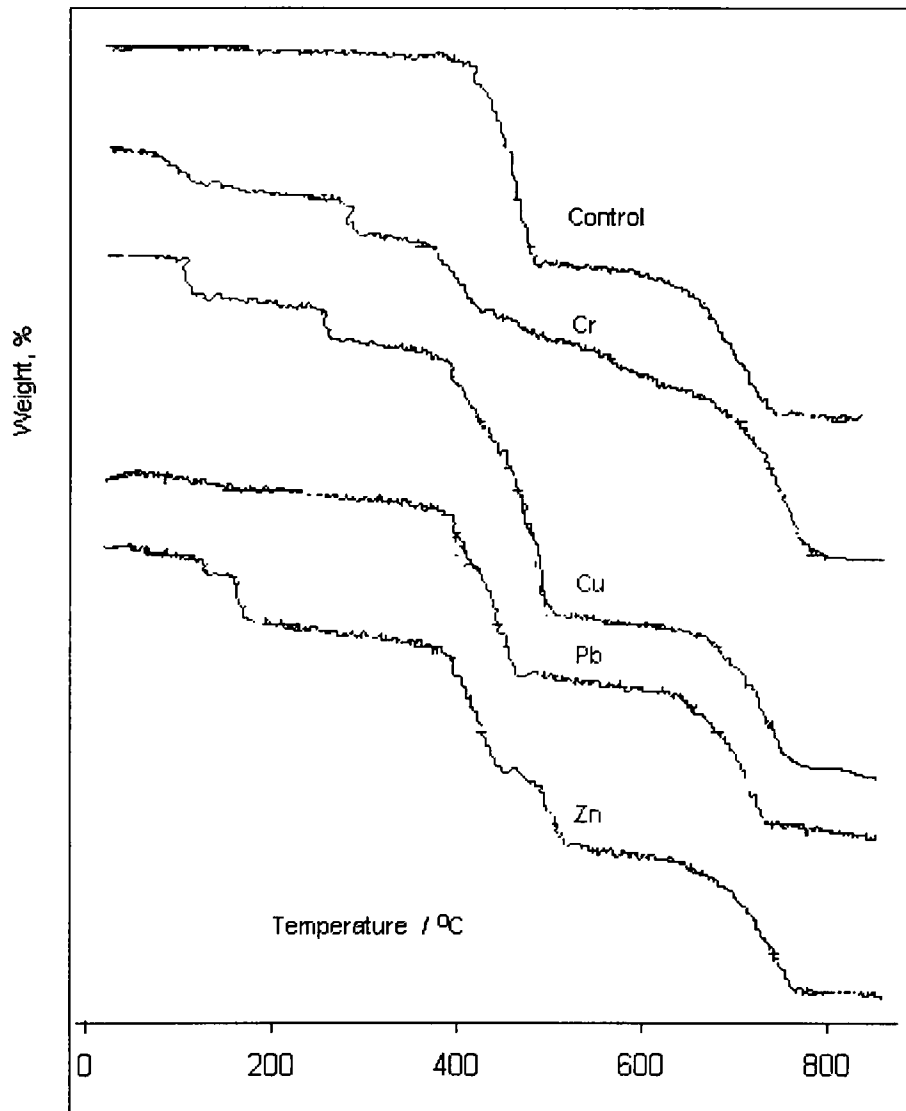


Fig. 3-11. TG curves of hydrated calcium oxide pastes

The DTA and TG curves of hydrated Pb-doped calcium oxide pastes were very similar to those of the control paste except for the obvious lower dehydration temperature of portlandite. It is noted that the decomposition temperature of portlandite shifted from 420-500°C to 390-450°C, indicating that Pb substituted for Ca in portlandite and reduced the thermal stability of portlandite. There was no endothermic or exothermic peak related to dehydroxylation of  $\text{Pb}(\text{OH})_2$ , indicating that the amount of  $\text{Pb}(\text{OH})_2$  in the paste was very

limited. In the Pb -doped paste, no double hydroxides were formed, in accordance with examinations based on XRD.

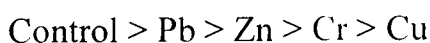
In the hydrated Zn -doped paste, there appeared five major endothermic peaks. Correspondingly, the TG curve shows five steps of mass loss. The mass loss in 100-200°C was attributed to the evaporation of structural water in calcium zincate ( $\text{CaZn}_2(\text{OH})_6 \cdot 2\text{H}_2\text{O}$ ) and dehydroxylation of  $\text{Zn}(\text{OH})_2$ . The second and third endothermic peaks and corresponding mass loss steps can be attributed to the decomposition of calcium zincate.



The fourth endothermic peak and corresponding mass loss step occurring in the Zn -doped paste arose from dehydroxylation of portlandite. The last endotherm and mass loss step were due to decomposition of calcium carbonate. Calculated portlandite content and calcium carbonate content were 40.4% and 25.5%, respectively.

It is noted that in all pastes doped with heavy metals, the portlandite decomposition temperature was lower compared to the control sample. In addition, in the DTA and TG curves, the decomposition temperature of calcium carbonate in the control paste occurred at 650-800°C, whereas in the heavy metal-doped pastes calcium carbonate decomposition ranges were: Cr 650-800°C, Cu 680-770°C, Pb 650-750°C and Zn 660-780°C, respectively. These results indicated that heavy metals could substitute for calcium in portlandite and calcium carbonate and change their thermal stabilities.

The amount of portlandite in the hydrated pastes of calcium oxide in the presence or absence of heavy metals was in the sequence:



Thermal analyses confirmed that all heavy metals investigated retarded the formation of portlandite. The above sequence was consistent with the XRD analyses, with reference to the intensities of portlandite at  $18^\circ 2\theta$ . In other words, the differences in reflection peak

intensities between pastes under the same operating conditions reflected the differences in phase contents. These differences should not be ignored, although many factors such as polarisation factor, Lorenz factor, multiplicity factor may influence the intensity of the XRD peak (Cullity, 1978).

As all samples investigated were dry, the total mass loss of the paste reflected the degree of hydration. The degree of hydration of calcium oxide with or without heavy metals can, therefore, be arranged in the order:

$$\text{Cu} > \text{Cr} > \text{Zn} > \text{Pb} = \text{Control}$$

The sequence discrepancy between the degree of hydration and the portlandite content can be attributed to natural carbonation and the formation of double hydroxides of calcium and heavy metals. The latter could be more important, because the content of portlandite plus calcium carbonate for each paste was in the sequence:

$$\text{Control} > \text{Pb} = \text{Cr} > \text{Zn} > \text{Cu}$$

By comparing the above sequence with the sequence of the degree of hydration, the amount of double hydroxide was in the order:

$$\text{Cu} > \text{Zn} > \text{Cr}$$

To sum up, when calcium oxide was hydrated in the presence of heavy metals, the degree of hydration was not reflected by the amount of portlandite formed. Although heavy metals promoted the hydration of calcium oxide, they inhibited the precipitation of portlandite. In addition to double hydroxides, calcium carbonate was identified in this work. From the calcium carbonate contents in the pastes shown in the Table 3-6, Cr and Cu promoted natural carbonation, and this was in agreement with XRD intensities recorded for calcite.

#### **3.3.4.2 Carbonated pastes**

The DTA curves of carbonated calcium oxide pastes aged 1 month are presented in Fig. 3-12. The simultaneous TG curves are shown in Fig. 3-13. Table 3-7 summarises the

mass loss in three major temperature ranges. It is noted that all curves of carbonated pastes of calcium oxide were similar to those of their hydrated analogues except that no portlandite endothermic peak and corresponding mass loss step occurred.

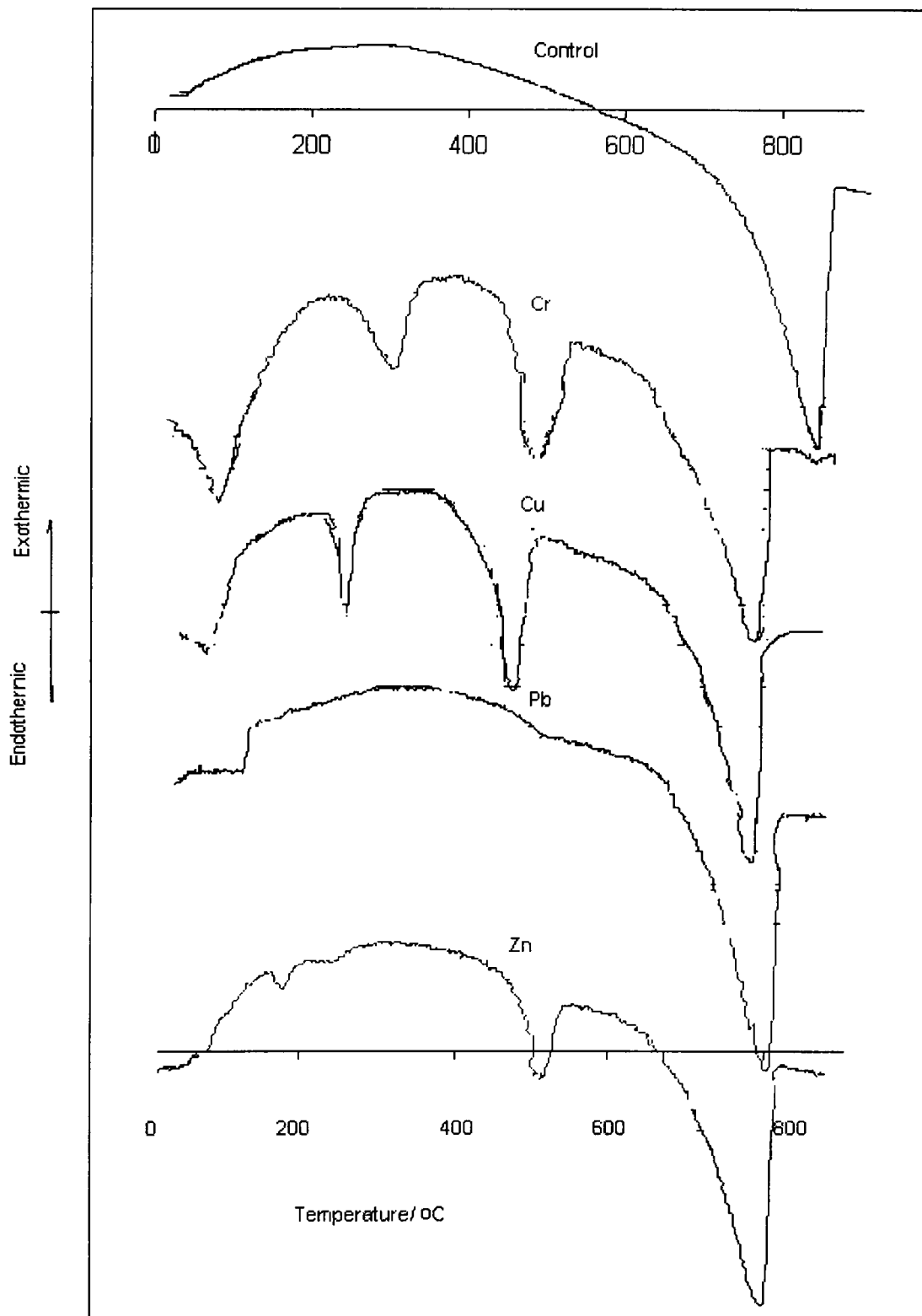


Fig. 3-12. DTA curves of the carbonated pastes of calcium oxide

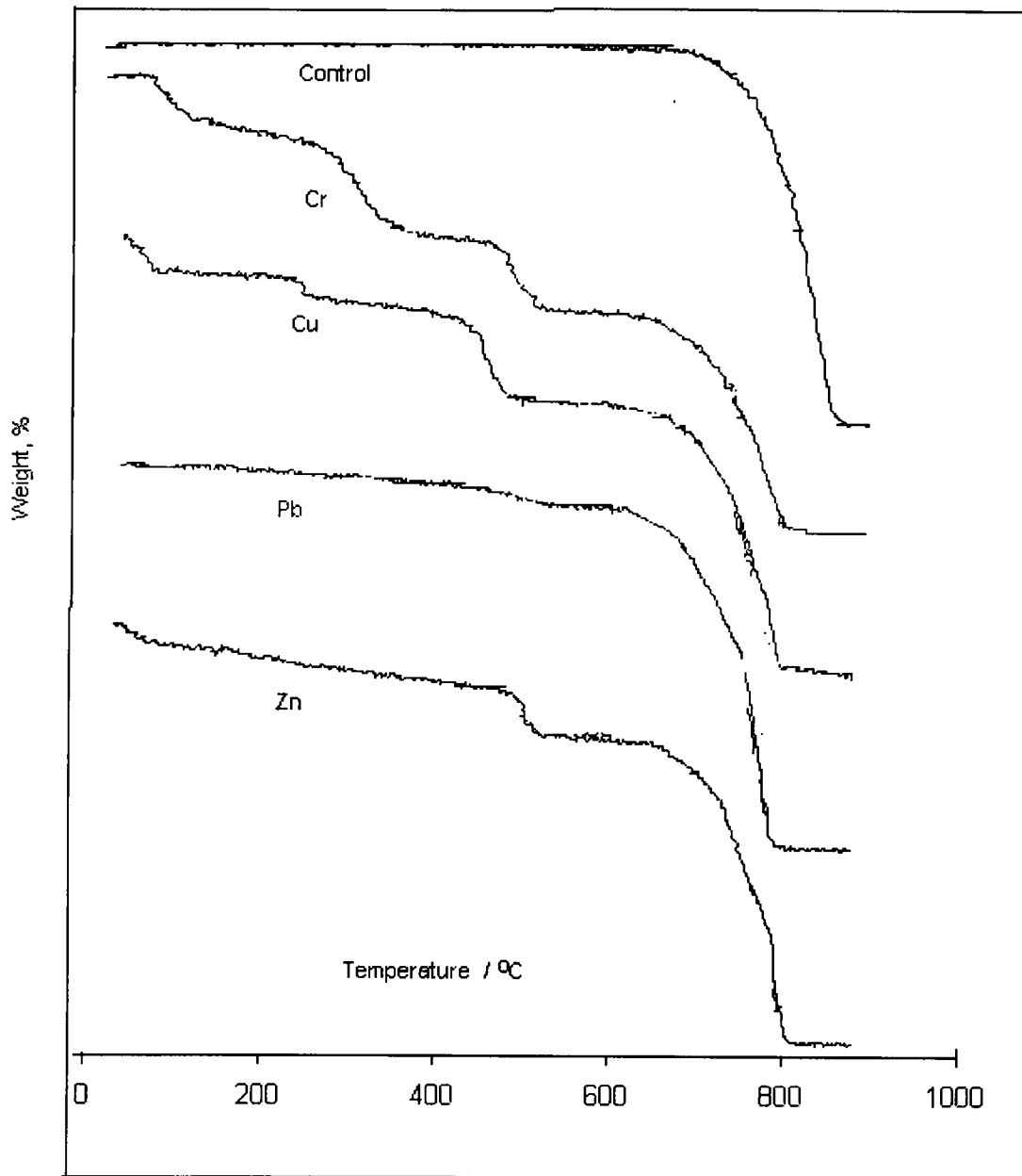


Fig. 3-13. The TG curves of the carbonated pastes of calcium oxide

In the control carbonated paste of calcium oxide, the endothermic peak of calcite decomposition appeared at 650-860°C in the DTA curves and the corresponding one step of mass loss can be seen in the TG curves. According to the amount of mass loss, it is calculated that in the control paste the calcite content was 93.4%, which demonstrates that the degree of carbonation was very high and the method for measuring the content of calcite using TG data was reliable. TG results indicated that there was very little free

water (0.1%) or calcium hydroxide (0.2%) in the control carbonated paste of calcium oxide.

Table 3-7. Thermal analysis results of carbonated pastes of calcium oxide (mass loss at indicated temperature, %)

Samples	Control	Cr	Cu	Pb	Zn
20-250°C	0.1	7.7	7.4	1.6	7.4
250-600°C	0.2	18.4	11.9	3.4	8
600-1100°C	41.1	24.4	29.4	37.4	33.2
Total mass loss	41.4	50.5	48.7	42.4	48.6
CaCO <sub>3</sub> content	93.4	55.2	66.8	84.6	75.1

In the carbonated Cr -doped paste of calcium oxide, there were four endothermic peaks in the DTA curve and four obvious mass loss steps, which were located at 100-120°C, 250-340°C, 450-540°C and 650-800°C, respectively. The first endothermic peak can be attributed to the loss of chemically and physically bound water in the paste. The second endothermic peak could be due to the dehydration of double hydroxide of calcium and chromium (Ca<sub>2</sub>Cr(OH)<sub>7</sub>·3H<sub>2</sub>O), which corresponded to the second mass loss step. The third mass loss step arose from the dehydroxylation of double hydroxide of calcium and chromium. The last mass loss step corresponds to the fourth endothermic peak at 650-800°C and was due to the decomposition of calcium carbonate. The calcium carbonate content in the Cr -doped paste was 55.2%.

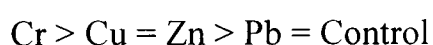
The carbonated Cu -doped paste exhibited similar endothermic peaks and mass loss steps to the carbonated Cr -doped paste, but the temperature ranges were different. The first endothermic peak (100-120°C) arose from the water loss of chemical bound water in the paste. The second and third peaks (240-270°C, 440-500°C) indicated the presence of double hydroxide of copper and calcium (2Ca(OH)<sub>2</sub>·4Cu(OH)<sub>2</sub>·H<sub>2</sub>O) in the carbonated Cu-doped paste of calcium oxide and were in good agreement with XRD results. The endothermic peak at 680-800°C was due to decomposition of calcium carbonate. According to mass loss, the calculated calcium carbonate content was 66.8%.

The DTA and TG curves of Pb -doped carbonated paste of calcium oxide were similar to those of the control paste, unlike other heavy metal -doped carbonated pastes of calcium oxide. The decomposition temperature of calcite was, however, much narrower and lower (660-800°C) compared to the control carbonated paste. In Pb -doped sample, the calcium carbonate content was determined as 84.6%.

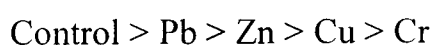
In the Zn -doped paste, three major endothermic peaks were recorded. Correspondingly, the TG curve shows three steps of mass loss. The steady mass loss at temperatures of 100-480°C could be attributed to dehydration of double hydroxide of calcium and zinc, i.e. calcium zincate ( $\text{CaZn}_2(\text{OH})_6 \cdot 2\text{H}_2\text{O}$ ). The endothermic peak and mass loss at 480-540°C arose from the decomposition of calcium zincate. The third endothermic peak and corresponding step of mass loss was due to the decomposition of calcium carbonate. The evaluated calcium carbonate content in the carbonated Zn-doped paste of calcium oxide was 75.1%.

It was noted that the decomposition temperature ranges of calcium carbonate in all heavy metal -doped pastes were close, but were different from that of calcite in the control sample. The shift of decomposition temperature of calcium carbonate could be attributed to adsorption of heavy metals on the surface of calcium carbonate or heavy metal incorporation into the lattice of calcium carbonate.

According to mass loss the degree of carbonation in the carbonated pastes of calcium oxide was in the following increasing sequence:



The calcium carbonate content was in the increasing sequence:



The above sequence is consistent with the examination of peak intensities of calcite  $29.5^\circ 2\theta$  by XRD. The sequence discrepancy between the degree of carbonation and the calcium carbonate content was due to the formation of double hydroxides of calcium and heavy metals.

### 3.4 Summary

The hydration of calcium oxide pastes and suspensions in the presence or absence of heavy metals was examined and compared with the corresponding calcium hydroxide systems. The reaction products of calcium oxide or calcium hydroxide with heavy metals were also examined after carbonation. Based on the examination of XRD and DTA/TG results, the following conclusions can be drawn.

- Heavy metals promoted the hydration of calcium oxide, but inhibited the formation of portlandite. Heavy metals promoted the carbonation of calcium oxide and calcium hydroxide.
- The double hydroxides of heavy metals and calcium,  $\text{Ca}_2\text{Cr}(\text{OH})_7 \cdot 3\text{H}_2\text{O}$ ,  $2\text{Ca}(\text{OH})_2 \cdot 4\text{Cu}(\text{OH})_2 \cdot \text{H}_2\text{O}$  and  $\text{CaZn}_2(\text{OH})_6 \cdot 2\text{H}_2\text{O}$ , were formed in all systems investigated. In suspensions, they existed as crystals and in pastes most of them were amorphous. These compounds were very stable in hydrated conditions. Upon carbonation, they were stable for at least three months in carbonated suspensions of calcium oxide with heavy metal; and at least two weeks for carbonated suspensions of calcium hydroxide with heavy metal.
- The precipitation of double hydroxides corresponded with a decrease in the content of portlandite and calcium carbonate in the hydrated and carbonated systems, respectively.
- The reaction products of calcium oxide with heavy metals exhibited some differences from those of calcium hydroxide with heavy metals. For example, more double hydroxides and heavy metal hydroxides formed in hydrated calcium oxide systems; metastable polymorphs of calcium carbonate and double hydroxides lasted longer in carbonated calcium oxide systems than in carbonated calcium hydroxide systems.
- Heavy metals influenced the polymorphism and decomposition temperature of calcium carbonate. This was due to the adsorption of heavy metal ions on the surface of calcium carbonate or the incorporation in the lattice of calcium carbonate. Heavy metals reduced the dehydroxylation temperature of portlandite.

## Chapter 4

### Investigation of tricalcium silicate/heavy metal systems

#### 4.1 Background

As described in Chapter 1, alite is the most abundant phase of Portland cement and dominates the performance of Portland cement. As tricalcium silicate is the pure form of alite, it is no surprise, therefore, that the reactions of tricalcium silicate ( $C_3S$ ) with water as well as carbon dioxide, in the presence or absence of heavy metals, are important to cement-based *s/s* of waste and contaminated soil containing heavy metals (Cocke *et al.*, 1989; Komarneni *et al.*, 1988; Glasser, 1997).

The hydration of  $C_3S$  has been extensively investigated and a divergence of opinions exists on the exact nature of the reactions of  $C_3S$  with water (Stein and Stevels, 1964; Nonat, 1997; Richardson and Groves 1993). A gel-model and a crystal-model have been forwarded to explain the hydration of  $C_3S$  and cement (see Chapter 1). The gel model has been demonstrated to be useful in explaining the retardation of heavy metal wastes in hydrated  $C_3S$  or cement systems due to the formation of insoluble gelatinous hydroxide of metal cations on the surface of  $C_3S$  (Conner, 1990; Cocke *et al.*, 1989). In addition, the ways heavy metals affect hydration reactions of  $C_3S$  or cement have largely focussed upon adsorption processes; and a number of models, including the di-layer model, the triple layer model and the charge-dispersal model, have been developed to understand the intrinsic mechanism involved in cement-based *s/s* processes (Yousuf and Mollah, 1995).

The essential hydration products of  $C_3S$  are portlandite and calcium silicate hydrate gel (C-S-H gel), whose structure and composition are not fully understood at present. Its crystalline analogues, i.e. the calcium silicate hydrate minerals such as torbermorite and jennite, are characterised by sheet-like structures with  $Ca(OH)_2$  layers, sandwiched by silicate tetrahedra. The tetrahedral form silicate chains with lengths of 2, 5, 8 (tetrahedra termed dimer, pentamer, octamer, respectively). The interlayer spaces, which are occupied by  $Ca^{2+}$  cations,  $OH^-$  anions and  $H_2O$  molecules, whose content affects the weak bonding between adjacent sheets, provides further variation (Taylor, 1986; 1993).

However, there is no convincing evidence that structure of C-S-H gel generated from  $C_3S$  or cement hydration stacks like the crystalline structure of calcium silicate hydrates described above (Glasser, 1997).

Hydration products of  $C_3S$  or cement readily undergo carbonation as a result of exposure to carbon dioxide gas and moisture (Klich *et al.*, 1999). As previously described, carbonation is a complicated physicochemical process, involving  $CO_2$  solution and dissolution in aqueous media and subsequent interaction with anhydrous clinker and hydration products (Berger *et al.*, 1972). The factors that influence carbonation include the partial pressure of  $CO_2$ , the water/solid ratio, temperature, time and the presence of admixtures. These were discussed by Goto *et al.* (1995), Slegers and Rouxhet (1976) and Suzuki (1985).

In addition to C-S-H gel (with very low Ca/Si ratio), calcium carbonate and silica gel are major carbonation products of  $C_3S$  and Portland cement. Silica gel has usually been ascribed to the condensation of  $Si(OH)_4$  into siloxane chains, then branching and cross-linking to form a three-dimensional network.

The effects of carbonation on concrete and cemented waste forms are potentially of great importance where durability is concerned. Furthermore, there is mounting evidence that during the accelerated carbonation of anhydrous and freshly mixed cement pastes, their ability to retain certain heavy metals may be enhanced (Hills *et al.*, 1994). In the carbonated cement/waste systems, heavy metals may be incorporated by precipitation as hydroxyl-carbonate or carbonate. And this was discussed by Bonen and Sarkhar (1995), Walton *et al.* (1997) and Macias (1997). Unfortunately, no convincing hard evidence has been published in the literature and further work remains to be done because of the complexities of characterisation of carbonate systems.

Solid-state high resolution  $^{29}Si$  NMR is an efficient method for the structural investigation of solid silicates and aluminosilicates (Lippmaa *et al.*, 1982; Brough *et al.*, 1996; Lin *et al.*, 1997). The  $^{29}Si$  chemical shifts display a regular dependence upon the degree of condensation of silica-oxygen tetrahedra. The total range of  $^{29}Si$  shifts in silicates (about 50ppm) can be divided into well-separated ranges for:

- 1) mono-silicates Q0 (-66 to -74ppm from TMS) or isolated tetrahedra, i.e. without shared O atom with neighbouring tetrahedra;
- 2) di-silicates and chain end groups Q1 (-77 to -82ppm), one shared O atom with neighbouring tetrahedra;
- 3) chain middle groups Q2 (-85 to -89ppm), two shared O atoms;
- 4) chain branching sites Q3 (-90 to -100ppm), three shared O atoms; and
- 5) three dimensional cross-linked framework Q4 (-103 to -115ppm, four shared O atoms with neighbouring tetrahedra.

Although cement-based s/s has been widely used in the treatments of industrial residues and contaminated soil containing metallic pollutants (Wiles, 1987; Conner, 1990; Trussel and Spence, 1994), the effects of heavy metals on the cement reactions and mechanisms of heavy metal immobilisation are not yet fully defined. In order to extend existing s/s techniques and take measures to prolong the life of cement-based solidified waste forms, there is an urgent need to examine the immobilisation mechanisms of heavy metals at a fundamental level (Wiles, 1987; Bozkurt *et al.*, 2000).

In this chapter, hydrated and carbonated C<sub>3</sub>S pastes and aqueous suspensions containing the selected heavy metals, namely Cu, Pb, Zn and Cr, have been investigated. The effect of these metals on phase development was evaluated up to one year of age by X-ray powder diffraction (XRD), thermal analyses (DTA/TG) and <sup>29</sup>Si solid state magic angle spinning/nuclear magnetic resonance (NMR) techniques.

## ***4.2 Experimental***

### **4.2.1 Materials**

Tricalcium silicate was synthesised from CaCO<sub>3</sub> and SiO<sub>2</sub> (Aldrich Chemical Company, 98% purity) (see Appendix A). Copper, lead, zinc and chromium nitrate salts (BCD Ltd, 98 % purity) were dissolved in de-ionised water at concentrations of 5w/w % and 10w/w % (by heavy metal ion weight).

## **4.2.2 Methods**

### **4.2.2.1 Hydration**

In the preparation of hydrated pastes of  $C_3S$ , 3g of  $C_3S$  was mixed with the 10 % w/w solutions of heavy metal nitrates or de-ionised water at a solid/liquid ratio of 10:4.

### **4.2.2.2 Accelerated carbonation**

Fresh  $C_3S$  pastes were prepared as above and exposed to 100%  $CO_2$  in the carbonation chamber described in Chapter 2.

### **4.2.2.3 Suspension studies**

Heavy metal nitrate solutions with concentrations of 0% and 5% w/w (by metal ion mass) were mixed with ground  $C_3S$  at a solid/liquid ratio of 1:10. The suspensions were placed in sealed containers and agitated, and pH was measured at regular time intervals with a pH meter (Philips DW9418). In order to effect carbonation, suspensions were placed in the carbonation chamber at 0.3MPa for 40 minutes prior to the measurements of pH values. This cycle of exposure to  $CO_2$  followed by measuring of pH was repeated until the stable pH values were obtained.

## **4.2.3 X-ray powder diffraction (XRD)**

A Siemens D500 diffractometer and Kristalloflex 810 generator (CuK-alpha radiation, 40KV, 40mA) were used to identify the crystalline products present in the pastes or suspensions both before and after carbonation. The finely ground samples (<50  $\mu m$ ) were examined between  $5-40^\circ 2\theta$  at a scanning rate of  $1^\circ 2\theta$  per minute. The diffractograms were obtained with Diffplus and analysed using Bruker/AXS EVA.

#### **4.2.4 Thermal analysis (DTA/TG)**

In this work, a Stanton Redcroft STA 780 Simultaneous Thermal Analyser was used to conduct DTA/TG analyses. Samples (20 mg) were ground with an agate mortar and pestle to less than 50 microns and packed in the crucible of 5.8mm diameter and 4 mm high and made from rhodium-platinum. Samples were examined at a heating rate of 10°C/min under flowing nitrogen (40cm<sup>3</sup>/min) from 30-1100°C.

#### **4.2.5 Solid-state magic angle spinning / nuclear magnetic resonance**

In this work, C-S-H gel was studied by magic angle spinning/nuclear magnetic resonance (MAS/NMR) spectroscopy. <sup>29</sup>Si solid state NMR spectra were recorded on a Varian Infinity Plus-300 spectrometer equipped with a 7.1T magnet in which the resonance frequency for <sup>29</sup>Si is 59.49 MHz. To narrow the resonance peaks, <sup>29</sup>Si NMR spectra of hydrated or carbonated C<sub>3</sub>S pastes with or without heavy metals were obtained on a spin rate of 6KHz. It was operated at relaxation T<sub>1</sub>>>30s with a relaxation delay of 10s. The curing time of all samples for NMR experiments was 1 year after hydration or accelerated carbonation.

### **4.3 Results and discussion**

#### **4.3.1 Hydration**

Tricalcium silicate is thermodynamically unstable due to non-regular co-ordination, and its reactivity with water results in the formation of a silica-rich layer (inner C-S-H gel) on the surface of C<sub>3</sub>S grains. Meanwhile, plate-like portlandite crystallites grow in pore space followed by outer C-S-H gel precipitation. Fig. 4-1 shows the diffractograms obtained from hydrated C<sub>3</sub>S pastes at 28 days with or without heavy metals. The main differences observed involved the intensities of portlandite and C<sub>3</sub>S peaks at 18.1°, 34°, 28.5° and 29.5° 2θ and 32°, 32.7° and 34.4° 2θ, respectively. For the convenience of comparison, the intensities of C<sub>3</sub>S (with reference to the peak at 32° 2θ) and portlandite (with reference to the peak at 18.1° 2θ) in various hydrated C<sub>3</sub>S pastes are presented in

Fig. 4-2. Obviously, Cu and Cr promoted the hydration of C<sub>3</sub>S and Zn inhibited the hydration of C<sub>3</sub>S. In the Cu -doped C<sub>3</sub>S paste, the peaks of C<sub>3</sub>S almost vanished (see Fig. 4-1). It was also noted that heavy metals inhibited the formation of portlandite. These phenomena will be investigated further with C<sub>3</sub>S suspensions and other techniques such as DTA/TG.

It is worth noting that in hydrated pastes (shown in Fig. 4-1), the intensities of X-ray reflections at 18.1° and 34.1° 2θ, which belong to portlandite, (001) and (101) respectively, were in different orders, *i. e.*

Control > Zn<sup>2+</sup> > Cr<sup>3+</sup> > Pb<sup>2+</sup> > Cu<sup>2+</sup>, and

Control > Cr<sup>3+</sup> > Pb<sup>2+</sup> > Cu<sup>2+</sup> > Zn<sup>2+</sup>

The differences in intensity observed can arise from several effects such as preferred orientation of the crystallites in the samples, the crystal structure and atom position variations of portlandite (Cullity, 1978). The exact reason is not known and needs further studies.

The diffractograms obtained from one-month old hydrated pastes also show peaks corresponding to calcite. This indicates that some carbonation occurred during sample preparation and storage, even though samples were sealed in plastic screw top bottles.

To further study the effects of heavy metals on the hydration of C<sub>3</sub>S, C<sub>3</sub>S suspensions with or without heavy metals were used. The pH of the suspensions of C<sub>3</sub>S is given in Fig. 4-3. In the absence of heavy metals, a pH of 12.4 was recorded, which was close to the pH of the saturated solution of pure portlandite. Additions of heavy metal nitrates decreased pH due to hydrolysis of heavy metal cations. For example, at a concentration of 50 g/l, the initial pH values of C<sub>3</sub>S suspensions with Cu<sup>2+</sup>, Pb<sup>2+</sup>, Zn<sup>2+</sup> and Cr<sup>3+</sup> were 6.3, 6.7, 8.4 and 8.5, respectively. These pH values increased with time due to the hydration of C<sub>3</sub>S at different rates, demonstrating that heavy metals behaved different in C<sub>3</sub>S hydration.

It is known that in low pH media the precipitation of portlandite is inhibited. As a consequence, X-ray intensities of portlandite were lower in the diffractograms obtained from these materials (see Figs. 4-1 and 4-4). The amount of portlandite and other

compounds formed as well as  $C_3S$  decomposition influenced the Ca/Si ratio of C-S-H gel in the hydrated  $C_3S$  pastes, which is examined with DTA/TG techniques in the latter part of this chapter.

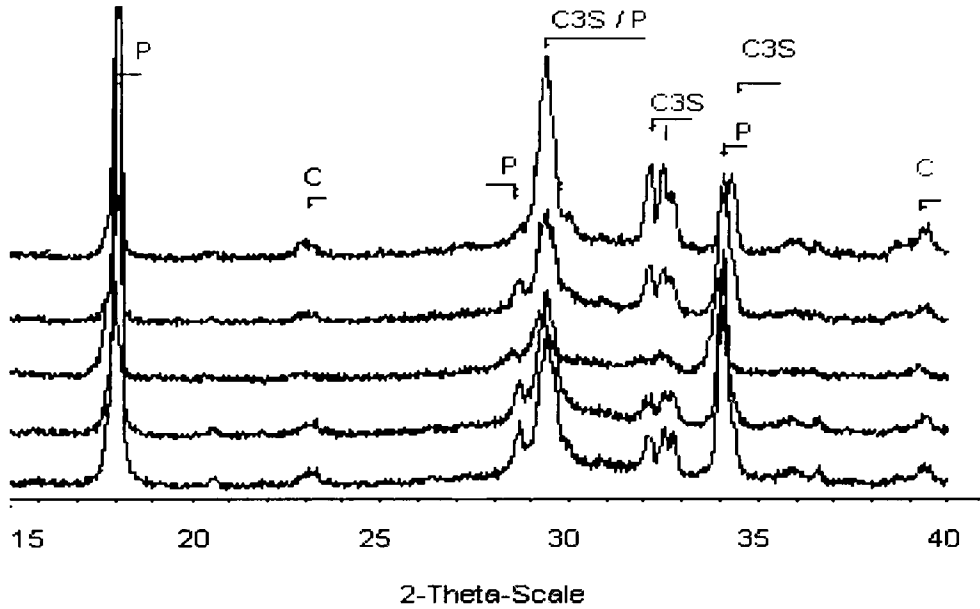


Fig. 4-1. Diffractograms of one-month old  $C_3S$  hydrated pastes (From bottom to top are: control,  $Cr^{3+}$ ,  $Cu^{2+}$ ,  $Pb^{2+}$ , and  $Zn^{2+}$ -doped pastes, Legend: C = calcite, P = portlandite)

The crystalline products of hydrated  $C_3S$  suspensions in the presence or absence of heavy metals at different hydration time are summarised in Table 4-1. According to the variations in X-ray reflection peaks of  $C_3S$  with time, these heavy metals,  $Cu^{2+}$ ,  $Pb^{2+}$  and  $Cr^{3+}$ , promoted the hydration of  $C_3S$  (see Table 4-1). It is also noteworthy that these heavy metals promoted the carbonation of  $C_3S$  suspensions.

Fig. 4-4 presents the diffractograms obtained from hydrated  $C_3S$  suspensions at the age of three months. In contrast to  $C_3S$  pastes containing heavy metals, in hydrated  $C_3S$  suspensions with heavy metals layered double hydroxides of heavy metals and calcium including  $Ca_2Cr(OH)_7 \cdot 3H_2O$ ,  $Ca_2(OH)_4 \times Cu(OH)_2 \cdot mH_2O$  and  $CaZn_2(OH)_6 \cdot 2H_2O$  were

observed. In the hydrated C<sub>3</sub>S suspensions these compounds crystallised, because for all species there were enough mobility and enough time to undergo proper orientation and alignment before bonding into a structure. It was also noted that the control hydrated C<sub>3</sub>S suspension generated the most intense reflections of portlandite, in accordance with the hydrated C<sub>3</sub>S pastes. This confirmed that heavy metals inhibited the precipitation of portlandite due to their hydrolysis with the consequence of reduction of C<sub>3</sub>S suspension pH values.

Table 4-1. The phase development in hydrated C<sub>3</sub>S suspensions

Sample	Effect	Phases identified by XRD		
		14 days	28 days	3 months
Control		Portlandite, C <sub>3</sub> S	Portlandite (I), C <sub>3</sub> S	Portlandite (I)
Cr	promoter	Ca <sub>2</sub> Cr(OH) <sub>7</sub> .3H <sub>2</sub> O Portlandite	Portlandite, Ca <sub>2</sub> Cr(OH) <sub>7</sub> .3H <sub>2</sub> O	Portlandite (I), Calcite, Ca <sub>2</sub> Cr(OH) <sub>7</sub> .3H <sub>2</sub> O
Cu	promoter	Portlandite, CaCuDH	Portlandite, CaCuDH	Portlandite, CaCuDH, Calcite
Pb	promoter	Portlandite	Portlandite	Portlandite, Calcite
Zn	inhibitor	CaZn <sub>2</sub> (OH) <sub>6</sub> .2H <sub>2</sub> O C <sub>3</sub> S	CaZn <sub>2</sub> (OH) <sub>6</sub> .2H <sub>2</sub> O C <sub>3</sub> S	CaZn <sub>2</sub> (OH) <sub>6</sub> .2H <sub>2</sub> O, C <sub>3</sub> S, Vaterite

Note: I-Increase of intensity, D-Decrease of intensity, CaCuDH-Ca<sub>2</sub>(OH)<sub>4</sub>xCu(OH)<sub>2</sub>.mH<sub>2</sub>O (d-space 0.931, 0.646, 0.455, 0.322 nm).

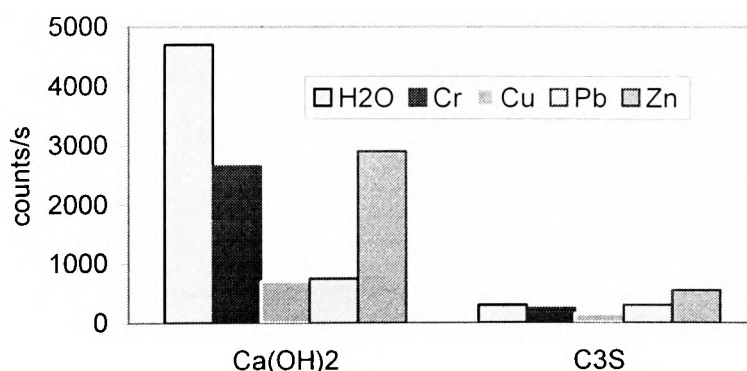


Fig. 4-2. XRD intensity of main phases in one-month old hydrated C<sub>3</sub>S pastes

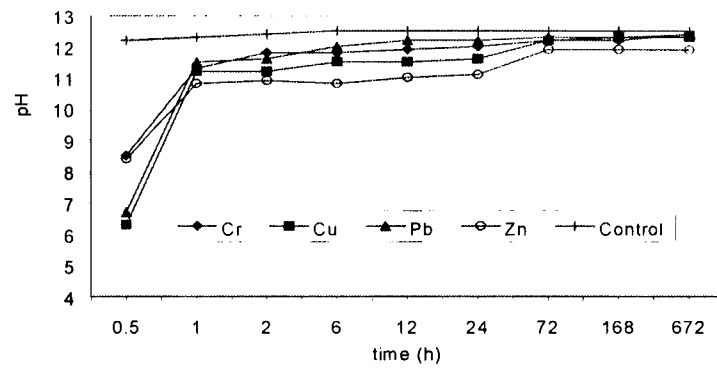


Fig. 4-3. The pH of C<sub>3</sub>S suspensions

As shown in Fig. 4-4, there were no portlandite peaks in the diffractogram obtained from the hydrated Zn -doped C<sub>3</sub>S suspension. Reflection for C<sub>3</sub>S and calcium zincate (CaZn<sub>2</sub>(OH)<sub>6</sub>.2H<sub>2</sub>O) were detected. In fact, in Zn -doped C<sub>3</sub>S suspension, the pH value was below 12 and there were no obvious differences in the XRD patterns for Zn -doped C<sub>3</sub>S suspension at 1 month to 6 months of age, indicating that Zn severely inhibited the hydration of C<sub>3</sub>S. This retardation effect on the hydration of C<sub>3</sub>S could arise from the formation of CaZn<sub>2</sub>(OH)<sub>6</sub>.2H<sub>2</sub>O on C<sub>3</sub>S surfaces, inhibiting the action with water (Yousuf and Mollah, 1995). In contrast, the acceleration effect of Cu, Cr and Pb on the hydration of C<sub>3</sub>S could be attributed to the attack of H<sup>+</sup> resulting from hydrolysis of heavy metals, supporting the theory put forward by Taylor (1997). It is worthy to mention that double hydroxides formed in the Cr or Cu -doped C<sub>3</sub>S suspensions including Ca<sub>2</sub>Cr(OH)<sub>7</sub>.3H<sub>2</sub>O and Ca<sub>2</sub>(OH)<sub>4</sub>Cu(OH)<sub>2</sub>.mH<sub>2</sub>O may not precipitate on the surface of C<sub>3</sub>S and did not keep water from contacting C<sub>3</sub>S, differing from calcium zincate. The interaction mechanism will be discussed further later in this chapter and in the general discussion (Chapter 8).

The diffractograms of one-year old C<sub>3</sub>S pastes are shown in Fig. 4-5. As expected, the intensities of C<sub>3</sub>S peaks were lower than that of the one-month old pastes, indicating that hydration had continued with time.

As mentioned above, some carbonation took place during sample preparation and storage, which may have resulted from CO<sub>2</sub> contained in the original mix water or from air trapped within the sample bottle. As a consequence, in addition to calcite, which was detected in all the pastes examined, vaterite was observed at 25° and 27.1° 2θ in Zn<sup>2+</sup>, Pb<sup>2+</sup> and Cu<sup>2+</sup> -doped pastes, indicating that metals influenced the polymorphism of the calcium carbonate formed.

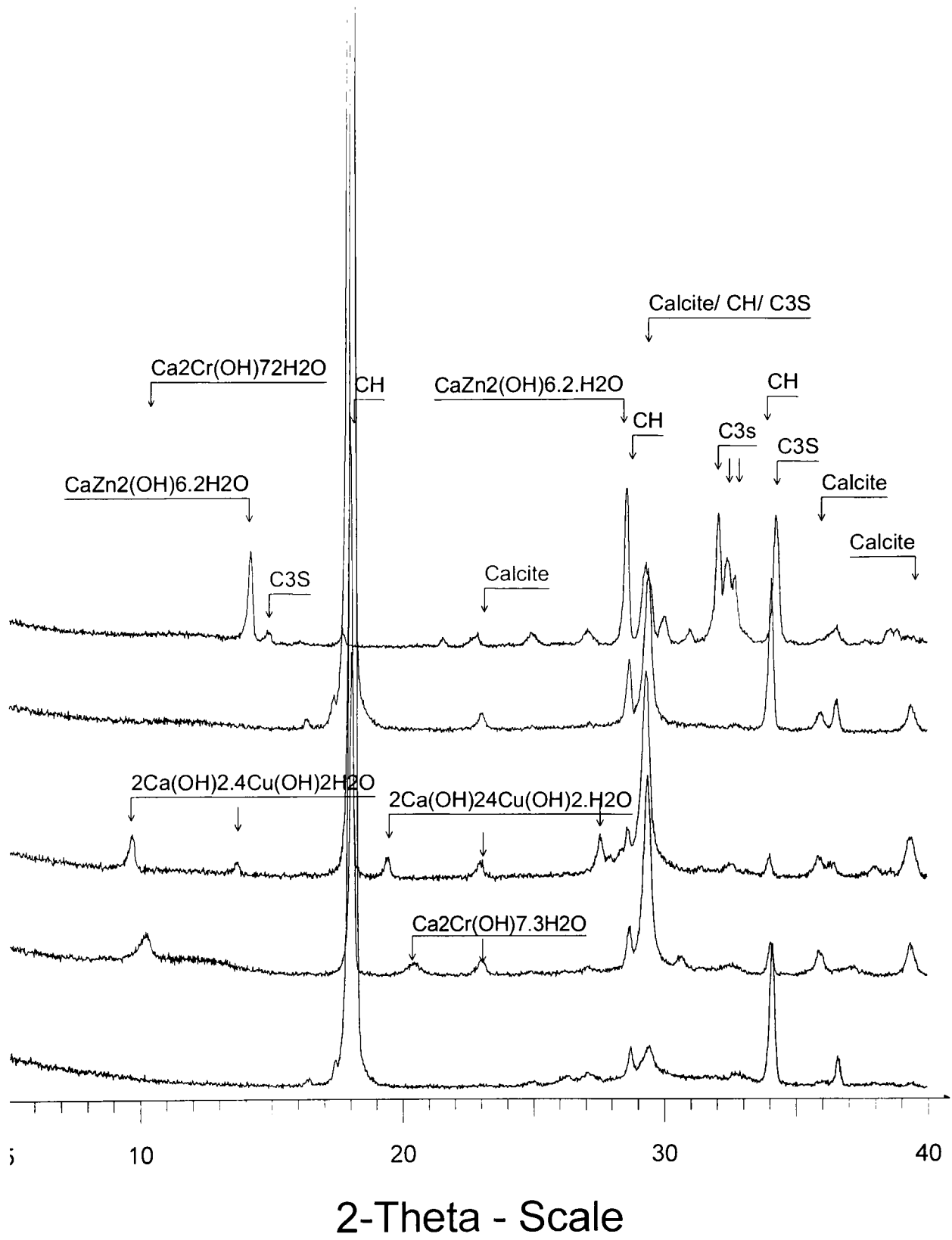


Fig. 4-4. Diffractograms of C<sub>3</sub>S suspensions at the age of three months (From bottom to top are: control, Cr<sup>3+</sup>, Cu<sup>2+</sup>, Pb<sup>2+</sup>, and Zn<sup>2+</sup>-doped suspensions)

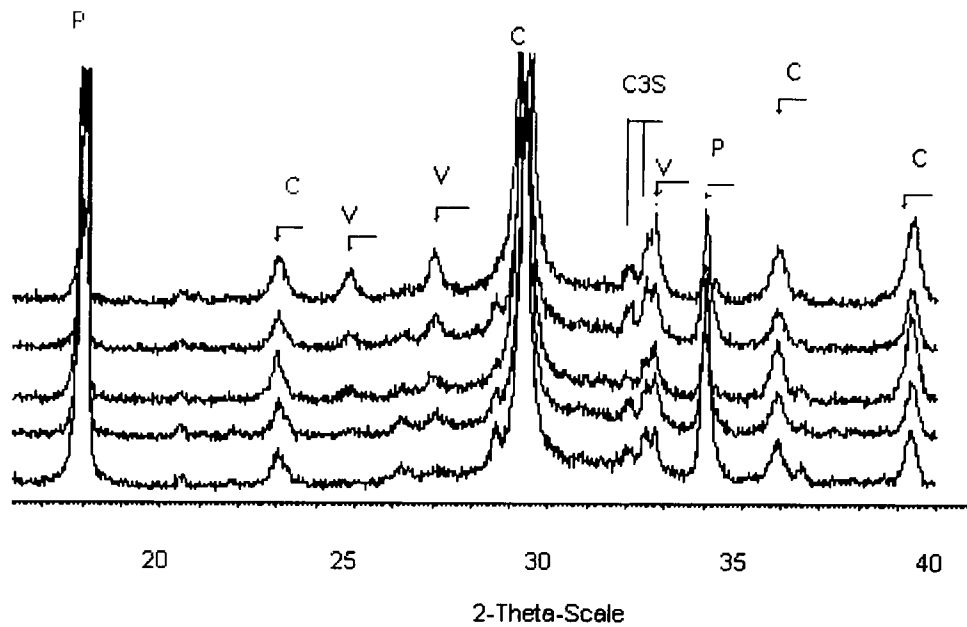


Fig. 4-5. Diffratograms of one-year old hydrated  $C_3S$  pastes

(From bottom to top are: control,  $Cr^{3+}$ ,  $Cu^{2+}$ ,  $Pb^{2+}$ , and  $Zn^{2+}$ -doped pastes, Legend: C = calcite, P = portlandite, V = vaterite)

Compared to one-month old hydrated  $C_3S$  pastes, the intensity of portlandite peaks in one-year old pastes were greater in all samples. The intensities of the portlandite peaks in the  $Cu^{2+}$ -doped paste increased most drastically. It was also noted that the differences between hydrated  $C_3S$  pastes with or without heavy metals of one year of age were very limited in respect of the reflection peak intensities of  $C_3S$  and portlandite.

The DTA curves and simultaneous TG curves of hydrated  $C_3S$  pastes aged 1 month with or without heavy metals are presented in Figs. 4-6 and 4-7. The results are summarised in Table 4-2. The similarity between the DTA curves of hydrated calcium oxide pastes with heavy metals and those of hydrated  $C_3S$  pastes with heavy metals suggests that double hydroxides of heavy metal and calcium such as  $Ca_2Cr(OH)_7 \cdot 3H_2O$ ,  $Ca_2(OH)_4xCu(OH)_2 \cdot mH_2O$  and  $CaZn_2(OH)_6 \cdot 2H_2O$  formed in these systems. The formations of amorphous double hydroxides associated with heavy metals in the hydrated heavy metal -doped  $C_3S$  pastes were responsible for many endothermic reactions occurred during the heating processes. As described earlier, in the  $C_3S$  suspensions doped with heavy metals these double hydroxides were identified as crystalline phases using XRD. It

is noted that the TG curves of hydrated  $C_3S$  were very different from those of hydrated calcium oxide. In other words, the amount of products changed significantly.

As shown in Fig. 4-6, heavy metals caused the enlargement of the exothermic peak at 110-200°C. From the curves of DTA/TG it can be seen that the heavy metals influenced the formation of portlandite, decreasing of the endothermic peak intensity and weight loss corresponding to the dehydroxylation of calcium hydroxide.

In the control paste, the endothermic peaks of portlandite dehydroxylation at 460-510°C and calcite decomposition at 650-750°C were observed. The presence of calcite can be attributed to carbonation during the sample preparation and storage. It was noted that the mass loss was continuous from 30°C to 800°C. Excluding a very small initial loss of weight due to evaporation of water from the paste, largely in C-S-H gel, at 110°C approximately, two steps of mass loss in the TG curve corresponding to dehydroxylation of portlandite and decomposition of calcite were notable. According to the amount of mass loss, the portlandite content and calcite content in the control paste were 16.7% and 16.81%, respectively. TG results indicate that the free water and combined water in C-S-H gel were 5.9%.

In the hydrated chromium-doped  $C_3S$  paste, there were five major endothermic peaks in the DTA curves, located at 50-170°C, 280-310°C, 390-430°C, 450-500°C and 650-780°C. The first endothermic peak can be attributed to the evaporation of physically and chemically bound water in C-S-H gel in the paste. The second peak could be due to the dehydration of double hydroxide of calcium and chromium ( $Ca_2Cr(OH)_7 \cdot 3H_2O$ ). This peak was exactly in the same range of temperature as endotherm of  $Ca_2Cr(OH)_7 \cdot 3H_2O$  in the hydrated Cr-doped calcium oxide paste. The third peak arose from the decomposition of double hydroxide of calcium and chromium. The fourth endothermic peak and corresponding to mass loss can be attributed to dehydroxylation of  $Ca_2Cr(OH)_7 \cdot 3H_2O$  and dehydroxylation of portlandite. The fifth endothermic peak at 650-800°C was due to the decomposition of calcium carbonate. The calculated portlandite content in the hydrated Cr-doped paste was 5.5%, but the actual portlandite content might be lower than that, because the mass loss in the range of 390-430°C includes the dehydroxylation of double hydroxide. The calcium carbonate content in the Cr-doped paste (29.32%) was much

higher than that in the control paste (16.81%), indicating that the presence of chromium promoted the natural carbonation of the C<sub>3</sub>S paste.

The hydrated Cu-doped C<sub>3</sub>S paste also exhibited similar endothermic peaks to the hydrated Cu-doped calcium oxide paste, but the mass loss steps occurred continuously in the temperature range of 30-860°C with different slopes at different temperatures. The endothermic peak and mass loss corresponding to portlandite was very small, which indicated that its content was very limited, as indicated by XRD. The endothermic peak in the temperature range of 250-400°C was due to the decomposition of double hydroxide of copper and calcium (Ca<sub>2</sub>(OH)<sub>4</sub>xCu(OH)<sub>2</sub>.mH<sub>2</sub>O). The dehydroxylation mechanism of this compound was presented in Chapter 3. The calculated portlandite content and calcium carbonate content were 5.4% and 29.32%, respectively.

The DTA curve and TG curve of the hydrated Pb-doped C<sub>3</sub>S paste was similar to those of the control paste. The mass loss of portlandite was, however, smaller than that of the control paste. The calculated portlandite content was 7.1% and calculated calcium carbonate content was 27.72%.

In the hydrated Zn -doped C<sub>3</sub>S paste, there were three endothermic peaks. The mass loss in 170-200°C was attributed to the dehydration of calcium zincate (CaZn<sub>2</sub>(OH)<sub>6</sub>.2H<sub>2</sub>O) in the paste. The second endothermic peak could arise from the dehydroxylation of calcium zincate (CaZn<sub>2</sub>(OH)<sub>6</sub>.2H<sub>2</sub>O). The third endothermic peak was due to the decomposition of calcium carbonate. No endothermic peak of the dehydroxylation of portlandite was detected and consistent with the XRD results. The calcium carbonate content, according to the mass loss, was 12.27%.

It was noted that in the C<sub>3</sub>S pastes doped with heavy metals, the decomposition temperature of calcium carbonate shifted upwards, compared to the control C<sub>3</sub>S paste, possibly due to these metal substitutions for calcium in calcium carbonate or the adsorption of heavy metals on the surface of calcium carbonate.

As all samples investigated were dry, the total mass loss of the paste reflected the degree of hydration. According to total mass loss the degree of hydration was in the sequence:

Cr > Cu > Pb > Control > Zn

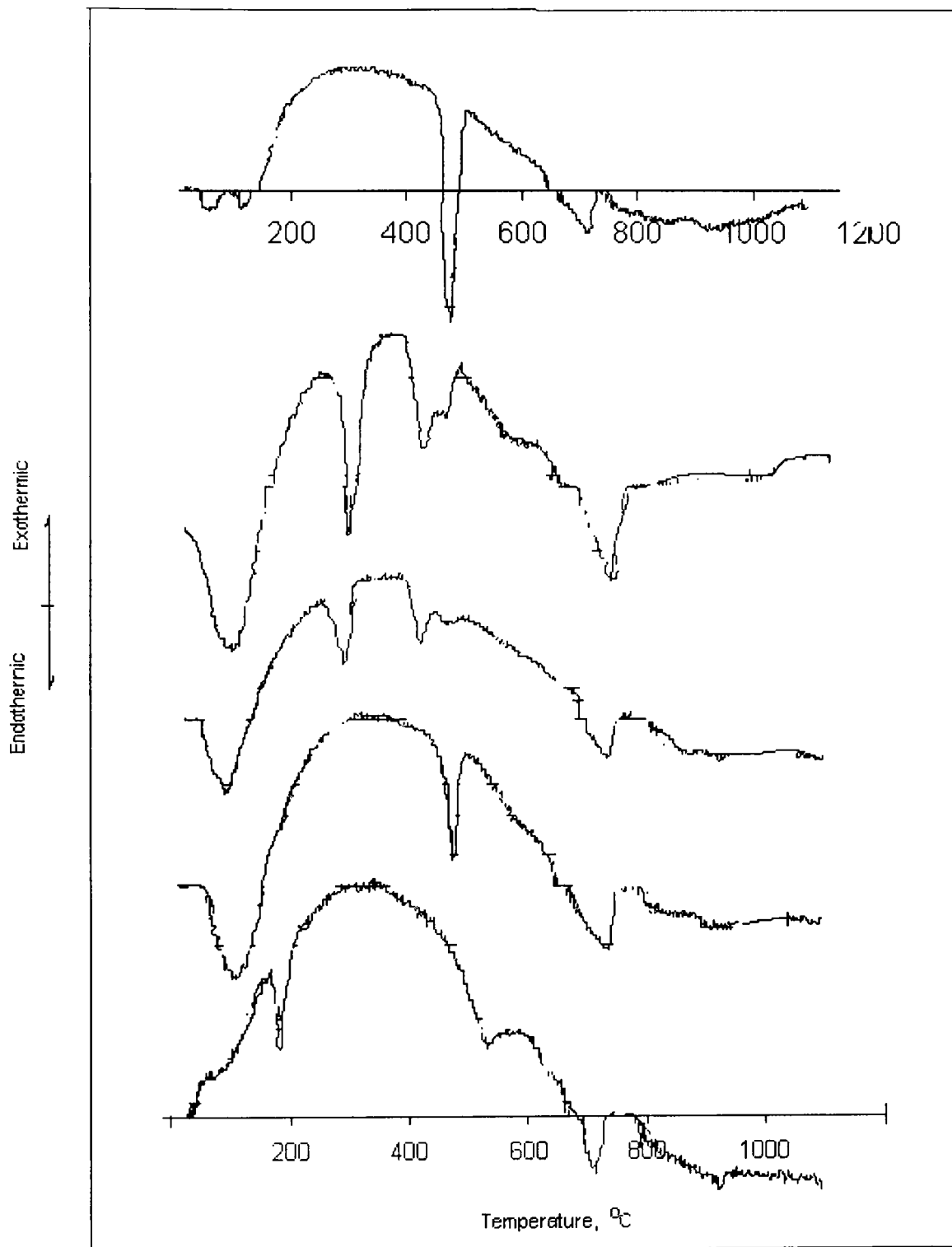


Fig. 4-6. DTA curves of hydrated  $C_3S$  pastes  
(From top to bottom are: control, Cr, Cu, Pb, and Zn -doped samples)

Table 4-2. Thermal analysis results of hydrated  $C_3S$  pastes (mass loss at indicated temperature, %)

Samples	Control	Cr	Cu	Pb	Zn
20-250°C	5.9	12.1	12.3	11.5	4.2
250-600°C	6.9	12.1	10.7	6.9	4.6
600-1100°C	7.4	12.9	12.9	12.2	5.4
Total mass loss	20.2	37.1	35.9	30.6	14.2
Ca(OH) <sub>2</sub> content	16.7	5.5	5.4	7.1	0
CaCO <sub>3</sub> content	16.81	29.32	29.32	27.72	12.27

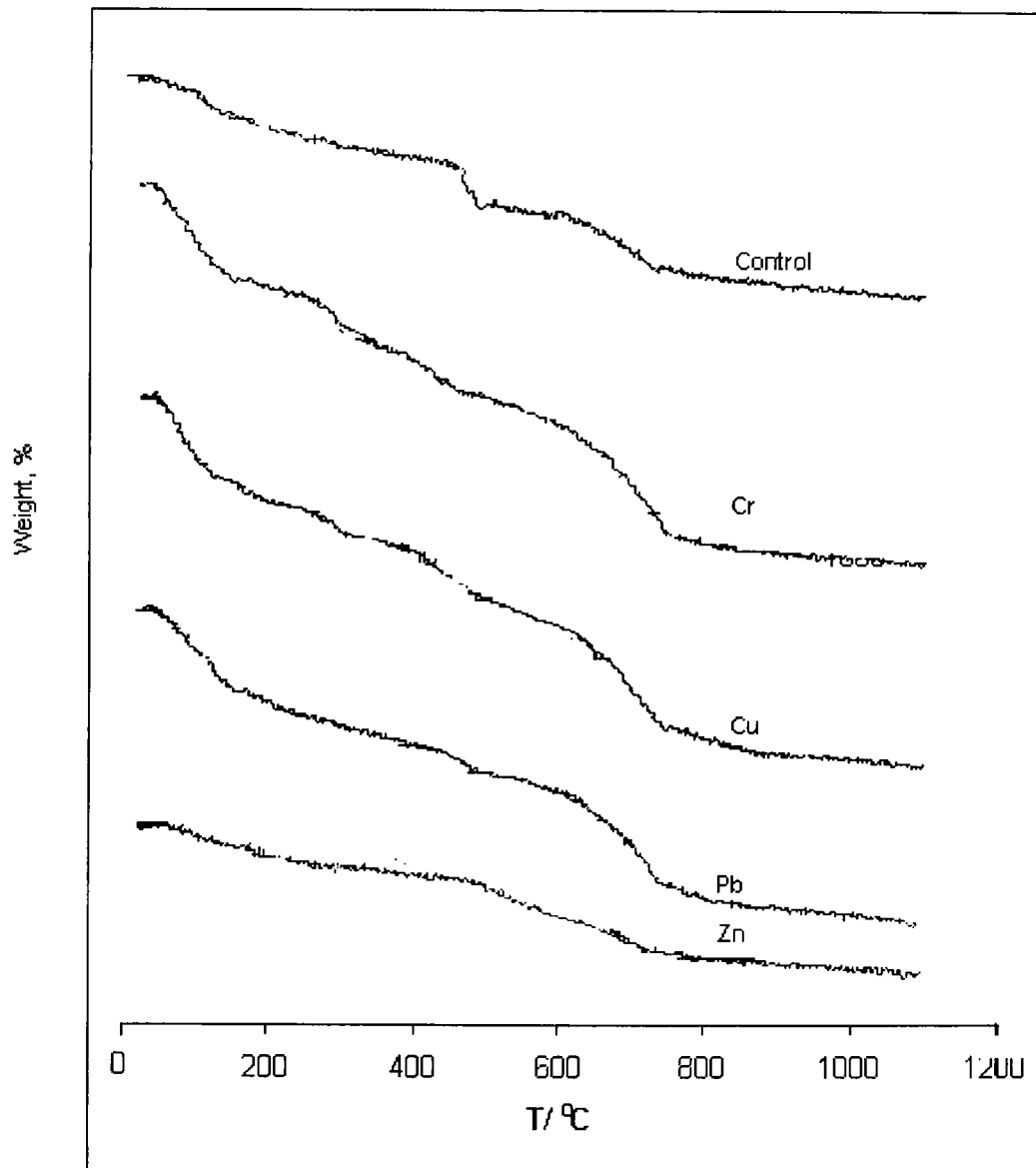


Fig. 4-7. TG curves of hydrated  $C_3S$  pastes  
(From top to bottom: control,  $Cr^{3+}$ ,  $Cu^{2+}$ ,  $Pb^{2+}$ , and  $Zn^{2+}$ -doped pastes)

Table 4-3. The evaluation of average Ca/Si ratio in C-S-H gel derived from thermal analysis results

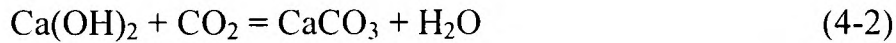
Content (%)	Control	Cr	Cu	Pb	Zn
Ca(OH) <sub>2</sub>	16.7	5.5	5.4	7.1	0
CaCO <sub>3</sub>	16.81	29.32	29.32	27.72	12.27
H <sub>2</sub> O	12.8	24.2	23.0	18.4	8.8
C <sub>3</sub> S	87.2	75.8	77.0	81.6	91.2
T Ca	45.89	39.89	40.53	42.95	48
T Si	10.73	9.32	9.47	10.04	11.22
Ca in CH	9.02	2.97	2.91	3.84	0.76
Ca in CC	6.72	11.73	11.73	11.09	4.91
Ca in C-S-H	30.15	25.19	25.89	28.02	42.33
Si in C-S-H	10.73	9.32	9.47	10.04	11.22
Ca/Si, α:100%	1.97	1.89	1.91	1.95	2.64
Ca/Si, α: 80%	1.71	1.61	1.64	1.69	2.61

Thermal analyses in this work confirmed that Pb<sup>2+</sup>, Cu<sup>2+</sup> and Cr<sup>3+</sup> promoted hydration of C<sub>3</sub>S, whereas Zn<sup>2+</sup> retarded the hydration of C<sub>3</sub>S. It is worth noting that the degree of hydration was not in accordance to the amount of portlandite observed. TG results demonstrated that the amount of portlandite in the C<sub>3</sub>S pastes was in the increasing order:

$$\text{Control} > \text{Pb} > \text{Cr} = \text{Cu} \gg \text{Zn}$$

DTA/TG results confirmed that heavy metals retarded the formation of portlandite, which are consistent with the examination by XRD, with reference to the peak intensities of portlandite at 18.1° 2θ and C<sub>3</sub>S at 32-33° 2θ. In other words, the differences in intensities of X-ray reflection peaks between pastes under the same operating conditions reflect the content of the phases. From DTA/TG results (Table 4-2), it can be seen that heavy metals investigated promoted the natural carbonation except Zn. These results are also consistent with the results of the investigation by XRD.

It is possible to estimate the average Ca/Si ratio of C-S-H gel according to the amount of portlandite and calcite in the samples using the following reactions.



The calculation results are presented in Table 4-3. The average Ca/Si ratio of C-S-H gel in different pastes at the different degrees of hydration ( $\alpha$ ) was in the range of 1.6-1.9 for most of the pastes. It should point out that the calculated Ca/Si ratio of C-S-H gel in the Zn -doped  $\text{C}_3\text{S}$  paste was not very accurate, because the degree of hydration may be much lower than 80% due to the retardation of calcium zincate. If the formation of double hydroxides of calcium and heavy metals was taken into account, the ratios of C-S-H gel in heavy metal -doped pastes may have been lower than values showed in Table 4-3.

### 4.3.2 Accelerated carbonation

Fig. 4-8 shows the pH of  $\text{C}_3\text{S}$  suspensions with an increasing number of carbonation cycles. The pH decreased when the number of carbonation cycles increased. It was also noted that pH increased with time away from contacting with  $\text{CO}_2$  due to decomposition of  $\text{C}_3\text{S}$ , if carbonation of  $\text{C}_3\text{S}$  was not complete. For example, at the 3<sup>rd</sup> cycle of carbonation, the pH values of  $\text{C}_3\text{S}$  suspensions reached 10 or above at < 2 hours, indicating that anhydrous  $\text{C}_3\text{S}$  was present and able to hydrate.

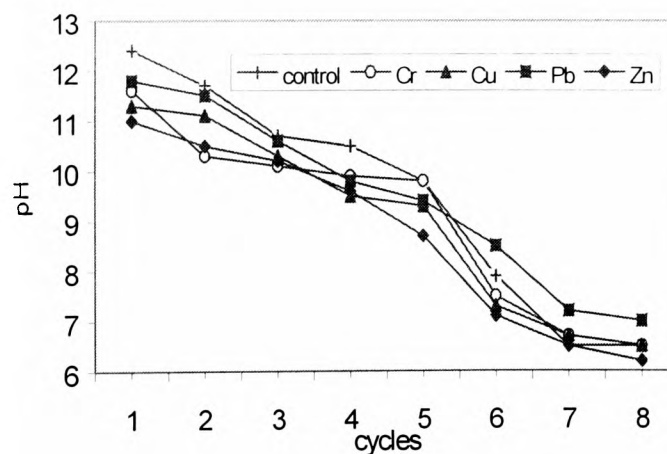


Fig. 4-8. The pH of  $\text{C}_3\text{S}$  suspensions, 1 hour after carbonation

Fig. 4-9 shows that after 8 cycles of carbonation the suspension pHs were <9 and stable up to 10 days of age, indicating that carbonation was complete and no anhydrous  $C_3S$  remained.

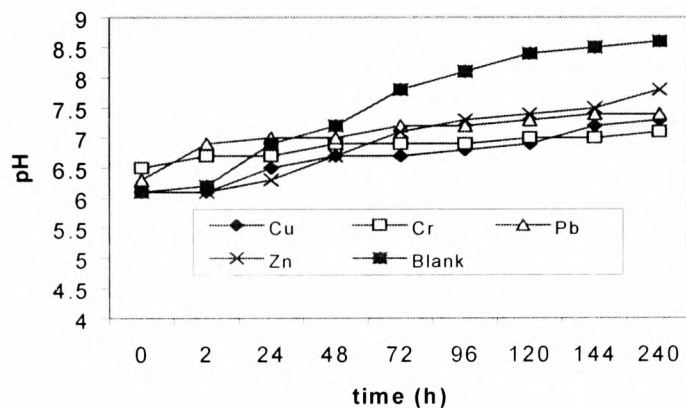


Fig. 4-9. The pH of  $C_3S$  suspensions after 8 cycles of carbonation

The pHs of carbonated metal hydroxides placed in water as suspensions are shown in Fig. 4-10. The similarity between the suspensions in Figs. 4-9 and 4-10 suggests that the carbonation was complete.

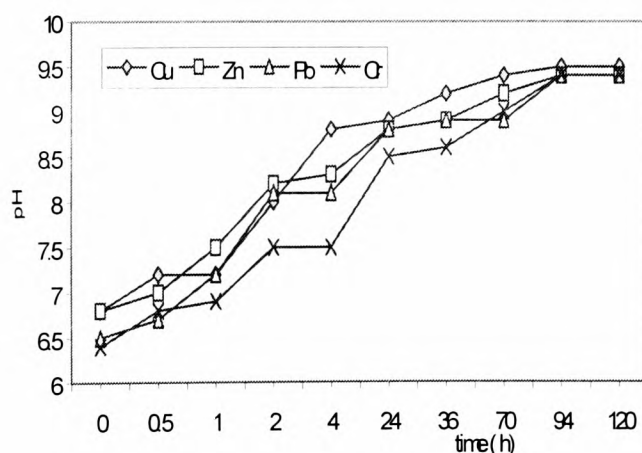


Fig. 4-10. The pH of carbonated metal hydroxide suspensions

The diffractograms obtained from carbonated  $C_3S$  suspensions in the absence or presence of heavy metals after 8 cycles of carbonation are presented in Figs. 4-11 and 4-12. Table

4-4 summarises the XRD results of carbonated C<sub>3</sub>S suspensions at different times. The main peaks of C<sub>3</sub>S between 32-33° 2θ were absent in all samples, indicating that the carbonation was complete. Although the essential product of carbonated C<sub>3</sub>S suspensions was calcite, it needs to address some points here.

In the carbonated Zn -doped suspension of C<sub>3</sub>S at 2 weeks of age, the calcium zincate (CaZn<sub>2</sub>(OH)<sub>6</sub>·2H<sub>2</sub>O) was detected by XRD. It vanished after that time. No other heavy metal compounds were detectable at any time, unlike the hydrated C<sub>3</sub>S suspensions, in which double hydroxides of heavy metal and calcium, Ca<sub>2</sub>(OH)<sub>4</sub>xCu(OH)<sub>2</sub>.mH<sub>2</sub>O, CaZn<sub>2</sub>(OH)<sub>6</sub>·2H<sub>2</sub>O, and Ca<sub>2</sub>Cr(OH)<sub>7</sub>·3H<sub>2</sub>O were present. Without doubt, in the carbonated C<sub>3</sub>S suspensions, heavy metal ions were absorbed by calcium carbonate or low Ca/Si ratio C-S-H gel including silica gel.

Aragonite and vaterite, the metastable polymorphs of calcium carbonate, were identified in the Zn<sup>2+</sup> -doped samples. The peaks of aragonite are located at 26.5°, 27.2°, 33.1°, 37.2°, 37.7° and 38.5° 2θ. Vaterite (25° and 27° 2θ) has a hexagonal structure and is similar to aragonite (orthorhombic) but differs appreciably from calcite (rhombohedral). Interestingly, it was noted that the peak intensities of calcite were very weak in the carbonated Zn -doped suspension of C<sub>3</sub>S. The presence of aragonite and vaterite in the Zn<sup>2+</sup>-doped samples could be attributed to partial zinc ion adsorption on the surface of calcium carbonate with a consequent improvement in the stability of these metastable phases.

The diffractograms of the carbonated C<sub>3</sub>S pastes after 8 cycles of carbonation are shown in Fig.4-13. As expected, calcite was major product of C<sub>3</sub>S carbonation in all pastes. Aragonite was identified in the Cu<sup>2+</sup> -doped paste (at 26.5°, 33.1° and 38.5° 2θ). The main peaks of C<sub>3</sub>S between 32-33° 2θ were absent in all pastes.

The accelerated carbonated pastes cured in CO<sub>2</sub> bags for one year did not change their diffractograms very much (Fig. 4-14). After one year, in the Cu<sup>2+</sup> -doped paste both calcite and aragonite were present, indicating that it had transformed to calcite in accordance with the Ostwald step rule. The presence of aragonite in the Cu -doped paste could be attributed to partial Cu<sup>2+</sup> substitution for Ca<sup>2+</sup> or adsorption on the surface of calcium carbonate, consequently affecting the conversion of CaCO<sub>3</sub>. The X-ray reflection

intensities of the main peaks of  $C_3S$  (between  $32-33^\circ 2\theta$ ) were lower in the carbonated samples than those in the hydrated samples at the same age, indicating that more of this phase had reacted in the former.

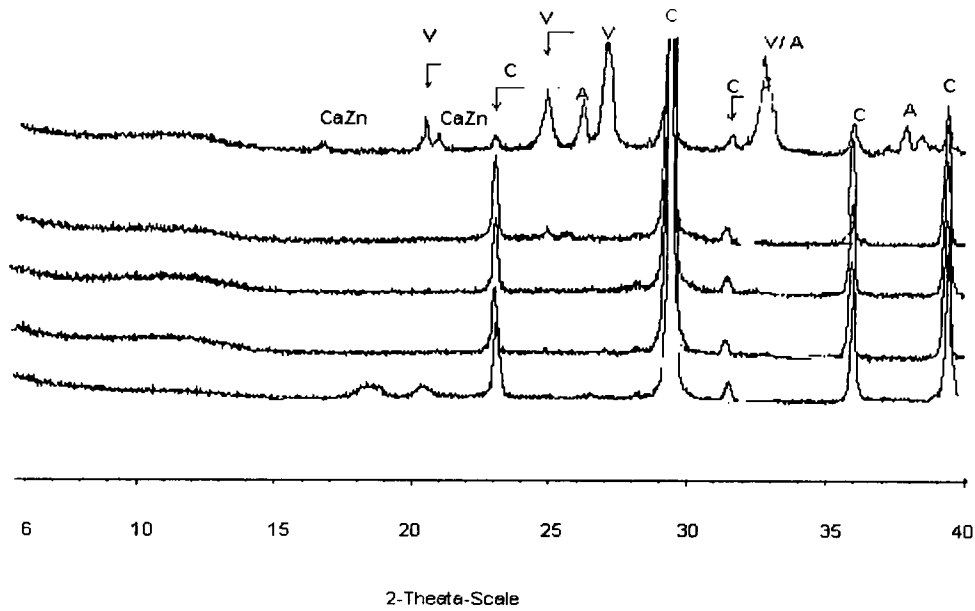


Fig. 4-11. Diffractograms of carbonated  $C_3S$  suspensions at the age of 2 weeks

(From bottom to top: control, Cr, Cu, Pb, and Zn -doped samples, Legend: C = calcite, A = aragonite, V = vaterite, CaZn = calcium zincate)

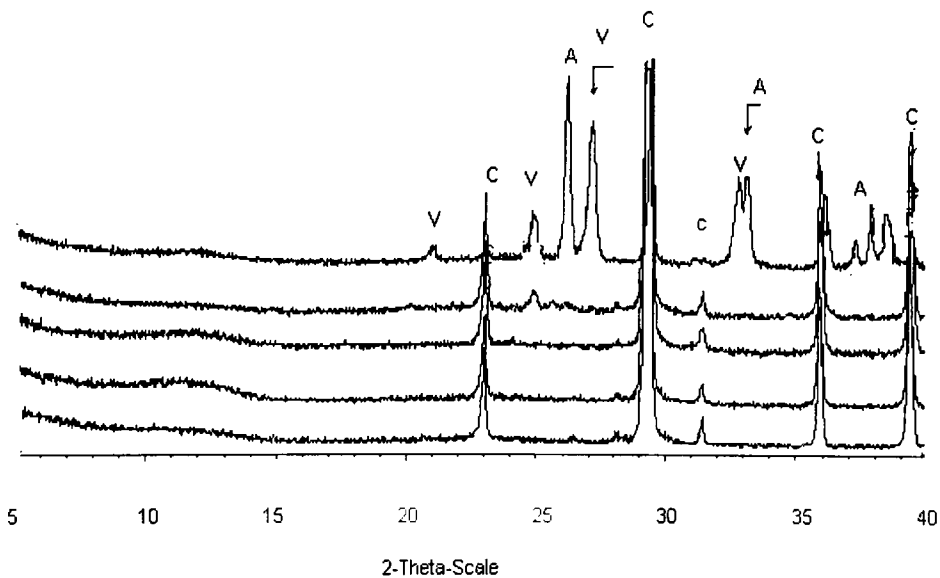


Fig. 4-12. Diffractograms of carbonated  $C_3S$  suspensions at the age of 1 month

(From bottom to top: control, Cr, Cu, Pb and Zn -doped samples, Legend: C = calcite, A = aragonite, V = vaterite)

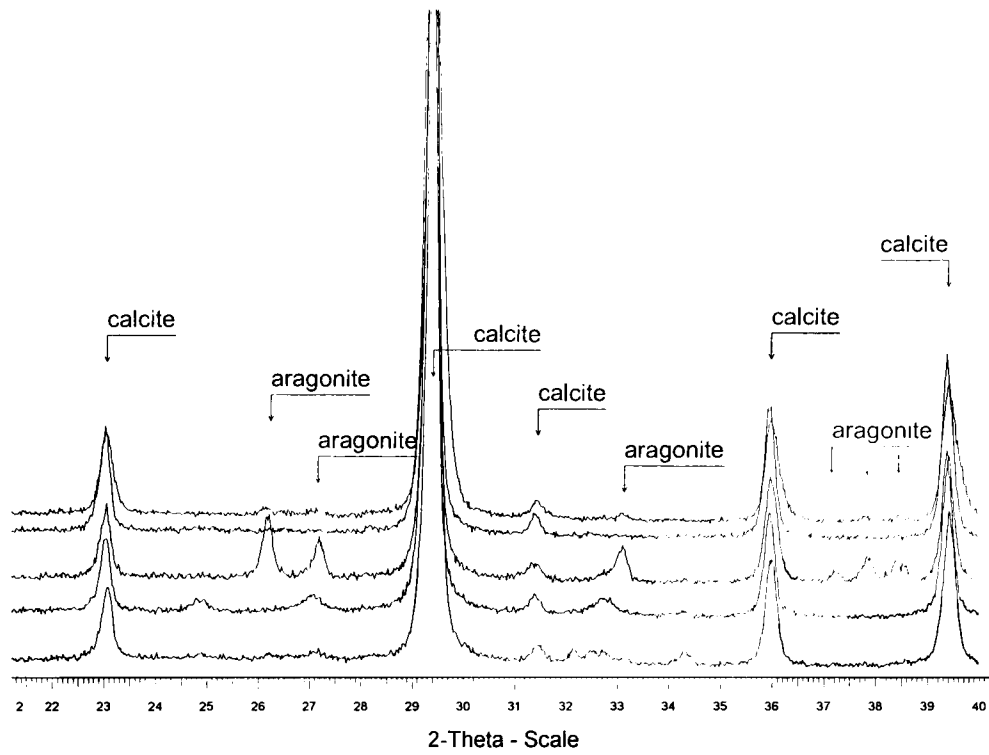


Fig. 4-13. Diffractograms of carbonated  $C_3S$  pastes aged 1 month (From bottom to top: control,  $Cr^{3+}$ ,  $Cu^{2+}$ ,  $Pb^{2+}$ , and  $Zn^{2+}$ -doped pastes)

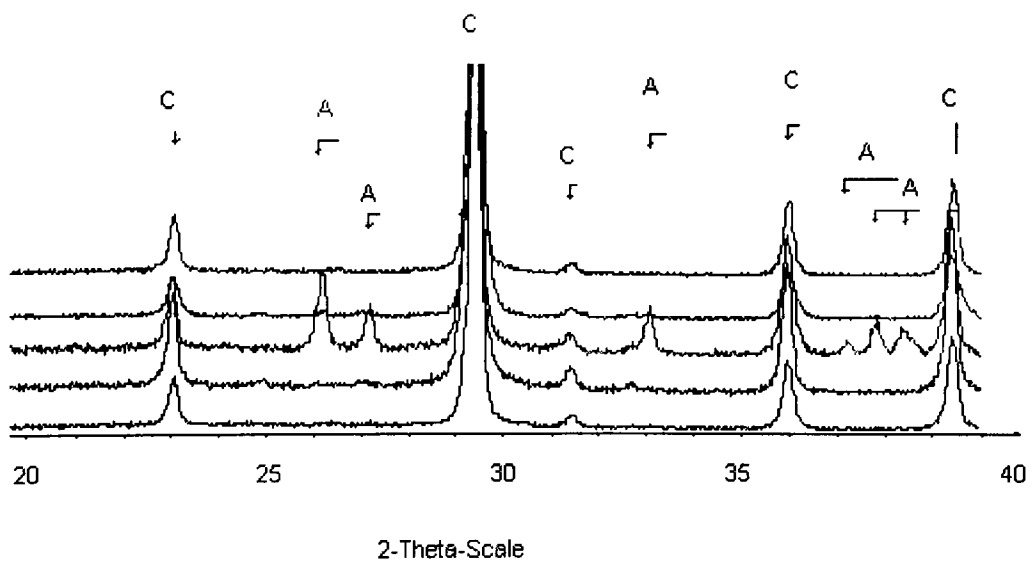


Fig. 4-14. Diffractograms of carbonated  $C_3S$  pastes aged 1 year (From bottom to top: control,  $Cr^{3+}$ ,  $Cu^{2+}$ ,  $Pb^{2+}$ , and  $Zn^{2+}$ -doped pastes, Legend: C = calcite, A = aragonite, V = vaterite)

Table 4-4. Phase development in carbonated C<sub>3</sub>S suspensions

Sample	Phases identified by XRD		
	14 days	28 days	3 months
Contr.	Calcite	Calcite	Calcite
Cr	Calcite	Calcite	Calcite
Cu	Calcite	Calcite	Calcite
Pb	Calcite, Vaterite	Calcite, Vaterite	Calcite
Zn	Calcite, Aragonite, Vaterite, CaZn <sub>2</sub> (OH) <sub>6</sub> 2H <sub>2</sub> O	Calcite, Aragonite, Vaterite	Calcite, Aragonite, Vaterite

In order to characterise the carbonation products of C<sub>3</sub>S and to explore the mechanism of incorporation of heavy metal in the carbonated C<sub>3</sub>S pastes, the thermal analysis techniques were employed. The DTA curves and simultaneous TG curves of carbonated C<sub>3</sub>S aged one month are presented in Figs. 4-15 and 4-16. Table 4-5 presents the thermal analysis results and estimated content of calcium carbonate.

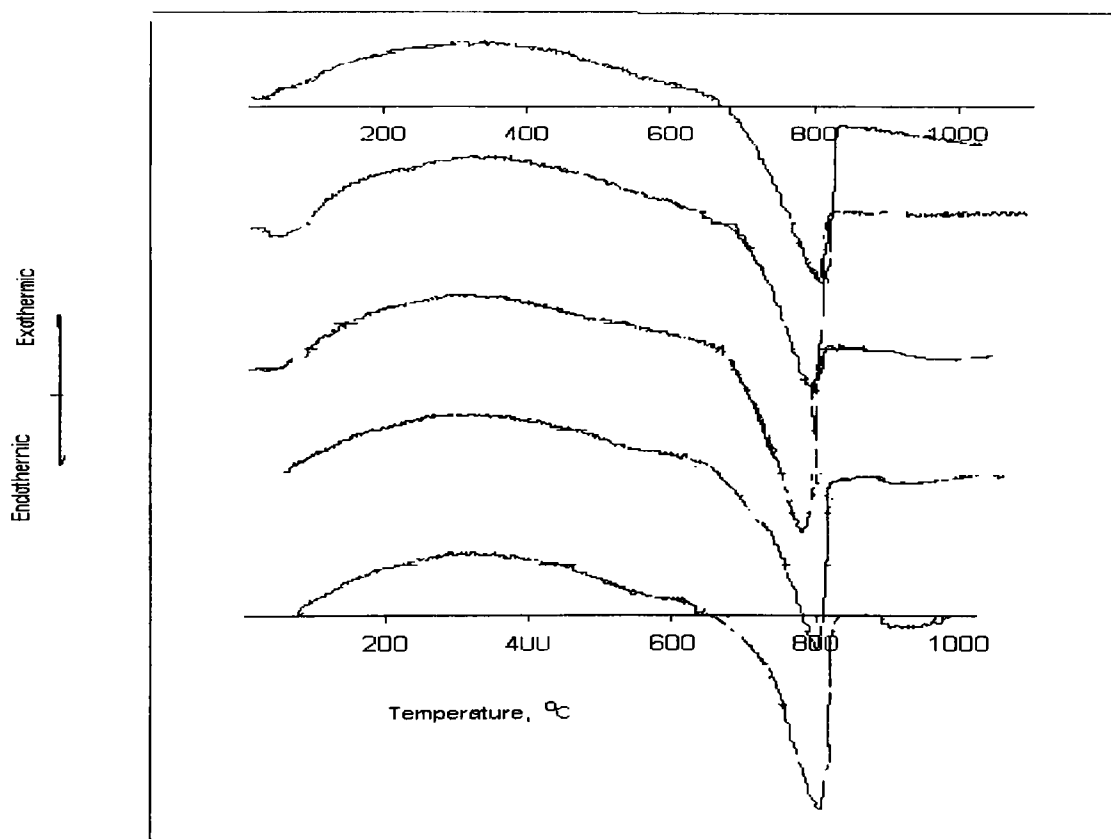


Fig. 4-15. DTA curves of carbonated C<sub>3</sub>S pastes  
(From top to bottom: control, Cr<sup>3+</sup>, Cu<sup>2+</sup>, Pb<sup>2+</sup>, and Zn<sup>2+</sup>-doped pastes)

Table 4-5. Thermal analysis results of carbonated C<sub>3</sub>S pastes (mass loss at indicated temperature, %)

Samples	Control	Cr	Cu	Pb	Zn
20-250°C	3.1	5.2	3.6	2.3	3.3
250-600°C	4.2	5.5	5.6	4.4	5.4
600-1100°C	33.4	31.1	31.7	32	32
Total mass loss	40.7	41.8	40.9	38.7	40.7
CaCO <sub>3</sub>	75.9	70.68	72.04	72.73	72.72
T Ca in the paste	31.21	30.63	31.1	32.26	31.21
T Si in the paste	7.29	7.16	7.27	7.54	7.29
Ca in C-S-H gel	0.85	2.36	2.28	3.17	2.12
Ca/Si (average)	0.08	0.23	0.22	0.29	0.20

In all carbonated pastes, the only endothermic peak for calcite decomposition was detected, which excludes the formation of amorphous compounds associated with heavy metals. Correspondingly, one mass loss step due to decomposition of calcium carbonate in the TG curve was very steep. According to the amount of mass loss, it was calculated that in the control paste, Cr, Cu, Pb and Zn -doped pastes the calcium carbonate contents were 69%, 63%, 65%, 65% and 66%, respectively. Based on the thermal analysis results, we can calculate the average Ca/Si ratio of C-S-H in the carbonated pastes of C<sub>3</sub>S (Table 4-5). The average ratio of C-S-H gel was in the range of 0.08-0.29. It can be concluded that the carbonation resulted in the formation of very low Ca/Si ratio C-S-H gel; the average ratio of Ca/Si in the carbonated heavy metal -doped C<sub>3</sub>S pastes was slightly higher than that of the control C<sub>3</sub>S paste.

In all experiments conducted with carbonated C<sub>3</sub>S in the presence of heavy metals, no metal-containing compounds were detected in the carbonated pastes and fully carbonated C<sub>3</sub>S suspensions, despite the high levels of metal doping. It is noted that the presence of heavy metals did influence the polymorphism and conversion rate of crystalline calcium carbonate. In addition, it is noted that the decomposition temperature ranges of calcium carbonate in all heavy metal -doped pastes were close but different from that in the carbonated C<sub>3</sub>S control paste. The downwards shift of decomposition temperature of

calcium carbonate could be attributed to adsorption of heavy metals on the surface of calcium carbonate or heavy metal entries into the lattice of calcium carbonate. As a result, the thermal stability of calcium carbonate decreased.

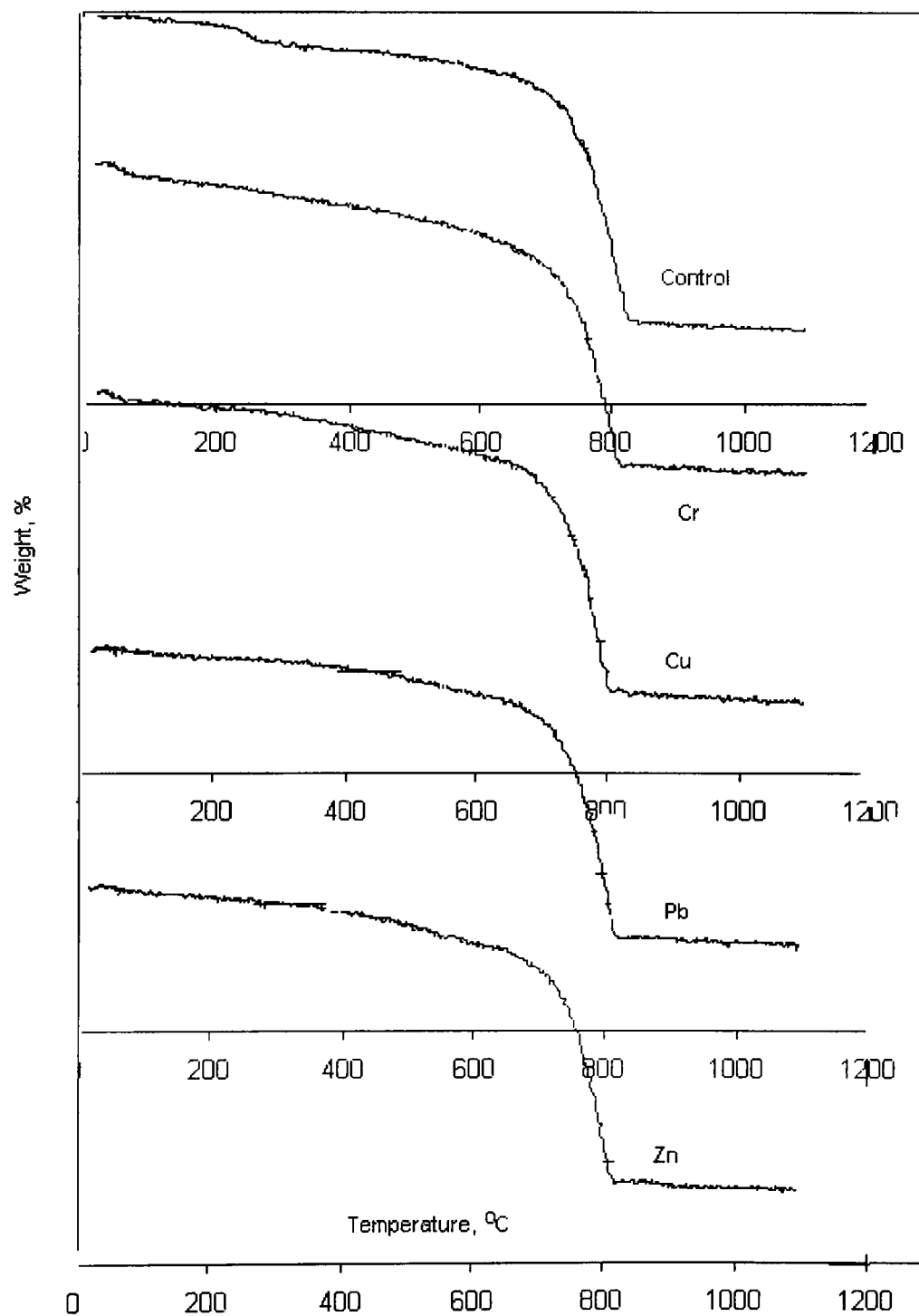


Fig. 4-16. TG curves of carbonated C<sub>3</sub>S pastes  
(From top to bottom: control, Cr<sup>3+</sup>, Cu<sup>2+</sup>, Pb<sup>2+</sup>, and Zn<sup>2+</sup>-doped pastes)

Heavy metal substitution for calcium occurs in the nature frequently (Deer *et al.*, 1982). Smithsonite ( $\text{ZnCO}_3$ ) and cerrusite ( $\text{PbCO}_3$ ) can occur naturally and are related structurally to calcite and aragonite;  $\text{CaBa}(\text{CO}_3)_2$  is also found in nature and has a similar structure to aragonite.

In mineralogy, the calcium atom position in portlandite and calcite can be replaced by different elements including Cd, Mn, Fe(2), Co, Ni, Zn, Mg, Sr, Ba, and Pb to form solid solutions, in which the electric configuration rather than ionic size influences M-O bond length and substitution (Deer *et al.*, 1982).

It should point out that the amount of substitution of heavy metal ions for calcium ions in the lattice of calcium carbonate might be very limited, because there was no observable XRD peak shift of calcium carbonate in the diffractograms of the carbonated samples. If a large number of heavy metal ions entered the lattice of calcium carbonate, the dimension of unit cell will have changed with resultant change of the  $2\theta$  position.

Besides C-S-H gel, fresh calcium carbonate also has a high capacity of absorbing heavy metal ions due to chemical adsorption. This is the reason that the carbonated pastes and suspensions of  $\text{C}_3\text{S}$  in the presence of heavy metals were devoid of heavy metal compounds.

#### **4.3.3 Silicate polymerisations in the hydrated and carbonated $\text{C}_3\text{S}$ pastes**

According to the DTA/TG results, the hydrated  $\text{C}_3\text{S}$  pastes were dominated by C-S-H gel (around 65% by mass). In the carbonated pastes the content of low Ca/Si ratio C-S-H or silica gel was close to 30%. The structures and properties of C-S-H gel influenced the incorporation of heavy metals (Cong and Kirkpatrick, 1996; Sun *et al.*, 1999).

Solid state magic angle spinning/nuclear magnetic resonance (MAS/NMR) was employed to study the structure of calcium silicate gel in the  $\text{C}_3\text{S}$  pastes at the age of one year. High resolution solid  $^{29}\text{Si}$  NMR techniques provided valuable molecular information.

Fig. 4-17 shows the  $^{29}\text{Si}$  NMR spectra of hydrated  $\text{C}_3\text{S}$  pastes with or without heavy metals. The differences in the polymerisation of calcium silicate hydrate gel are

summarised in Table 4-6. The degree of hydration of  $C_3S$ , average length (in terms of number of Si) in C-S-H gel ( $\Psi$ ), connectivity ratio ( $C$ ) and Ca/Si ratio were determined by the following equations (Engelhardt and Michel, 1987; Lin *et al.*, 1997):

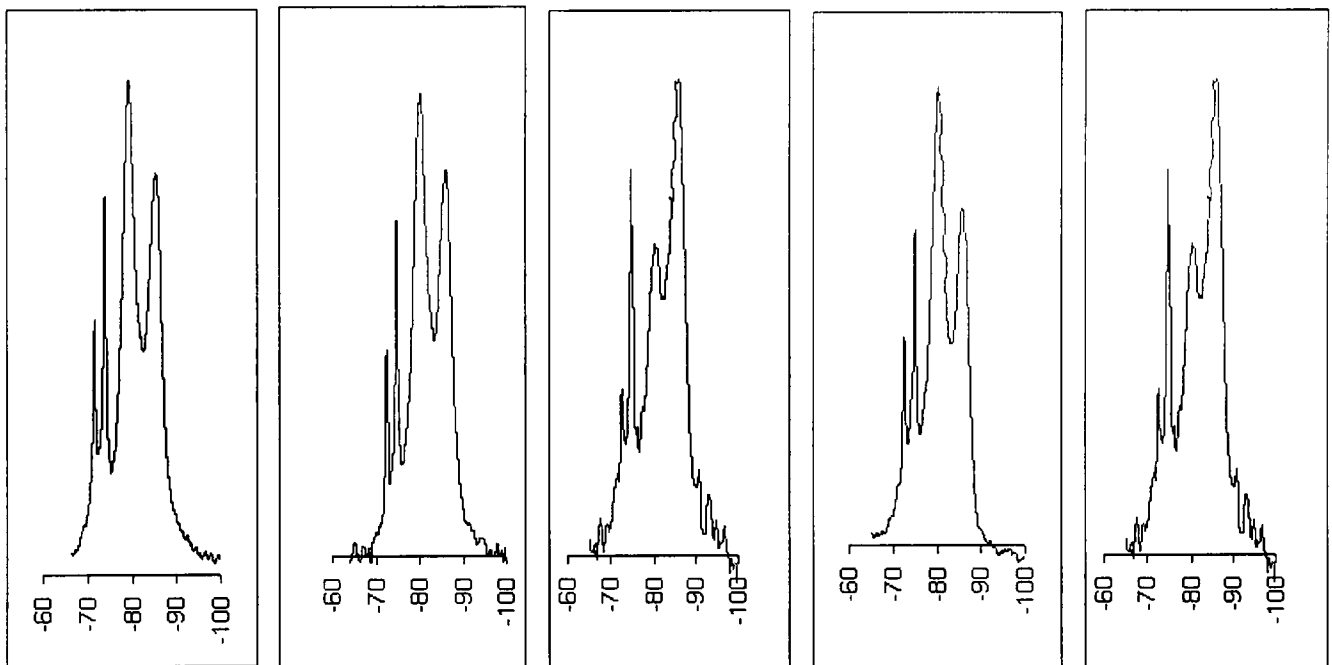
$$\Psi = 2(1 + I(Q_2)/I(Q_1)), \text{ and}$$

$$C = (Q_1 + 2Q_2 + 3Q_3 + 4Q_4)/(Q_1 + Q_2 + Q_3 + Q_4)$$

$$\text{Ca/Si} = 2Q_0 + 1.5 Q_1 + Q_2 + 0.3Q_3$$

Where  $I(Q_0)$ ,  $I(Q_1)$ ,  $I(Q_2)$  are the integral intensity at 74ppm, -80ppm and -85ppm, respectively.  $Q_0$ ,  $Q_1$ ,  $Q_2$ ,  $Q_3$  and  $Q_4$  are percentages of respective species.

According to Lippmaa *et al.* (1982), the spectra of  $C_3S$  consists at least six narrow lines in the range from -69.3 to -74.5ppm. The line at -73.7ppm is the most intense one. In this study, two peaks of  $C_3S$  lay at in -72ppm and -75ppm, which were characteristic for the mono-silicate group ( $Q_0$ ).



Chemical shifts from TMS, ppm

Fig. 4-17.  $^{29}\text{Si}$  NMR spectra of hydrated  $C_3S$  pastes with or without heavy metals (From left to right are control,  $\text{Cr}^{3+}$ ,  $\text{Cu}^{2+}$ ,  $\text{Pb}^{2+}$ , and  $\text{Zn}^{2+}$ -doped pastes, respectively)

The degree of hydration was calculated according to:

$$\alpha = 1 - I(Q0)/I^0(Q0)$$

Where  $I^0(Q0)$  is raw  $C_3S$  intensity at  $-74\text{ppm}$ . As shown in Table 4-6, the value of  $\alpha$  is in good agreement with sum of hydrated species ( $\sum Q^* = Q1+Q2+Q3$ ).

As mentioned earlier,  $Zn^{2+}$  had the capacity of retarding the hydration of  $C_3S$  at early age. In one year of age there were no obvious differences in the diffractograms of Zn -doped and other  $C_3S$  pastes. According to NMR results, in the longer term, for example, 1 year, all the heavy metals investigated slightly promoted the hydration of  $C_3S$ .

Table 4-6.  $^{29}\text{Si}$  NMR data of hydrated  $C_3S$  pastes (species proportion, %)

Sample	Control	Cr	Cu	Pb	Zn
Q0, 72ppm	16.08	14.97	10.91	15.43	15.2
Q0, 75ppm	24.51	24.15	25.40	23.66	20.53
Q1, 80ppm	32.94	33.53	21.43	34.57	17.86
Q2, 87ppm	26.47	27.35	33.33	26.34	34.50
Q3, 93ppm	0	0	8.90	0	11.91
$\sum Q^*$	59.41	60.88	63.69	60.91	64.27
$\alpha$	58.60	60.80	63.4	62.00	65.20
C	1.45	1.44	1.8	1.43	1.82
Ca/Si	1.57	1.56	1.41	1.56	1.36
Psi	3.62	3.66	5.11	3.52	5.86

Note:  $\sum Q^* = Q1+Q2+Q3$

Increasing hydration of  $C_3S$  resulted in the increased condensation of silicate from single tetrahedron (mono-silicate) to end groups and chain middle groups. It is interesting to note that in the control paste,  $Cr^{3+}$ - and  $Pb^{2+}$ -doped  $C_3S$  pastes,  $Q1 > Q2$ , but in  $Cu^{2+}$ - and  $Zn^{2+}$ -doped pastes,  $Q2 > Q1$ , which means a high condensation of C-S-H gel in the  $Cu^{2+}$ - and  $Zn^{2+}$ -doped pastes.

Heavy metals promoted the polymerisation of C-S-H gel except for  $Pb^{2+}$ . Correspondingly, the values of connectivity of C-S-H gel in heavy metal-doped pastes

were larger than that of the control paste except for the  $\text{Pb}^{2+}$ -doped paste. As the connectivity ratio is related to the statistical average chain length of hydrated species, the values of connectivity ratio (C)/Psi were in the range from 2.5 to 3.2 for the hydrated  $\text{C}_3\text{S}$  pastes for this study.

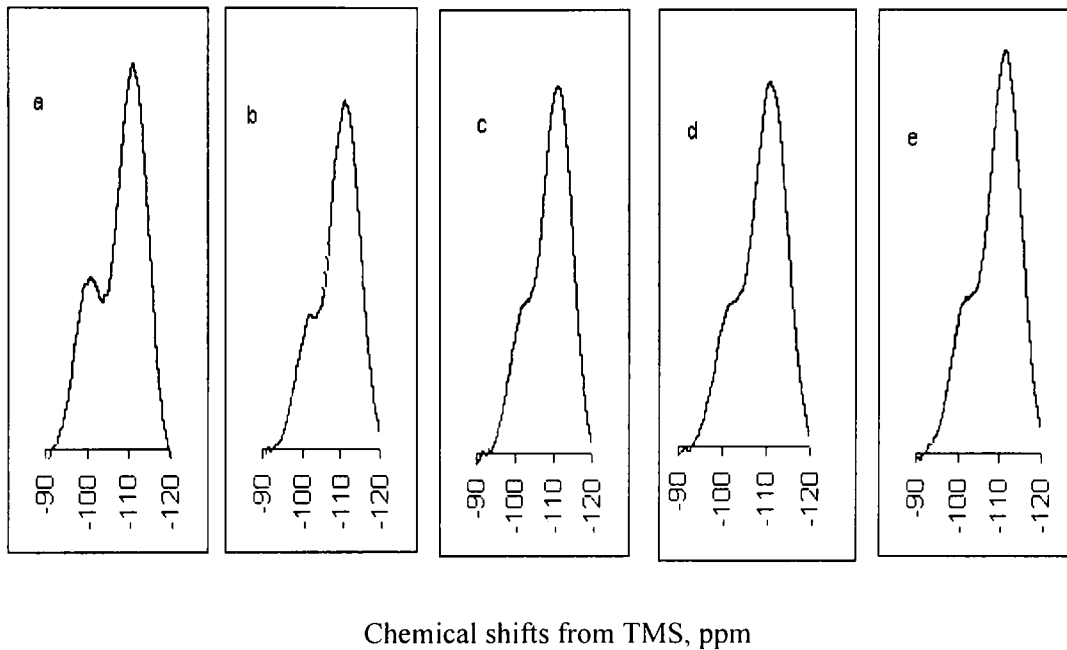


Fig. 4-18.  $^{29}\text{Si}$  NMR spectra of carbonated  $\text{C}_3\text{S}$  pastes with or without heavy metals (From left to right are control,  $\text{Cr}^{3+}$ ,  $\text{Cu}^{2+}$ ,  $\text{Pb}^{2+}$ , and  $\text{Zn}^{2+}$ -doped pastes, respectively)

According to the charge balance, we can calculate the Ca/Si ratio of C-S-H gel, *i.e.*

$$\text{Ca/Si} = 2\text{Q}_0 + 1.5\text{Q}_1 + \text{Q}_2 + 0.3\text{Q}_3$$

The calculated Ca/Si ratios of C-S-H gel of one year old hydrated  $\text{C}_3\text{S}$  pastes were in the range of 1.36-1.57, which are in the agreement with calculations based on the thermal analyses. Cu and Zn, which promoted the polymerisation of C-S-H gel, lowered the Ca/Si ratio of C-S-H gel.

$^{29}\text{Si}$  NMR spectra of 1 year old carbonated  $\text{C}_3\text{S}$  pastes are presented in Fig. 4-18 and Table 4-7. The carbonation of  $\text{C}_3\text{S}$  resulted in the condensation of silicates from isolated tetrahedron to branching sites and three-dimensional frameworks.

Q0 species of C<sub>3</sub>S disappeared from all the carbonated pastes, in contrast to the hydrated samples. Therefore, the degree of carbonation should be 100%. The end groups and middle groups of silicates were not detected in the carbonated C<sub>3</sub>S pastes. The branching sites were very strong and framework sites were the dominant species.

The Ca/Si ratios of C-S-H gel in the carbonated C<sub>3</sub>S pastes were around 0.16 (see Table 4-7), which were consistent with DTA/TG results. NMR results confirm that accelerated carbonation promoted the condensation of silicates to form very low Ca/Si ratio C-S-H gel (Q3 species) and SiO<sub>2</sub> gel (Q4 species).

Table 4-7. <sup>29</sup>Si NMR spectra data of carbonated C<sub>3</sub>S pastes (species proportion, %)

Samples	Q3, 100ppm	Q4, 110ppm	FWHH (ppm)		Ca/Si (average)	C
			Q3	Q4		
Control	33.96	66.04	12	11	0.17	3.66
Cr	32.69	67.31	9	11	0.16	3.67
Cu	30.00	70.00	10	11	0.15	3.70
Pb	33.33	66.67	10	11	0.17	3.69
Zn	32.69	67.31	12	11	0.16	3.67

Note: FWHM means full width of half maximum of peak

From the relationship of the connectivity (C) and the average length of tetrahedra (Psi) obtained in the hydrated C<sub>3</sub>S pastes, it is estimated that the average length of tetrahedral in the carbonated C<sub>3</sub>S pastes could be in the range from 9 to 12. The structural models of C-S-H gel are discussed in the next section.

#### 4.3.4 Structural models of C-S-H gel

From the suspension pH studies and results of XRD, DTA/TG and NMR, in the hydrated C<sub>3</sub>S pastes, the phases present were C-S-H gel, portlandite and double hydroxides of heavy metal and calcium. The behaviour of heavy metals varied and was different from the control system. In addition to the formation of double hydroxides, heavy metals inhibited the precipitation of portlandite and promoted the hydration of C<sub>3</sub>S, even though at the early period of hydration, Zn exhibited retarding effect. As a result, heavy metals

especially Cu and Zn, lowered the Ca/Si ratio of C-S-H gel and promoted the polymerisation of C-S-H gel at one year of age.

In the carbonated C<sub>3</sub>S pastes (with a pH around 8), silica gel, calcite, aragonite and vaterite precipitated (see Table 4-8). Low ratio Ca/Si C-S-H gel also existed, although in principle complete carbonation renders C-S-H gel under-saturated and transferred to acid insoluble silica gel. The differences between carbonated C<sub>3</sub>S pastes with or without heavy metal were small.

As described earlier, the reactions of C<sub>3</sub>S can be referred to as the condensation of monomeric SiO<sub>4</sub> units to higher condensed silicates. Hydration resulted in end groups (Q1) and Q2 species. After carbonation, branching sites (Q3) and three-dimensional frameworks (Q4 species) were present, leading to an increasing diamagnetic shielding of the <sup>29</sup>Si nuclei.

There are a number types of essential models regarding the structure of C-S-H gel, i.e. Glasser's isolated disilicate model (Glasser, 1992) and Richardson-Groves' linear single chain model (Richardson and Groves, 1993; 1997; Richardson, 2000). These models all are based on Taylor's model, in which C-S-H gel contains at least two kinds of crystalline structures of calcium silicate hydrates such as tobermorite or jennite (Taylor, 1997).

Table 4-8. Phases of C<sub>3</sub>S pastes

pH	Phases	Remarks
8.5-7.5	C-S-H [Ca/Si (average): 0.15-0.17 with NMR (1 year); 0.08-0.29 with TG (1 month)], SiO <sub>2</sub> , CaCO <sub>3</sub>	Carbonation
11.7-8.5	C-S-H (Ca/Si moderate), SiO <sub>2</sub> , Ca(OH) <sub>2</sub> , CaCO <sub>3</sub>	Transition
>11.7	C-S-H [Ca/Si (average): 1.36-1.57 with NMR (1 year): 1.61-1.97 with TG (1 month)], double hydroxides, Ca(OH) <sub>2</sub>	Hydration

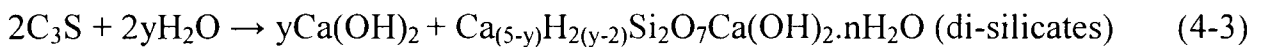
In C<sub>3</sub>S or cement pastes, calcium silicate hydrate gel (C-S-H) is a structure very far from equilibrium and is thermodynamically unstable at ambient temperature. It comprises a large and complex family of phases, with varying compositions. For example, it is likely that a continuous range of composition of C-S-H gel may exist in C<sub>3</sub>S or cement pastes.

Furthermore, C-S-H gel is a highly disordered amorphous phase in cement or C<sub>3</sub>S pastes and there is no hard evidence that links C-S-H gel and crystalline calcium silicate hydrate minerals. Additionally, for high disordered amorphous C-S-H gel, it is unlikely that silicon only adopts numbers of (3m-1), as indicated in the Richardson-Groves' model. In fact, dimer, trimer, tetramer, pentamer and octamer were identified in his experiments (Richardson, 1999).

It is also worthy to note that Glasser's model does not explain the Q2, Q3 species. The Richardson-Groves' linear single chain model excludes the presence of Q3 species. In this work, Q3 species were present in the hydrated Cu and Zn -doped C<sub>3</sub>S pastes. For the carbonated C<sub>3</sub>S pastes, where Q4 and Q3 species were only detectable species, there is no model available to describe these species at present. Based on the results of <sup>29</sup>Si NMR studies, the structural models of C-S-H and reactions in the presence or absence of heavy metals are described as following:

#### 4.3.4.1 In the control hydrated C<sub>3</sub>S paste:

Q1 species:



$$y = 1, 2, 3, 4, Ca/Si = (6-y)/2$$

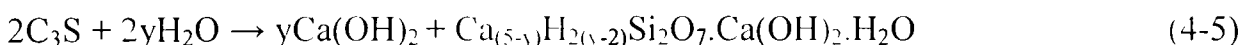
If we substitute 5-y = x, it reduces to Glasser's model of C-S-H (Glasser *et al.*, 1987).

Q2 species:



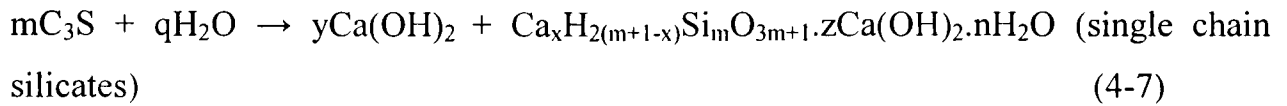
$$m=3, 4, 5, 6, 7, 8; n>0; z=0,1, 2, 3, \text{ etc. } Ca/Si=(x+z)/m$$

Q1 and Q2 species (alternative combination 1):



$m = 3, 4, 5, 6, 7, 8; n > 0; z = 0, 1, 2, 3, \text{ etc.}$

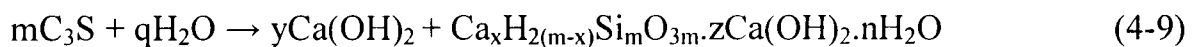
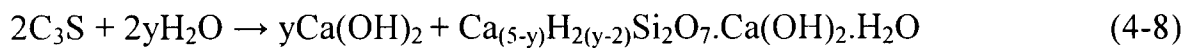
Q1 and Q2 species (alternative combination 2):



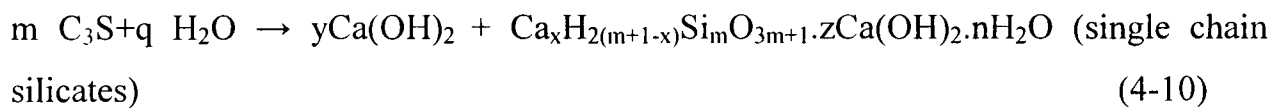
$m = 3, 4, 5, 6, 7, 8; n > 0; z = 0, 1, 2, 3, \text{ etc.}$

If we substitute  $m = 3n-1$ , it reduces to the Richardson-Groves' model of C-S-H (Richardson and Groves, 1993)

Q1 and Q2 species (alternative combination 3):



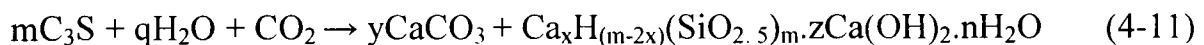
$m = 3, 4, 5, 6, 7, 8; n > 0; z = 0, 1, 2, 3, \text{ etc.}$



$m = 3, 4, 5, 6, 7, 8; n > 0; z = 0, 1, 2, 3, \text{ etc.}$

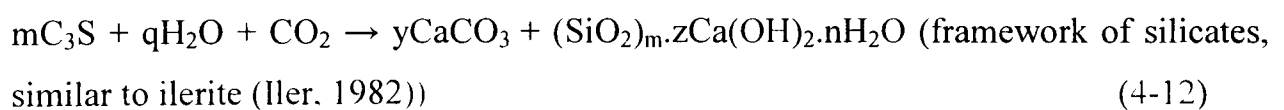
#### 4.3.4.2 In the control carbonated C<sub>3</sub>S paste

Q3 species:



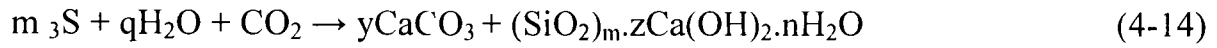
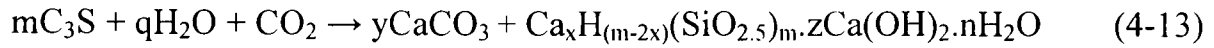
$m$  should be a very big number, because no Q1 and Q2 species appeared in the carbonated C<sub>3</sub>S pastes;  $n > 0; z = 0, 1, 2, 3, \text{ etc.}$

Q4 species:



m should be a very big number; n>0; z=0, 1, 2, 3, *etc.*

Q3 and Q4 species:



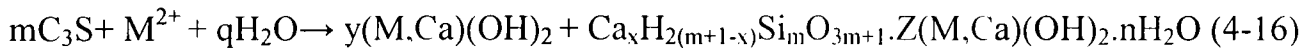
m should be a very big number; n>0; z=0,1, 2, 3, *etc.*

#### 4.3.4.3 In the hydrated C<sub>3</sub>S pastes with heavy metals

Hydration of heavy metal results in the reduction of pH:



Due to the hydration C<sub>3</sub>S, pH will increase and MOH)<sub>2(aq)</sub> or M(OH)<sub>3(aq)</sub> will form. The reaction products of C<sub>3</sub>S with water and carbon dioxide have a good capacity to absorb heavy metal cations and heavy metal hydroxides, because of the large surface area and meta-stability of C-S-H gel and other phases. In disordered C-S-H gel, the incorporation of heavy metal is similar to the structure of glass. Heavy metals act as network modifiers or network intermediates, as shown in Fig. 4-19. If the amount of heavy metal is large enough, precipitation and co-precipitation can occur and form three-dimensional amorphous structures. In the hydration of C<sub>3</sub>S, heavy metal hydroxides could substitute for Ca(OH)<sub>2</sub> in C-S-H gel and co-precipitate with Ca(OH)<sub>2</sub>:



m=3, 4, 5, 6, 7, 8, *etc.*; n>0; z > 1

#### 4.3.4.4 In the carbonated C<sub>3</sub>S pastes with heavy metals

In accelerated carbonated C<sub>3</sub>S pastes, heavy metal hydroxides or carbonates or hydroxyl carbonates can substitute for Ca(OH)<sub>2</sub> in the C-S-H gel {(SiO<sub>2</sub>)<sub>m</sub> · zCa(OH)<sub>2</sub> · nH<sub>2</sub>O} and co-precipitate with CaCO<sub>3</sub>, affecting polymorphism of calcium carbonate:

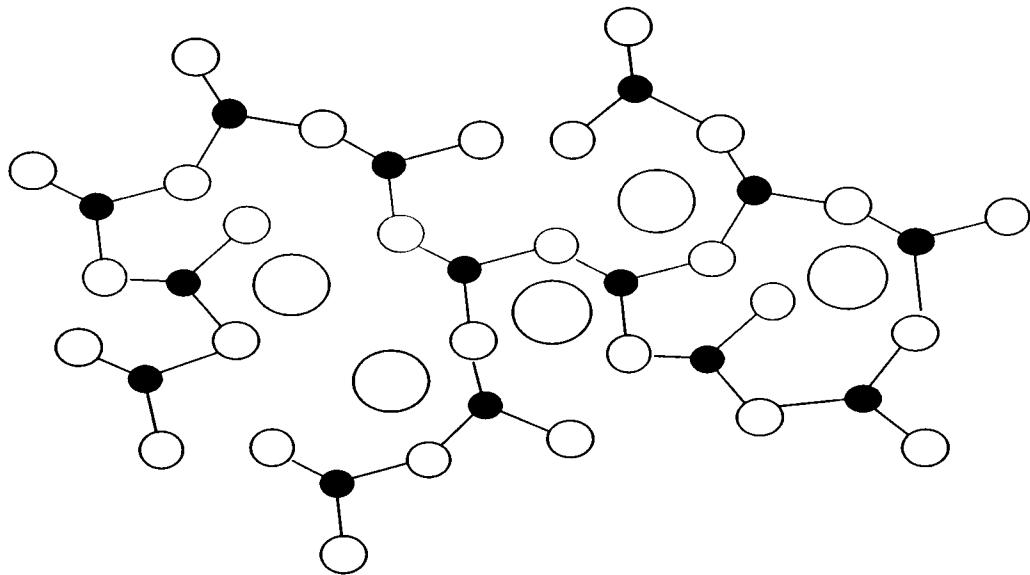
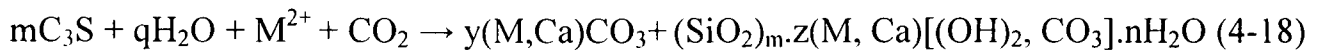
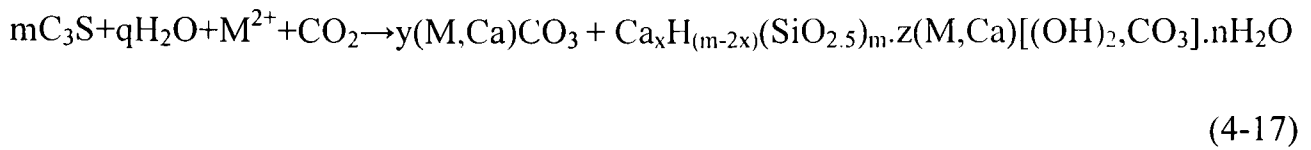


Fig. 4-19. The incorporation model of heavy metal in calcium silicate hydrate gel (Solid spheres stand for silicate atom; white spheres represent oxygen; and large grey spheres represent calcium or heavy metal cations (after Iler, 1982))

#### 4.4 Summary

Tricalcium silicate pastes and aqueous suspensions doped with nitrate salts of  $Zn^{2+}$ ,  $Pb^{2+}$ ,  $Cu^{2+}$  and  $Cr^{3+}$  were examined at different times by X-ray powder diffraction (XRD), thermal analysis (DTA/TG) and  $^{29}Si$  solid state magic angle spinning/nuclear magnetic resonance (MAS/NMR) techniques. The effects of heavy metals on the hydrated and carbonated products of  $C_3S$  were recorded. The following conclusions can be drawn:

- Heavy metals had different effects on the hydration of  $C_3S$ . For 1 month-old pastes, it was found that  $Cu^{2+}$  and  $Cr^{3+}$  acted as accelerators of hydration, whereas  $Zn^{2+}$  retarded hydration. After one year, all heavy metals slightly increased the degree of  $C_3S$  hydration based on NMR results. Heavy metals, especially Cu and Zn, increased the polymerisation of C-S-H gel.
- The double hydroxides  $Ca_2Cr(OH)_7 \cdot 3H_2O$ ,  $2Ca(OH)_2 \cdot 4Cu(OH)_2 \cdot H_2O$  and  $CaZn_2(OH)_6 \cdot 2H_2O$  were identified in the hydrated  $C_3S$  suspensions as crystalline phases and in the hydrated  $C_3S$  pastes as amorphous phases. These compounds were very stable in hydrated  $C_3S$  systems.
- Heavy metal hydrolysis reduced the pH and inhibited the precipitation of portlandite based on the XRD and DTA/TG examinations. The relative intensity changes of portlandite at  $18.1^\circ$  and  $34.2^\circ$   $2\theta$ , and the dehydroxylation temperature shifts of portlandite indicated the co-existence of heavy metals with portlandite, in addition to the formation of double hydroxides.
- Heavy metals were absorbed in fully carbonated  $C_3S$  suspensions and pastes based on XRD and thermal analysis results. Heavy metals affected the polymorphism and quantity of calcium carbonate and changed the decomposition temperature of calcium carbonate, demonstrating that heavy metals may be absorbed on the surface of calcium carbonate or incorporated into the lattice of calcium carbonate.
- The carbonation of  $C_3S$  pastes was difficult to avoid, but complete carbonation of  $C_3S$  in the laboratory was not straightforward. Suspension pH studies, XRD and NMR confirmed that at least 8 cycles of contacting with carbon dioxide, crushing and grinding were required before residual  $C_3S$  was no longer detected.
- The degree of reactivity of  $C_3S$  was greater during carbonation than during hydration.
- Solid state magic angle spinning/nuclear magnetic resonance (MAS/NMR) showed that in the hydrated control and  $Cr^{3+}$ -,  $Pb^{2+}$ -doped  $C_3S$  pastes, Q1 groups were dominant, but in the hydrated  $Cu^{2+}$ - and  $Zn^{2+}$ -doped pastes, Q2 groups were dominant. The length of silicates (C-S-H gel) was in the order:  $Zn^{2+} > Cu^{2+} > Cr^{3+} > Control > Pb^{2+}$ .

- Heavy metal cations could be adsorbed or co-precipitate with calcium silicate hydrate gel. As a consequence of this, Ca/Si ratio of C-S-H gel varied. According to NMR results, the average Ca/Si ratio of C-S-H gel was in the range of 1.36-1.57 for hydrated  $C_3S$  pastes doped with different heavy metals. This was consistent with the calculation from the DTA/TG results.
- Carbonation promoted the condensation of silicates to form very low Ca/Si ratio C-S-H gel. In the carbonated pastes, based on NMR and DTA/TG analyses, the estimated average Ca/Si ratio was 0.08-0.29.
- Structural models of C-S-H gel and heavy metal incorporation in C-S-H and silica gel have been postulated.

## Chapter 5

### Investigation of aluminium-bearing phase/heavy metal systems

#### 5.1 Background

In the previous chapters, heavy metal -doped suspensions and pastes of calcium oxide, calcium hydroxide, tricalcium silicate have been examined with XRD, DTA/TG and NMR techniques. The results were in agreement one another and provided an insight into the reactions and encapsulation of heavy metals. This chapter investigates the systems of pure cement phases containing aluminium with or without heavy metals using XRD.

Among the minerals present in Portland cement, aluminate ( $C_3A$ ) is the most reactive towards water and is believed to have a significant influence on the early hydration and rheology of Portland cement (Taylor 1990, Glasser *et al.*, 1999).

$C_{12}A_7$  is an intermediate or minor phase formed during the production of  $C_3A$  in Portland cement, which may also affect the hydration of Portland cement. Both CA and  $C_{12}A_7$  are the most important phases of calcium aluminate cement and have a significant role in the hydration of calcium aluminate cement (CAC) and the performance of CAC concrete (Taylor, 1990). Ferrite is poorly hydraulic and does not make a significant low contribution to strength of concrete, but  $Fe_2O_3$  can substitute for  $Al_2O_3$  in ettringite, monosulfate and hydrogarnet (Klich *et al.*, 1990; 1999).

Taylor (1997) and Glasser (1997) claimed that cement phases containing aluminium, such as  $C_3A$ ,  $C_{12}A_7$ , CA and  $C_4AF$ , influence the strength and durability of concrete and effectiveness of cement-based solidification/stabilisation of wastes. The reaction rate and degree of the above phases are dependent on phase composition, temperature, water/solid ratio, particle shape and size, and the presence of accelerators or retarding agents (Berger *et al.*, 1972; Slegers and Rouxhet, 1976).

In the absence of gypsum, the hydration products of  $C_3A$  are  $CAH_{10}$ ,  $C_2AH_x$ ,  $C_4AH_x$  and hydrogarnet ( $C_3AH_6$ ). The conversion of  $CAH_{10}$ ,  $C_2AH_x$ ,  $C_4AH_x$  to hydrogarnet results in the mechanical strength loss or other durability problems. In the presence of gypsum,

monosulfoaluminate and ettringite are the main hydration products of  $C_3A$  (Moore and Taylor, 1968; 1970).

The hydration of CA and  $C_{12}A_7$  has not been studied in depth. It is believed that the hydration products of these phases are very similar to those of  $C_3A$ , *i.e.*  $CAH_{10}$ ,  $C_2AH_x$ ,  $C_4AH_x$  and hydrogarnet in the absence of gypsum; and monosulfoaluminate and ettringite in the presence of gypsum (Poellmann *et al.*, 1993; Jeffrey, 1996).

If the amount of gypsum is not sufficient and is consumed, ettringite will change into monosulfoaluminate, which coexists with some hexagonal and cubic calcium aluminate hydrates, for example, gehlenite hydrate, hydrogarnet (Gougar *et al.*, 1996).

The mechanisms of conversion of hydration products such as hexagonal aluminate hydrate, cubic aluminate, ettringite and monosulphate are not yet fully understood, although much research work has been conducted (Damidot and Glasser, 1992; 1993a; 1993b; 1995; Glasser *et al.*, 1999). The effects of heavy metals on the hydration of cement phases containing aluminium and conversions of hydration product are not known at present and require investigation in respect of cement-based s/s.

Carbonation neutralises the alkalinity of hydrated pastes of cement and reduces the solubility of some metal compounds. This may offer some important advantages in the protection of the environment. Smith *et al.* (1997) have demonstrated that the precipitation of calcite due to carbonation can affect the incorporation of heavy metals, because heavy metals may co-precipitate with the calcite forming solid solutions. Bonen and Sarkar (1995) have found that carbonation can have a profound effect on the leaching characteristics of heavy metals and on the microstructure of the cement binders.

The carbonation of  $C_3A$ ,  $C_4AF$ , CA and  $C_{12}A_7$  has not been fully studied, and knowledge of the potentially complicated reaction processes involving  $CO_2$  gas, especially in the presence of heavy metals, is very limited. Thus, the present work seeks to identify the reaction products of these phases. This chapter provides some evidences of major differences in hydrated and carbonated cement phases containing aluminium ( $C_3A$ , CA,  $C_{12}A_7$  and  $C_4AF$ ) in the presence or absence of  $Cu^{2+}$ ,  $Cr^{3+}$ ,  $Pb^{2+}$  and  $Zn^{2+}$ , with or without gypsum.

## ***5.2 Experimental***

### **5.2.1 Materials**

Pure cement phases containing aluminium ( $C_3A$ ,  $CA$ ,  $C_{12}A_7$  and  $C_4AF$ ) were synthesised from  $CaCO_3$  and  $Al_2O_3$  or  $Fe_2O_3$  (Aldrich Chemical Company, 98% purity) (see Appendix A). Copper, lead, zinc and chromium nitrate salts (BCD Ltd, 98 % purity) were dissolved in de-ionised water at concentrations of 5%w/w and 10%w/w (by heavy metal ion weight).

### **5.2.2 Methods**

#### **5.2.2.1 Hydration**

Hydrated paste preparations involved blending 3g of  $C_3A$ ,  $CA$ ,  $C_{12}A_7$  and  $C_4AF$  with 0% or 10% heavy metal solutions (by metal ion weight) at a solid/liquid ratio of 10:4, respectively. These samples were kept in sealed containers for examinations by XRD at 1 month and 1 year of age.

#### **5.2.2.2 Accelerated carbonation**

Accelerated carbonation of pure cement phases containing aluminium involved preparing the pastes under the same conditions as for the hydration studies prior to exposure to 100%  $CO_2$  for 30min in a reaction chamber. Once samples were removed they were ground to less than 0.03mm with a pestle and mortar prior to placement back in the reaction chamber and carbonated. This procedure was repeated for 8 cycles. Carbonated samples were stored in sealed  $CO_2$  -bags for 1 month and 1 year.

#### **5.2.2.3 Suspension studies**

Heavy metal nitrate solutions with concentrations of 0% and 5% w/w (by metal ion weight) were mixed with ground pure cement phases at a solid/liquid ratio of 1:10. The

suspensions were placed in sealed containers and agitated. In order to effect carbonation, suspensions were placed in the carbonation chamber (see Chapter 2).

#### **5.2.2.4 X-ray powder diffraction (XRD)**

A Siemens D500 diffractometer and Kristalloflex 810 generator (CuK-alpha radiation, 40KV, 40mA) were used to identify the crystalline products present in the pastes or suspensions both before and after carbonation. The finely ground samples (<30µm) were examined between 5-40° 2θ at a scanning rate of 1° 2θ per minute. The diffractograms were obtained with Diffplus and analysed using Bruker/AXS EVA software.

### **5.3 Results and discussion**

#### **5.3.1 C<sub>3</sub>A in the absence of gypsum**

##### **5.3.1.1 Hydration**

The diffractograms obtained from one month and one year old hydrated C<sub>3</sub>A pastes are presented in Figs. 5-1 and 5-2, respectively. First of all, no CAH<sub>10</sub> was detected in any of the pastes by XRD despite the low ambient laboratory temperature (17°C). Anhydrous C<sub>3</sub>A was detectable in all hydrated pastes at one month of age, but it was not detected in the Cu, Pb and Zn -doped hydrated pastes at the age of one year. The reflection peaks for anhydrous C<sub>3</sub>A (at 33.2° 2θ) were strong in the Cr<sup>3+</sup>-doped paste and evident in the control hydrated paste aged 1 year. From this observation it was deduced that Cr<sup>3+</sup> did not appear to accelerate hydration, unlike the other metals, which promoted the hydration of C<sub>3</sub>A.

The major hydration products observed were hydrogarnet (C<sub>3</sub>AH<sub>6</sub>), calcium monoaluminate (C<sub>4</sub>AH<sub>19</sub>), gehlenite hydrate (C<sub>2</sub>AH<sub>8</sub>) and calcium carboaluminate [C<sub>3</sub>A(CaCO<sub>3</sub>)H<sub>11</sub>, C<sub>3</sub>A(CaCO<sub>3</sub>)<sub>0.5</sub>H<sub>12</sub>]. Table 5-1 summarises the reaction products identified. In all pastes C<sub>4</sub>AH<sub>19</sub> and gehlenite hydrate (C<sub>2</sub>AH<sub>8</sub>) was absent after one year's hydration.

Table 5-1. Phases detected in the hydrated C<sub>3</sub>A pastes in the absence of gypsum

Sample	C <sub>2</sub> AH <sub>8</sub>	C <sub>3</sub> AH <sub>6</sub>	C <sub>3</sub> A(CaCO <sub>3</sub> ) <sub>0.5</sub> H <sub>12</sub>	C <sub>3</sub> A(CaCO <sub>3</sub> )H <sub>11</sub>	V	A	C
Contr-28d	p	p	a	p	a	a	a
Contr-1y	a	p	a	p	p	p	a
Cr-28d	p	p	p	p	a	a	a
Cr-1y	a	p	p	p	p	p	p
Cu-28d	p	p	p	p	a	a	p
Cu-1y	a	a	p	p	p	a	p
Pb-28d	p	p	p	p	a	a	p
Pb-1y	a	p	p	p	p	p	p
Zn-28d	p	a	p	p	a	a	a
Zn-1y	a	a	p	p	p	a	p

Note: p—present, a—absent, C = calcite, V = vaterite, A = aragonite

It is worth pointing out that in the Zn<sup>2+</sup>-doped paste, C<sub>3</sub>AH<sub>6</sub> was absent at any time, unlike the other pastes. In the Cr<sup>3+</sup> and Pb<sup>2+</sup>-doped pastes, the intensities of the C<sub>3</sub>AH<sub>6</sub> were very weak after one year. An examination of the phases detected by XRD, as shown in Fig. 5-3, indicates that other heavy metals also retarded the formation of C<sub>3</sub>AH<sub>6</sub>.

A further comparison of the diffractograms obtained from one month and one year old pastes indicates that C<sub>3</sub>AH<sub>6</sub> was more stable in the control paste than in heavy metal-doped pastes, even though there was evidence for the transformation of C<sub>3</sub>AH<sub>6</sub> to calcium carboaluminate in the control paste.

Heavy metals appeared to promote the formation of calcium carboaluminate (see Figs. 5-3 and 5-4), for example, in the Zn<sup>2+</sup>-doped paste the main reaction products identified were C<sub>3</sub>A(CaCO<sub>3</sub>)<sub>0.5</sub>H<sub>12</sub> and C<sub>3</sub>A(CaCO<sub>3</sub>)H<sub>11</sub>. It is worthy to note that C<sub>3</sub>A(CaCO<sub>3</sub>)<sub>0.5</sub>0.5H<sub>12</sub> was detected in the heavy metal -doped pastes, but was absent in the control pastes.

In the diffractograms obtained from metal-doped pastes aged one year, calcite was evident, whereas in the control paste it was absent. Vaterite was present in the Cu- and Zn-doped pastes. Gibbsite was detected in all the pastes. The diffractograms indicated

that the heavy metals influenced the polymorphism of calcium carbonate in the natural carbonation process.

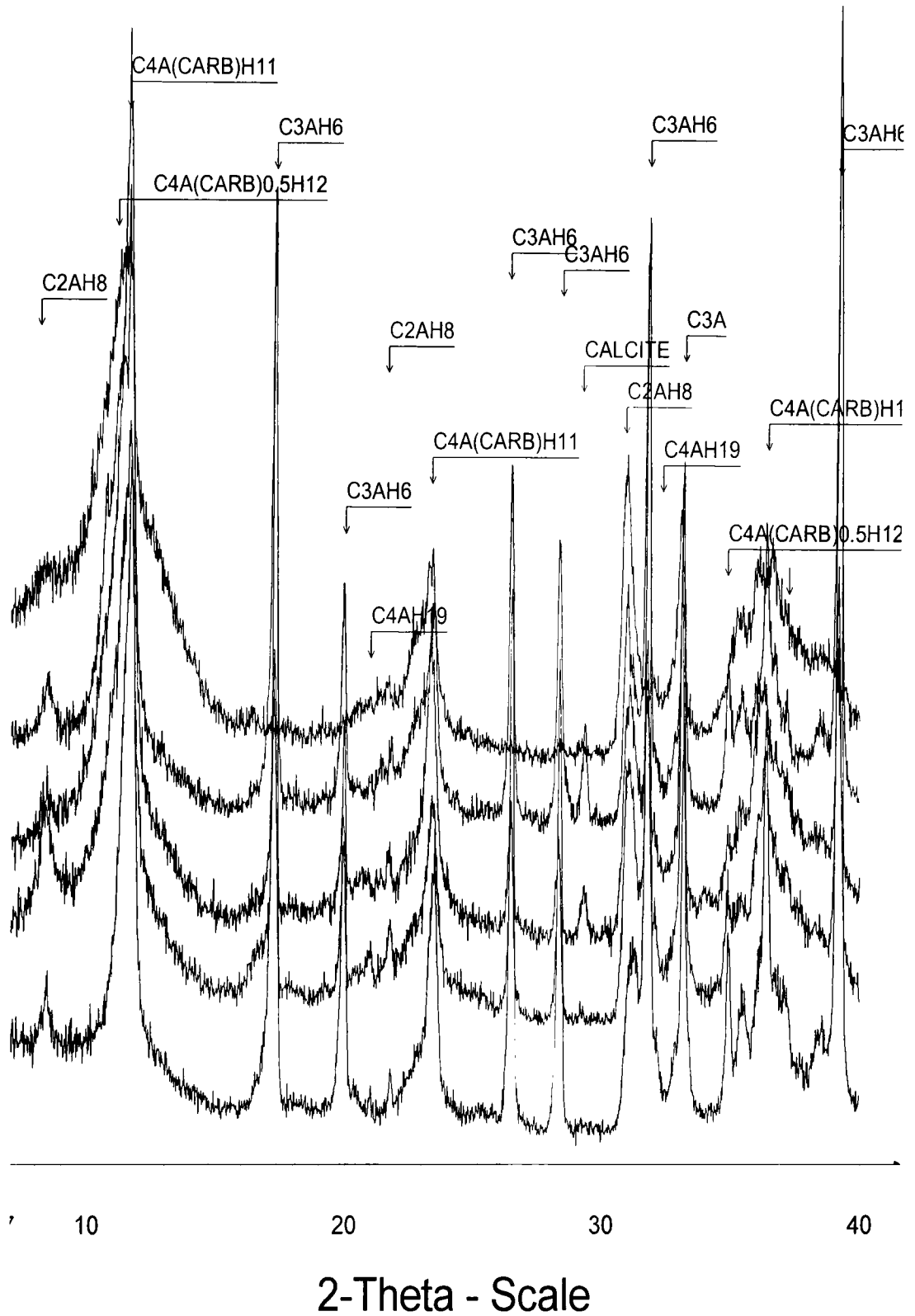


Fig. 5-1. Diffractograms of hydrated  $C_3A$  pastes aged 28-days  
(From bottom to top are control,  $Cr^{3+}$ ,  $Cu^{2+}$ ,  $Pb^{2+}$ , and  $Zn^{2+}$ -doped pastes, respectively)

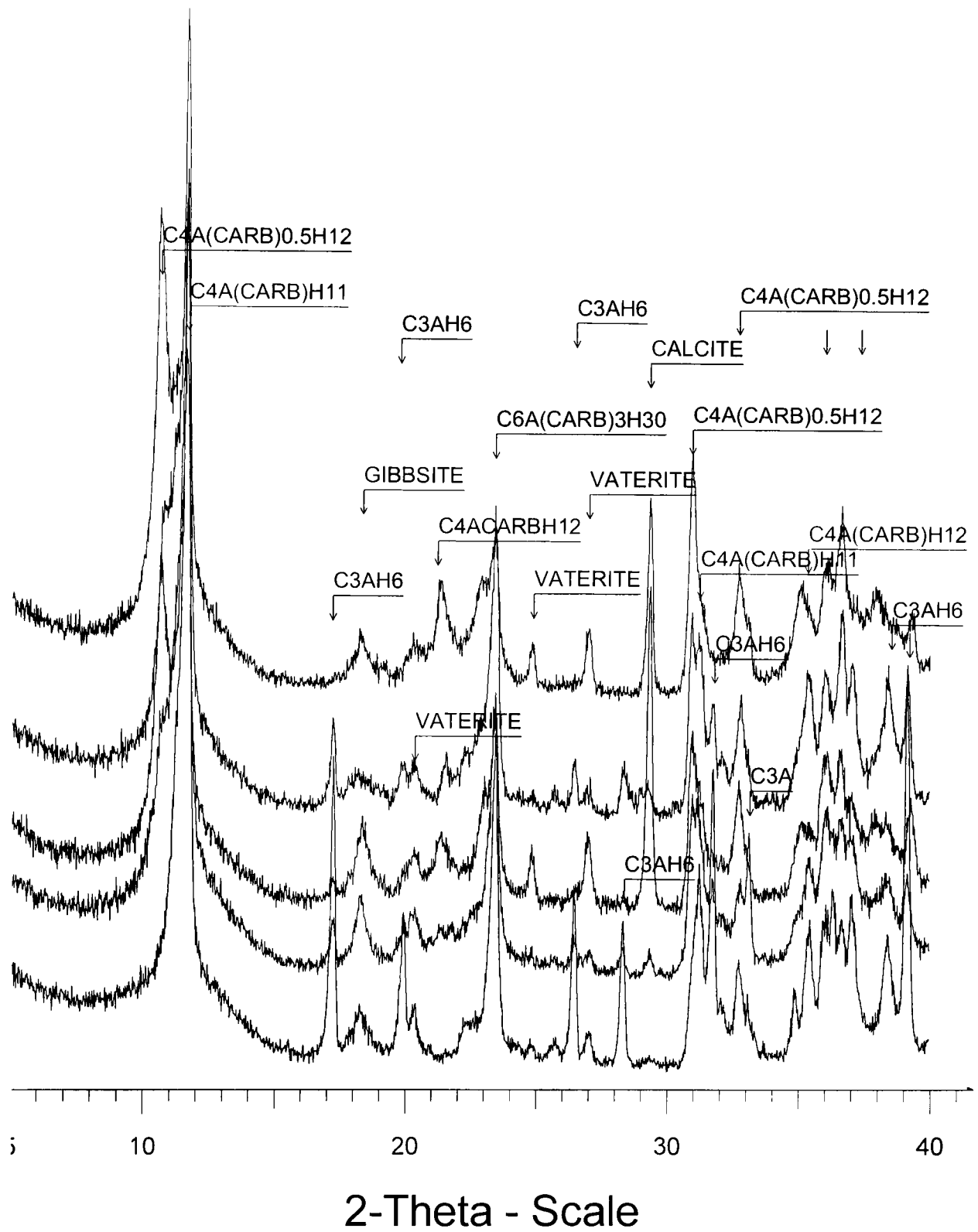


Fig. 5-2. Diffratograms of hydrated  $C_3A$  pastes aged 1 year,  
 (From bottom to top are control,  $Cr^{3+}$ ,  $Cu^{2+}$ ,  $Pb^{2+}$ , and  $Zn^{2+}$ -doped pastes, respectively)

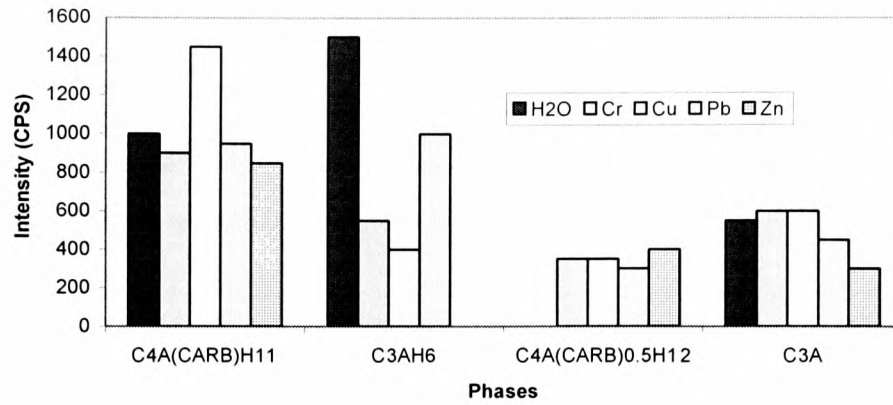


Fig. 5-3. The main phases in 28-day old hydrated  $C_3A$  pastes

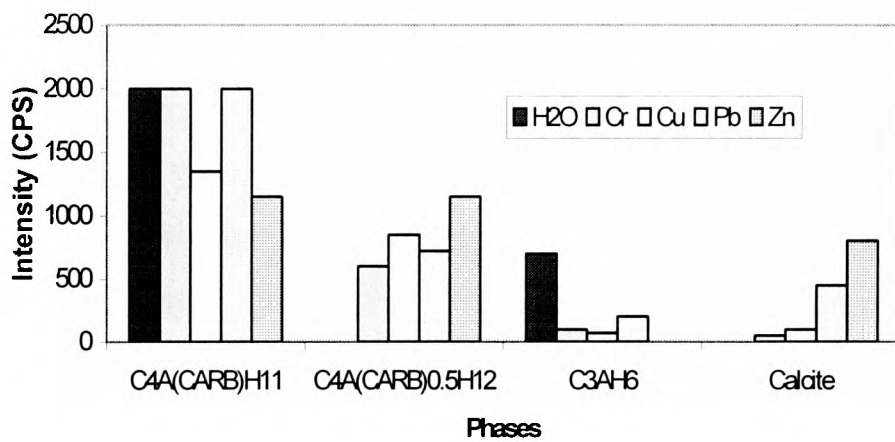


Fig. 5-4. The main phases in hydrated  $C_3A$  pastes at one year

To sum up, in the hydrated  $C_3A$  pastes containing heavy metal, heavy metals, especially zinc ions, inhibited the formation hydrogarnet ( $C_3AH_6$ ) and favoured the conversions of C-A-H phases to calcium carboaluminate and calcium carbonate eventually. In order to get more information on the interaction of heavy metal and  $C_3A$ , the suspensions of  $C_3A$  in the presence or absence of zinc nitrate were studied.

The reaction products identified by XRD in hydrated  $C_3A$  suspensions are presented in Table 5-2 and Fig. 5-5. In the control  $C_3A$  suspension, hydrogarnet and  $C_4AH_{13}$ ,  $C_4AH_{19}$  were detected. It is noted that the intensity of hydrogarnet increased with the time.

Correspondingly, the peak intensities of  $C_4AH_{13}$  and  $C_4AH_{19}$  decreased with the time, indicating that  $C_4AH_{13}$  and  $C_4AH_{19}$  were the initial products formed, transforming to hydrogarnet later.

In the  $Zn^{2+}$  -doped  $C_3A$  suspension, C-A-H including  $C_2AH_8$ ,  $C_2AH_5$ ,  $C_3AH_6$ ,  $C_4AH_{13}$  and  $C_4AH_{19}$  formed at 1 month and 3 months of age. Calcium carboaluminate was detected at 3 months. The difference in the hydration products of suspensions at different times confirmed that zinc retarded the formation of hydrogarnet by zinc inhibiting the conversions of  $C_2AH_8$ ,  $C_2AH_5$ ,  $C_4AH_{13}$  and  $C_4AH_{19}$  to this phase.

In the presence of zinc, the hydration products of the  $C_3A$  suspension differed from those of the  $C_3A$  paste. In the  $Zn^{2+}$  -doped paste, no hydrogarnet was detected, but in the hydrated suspension hydration with zinc ions, in addition to  $C_2AH_8$ ,  $C_2AH_5$ ,  $C_4AH_{13}$  and  $C_4AH_{19}$ , hydrogarnet was detected. The above study indicates that the suspension favoured the conversions of  $C_2AH_8$ ,  $C_2AH_5$ ,  $C_4AH_{13}$  and  $C_4AH_{19}$  to hydrogarnet, compared to the paste. In the  $Zn^{2+}$  -doped suspension at an age of 1 month, gibbsite was absent, but at an age of three months, gibbsite was detected, illustrating the ability of  $Zn^{2+}$  to retard the crystallisation of  $Al(OH)_3$ . It was also noted that at an age of 1 month, gibbsite and beohmite were identified in the control  $C_3A$  suspension, whereas in the control  $C_3A$  paste, they were not detected.

Table 5-2. Phase development in hydrated  $C_3A$  suspensions

Hydration time	Phases detected by XRD	
	Control	Zn -doped
1 month	$C_3AH_6$ , $C_4AH_{13}$ , $C_4AH_{19}$ , Gibbsite, Beohmite	$C_2AH_8$ , $C_2AH_5$ , $C_4AH_{13}$ , $C_4AH_{19}$ , $C_3AH_6$ , Beohmite
3 months	$C_3AH_6$ (I), $C_4AH_{13}$ (D), $C_4AH_{19}$ (D), Gibbsite	$C_4A(CaCO_3)_{0.5}H_{12}$ , $C_2AH_8$ (I), $C_2AH_5$ (D), $C_3AH_6$ , $C_4AH_{13}$ , $C_4AH_{19}$ , Gibbsite

Note: I-increased intensity; D-decreased intensity

In the hydrated  $Zn^{2+}$  -doped  $C_3A$  paste and suspension, no crystalline zinc compounds were observed, although suspension created more favourable environment for crystallisation of reaction products. From the examination of  $C_3A$  suspensions, it is

reasonable to exclude the formation of heavy metal compounds. Heavy metals were absorbed by C-A-H and other phases formed. As a result, atmospheric carbonation was facilitated during sample preparation and storage.

Table 5-3. The major phases detected by XRD in the carbonated C<sub>3</sub>A pastes

Sample	C <sub>3</sub> AH <sub>6</sub>	C <sub>3</sub> A(CaCO <sub>3</sub> ) <sub>0.5</sub> H <sub>12</sub>	C <sub>3</sub> A(CaCO <sub>3</sub> )H <sub>11</sub>	V	A	C	G
Control-28d	p	a	p	p	a	p	p
Control-1y	a	a	a	p	p	p	p
Cr-28d	p	p	a	p	a	p	a
Cr-1y	a	a	a	p	a	p	p
Cu-28d	p	p	a	p	a	p	a
Cu-1y	a	a	a	p	p	p	p
Pb-28d	p	a	p	p	a	p	p
Pb-1y	a	a	a	p	a	p	p
Zn-28d	a	p	a	p	a	p	a
Zn-1y	a	a	a	p	p	p	p

Note: p—present, a—absent, C—calcite, V—vaterite, A—aragonite, G—gibbsite

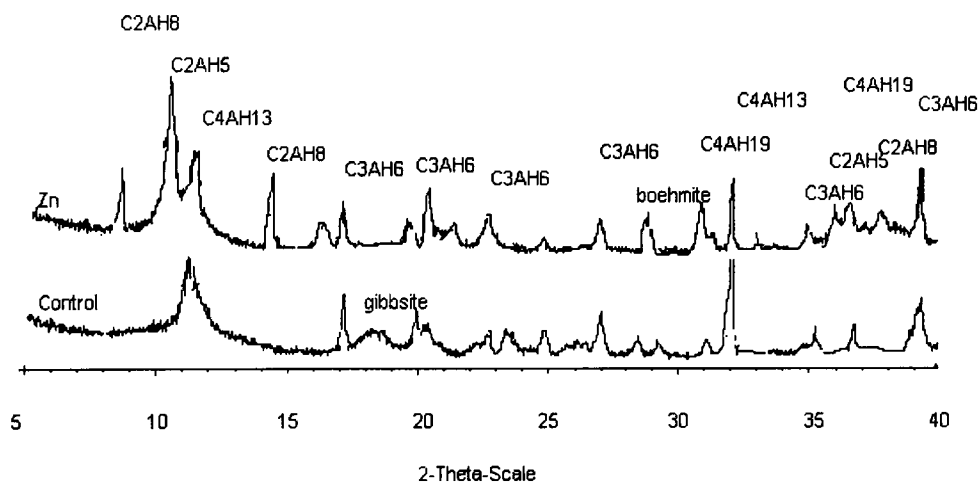


Fig. 5-5. Diffractograms of the hydrated C<sub>3</sub>A suspensions at the age of one month

### 5.3.1.2 Accelerated carbonation

The diffractograms obtained from 28 days old accelerated carbonated C<sub>3</sub>A pastes are shown in the Fig. 5-6. The main reaction products identified were calcite, vaterite,

carboaluminate ( $C_3A(CaCO_3)H_{11}$ ,  $C_3A(CaCO_3)_{0.5}H_{12}$ ), gibbsite and hydrogarnet ( $C_3AH_6$ ). The phases observed are summarised in Table 5-3.

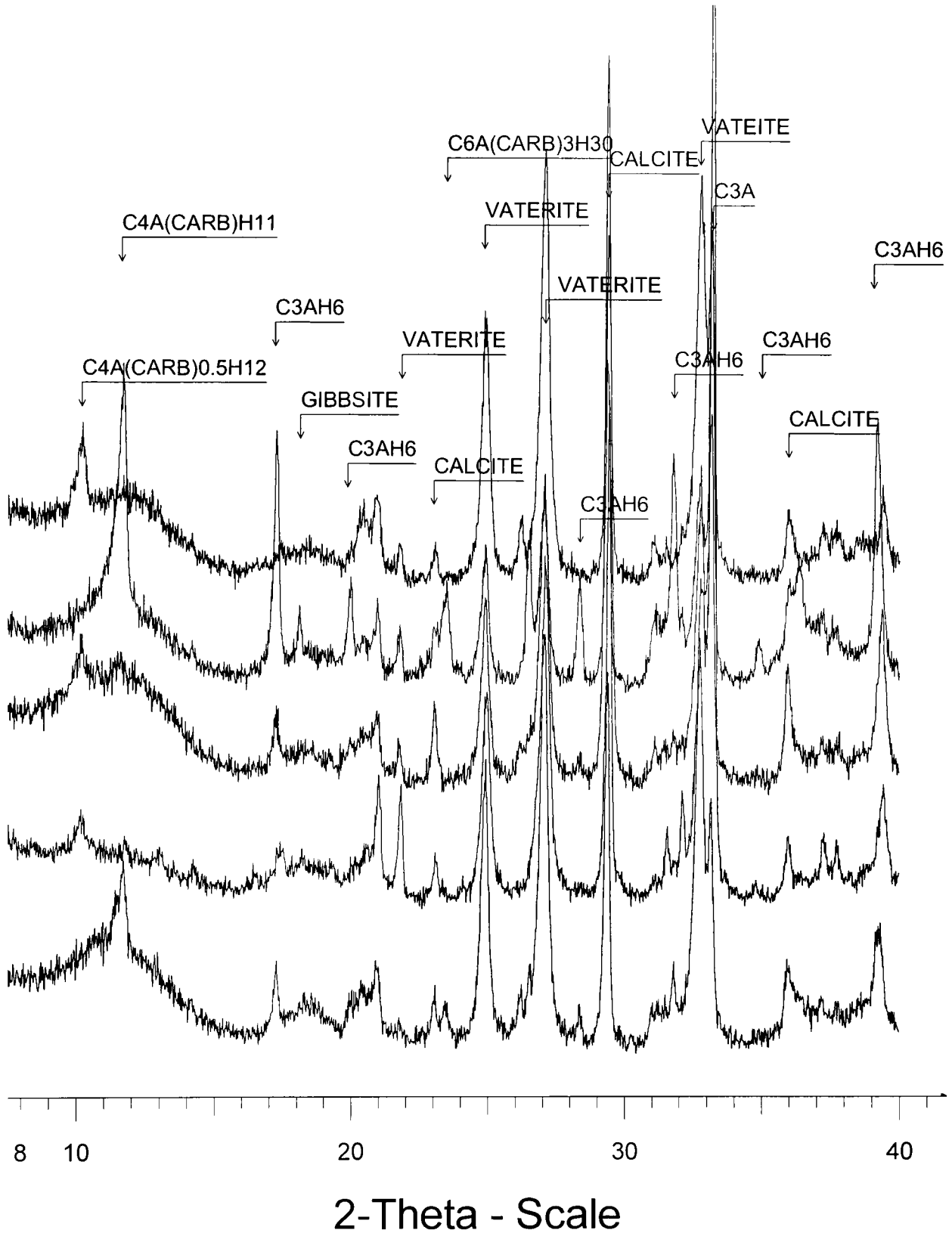


Fig. 5-6. Diffractograms of carbonated  $C_3A$  pastes at 28-days (From bottom to top are control,  $Cr^{3+}$ ,  $Cu^{2+}$ ,  $Pb^{2+}$ , and  $Zn^{2+}$ -doped pastes, respectively)

Compared with the carbonated heavy metal-doped  $C_3A$  paste, the intensities of reflections of anhydrous  $C_3A$  were lowest in the control paste and are shown in Fig. 5-7. The carbonated  $Pb^{2+}$ -doped paste had the strongest peaks recorded for  $C_3AH_6$  followed by the control paste. In the  $Cu^{2+}$  and  $Cr^{3+}$  -doped pastes, the intensities of  $C_3AH_6$  reflections were very weak.  $C_3AH_6$  was absent in the carbonated  $Zn^{2+}$ -doped  $C_3A$  paste.

The diffractograms obtained from accelerated carbonated pastes placed in  $CO_2$  bags for one year are shown in Fig. 5-8. Hydrogarnet and calcium carboaluminate were not detectable. Gibbsite, calcite and vaterite were identified in all the pastes. Strong reflections corresponding to aragonite occurred in the  $Zn^{2+}$  -doped paste,  $Cu^{2+}$  -doped paste and in the control paste; whereas in the  $Cr^{3+}$  and  $Pb^{2+}$ -doped pastes, aragonite was absent, indicating that heavy metals influenced the polymorphism of calcium carbonate.

According to the Ostwald step rule, vaterite transforms into calcite with aragonite being the intermediate product. A comparison of the carbonated 28 day and one year old samples showed that the intensities of peaks recorded for calcite increased, while those of vaterite became weaker. Aragonite appeared in only some of the pastes examined, indicating that Ostwald ripening had indeed occurred in these pastes.

The diffractograms obtained from carbonated  $C_3A$  suspensions at ages of 1 month and 3 months are shown in Fig. 5-9 and in Table 5-4. Upon carbonation, calcium carboaluminate and C-A-H phases transferred into calcite and gibbsite, with vaterite and aragonite as intermediates. The presence of zinc ions appeared to promote these conversions. It is noted that the presence of zinc stabilised the metastable polymorphs of calcium carbonate. It is worth noting that no crystalline zinc compounds were detected by XRD in the carbonated Zn -doped  $C_3A$  suspensions and pastes.

A comparison of the carbonated  $C_3A$  suspension and paste at 3 months of age, it was found that the former favoured the crystallisation of gibbsite and the conversion of vaterite and aragonite to calcite (Fig. 5-10).

There were no heavy metal compounds detected in the  $C_3A$  pastes, even in the  $C_3A$  suspensions, where species had mobility as well as enough time to undergo proper orientation and alignment before bonding into a structure. The above studies demonstrated that heavy metals could be incorporated in hydration or carbonation

products of C<sub>3</sub>A due to sorption phenomena or incorporation into the lattices of C-A-H, calcium carbonate or other phases formed.

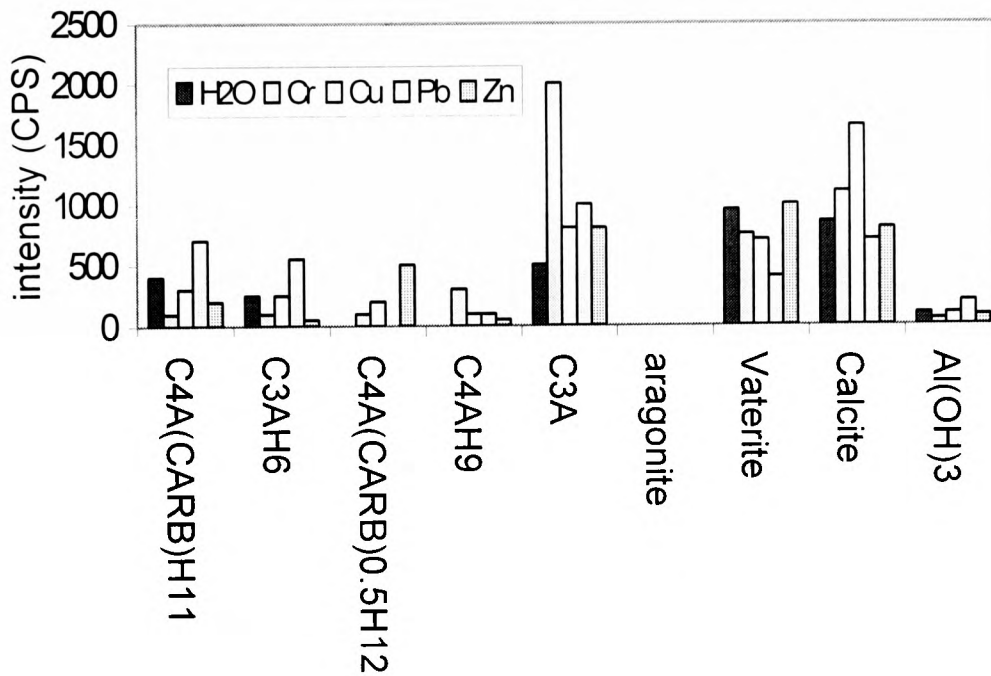


Fig. 5-7. Phases detected in the accelerated carbonated C<sub>3</sub>A pastes

Table 5-4. Phase development in the carbonated C<sub>3</sub>A suspensions

Time	Phases detected by XRD	
	Control	Zn -doped
2 weeks	C <sub>4</sub> A(CaCO <sub>3</sub> )H <sub>11</sub> , Calcite, Vaterite, Gibbsite, C <sub>3</sub> AH <sub>6</sub> , C <sub>4</sub> AH <sub>19</sub> , Boehmite	C <sub>4</sub> A(CaCO <sub>3</sub> ) <sub>0.5</sub> H <sub>12</sub> , C <sub>4</sub> A(CaCO <sub>3</sub> )H <sub>11</sub> , Calcite, Aragonite, Vaterite, Gibbsite,
1 month	C <sub>4</sub> A(CaCO <sub>3</sub> )H <sub>11</sub> (D), Gibbsite(I), Calcite(I)	C <sub>4</sub> A(CaCO <sub>3</sub> ) <sub>0.5</sub> H <sub>12</sub> (D), C <sub>4</sub> A(CaCO <sub>3</sub> )H <sub>11</sub> (D), Calcite(I), Aragonite, Vaterite, Gibbsite(I)
3 months	Gibbsite, Calcite(I),	C <sub>4</sub> A(CaCO <sub>3</sub> )H <sub>11</sub> (D), Gibbsite, Calcite(I), Aragonite(D)

Note: I-increased; D-decreased

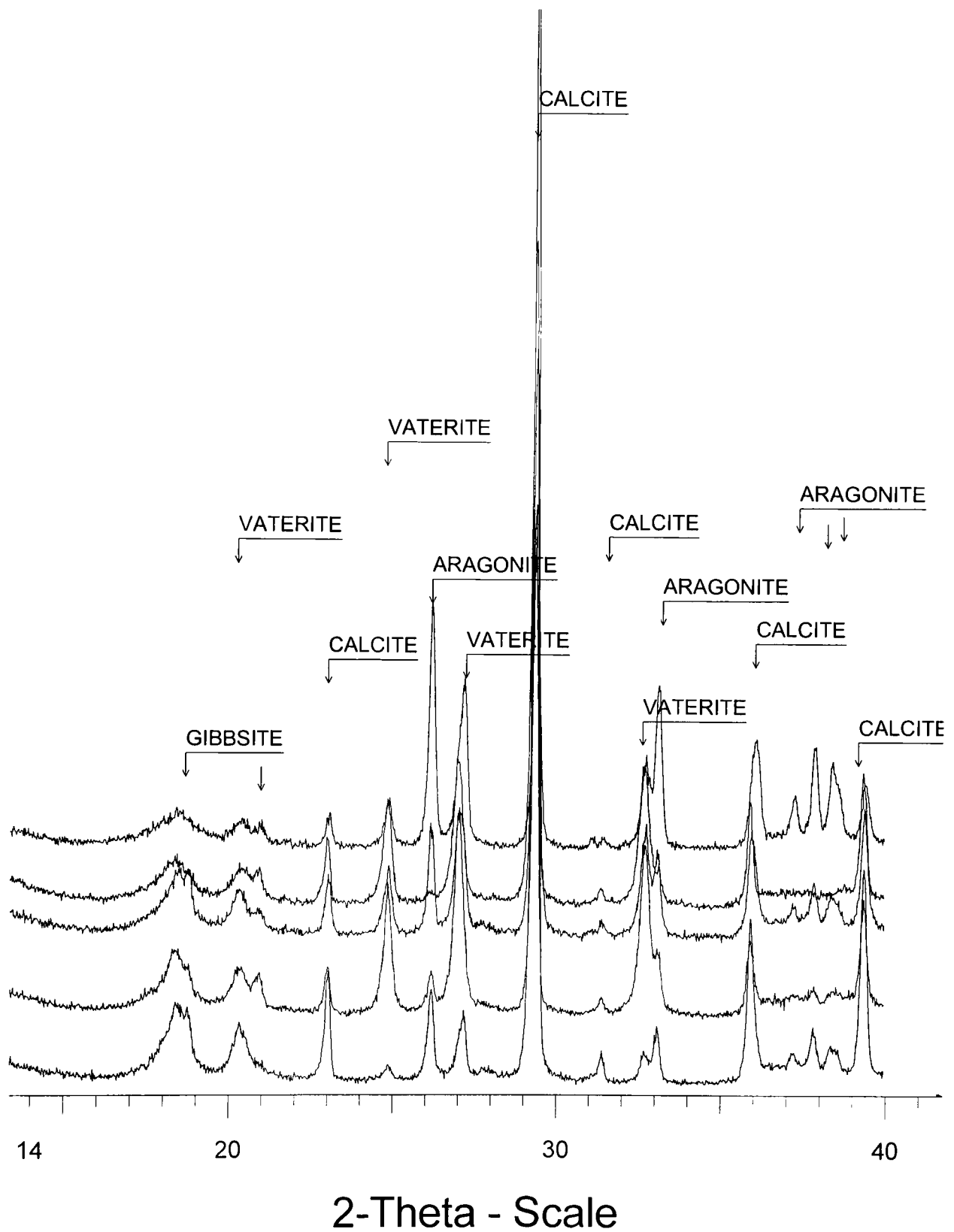


Fig. 5-8. Diffractograms of carbonated C<sub>3</sub>A pastes aged 1 year  
 (From bottom to top are control, Cr<sup>3+</sup>, Cu<sup>2+</sup>, Pb<sup>2+</sup>, and Zn<sup>2+</sup>-doped pastes, respectively)

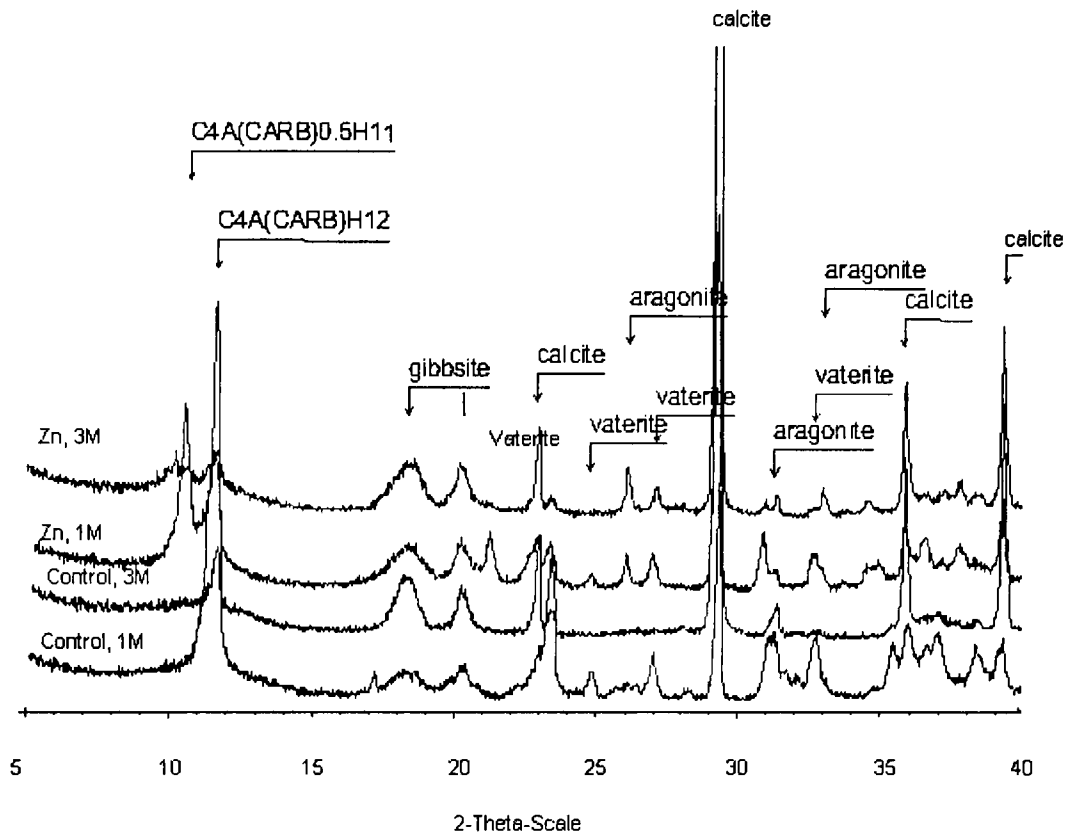


Fig. 5-9. Diffractograms of carbonated  $C_3A$  suspensions at different times

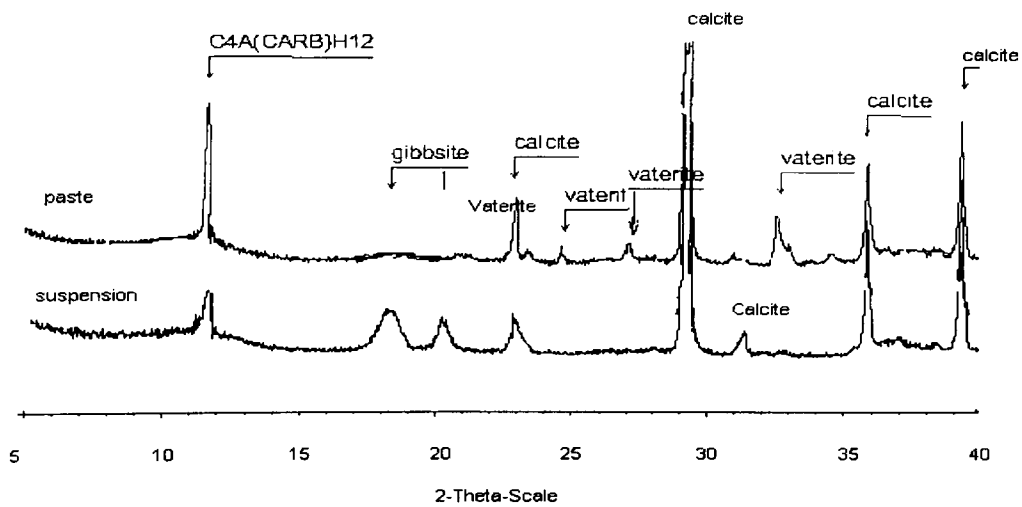


Fig. 5-10. Diffractograms of the carbonated  $C_3A$  suspension and paste at 3 months of age

## 5.3.2 C<sub>3</sub>A in the presence of gypsum

### 5.3.2.1 Hydration

The hydration products of metal-doped C<sub>3</sub>A pastes with gypsum are shown in Fig. 5-11. In the one-month old pastes, ettringite, gypsum and a small amount of anhydrous C<sub>3</sub>A were detected. Unlike the pastes obtained from hydrated C<sub>3</sub>A without gypsum, no products resulting from atmospheric carbonation were detected. It is noted that a very weak reflection for calcium monosulphoaluminate at 10.2° 2θ was detected in the control sample, differing from heavy metal -doped C<sub>3</sub>A pastes with gypsum.

The diffractograms obtained from C<sub>3</sub>A pastes in the presence of gypsum at one year of age are shown in Fig. 5-12. Compared with one-month old paste, very weak reflections for vaterite were observed at 24.5° and 27° 2θ. Boehmite was detected in all the pastes.

### 5.3.2.2 Accelerated carbonation

The diffractograms obtained from accelerated carbonated C<sub>3</sub>A with gypsum are shown in Fig. 5-13. The most obvious reflections belong to gypsum and C<sub>3</sub>A. However, in the Zn<sup>2+</sup>-doped paste, ettringite was detected. Weak reflections for vaterite and boehmite were detected in all pastes.

The diffractograms obtained from pastes at one year are shown in Fig. 5-14. The differences in peak intensities in the metal-doped pastes and the control paste were less obvious, compared to the diffractograms of one-month old pastes. It is noted that ettringite disappeared in the Zn<sup>2+</sup>-doped paste aged one year. Vaterite and aragonite were detected in all pastes. It is interesting to note that in the presence of gypsum calcite did not form in the carbonated C<sub>3</sub>A pastes excluding the Pb-doped C<sub>3</sub>A paste with gypsum.

It is worth pointing out that in the presence of gypsum, no heavy metal compounds were detected by XRD. Heavy metal ions were most likely incorporated in ettringite, substituting for calcium or aluminium (Moore and Taylor, 1968; 1970). For example, the chromium can replace aluminium (Glasser, 1992; 1993). As mentioned in Chapter 1, in ettringite, columns of Ca<sub>6</sub>(Al(OH)<sub>6</sub>·24H<sub>2</sub>O are lines of Al(OH)<sub>6</sub><sup>3-</sup> octahedrally bonded

with  $3\text{Ca}^{2+}$  ions. The layer structure can incorporate variable amounts of water as well as compounds including metal hydroxide (Grougar *et al.*, 1996).

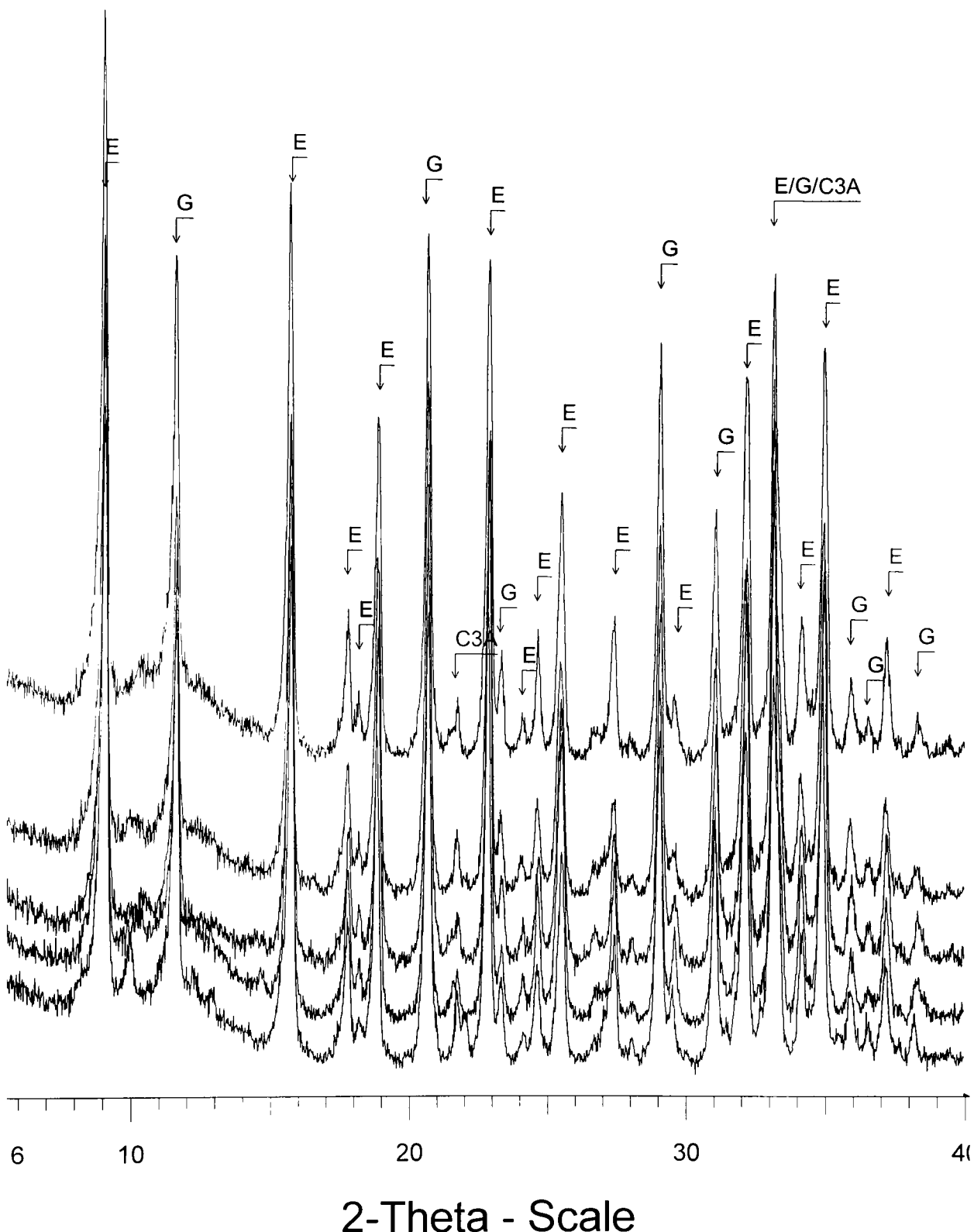


Fig. 5-11. Diffractograms of hydrated 28 day old  $\text{C}_3\text{A}$  pastes in the presence of gypsum (From bottom to top are control,  $\text{Cr}^{3+}$ ,  $\text{Cu}^{2+}$ ,  $\text{Pb}^{2+}$ , and  $\text{Zn}^{2+}$ -doped pastes, respectively, Legend: G = Gypsum, E = ettringite)



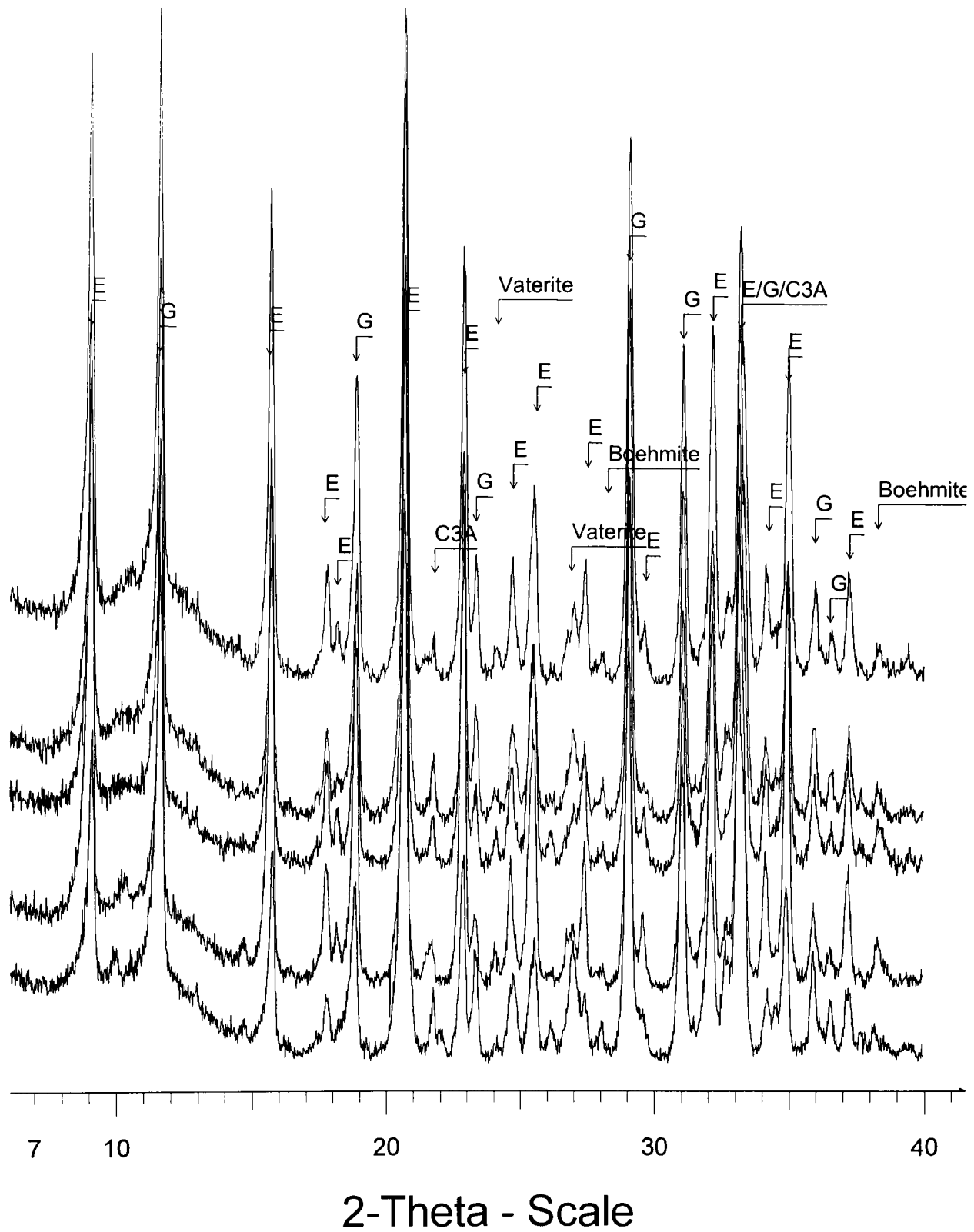


Fig. 5-12. Diffractograms of hydrated 1 year old  $C_3A$  pastes in the presence of gypsum (From bottom to top are control,  $Cr^{3+}$ ,  $Cu^{2+}$ ,  $Pb^{2+}$ , and  $Zn^{2+}$ -doped pastes, respectively, Legend: G = Gypsum, E = ettringite)

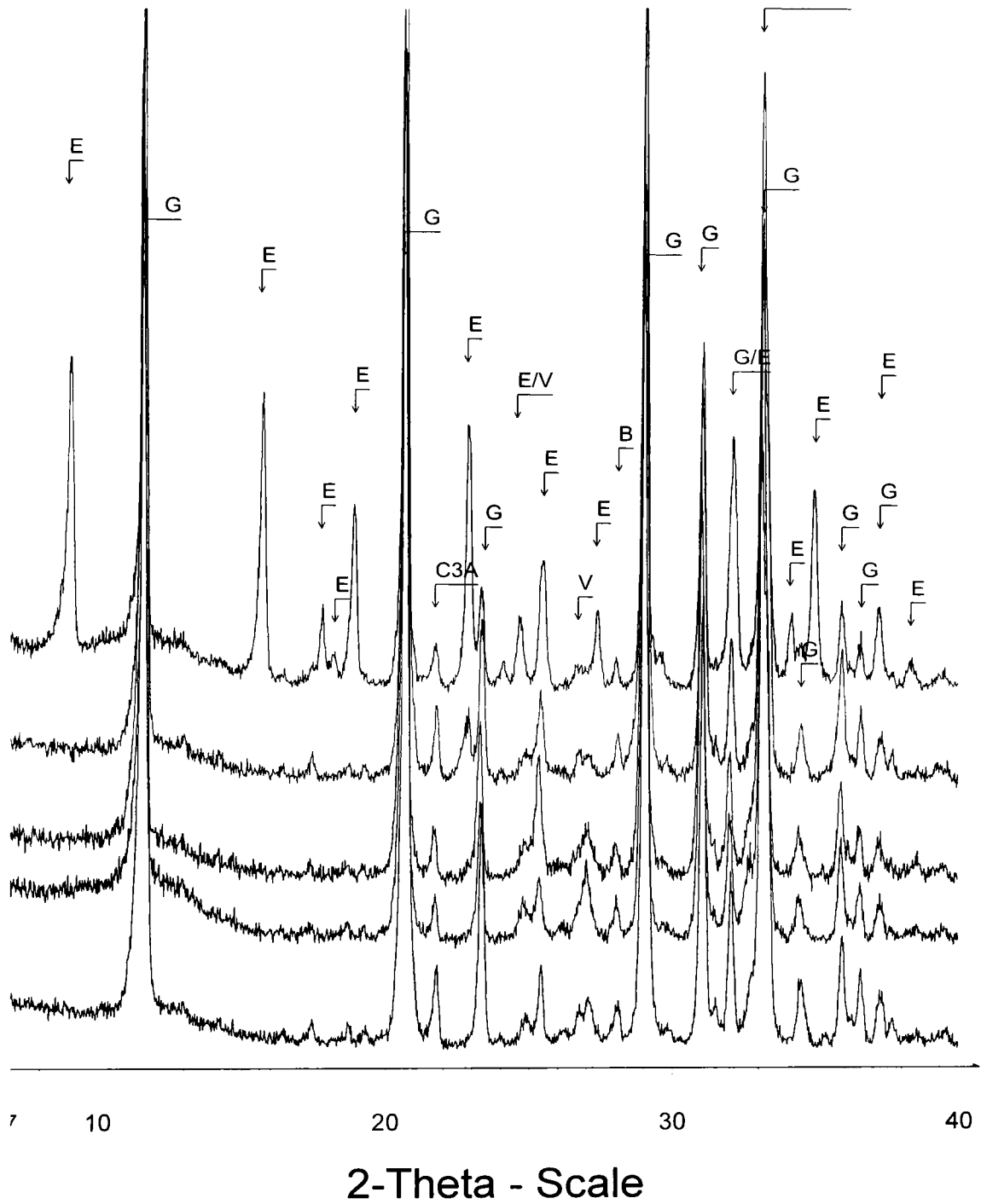


Fig. 5-13. Diffractograms of carbonated C<sub>3</sub>A pastes aged 1 month with gypsum (From bottom to top are control, Cr<sup>3+</sup>, Cu<sup>2+</sup>, Pb<sup>2+</sup>, and Zn<sup>2+</sup>-doped pastes, respectively.

Legend: G = Gypsum, E = ettringite, V = vaterite, B = boehmite)

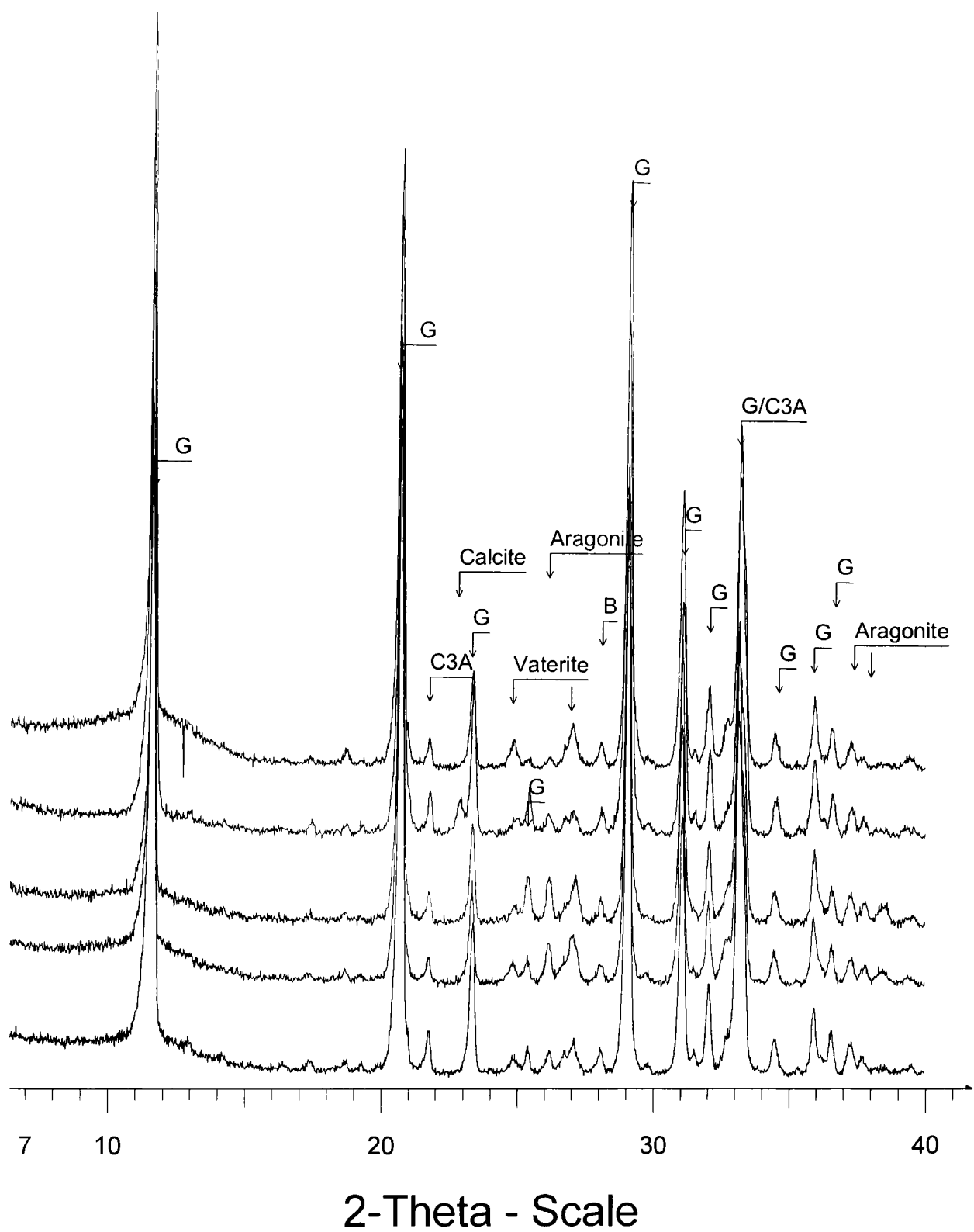


Fig. 5-14. Diffractograms of carbonated C<sub>3</sub>A pastes aged 1 year with gypsum (From bottom to top are control, Cr<sup>3+</sup>, Cu<sup>2+</sup>, Pb<sup>2+</sup>, and Zn<sup>2+</sup>-doped pastes, respectively, Legend: G = Gypsum, E = ettringite)

### 5.3.3 C<sub>12</sub>A<sub>7</sub>, CA and C<sub>4</sub>AF

The diffractograms of hydrated and carbonated C<sub>12</sub>A<sub>7</sub>, CA and C<sub>4</sub>AF are presented in Appendix 2 for clarity. Main findings are described as follows:

#### 5.3.3.1 Hydration

In the control hydrated C<sub>12</sub>A<sub>7</sub> paste aged 28 days, C<sub>4</sub>AH<sub>13</sub>, C<sub>4</sub>A(CaCO<sub>3</sub>)H<sub>11</sub>, C<sub>4</sub>A(CaCO<sub>3</sub>)<sub>0.5</sub>H<sub>12</sub>, gibbsite, vaterite and calcite were detected. The Cr<sup>3+</sup>-doped paste gave similar reflections to the control paste but the intensities of these peaks were much weaker. In addition, poorly crystalline calcium carboaluminate was detected in the Cr<sup>3+</sup>-doped paste. In the other heavy metal-doped pastes the major reflections belonged to anhydrous C<sub>12</sub>A<sub>7</sub>. It should note that in the Cu<sup>2+</sup>, Pb<sup>2+</sup>, and Zn<sup>2+</sup>-doped pastes, the peak at 29.45° 2θ was assigned to calcite. There were very broad reflections of poorly crystalline calcium carboaluminates in the Cu<sup>2+</sup>-doped C<sub>12</sub>A<sub>7</sub> paste. According to the main peak intensities of C<sub>12</sub>A<sub>7</sub> at 18° and 32.5° 2θ, heavy metals generally inhibited the hydration of C<sub>12</sub>A<sub>7</sub>.

In C<sub>12</sub>A<sub>7</sub> pastes sealed for one year, the degree of hydration increased greatly with time. Compared with one-month old control pastes, gibbsite and calcite reflections at one year were much stronger. C<sub>4</sub>A(CaCO<sub>3</sub>)<sub>0.5</sub>H<sub>12</sub>, gibbsite, vaterite and aragonite were identified in the heavy metal -doped pastes except for the Pb<sup>2+</sup>-doped paste. According to the intensities of C<sub>12</sub>A<sub>7</sub> reflections, heavy metals severely inhibited the hydration of C<sub>12</sub>A<sub>7</sub>.

The crystalline compounds identified by XRD in 28 days old hydrated CA pastes were calcium hemicarboxylate (C<sub>3</sub>A(CaCO<sub>3</sub>)<sub>0.5</sub>H<sub>12</sub>) and calcium monocarbonate (C<sub>3</sub>A(CaCO<sub>3</sub>)H<sub>11</sub>) as well as C<sub>4</sub>AH<sub>19</sub>. CAH<sub>10</sub> was also detected in the control paste. In these experiments CA carbonation was due to the small amount of CO<sub>2</sub> in the atmosphere in the preparation and testing of samples, despite the fact that samples were well sealed in bottles. Based on the intensity of CA at 30° 2θ, heavy metals promoted the hydration of this phase.

In the diffractograms of hydrated CA pastes aged one year, interestingly, compared to one-month old pastes, the peaks of calcium carboaluminate disappeared. and the peaks of

vaterite, calcite and  $C_4AH_{19}$  became stronger. In addition, gibbsite was more obvious in one year old hydrated pastes, especially in  $Zn^{2+}$ ,  $Cu^{2+}$  and  $Cr^{3+}$  -doped CA pastes.

It was noted that the heavy metal -doped ferrite pastes did not set and harden properly with the exception of the  $Cr^{3+}$ -doped paste. The major hydration products identified in the control hydrated paste of  $C_4AF$  were  $C_2(A,F)H_8$ ,  $C_4(A,F)(CaCO_3)H_{11}$  and  $C_4(A,F)(CaCO_3)_{0.5}H_{12}$ . According to the diffractograms and experimental observations, heavy metals strongly inhibited the hydration of  $C_4AF$ . In the  $Cr^{3+}$ -doped paste,  $C_4(A,F)(CaCO_3)_{0.5}H_{12}$  and  $C_4AF$  were identified, whereas in  $C_4AF$  pastes doped with other heavy metals, the most X-ray reflection peaks belonged to  $C_4AF$ .

After one year, the main reflection peaks of hydrated  $C_4AF$  pastes did not change significantly. It was noted that the peaks for hydrogarnet and vaterite in the control paste became stronger (see Appendix 2).  $C_2AH_8$  that was originally observed in the control paste at 28 days had a lower intensity at one year. In the  $Zn^{2+}$  -doped paste the peaks for  $C_4(A,F)(CaCO_3)_{0.5}H_{12}$  were detected.

The degree of  $C_4AF$  hydration did not increase appreciably with time.  $C_4AF$  had low hydraulic activity, which was further inhibited by the presence of heavy metals.

### 5.3.3.2 Accelerated carbonation

In the diffractograms of carbonated  $C_{12}A_7$  pastes aged one month, most peaks belonged to anhydrous  $C_{12}A_7$ , indicating that the degree of carbonation was very low. In the control and  $Cr^{3+}$ -doped  $C_{12}A_7$  pastes calcite and vaterite were detectable, whereas in other  $C_{12}A_7$  pastes only vaterite was detected.

Calcite, vaterite and aragonite were detectable in carbonated  $C_{12}A_7$  pastes aged one year. In the one year old  $Zn^{2+}$ -doped  $C_{12}A_7$  paste,  $C_4A(CaCO_3)_{0.5}H_{12}$  and  $C_4A(CaCO_3)H_{11}$  were apparent. The results from X-ray diffractometry for carbonated  $C_{12}A_7$  pastes illustrated the retarding effects of heavy metals on the carbonation of  $C_{12}A_7$ .

The carbonation products of CA were calcite and vaterite. According to the intensities recorded for CA at  $30^\circ 2\theta$  and the intensities of calcite at  $29.5^\circ 2\theta$ , heavy metals slightly promoted the carbonation of CA.

The similarity between the diffractograms of carbonated CA pastes at different ages (1 month and 1 year) indicated that the degree of CA carbonation increased only slightly with time. CA was resistant to carbonation under these conditions.

The diffractograms of carbonated  $C_4AF$  pastes with or without heavy metals indicated that heavy metal doping inhibited the carbonation of this phase. In the control carbonated  $C_4AF$  paste calcite was detected, whereas the main X-ray reflections belonged to  $C_4AF$  in the heavy metal-doped pastes. This indicates that no carbonation products were detected by XRD in the heavy metal -doped  $C_4AF$  pastes.

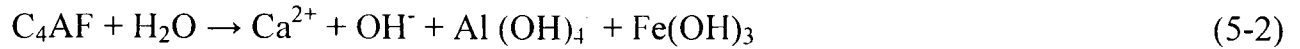
The XRD patterns of one year old carbonated  $C_4AF$  pastes showed very similar patterns to one-month old pastes, indicating that  $C_4AF$  was resistant to carbonation. The only noticeable difference was that in the control carbonated  $C_4AF$  paste aged one year the intensities of X-ray diffraction peaks of gibbsite, calcite, aragonite and vaterite were stronger compared to the control paste age one month. Heavy metals inhibited the carbonation of  $C_4AF$ , according to the examination based on XRD.

#### ***5.4 Further discussion---reactivity of phases containing aluminium***

The foregoing results and discussion illustrated that there were obvious differences in the behaviour of pure cement phases containing aluminium during hydration and carbonation. Table 5-5 summarises the results based on the examination of XRD. Comparing the hydrated pastes with their carbonated analogues as well as starting materials, it can be seen that these phases were more easily hydrated than carbonated.

To explain the reactivity of cement phases containing aluminium, the suspensions of these phases were examined. In pure cement phases,  $C_3A$ ,  $C_{12}A_7$ , CA and  $C_4AF$ , the calcium ions link the  $AlO_4^-$  tetrahedral and are co-ordinated to oxygen ions that are not linked to  $Al^{3+}$ . This open structure readily allows water interaction, because CaO is the favoured site for water attack (Taylor, 1997). On the contact with water, the phases of

cement decompose and hydrate. The decompositions of these phases are shown in the following equations:



According to products identified by XRD in this work, the reactions of calcium aluminates and ferrite with water or carbon dioxide can be presented as Eqs. 3-7.

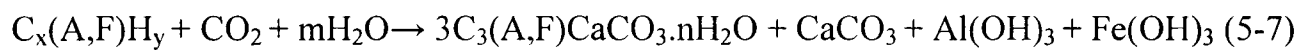
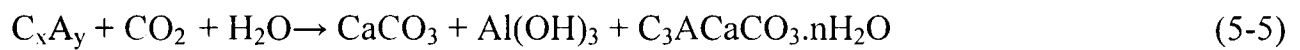
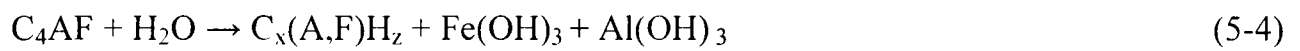


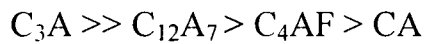
Table 5-5. A comparison of pure cement phases containing aluminium

Phases	Reaction	Comments
C <sub>3</sub> A	Hydration: fast Carbonation: moderate	The degree of reaction was high and increased with time
C <sub>12</sub> A <sub>7</sub>	Hydration: moderate Carbonation: slow	The degree of hydration was moderate and increased drastically with time, but the degree of carbonation was low and increased only slightly with time
CA	Hydration: slow Carbonation: slow	The degree of reaction was low and increased only slightly with time
C <sub>4</sub> AF	Hydration: slow Carbonation: slow	The degree of hydration was low and increased with time, but the degree of carbonation was very low and increased only slightly with time

In the absence of heavy metals, the calcium that enters solution and the resulting hydrolysis are the most important factors affecting the suspension pH and consequently

dominate the hydration of these phases. The calcium oxide content of these phases is presented in Table 5-6. Table 5-6 also shows the equilibrium pH values of pure cement phase suspensions. The suspensions of pure cement phases reached their equilibrium pH at different rates. C<sub>3</sub>A suspensions only took a few seconds after contacting water, but the suspensions of C<sub>4</sub>AF, C<sub>12</sub>A<sub>7</sub> and CA needed a few minutes more.

It is noted that the sequence of equilibrium pH values and the rates of reaching equilibrium pH values are consistent with the CaO content and the reactivity of the phases identified by XRD. The higher calcium oxide content of cement phases is, the higher of suspension pH values and higher the reactivity of cement phases. In the control pastes, the reactivity of these phases can be arranged in the sequence:



The presence of heavy metal ions lowered the suspension pH values recorded due to hydrolysis of heavy metal ions. As a result, the hydration rates and degrees of cement phases containing aluminium varied.

Table 5-6. The pH of pure cement phase suspensions

Phase	C <sub>3</sub> A	CA	C <sub>4</sub> AF	C <sub>12</sub> A <sub>7</sub>
pH	12.4	11.5	12.0	11.8
CaO (%)	62.22	35.44	46.09	48.48

In order to study the reactivity of pure cement phases containing aluminium in carbonation processes, the pH values of carbonated suspensions were measured. Fig. 5-15 shows the relationship of carbonation cycles with suspension pH values, which were measured one hour after the suspensions were removed from contacting with carbon dioxide. The suspension pH values decreased with the increase in the number of carbonation cycles. Fig. 5-15 also confirmed that there were differences in carbonation rate between different phases, as the suspension pH depended on both the degree of carbonation and the rate of decomposition of phases. When carbonation was incomplete,

the suspension pH rose very quickly and went up to high alkalinity shortly after removal from contact with CO<sub>2</sub>. This was due to the decomposition of anhydrous cement phases.

After the 8<sup>th</sup> carbonation cycle, the pH values of most suspensions were stable and below 8 (Fig. 5-16), indicating that 8 cycles of carbonation procedure are suitable procedure for accelerated carbonation of pure CA, C<sub>12</sub>A<sub>7</sub> and C<sub>4</sub>AF. The degree of carbonation of CA, C<sub>12</sub>A<sub>7</sub> and C<sub>4</sub>AF were very low at one year after carbonation. The low reactivity of these phases upon carbonation can be attributed to the precipitation of Al(OH)<sub>3</sub> and Fe(OH)<sub>3</sub> on the surfaces of C<sub>3</sub>A, C<sub>12</sub>A<sub>7</sub>, C<sub>4</sub>AF and CA, blocking the further reactions (Taylor, 1990; Berger *et al.*, 1972).

Heavy metals retarded the carbonation of C<sub>3</sub>A, C<sub>12</sub>A<sub>7</sub> and C<sub>4</sub>AF. The retardation could be attributed to heavy metal ion adsorption on the surfaces of C<sub>3</sub>A, C<sub>12</sub>A<sub>7</sub> and C<sub>4</sub>AF phases when calcium ions entered solutions due to structure meta-stability (Brady and Weil, 1996; Wang and Vipulanandan, 2000; Cheng and Bishop, 1992). The adsorption of heavy metal ions formed an impermeable carbonate coating and blocked the carbonation (Glasser *et al.*, 1999; Lin *et al.*, 1993; 1997).

According to experimental observation, examination of XRD results and suspension pH measurements, reactivity of C<sub>3</sub>A was higher than that of C<sub>3</sub>S in hydration, but lower than that of C<sub>3</sub>S in carbonation.

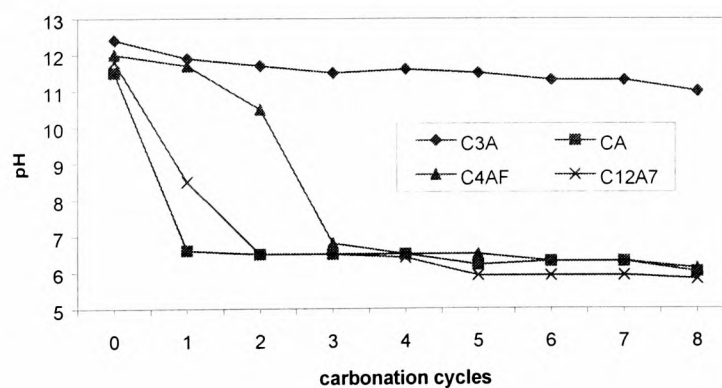


Fig. 5-15. The pH of pure cement phase suspensions, 1 hour after carbonation

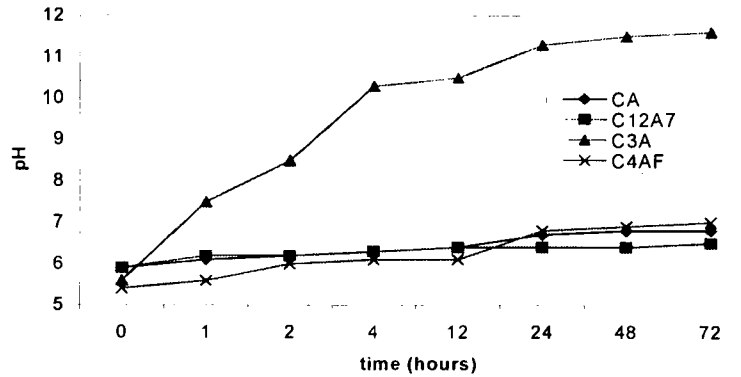


Fig. 5-16. The pH of pure cement phase suspensions after 8 cycles of carbonation

### 5.5 Summary

The present work investigated the reactions of pure cement phases containing aluminium with water and carbon dioxide in the presence or absence of selected heavy metal nitrates ( $Zn^{2+}$ ,  $Pb^{2+}$ ,  $Cu^{2+}$  and  $Cr^{3+}$ ) with and without gypsum. Changes induced by the presence of the heavy metals on the reaction products were examined by suspension pH measurements and X-ray diffractometry. The chemical reaction activities of  $C_3A$ ,  $C_{12}A_7$ , CA and  $C_4AF$  were studied and compared. The main conclusions are:

- Heavy metals inhibited the hydration reactions of  $C_{12}A_7$  and  $C_4AF$ , but slightly promoted the hydration reactions of  $C_3A$  and CA. Heavy metals inhibited the carbonation reactions of  $C_3A$ ,  $C_{12}A_7$  and  $C_4AF$ , but slightly promoted the carbonation of CA.
- In the absence of gypsum the hydration products of  $C_3A$  were primarily hydrogarnet, gehlenite hydrate,  $C_4AH_x$  and calcium carboaluminate, but in the  $Zn^{2+}$ -doped  $C_3A$  paste, hydrogarnet was not detected. Heavy metals, especially  $Zn^{2+}$ , inhibited the formation of hydrogarnet and promoted the transformation of C-A-H into calcium carboaluminate and eventually into calcium carbonate. During carbonation of  $C_3A$ ,  $C_{12}A_7$ , CA and  $C_4AF$ , the polymorphism of calcium carbonate was affected by the presence of heavy metals.

- In the presence of gypsum, the reaction products of  $C_3A$  appeared much more stable than those in the absence of gypsum. The effect of heavy metals on both the hydration or carbonation of  $C_3A$  with gypsum was less pronounced, compared to the results obtained in the absence of gypsum.
- The reactivity of  $C_3A$ ,  $C_{12}A_7$ ,  $CA$  and  $C_4AF$  in carbonation was much lower than in hydration.

## Chapter 6

### Phase development in heavy metal -doped Portland cement pastes and suspensions

#### 6.1 Background

The previous chapters examined the hydration and carbonation reactions of calcium oxide, calcium hydroxide and main pure cement phases in the presence or absence of heavy metals.

Cement clinkers are inherently thermodynamically unstable due to their small particle size, non-regular co-ordination and the deformation of their crystal structure resulting from the presence of metal ion impurities. For example, alite is stable only above 1250°C, in which the  $\text{Ca}^{2+}$  co-ordination number is 6 and  $\text{Al}^{3+}$  and  $\text{Mg}^{2+}$  ions distort the crystalline structure (Lea, 1970). In aluminate, the co-ordination numbers of calcium are different, as some are 6 co-ordinated and others are 12. Calcium ions link the tetrahedra  $(\text{SiO}_4)^{4-}$  or  $(\text{AlO}_4)^{5-}$  tetrahedra and are also co-ordinated to oxygen ions that are not linked to either  $\text{Si}^{4+}$  or  $\text{Al}^{3+}$ . It is this open structure that readily allows interaction with water (Taylor, 1990). According to Asavapisit *et al.* (1997), the hydration of cement proceeds three successive phases of reactions:

- dissolution of phases,
- precipitation of ettringite, C-S-H and portlandite, and
- interaction of hydration products

At the earliest stage of hydration, ettringite is formed, and a supersaturated solution of calcium hydroxide is also formed, from which portlandite crystallises. Following this a colloid solution coagulates, giving the typical hydro-gels of calcium silicate hydrate, which cause cement grains to cohere.

The reaction products can be considered as two parts, crystalline phases and amorphous phases. Crystalline phases in Portland cement pastes include portlandite, calcium carbonate and ettringite. Calcium silicate hydrate gel (C-S-H gel), the main substance of

hydrated or carbonated cement pastes, comprises a large and complex family of amorphous phases and displays varying composition (could incorporate aluminium and some other atoms). The impurities in the C-S-H gel such as aluminium, heavy metals and some anions such as  $\text{CO}_3^{2-}$  and  $\text{SO}_4^{2-}$  influence its structure (Richardson and Groves, 1993).

In cement pastes, Taylor (1990, 1993) claimed that when  $\text{Ca/Si} < 1$ , C-S-H and  $\text{SiO}_2$  coexist; when  $1 < \text{Ca/Si} < 2$ , C-S-H(1), i.e. low Ca/Si ratio calcium silicate hydrate gel—tobermorite-like gel forms; when  $2 < \text{Ca/Si} < 3$ , C-S-H(2), i.e. high Ca/Si ratio calcium silicate hydrate gel—jennite-like gel forms; and when  $\text{Ca/Si} > 3$ , C-S-H(2) and portlandite coexist.

The carbonation of cement is a chemical process that results in the formation of calcium carbonate and water (Suzuki, 1985; Taylor, 1990). Some minor phases, for example, ettringite, transform into calcium carbonate, hydrous alumina and gypsum upon carbonation (Berger *et al.*, 1972; Bozkurt *et al.*, 2000). During carbonation both free water and structurally bound water are liberated (Ngala and Page, 1997). This water reacts with anhydrous cement and facilitates carbonation through dissolution of  $\text{CO}_2$  gas, and the consequent dissolution of calcium (Goto *et al.*, 1995).

Cement may contain a significant amount of trace heavy metals resulting from the raw materials or fuel used during preparation (Murat and Sorrentino, 1996; Stephan *et al.*, 1999). Heavy metals present influence the rates and products of cement reactions with water or carbon dioxide (Chandra, 1997; Murat and Sorrentino, 1996; Trussel and Spence, 1994). Consequently, these metals may have a significant impact on the performance of cement and concrete.

When high concentrations of heavy metals are incorporated into hydrating cement, such as during s/s of waste, both setting and strength development may be significantly affected (Conner, 1990; Hills *et al.*, 1994; Johannesson and Utgenannt, 2001; Klich *et al.*, 1999). Yousuf and Mollah (1995) claimed that carbonation could change the characteristics of the clinker-C-S-H interface, affecting the long-term retention of heavy metals. More studies involving accelerated carbonation of cement-based solidified waste forms showed that the immobilisation of contaminants during leach testing could be significantly improved (Lange *et al.*, 1996).

A better understanding of the interactions of cement with heavy metals will lead to finding methods to improve the effectiveness of s/s (Conner, 1990; Bonen and Sarkhar, 1995). The present work seeks to examine carbonated Portland cement-metal mixtures by XRD, DTA/TG and  $^{29}\text{Si}$  and  $^{27}\text{Al}$  magic angle spinning/nuclear magnetic resonance (MAS/NMR) spectroscopy and compares the results obtained with their hydrated counterparts.

## **6.2 Experimental**

### **6.2.1 Materials**

Portland cement and chemicals used in this study were described in Chapter 2. Hydroxides of heavy metals were prepared by the slow addition of 10M NaOH solution to the solutions of heavy metal nitrates until a pH 8-9 was achieved and hydroxides were precipitated. The hydroxide slurry was allowed to settle for 1 hour and was then filtered through a 0.45 $\mu\text{m}$  membrane filter. Prior to oven drying, a portion of the cake described above was placed into a carbon dioxide chamber at a pressure of 0.3MPa for 3 days. Following carbonation the salts were dried and ground for use.

### **6.2.2 Methods**

#### **6.2.2.1 Hydration**

Hydrated pastes were prepared by mixing the metal nitrate solutions or de-ionised water with Portland cement in a 500ml beaker. The cement/liquid (C/L) ratio was 10:4, giving a content of heavy metal in the hydrated paste of 2% w/w. Mixtures were placed in screw top sealed containers and then stored at laboratory ambient temperature of around 17°C. Samples were examined at the ages of 28 days and one year.

#### **6.2.2.2 Accelerated carbonation**

Fresh cement pastes were prepared for accelerated carbonation under the same conditions as described above and were exposed to 100% CO<sub>2</sub> in a reaction chamber for a period of 30 minutes. Following this, pastes were removed and ground to <0.03mm with a pestle and mortar and placed back in the carbonation chamber for another 30 minutes. This

procedure was repeated 8 times. Accelerated carbonated samples were stored in containers in a CO<sub>2</sub> bags until examination time of 28 days and one year.

### **6.2.2.3 Carbonation of previously hydrated pastes**

The one month old hydrated cement pastes were ground to <0.03 mm with a pestle and mortar and mixed with water at a solid/water ratio 10:2 prior to exposure to carbon dioxide in a carbonation chamber for 30 minutes. Using the same procedure described in Chapter 2, the carbonation was completed after 5 cycles.

### **6.2.2.4 Cement suspension studies**

The pH of the heavy metal nitrate/cement suspensions at 0% and 5% metals addition, at a C/L ratio 1:10, was recorded with time using a Philips DW9418 pH meter. To obtain data on the progress of carbonation, heavy metal nitrate/cement suspensions with a C/L ratio of 1:10 were placed in a carbonation chamber for 40 minutes. They were then removed and the pH was measured before placement back in the chamber for a further period (40 minutes) of carbonation.

### **6.2.2.5 Thermal analysis (DTA/TG)**

A Stanton Redcroft STA 780 Simultaneous Thermal Analyser was used to conduct DTA/TG analyses. Samples (20 mg) were ground with an agate mortar and pestle to less than 50 microns and were packed in a crucible, which is 5.8mm dia. and 4 mm high and made from rhodium-platinum. Samples were examined at a heating rate of 10°C/min under flowing nitrogen (40cm<sup>3</sup>/min) from 30-900°C.

### **6.2.2.6 X-ray powder diffraction (XRD)**

A Siemens D500 diffractometer (CuK-alpha radiation; 40KV and 40mA) was used to identify the crystalline products present in the pastes before and after carbonation. Samples were ground to <0.03mm and a scanning range of 5-40° 2θ was chosen at a scanning rate of 1° 2θ per minute.

### 6.2.2.7 Nuclear magnetic resonance (NMR)

In this work,  $^{29}\text{Si}$  solid state NMR spectra were recorded on a Varian Infinity Plus-300 spectrometer equipped with a 7.1T magnet. The resonance frequency for  $^{29}\text{Si}$  was 59.49 MHz. The NMR experiments were operated at relaxation T1 2s pulse with a relaxation delay of 2s.  $^{29}\text{Si}$  chemical shifts were reported related to tetramethylsilane.

$^{27}\text{Al}$  solid-state NMR spectra were recorded on a JOEL JNM ECP-300 FT spectrometer equipped with a 6mm SH30T6/HS solid state probe and a 7.05T magnet in which the resonance frequency for  $^{27}\text{Al}$  was 78.31MHz.  $^{27}\text{Al}$  spectra were acquire with  $1\mu\text{s}$  pulses and recycle delay of 2s in order to minimise intensity distortion arising from quadrupolar effects. Aluminium NMR data were reported to the nearest 1ppm relative to aluminium cation and used solid aluminium nitrate as a reference to confirm acquisition parameters did not vary.

The curing time of all samples was 1 year after hydration or after accelerated carbonation. To avoid the broad resonance, spinning the sample (6 KHz) at the angle of  $54.7^\circ$  to the direction of the spectrometer magnetic field was used to acquire the silicon and aluminium data.

## 6.3 Results and discussion

### 6.3.1 Hydration

Fig. 6-1 shows the diffractograms obtained from Portland cement pastes after 28 days of hydration with or without heavy metals. The main differences involve the intensity of peaks of portlandite at, for example,  $18^\circ$ ,  $28.6^\circ$  and  $34^\circ$  ( $2\theta$ ), alite at  $32^\circ$  and  $32.7^\circ$  ( $2\theta$ ), and ettringite at  $9^\circ$ ,  $16^\circ$  and  $25.5^\circ$  ( $2\theta$ ).

A variation in intensities of the ettringite peaks, which was particularly large for  $\text{Cr}^{3+}$  and  $\text{Zn}^{2+}$ , was noticed. This indicated that these metals encouraged the formation of ettringite. Calcium carboaluminate ( $\text{C}_4\text{A}(\text{CARB})\text{H}_{11}$ ) was detected at  $11^\circ$   $2\theta$  in the  $\text{Cu}^{2+}$  -doped paste.

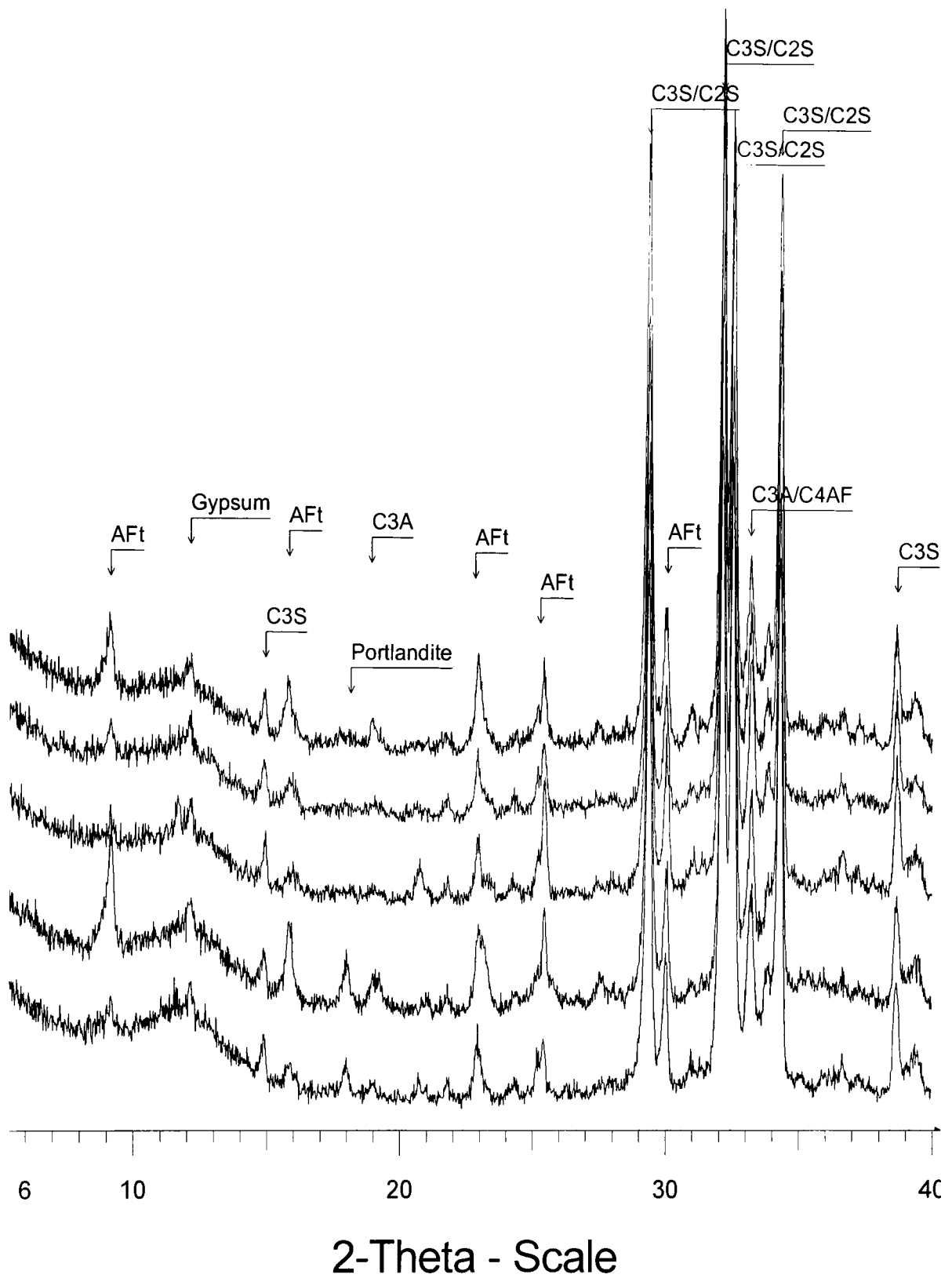


Fig. 6-1. Diffractograms for hydrated cement pastes aged one month  
 (From top to bottom are  $Zn^{2+}$ ,  $Pb^{2+}$ ,  $Cu^{2+}$ ,  $Cr^{3+}$  -doped and the control pastes)

The formation of portlandite is often used as an indication of cement hydration. Portlandite was detected in the control paste, but not in  $\text{Cu}^{2+}$ ,  $\text{Pb}^{2+}$  or  $\text{Zn}^{2+}$ -doped pastes. It is worthy to mention that in the  $\text{Cr}^{3+}$ -doped paste, the X-ray reflection peak at  $18.1^\circ 2\theta$  was assigned to AFt- $\text{Cr}_2\text{O}_3$ , not portlandite, combined with DTA/TG analysis techniques (see the later part of this section). According to the X-ray reflection peaks of portlandite in the various cement pastes, heavy metals ( $\text{Cr}^{3+}$ ,  $\text{Cu}^{2+}$ ,  $\text{Pb}^{2+}$  and  $\text{Zn}^{2+}$ ) retarded the precipitation of portlandite.

In cement pastes, amorphous phases of heavy metal compounds are inclined to form, because their saturation indices are too high; the nucleation and aggregation occur too fast; and species have not mobility as well as enough time to undergo proper orientation and alignment before bonding into a structure. The cement suspensions with or without heavy metal ions, therefore, were used to study and explain the retarding effect of heavy metals on the portlandite formation, and obtain more information on the phase development in the cement hydration process.

The crystalline products formed in cement suspensions are summarised in Table 6-1 at different times. Reflection peaks of alite in Cu, Cr and Pb -doped suspensions disappeared before those in the control suspension. In the Zn -doped suspension, alite was detectable even at 2 months of age. According to this,  $\text{Cu}^{2+}$ ,  $\text{Pb}^{2+}$  and  $\text{Cr}^{3+}$  promoted the hydration of cement, whereas Zn inhibited the hydration of cement.

Interestingly, the layered double hydroxides of calcium and heavy metals ( $\text{CaZn}_2(\text{OH})_6 \cdot 2\text{H}_2\text{O}$ ,  $\text{Ca}_2(\text{OH})_4 \times \text{Cu}(\text{OH})_2 \cdot m\text{H}_2\text{O}$  and  $\text{Ca}_2\text{Cr}(\text{OH})_7 \cdot 3\text{H}_2\text{O}$ ) were detected, as shown in Fig. 6-4, exhibiting the similarity to heavy metal -doped suspensions of calcium oxide, calcium hydroxide and tricalcium silicate.

The control suspension of Portland cement gave the most intense peaks of portlandite, whereas in heavy metal-doped suspensions the amount of portlandite was very limited even after three months of hydration. In the  $\text{Zn}^{2+}$ -doped cement suspension, there was no portlandite detected. These results were in agreement with those obtained from hydrated Portland cement pastes.

In the absence of heavy metals, the cement suspension had a very high pH (12.4), which closed to the saturation pH of portlandite (Fig. 6-3). In the presence of heavy metals, due to the hydrolysis of metal nitrate salts and hydration of cement, the suspension pH values

varied and initial pHs were 4.2, 5.8, 8.1 and 9.5 for  $\text{Cu}^{2+}$ ,  $\text{Zn}^{2+}$ ,  $\text{Pb}^{2+}$  and  $\text{Cr}^{3+}$ -doped suspensions, respectively (at the heavy metal concentration of 50 g/l).

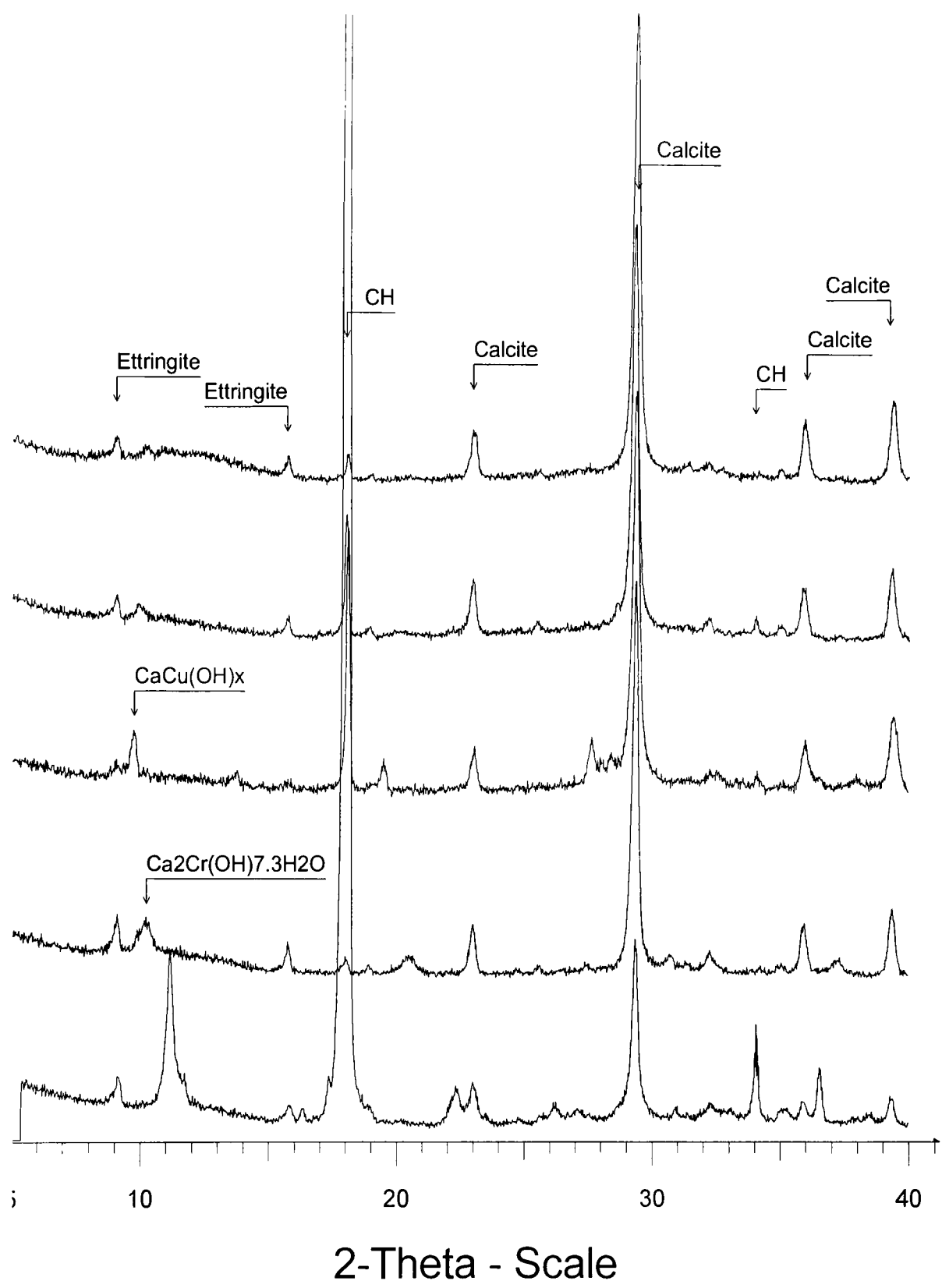


Fig. 6-2. Diffractograms of hydrated cement suspensions at the age of three months (From top to bottom are  $\text{Zn}^{2+}$ ,  $\text{Pb}^{2+}$ ,  $\text{Cu}^{2+}$ ,  $\text{Cr}^{3+}$  -doped and the control suspensions, respectively, Legend:  $\text{CaCu(OH)}_x = \text{Ca}_2(\text{OH})_{4x}\text{Cu(OH)}_2m\text{H}_2\text{O}$ )

Table 6-1. Phase development in hydrated Portland cement suspensions

Sample	Effect	Phases identified by XRD	
		14 days	3 months
Control		Portlandite (VS), Alite (M), Belite (M), Ettringite	Portlandite (VS), Ettringite, Calcite (w)
Cr	promoter	Alite (w), Belite (w), Ettringite, Monosulphate, Aragonite, $\text{Ca}_2\text{Cr}(\text{OH})_7\cdot 3\text{H}_2\text{O}$	Portlandite, Ettringite, Monosulphate, Calcite, $\text{Ca}_2\text{Cr}(\text{OH})_7\cdot 3\text{H}_2\text{O}$
Cu	promoter	Ettringite, Monosulphate, $\text{Ca}_2(\text{OH})_4\text{xCu}(\text{OH})_2\cdot \text{mH}_2\text{O}$ , Alite (w), Belite (w)	Portlandite, Ettringite, Monosulphate, $\text{Ca}_2(\text{OH})_4\text{xCu}(\text{OH})_2\cdot \text{mH}_2\text{O}$
Pb	promoter	Portlandite (w), Ettringite, Alite (w), Belite (w), Monosulphate	Portlandite, Ettringite, Monosulphate, Calcite
Zn	inhibitor	Alite (VS), Belite (VS), $\text{CaZn}_2(\text{OH})_6\cdot 2\text{H}_2\text{O}$ , Ettringite, Monosulphate,	Portlandite (w), Ettringite, Monosulphate, Calcite

Note:  $\text{Ca}_2(\text{OH})_4\text{xCu}(\text{OH})_2\cdot \text{mH}_2\text{O}$  (d-space 0.769, 0.395, 0.336, 0.319, 0.313 nm); VS-very strong, w-weak; M-moderate

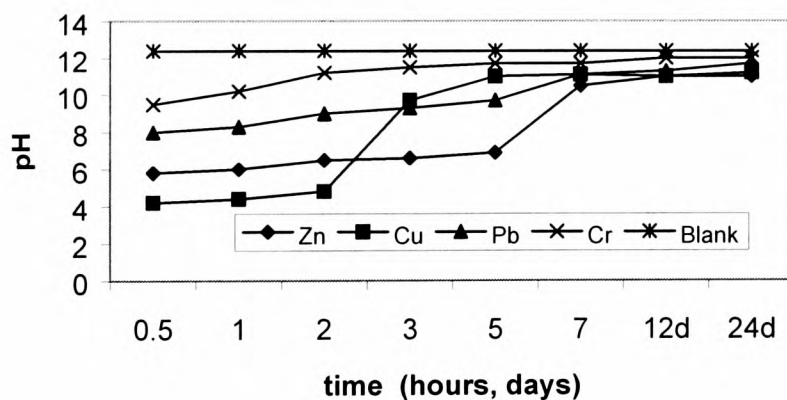
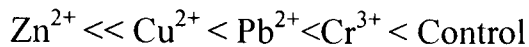


Fig. 6-3. pH values of cement suspensions with time

The suspension pH values of Portland cement with or without heavy metals increased with time and the pH values recorded after 24 days were in the order:



In the  $\text{Zn}^{2+}$ -doped cement suspension, the pH remained at less than 12 after three months of hydration (Fig. 6-3). The low pH values resulted from the heavy metal hydrolyses were responsible for the retardation of portlandite precipitation in heavy metal -doped cement pastes and suspensions.

Hydrated Portland cement pastes sealed in the plastic screw top bottles for one year were also examined by XRD. The diffractograms obtained from these pastes are presented in Fig. 6-4. A comparison with the diffractograms obtained from the 28 day-old (given in Fig. 6-1) showed that the intensities of X-ray reflections of portlandite and ettringite increased with time, particularly in the heavy metal-doped pastes. It was noticed that the intensities of reflection peaks for portlandite were compatible with the intensity variations of X-ray reflections recorded for alite (consumption of alite resulted in the reduction of peak intensities for alite).

In the heavy metal -doped cement pastes a broad peak at  $10-11.5^\circ 2\theta$  representing poorly crystalline carboaluminate was also observed, but in the control paste, this peak was absent. Despite careful sealing in the containers a minor amount of carbonation was evident at 1 year for the hydrated cement pastes. Calcite was detected in all cement pastes except for the  $\text{Cr}^{3+}$ -doped paste; vaterite was observed in all heavy metal -doped Portland cement pastes, showing that the polymorphism of calcium carbonate was strongly influenced by the presence of particular metals.

As described earlier, in the hydrated Portland cement suspensions doped with heavy metals the double hydroxides were detected by XRD. To confirm the formation of these compounds in the heavy metal -doped Portland cement pastes and to characterise other hydration products of cement further, DTA/TG techniques were employed. The DTA curves and simultaneous TG curves of hydrated cement pastes aged one month are present in Figs. 6-5 and 6-6. The thermal analysis results are summarised in Table 6-2.

In the control Portland cement paste, the endothermic peak at temperature  $80-130^\circ\text{C}$  arose from the evaporation of physically and chemically bound water, dehydration of C-S-H gel and decomposition of ettringite. It is apparent that there were the endothermic

peaks of portlandite dehydroxylation at 440-510°C and calcite decomposition at 680-780°C, which corresponded to two apparent steps of mass loss in the TG curve. According to the amount of mass loss, it is calculated that in the control paste the portlandite and calcite contents were 19.2% and 29.1%, by mass, respectively.

In the heavy metal -doped cement pastes, there was no endothermic peak of the dehydroxylation of portlandite and corresponding mass-loss step, excluding the formation of amorphous and crystalline portlandite. In other words, there was no portlandite formed at early age in the presence of heavy metals, supporting the XRD examination.

In the Cr<sup>3+</sup>-doped cement paste, endotherm corresponding to the dehydroxylation of the double hydroxide of calcium and chromium (Ca<sub>2</sub>Cr(OH)<sub>7</sub>·3H<sub>2</sub>O) at 260-340°C was recognised. In addition, the endothermic peaks of calcium carbonate decomposition and dehydration of C-S-H and ettringite were detected. Similarly, in the Cu-doped paste, two endotherms corresponding to double hydroxides of calcium and copper, namely Ca<sub>2</sub>(OH)<sub>4</sub>xCu(OH)<sub>2</sub>·mH<sub>2</sub>O, at 250-320°C and 400-430°C were apparent.

In Pb<sup>2+</sup>-doped and Zn<sup>2+</sup>-doped pastes endotherms for the dehydration of C-S-H and ettringite and the decomposition of calcium carbonate were detected. Differing from the hydrated Zn<sup>2+</sup>-doped C<sub>3</sub>S paste or calcium oxide paste, no endothermic peaks corresponding to CaZn<sub>2</sub>(OH)<sub>6</sub>·2H<sub>2</sub>O decomposition were observed in the hydrated Zn<sup>2+</sup>-doped Portland cement paste. This indicates that hydration products of Portland cement may have a stronger binding capacity for zinc ions in comparison to those of C<sub>3</sub>S or calcium oxide.

Table 6-2. Thermal analysis results of hydrated Portland cement pastes (mass loss at indicated temperature, %)

Samples	Control	Cr	Cu	Pb	Zn
20-250°C	11.1	12.3	7.8	7.5	8.6
250-600°C	9.9	17.3	12.6	10.9	15
600-1100°C	12.8	14.5	16.2	17.1	14.5
Total mass loss	33.8	44.1	36.6	35.6	38.1
Ca(OH) <sub>2</sub> content	19.2	0	0	0	0
CaCO <sub>3</sub> content	29.1	32.9	36.8	38.9	32.9

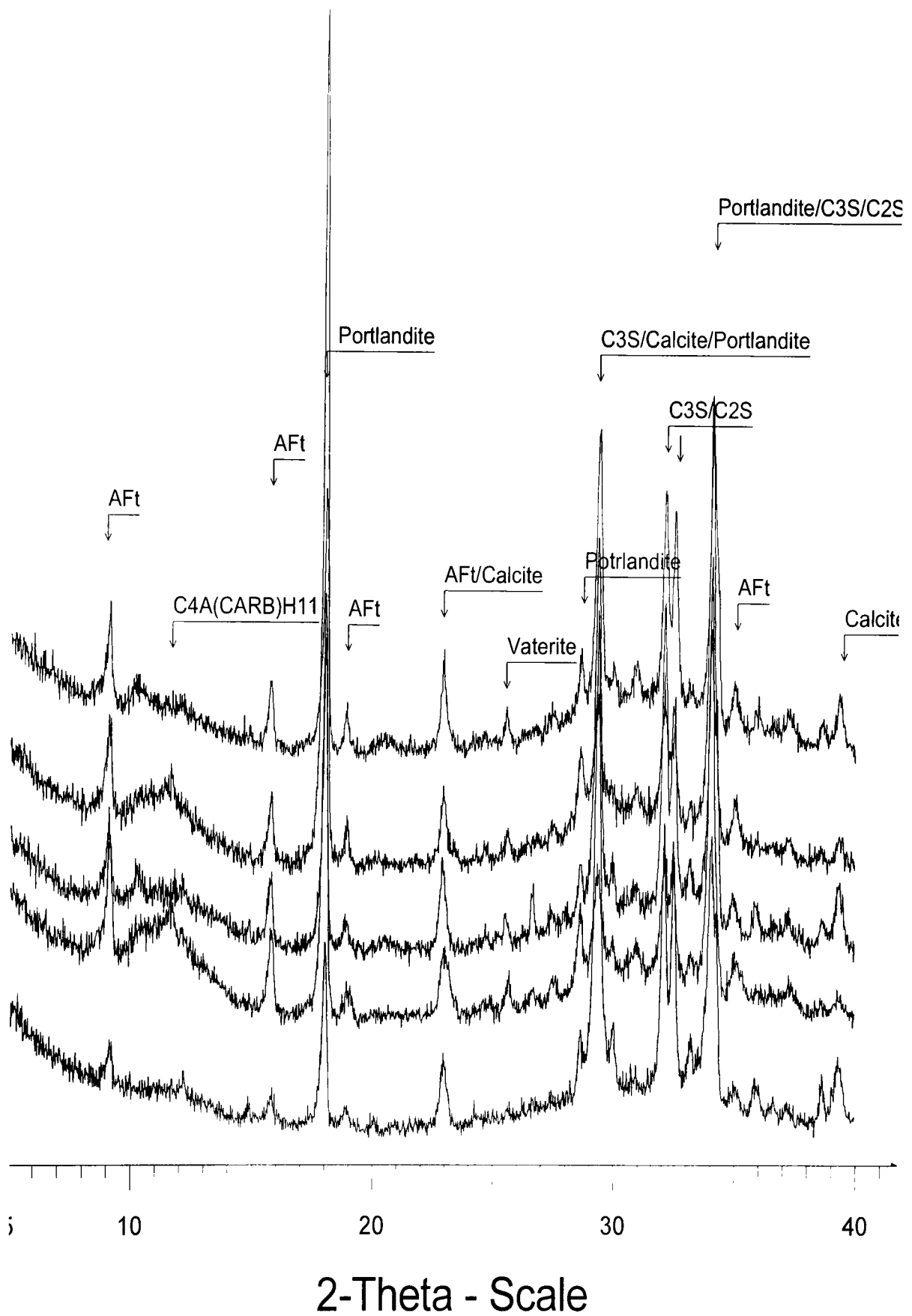


Fig. 6-4. Diffractograms of hydrated Portland cement pastes aged one year (From top to bottom are Zn<sup>2+</sup>, Pb<sup>2+</sup>, Cu<sup>2+</sup>, Cr<sup>3+</sup> -doped and the control pastes).

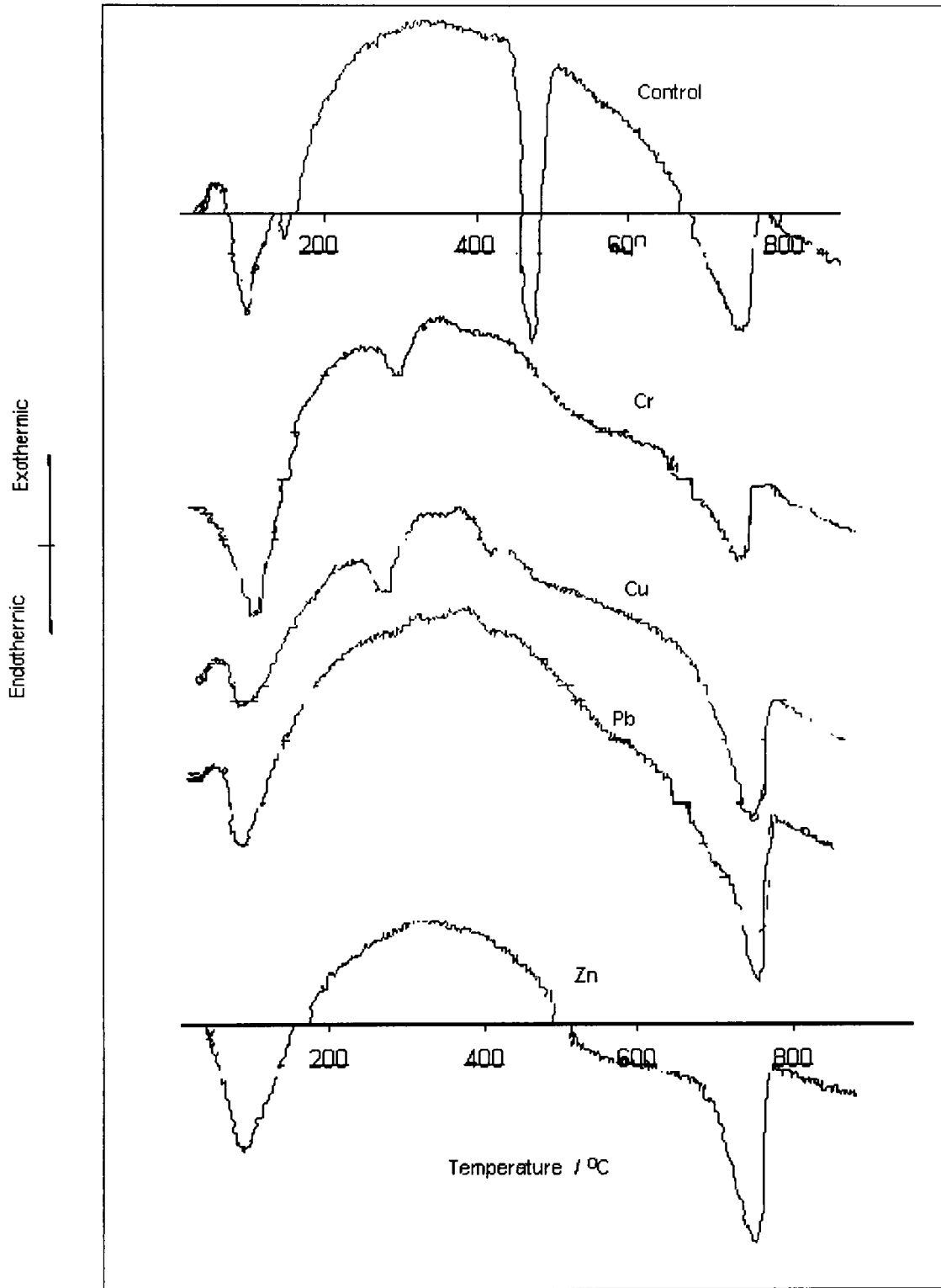


Fig. 6-5. DTA curves of hydrated Portland cement pastes

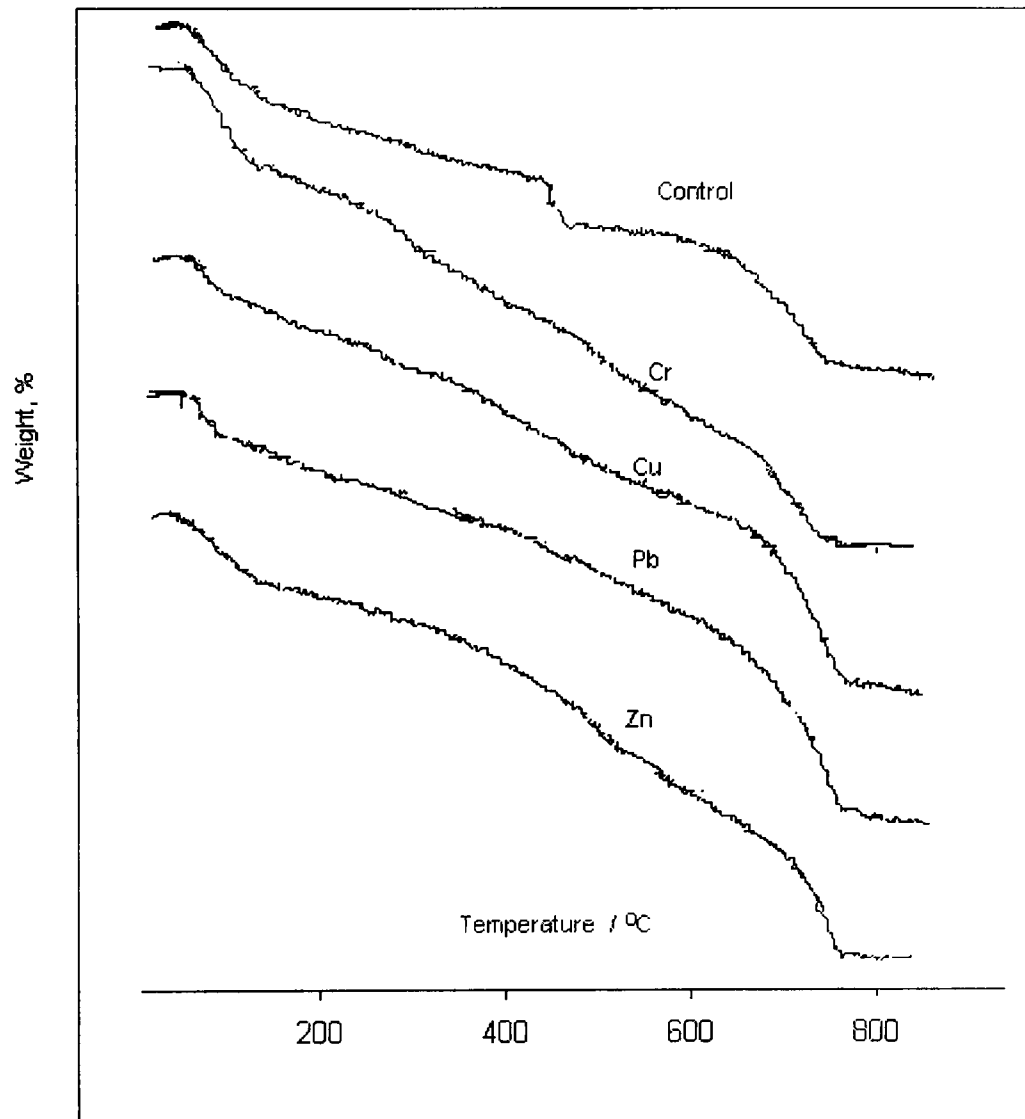


Fig. 6-6. TG curves of hydrated Portland cement pastes

The above observations revealed heavy metals inhibited the precipitation of portlandite at early age, but they promoted the hydration of cement as indicated by the consumptions of cement phases by XRD and total mass loss by TG. The calcium ions disassociated from cement phases combined with heavy metal ions to form double hydroxides. It is worthy to point out that the view that heavy metals retard the hydration of cement based on the formation of portlandite or heat evolution, which also depends mainly on the crystallisation of ettringite and portlandite, is not very accurate.

XRD examinations and thermal analyses of the hydrated Portland cement pastes (Table 6-2) indicate that the presence of heavy metals encouraged the formation of calcium carbonate in comparison to the control paste. This may be due to the low pH resulting

from hydrolyses of heavy metal ions. In low pH media, the calcium ions dissociated from cement phases quickly and combined with  $\text{CO}_3^{2-}$  in the solution, forming  $\text{CaCO}_3$ .

### 6.3.2 Accelerated carbonation

Data on the carbonation of Portland cement were obtained from measuring the pH of cement suspensions containing heavy metals at different times. The relationship between suspension pH and the number of carbonation cycles is shown in Fig. 6-7. It is apparent that heavy metals buffered the suspension pH. Initially, the pH values of suspensions containing metals were slightly higher than that of the control Portland cement suspension, but as carbonation proceeded, the opposite was observed. Fig. 6-8 shows the pH values of suspensions following the 8<sup>th</sup> cycle of carbonation. These suspensions maintained stable pH values below 9 at least for a period of 10 days, indicating that carbonation was complete.

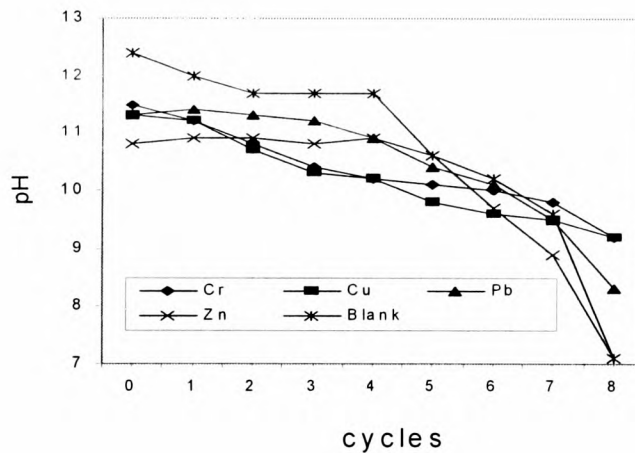


Fig. 6-7. Suspension pH for different carbonation cycles (measured 72 hours after carbonation)

In comparison, the pH values of carbonated metal hydroxides placed in water as suspensions are shown in Fig. 6-9, showing a similarity to the completely carbonated Portland cement suspensions doped with heavy metals.

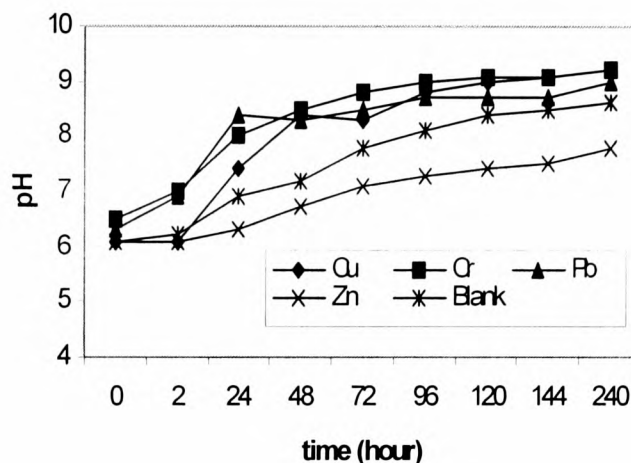


Fig. 6-8. pH of cement suspensions as function of time following the 8<sup>th</sup> cycle of carbonation

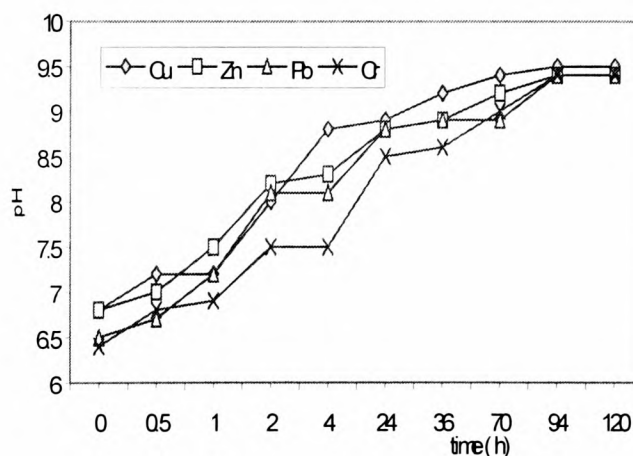


Fig. 6-9. Suspension pH of carbonated metal hydroxides

In the diffractograms of carbonated Portland cement suspensions (Fig. 6-10), no residual cement phases were observed, confirming the carbonation of cement suspensions was complete after 8 cycles of carbonation again.

In the carbonated cement suspensions in the presence or absence of heavy metal ions, as shown in Fig. 6-10, calcium carbonate (including calcite and vaterite) was detected with

XRD technique at 2 weeks, 1 month and 3 months of age. No heavy metal compounds were detected at any time, indicating that heavy metals were absorbed by carbonation products of cement such as calcium carbonate, C-S-H gel and silica gel.

The diffractograms obtained from carbonated cement pastes after 8 cycles of carbonation at the age of one month are shown in Fig. 6-11. Calcite, gypsum and minor trace of anhydrous alite and belite were observed in all pastes. Portlandite was not detectable in the carbonated cement pastes. As described before, in the  $\text{Cr}^{3+}$ -doped cement paste, the X-ray reflection at  $18.1^\circ 2\theta$  was due to the presence of Aft- $\text{Cr}_2\text{O}_3$ . Vaterite was absent in the  $\text{Cr}^{3+}$ -doped cement paste. Aragonite was identified in the  $\text{Cu}^{2+}$ -doped paste, and this indicated that copper stabilised aragonite.

The diffractograms of carbonated Portland cement pastes cured in the  $\text{CO}_2$ -bags for one year are presented in Fig. 6-12. Compared to one month old carbonated cement pastes, portlandite disappeared in the  $\text{Cr}^{3+}$ -doped paste; aragonite was still present in the  $\text{Cu}^{2+}$ -doped paste. The X-ray reflections of alite and belite in the one year old pastes were much weaker than those in the one month old pastes, indicating that cement carbonation continued with time.

The diffractograms obtained from the carbonated pastes, which were hydrated previously for one month, are shown in Fig. 6-13. The typical double peaks of alite and belite were absent, whereas in the accelerated carbonated cement pastes these peaks were present even after one year's storage described above. Moreover, only 5 cycles of carbonation procedure were required to effect complete carbonation of the 28 days old hydrated pastes, whereas 8 cycles of carbonation were necessary to completely carbonate cement pastes. According to this, it is concluded that the carbonation of hydration products of cement was much easier than accelerated carbonation of anhydrous cement.

To further investigate the carbonation products of cement, the thermal analysis techniques including differential temperature analysis and thermogravimetry were employed to examine the carbonated cement pastes with or without heavy metals.

The DTA curves and simultaneous TG curves of carbonated Portland cement pastes aged one month are presented in Figs. 6-14 and 6-15. The thermal analysis results are summarised in Table 6-3.

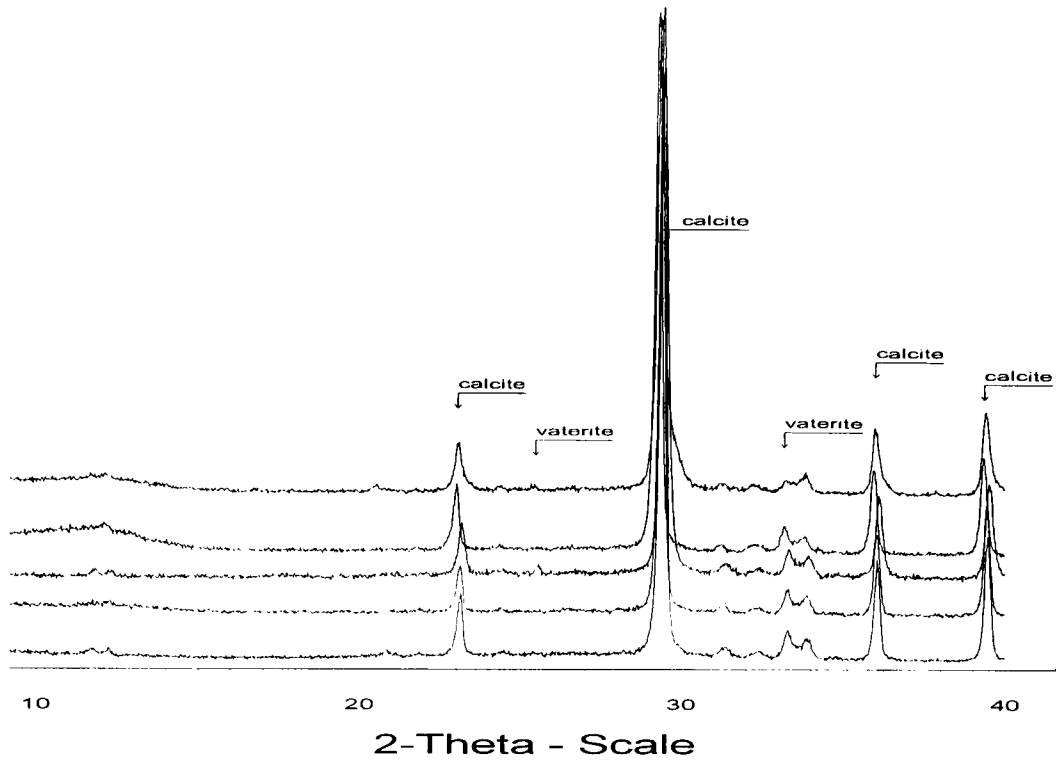


Fig. 6-10. Diffractograms of carbonated cement suspensions  
 (From top to bottom are  $Zn^{2+}$ ,  $Pb^{2+}$ ,  $Cu^{2+}$ ,  $Cr^{3+}$  -doped and control suspensions)

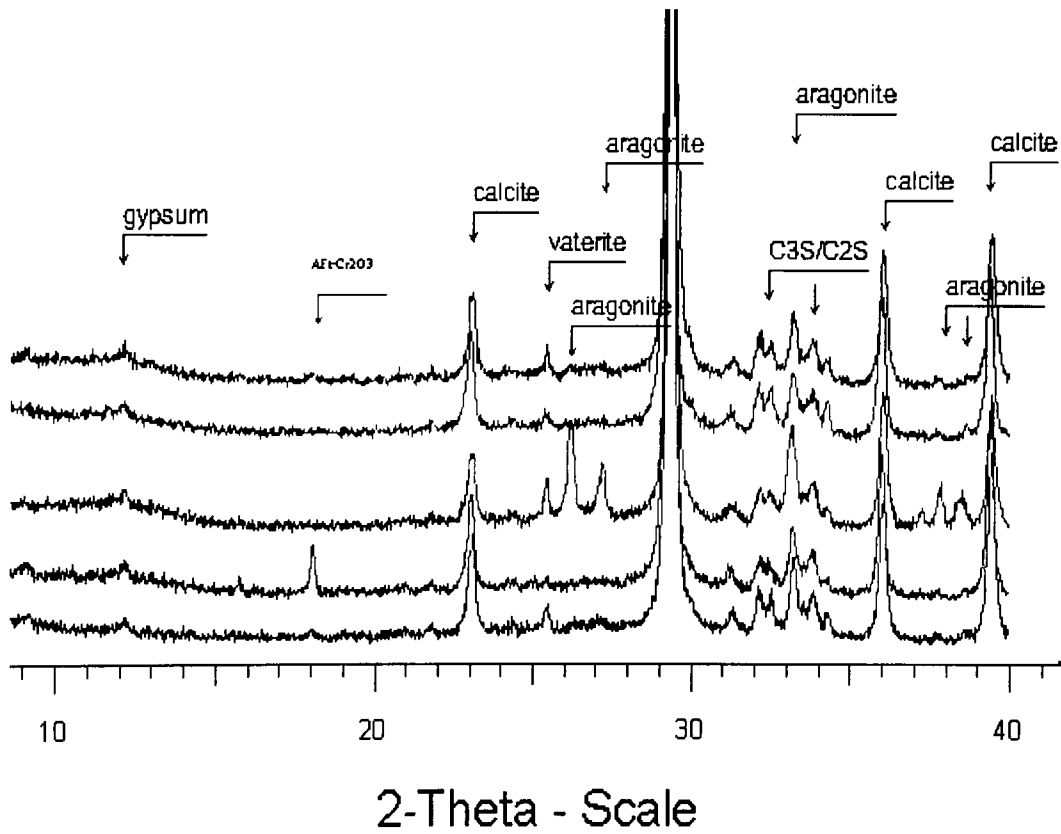


Fig. 6-11. Diffractograms of carbonated cement pastes aged one month  
 (From top to bottom are  $Zn^{2+}$ ,  $Pb^{2+}$ ,  $Cu^{2+}$ ,  $Cr^{3+}$  -doped and control pastes).

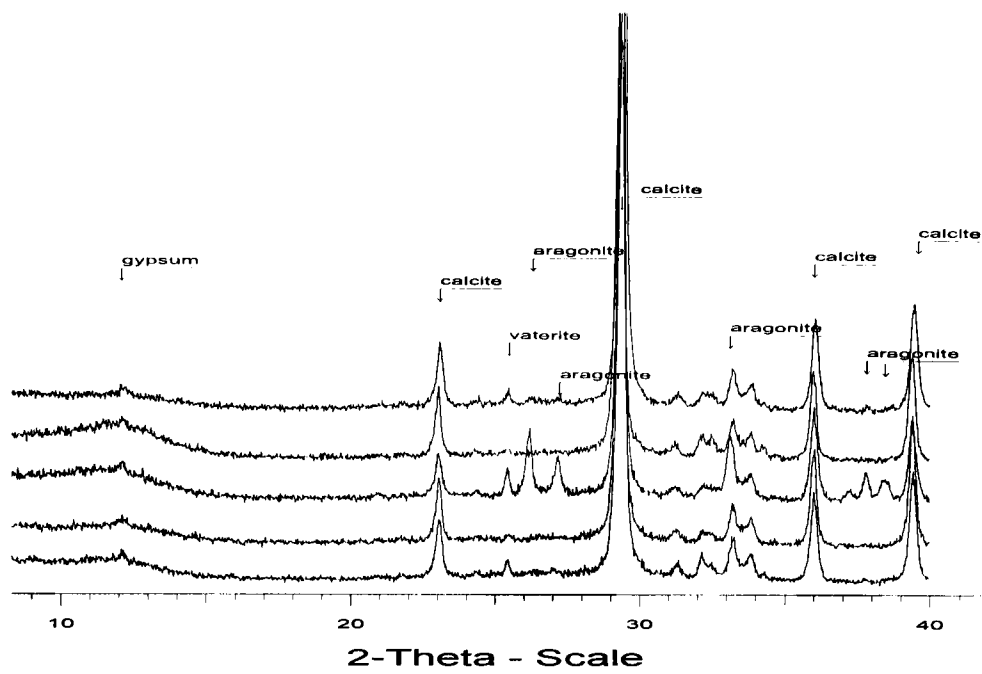


Fig. 6-12. Diffractograms of carbonated cement pastes aged one year  
 (From top to bottom are  $Zn^{2+}$ ,  $Pb^{2+}$ ,  $Cu^{2+}$ ,  $Cr^{3+}$  -doped and control pastes)

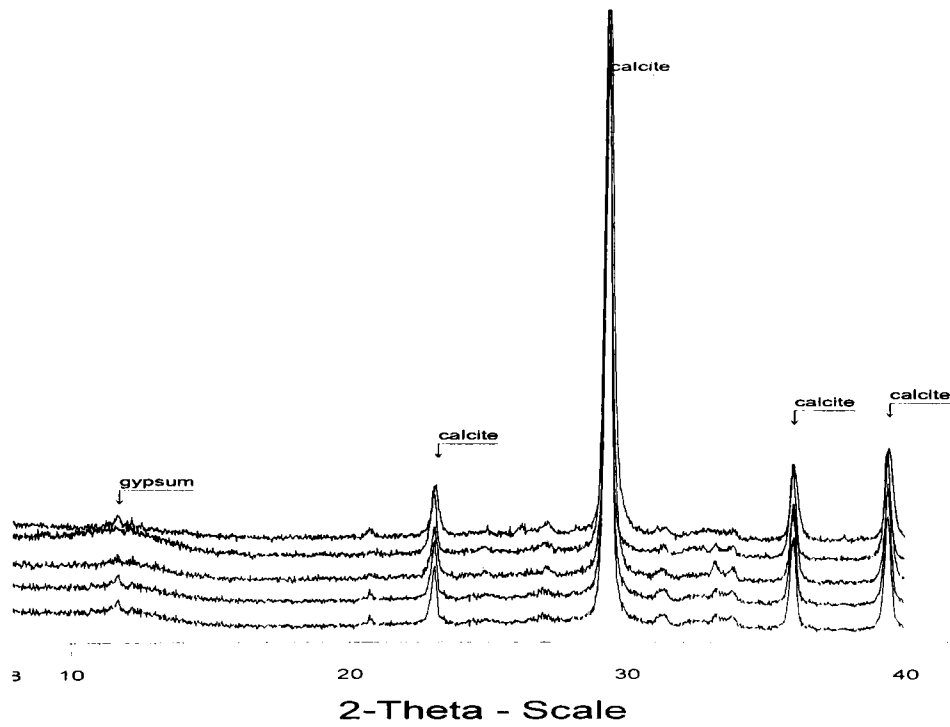


Fig. 6-13. XRD patterns of carbonation of 28-day old hydrated cement pastes  
 (From top to bottom are  $Zn^{2+}$ ,  $Pb^{2+}$ ,  $Cu^{2+}$ ,  $Cr^{3+}$  -doped and control pastes)

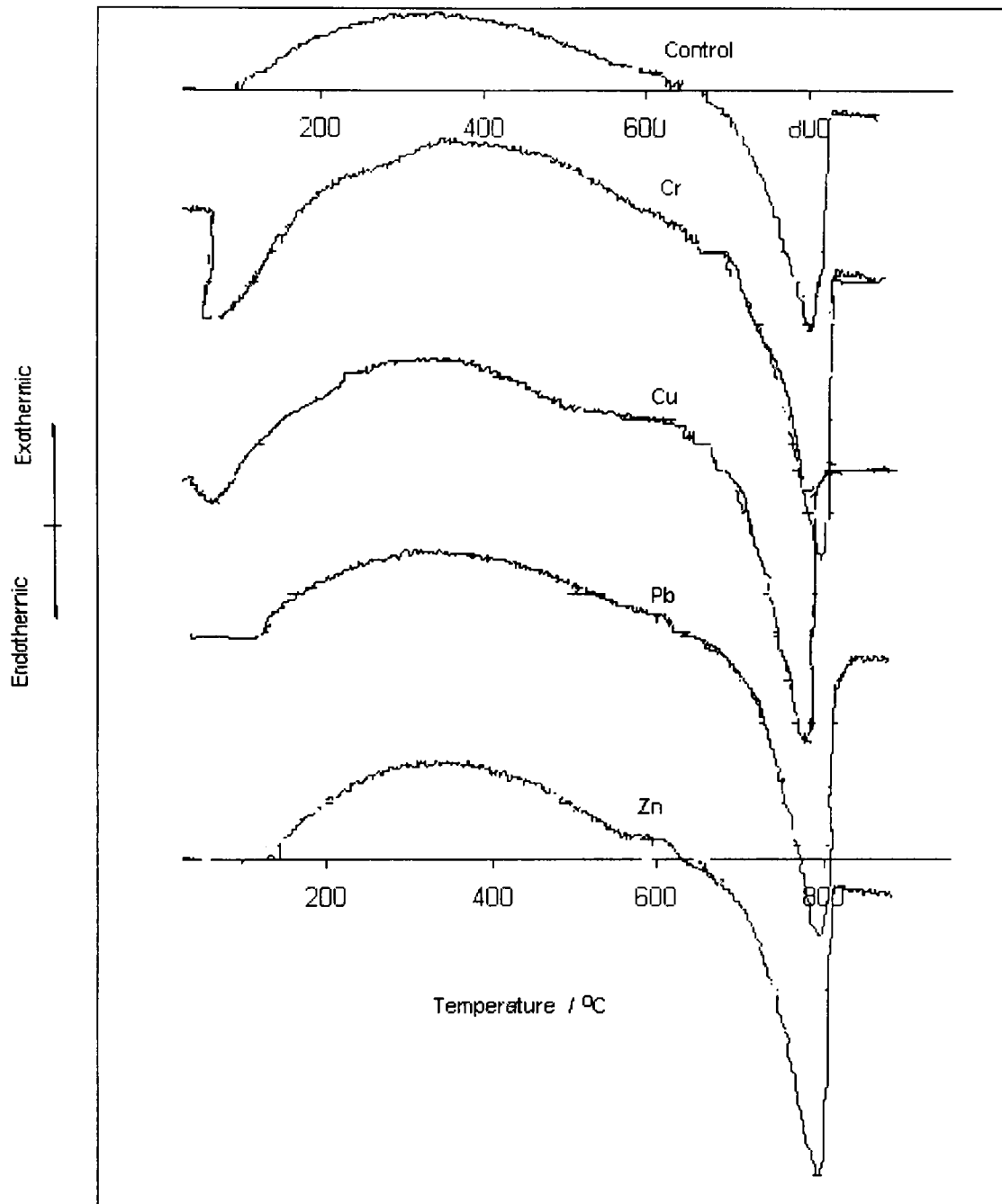


Fig. 6-14. DTA curves of carbonated Portland cement pastes

The endothermic peaks at 100-130°C in DTA curves of the Cr and Cu -doped carbonated cement pastes are assigned to the evaporation of water, which was combined physically and chemically with C-S-H gel or silica gel. In other pastes, this endotherm was not obvious, indicating that the amount of bound water in C-S-H gel or silica gel was very small. This is consistent with the mass loss in the TG curves.

In all pastes, there was an endothermic peak for calcite decomposition at 680-850°C. Correspondingly, mass loss due to decomposition of calcium carbonate in the TG curves

was very steep. According to the amount of mass loss, it is calculated that in the carbonated control Portland cement paste, Cr, Cu, Pb and Zn -doped Portland cement pastes the calcium carbonate contents were 65.9%, 55%, 54.5%, 60.7% and 56.8%, respectively.

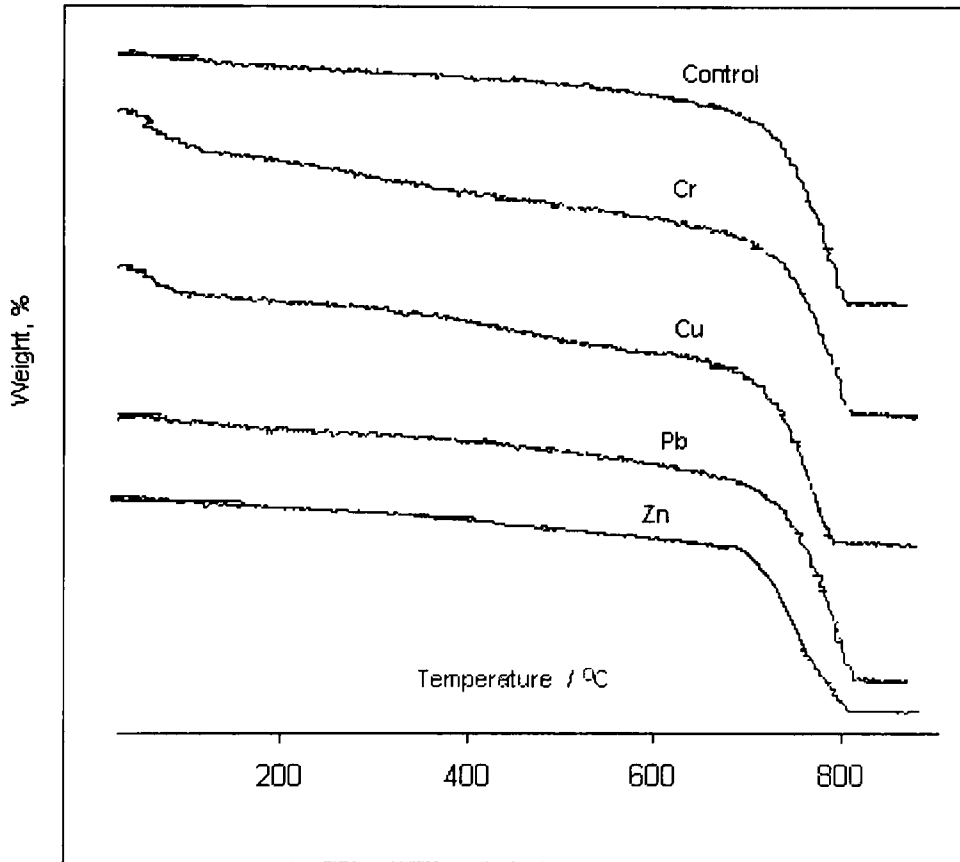


Fig. 6-15. TG curves of carbonated Portland cement pastes

The estimated Ca/Si ratios of C-S-H gel in various carbonated Portland cement pastes are also present in Table 6-4. In the control sample, the average ratio of Ca/Si of C-S-H was 0.29, demonstrating the presence of C-S-H gel with very low Ca/Si ratio. It is noted that the Ca/Si ratio of C-S-H gel in the carbonated heavy metal -doped cement pastes was higher than that in the control cement paste.

In all carbonated cement pastes, no endothermic or exothermic peaks associated with heavy metals were observed. Heavy metals shifted the decomposition temperature of calcium carbonate in DTA curves and influenced the Ca/Si ratio of C-S-H gel.

Table 6-3. Thermal analysis results of carbonated cement pastes (mass loss at indicated temperature, %)

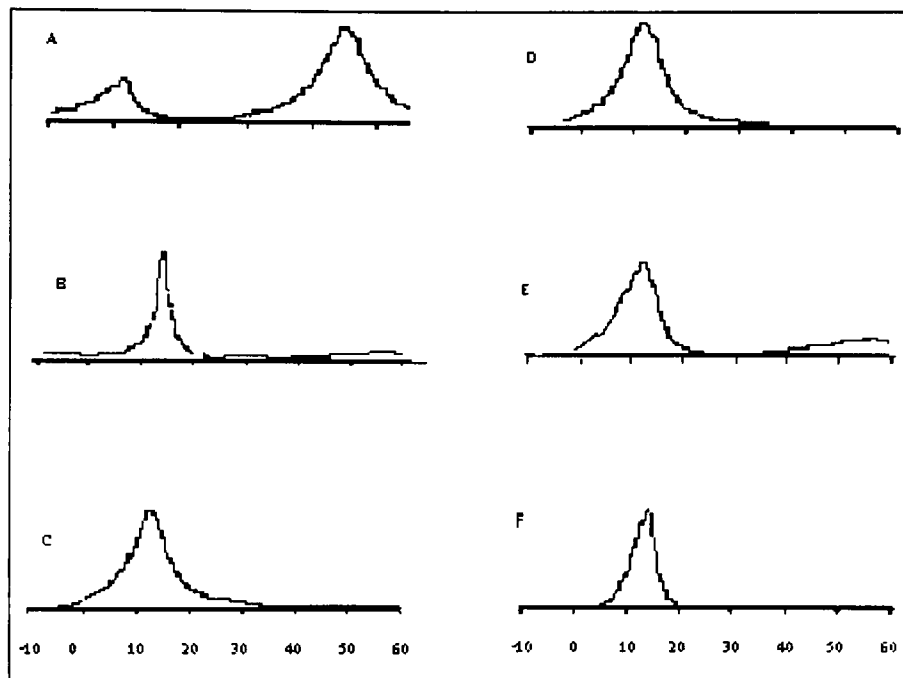
Samples	Control	Cr	Cu	Pb	Zn
20-250°C	2.7	8	7.3	2.2	3.6
250-600°C	3.6	5.9	5.6	4	6.9
600-1100°C	29	24.2	24	26.7	25
Total mass loss	35.3	38.1	36.9	32.9	35.5
CaCO <sub>3</sub> content	65.9	55.0	54.5	60.7	56.8
Cement in the paste	64.7	61.9	63.1	67.1	64.5
T Ca in the paste	29.1	27.8	28.4	30.2	29.0
T Si in the paste	6.5	6.2	6.3	6.7	6.5
Ca in C-S-H	2.7	5.8	6.6	5.9	6.28
Ca/Si in C-S-H	0.29	0.65	0.77	0.61	0.72

### 6.3.3 Characterisation of C-S-H gel in Portland cement pastes

Based on the thermal analysis results, the contents of calcium silicate hydrate gel were around 60% and 35-45% by mass in hydrated Portland cement pastes and carbonated Portland cement pastes, respectively (see Table 6-2 and Table 6-3). Without doubt, C-S-H gel played an important part in the immobilisation of heavy metals.

Calcium silicate hydrate gel is thermodynamically unstable and amorphous at ambient temperatures, and rather difficult to characterise. The properties of C-S-H and effects of heavy metals on the polymerisation of C-S-H gel were studied using NMR techniques in this work. The chemical shifts of <sup>29</sup>Si NMR and <sup>27</sup>Al NMR gave considerable insight into silicon and aluminium chemistry.

Fig. 6-16 presents the <sup>27</sup>Al NMR spectra of raw Portland cement and hydrated cement pastes with or without heavy metals. For raw cement, 4-coordinated (tetrahedral) and 6-coordinated (octahedral) aluminium can be clearly distinguished from each other at chemical shift positions of 80.12ppm and 12.8ppm, respectively.



Chemical shift from  $\text{Al}^{3+} (\text{H}_2\text{O})$ , ppm

Fig. 6-16.  $^{27}\text{Al}$  NMR spectra of hydrated Portland cement pastes

(A, B, C, D, E, and F stand for cement, control,  $\text{Cr}^{3+}$ ,  $\text{Cu}^{2+}$ ,  $\text{Pb}^{2+}$ , and  $\text{Zn}^{2+}$ -doped pastes)

It is well documented that in  $\text{C}_3\text{A}$  and aluminoferrites (e.g.  $\text{C}_4\text{AF}$ ) aluminium is in tetrahedral co-ordinated (Moore and Taylor, 1968; 1970), but aluminoferrites can not be detected by NMR techniques due to the close proximity of the ferromagnetic centres. Therefore, the signal at 80.12ppm was attributed to resonance of aluminium in  $\text{C}_3\text{A}$ . Obviously, this position (80.12ppm) indicated no silicon in aluminate phase.  $^{27}\text{Al}$  NMR signal at 12.8ppm was attributed to the small quantity of calcium aluminosilicate (aluminium in octahedra) in Portland cement. The microanalyses with EDS also confirmed the presence of calcium aluminosilicate (see Chapter 7).

After one year of hydration, as shown in Fig. 6-16 and Table 6-4, all aluminium was in octahedra (chemical shift 12ppm). In the most aluminium compounds in hydrated cement paste such as  $\text{CAH}_{10}$ ,  $\text{C}_4\text{AH}_{13}$ ,  $\text{C}_4\text{AH}_{19}$ ,  $\text{C}_3\text{AH}_6$ , boehmite, gibbsite, ettringite and monosulphate, aluminium is present in octahedra. In  $\text{C}_2\text{AH}_8$ , however, both 4 and 6 coordination numbers could be present. Combined with XRD results (Fig. 6-4), it can be assumed that aluminium in hydrated Portland cement pastes existed in ettringite and calcium aluminomonocarbonate. When compared to the  $^{27}\text{Al}$  MAS/NMR signals in heavy metal -doped cement pastes, the sharper peak in the control paste indicated that the

degree of crystallinity of ettringite and calcium aluminomonocarbonate were higher in the control paste.

Table 6-4. <sup>27</sup>Al NMR data of raw Portland cement and hydrated cement pastes

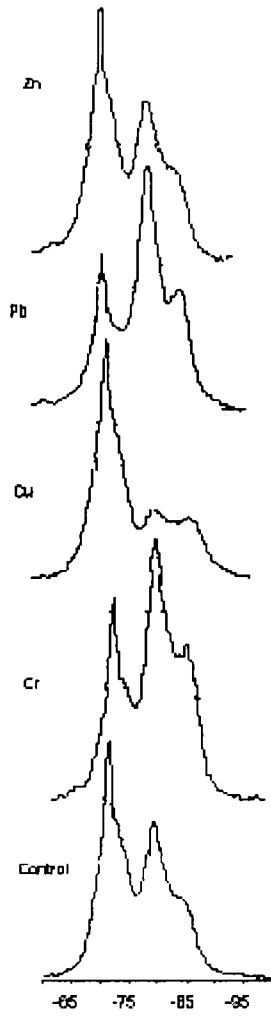
Samples	tetrahedra		octahedra		FWHM*
	Chemical	Proportion	Chemical	Proportion	
	shift, ppm	(%)	shift, ppm	(%)	
Raw cement	80.12	30.43	12.8	69.56	15
Control paste		0	13.2	100	3.05
Cr		0	12.7	100	8.26
Cu		0	11.4	100	8.74
Pb		0	11.8	100	9.11
Zn		0	11.8	100	4.83

Note: FWHM means full width at half maximum, ppm in octahedral

Fig. 6-17 shows the <sup>29</sup>Si NMR spectra of the hydrated Portland cement pastes. As <sup>27</sup>Al NMR results excluded the presence of aluminium in C-S-H gel (tetrahedrally coordinated), the <sup>29</sup>Si chemical shifts displayed a regular dependence upon the degree of condensation of silica-oxygen tetrahedra. The differences of polymerisation of silicates in hydrated Portland cement pastes are summarised in Table 6-5. Hydration of cement increased the condensation of silicate from the isolated tetrahedra to Q1 species and Q2 species.

It is interesting to note that the  $\alpha$  value (degree of hydration, calculated according to  $\alpha=1-I(Q0)/I^0(Q0)$ , see Chapter 4) was much lower than the sum of hydrated species ( $\sum Q^*= Q1+Q2$ , the more accurate indicator for the degree of hydration).

The average length of the silicate chain ( $\Psi$ ) was around 3.03-3.79. The Ca/Si ratio was estimated according to the charge balance and shown in Table 6-6. It is certain that heavy metals influenced the compositions and structures (e.g. polymerisation) of C-S-H gel. Some limited heavy metal ions, therefore, were incorporated in C-S-H gel. This will be investigated further with SEM/EDS in Chapter 7.



Chemical shift from TMS, ppm

Fig. 6-17.  $^{29}\text{Si}$  NMR spectra of hydrated Portland cement pastes

Table 6-5.  $^{29}\text{Si}$  data of hydrated Portland cement pastes (species proportion, %)

Samples	Q0, 72ppm	Q1, 82ppm	Q2, 85ppm	$\Sigma\text{Q}^*$	$\alpha$	C	Ca/Si	Psi
Control	50.45	31.15	18.4	49.55	38.59	1.37	1.66	3.27
Cr	29.33	47.49	23.18	70.67	61.4	1.32	1.53	3.03
Cu	63.77	19.25	16.98	36.23	38.31	1.47	1.74	3.79
Pb	32.57	42.49	24.94	67.43	52.63	1.37	1.54	3.2
Zn	50.15	32.84	17.01	49.85	38.43	1.34	1.66	3.11

Note:  $\Sigma\text{Q}^* = \text{Q1} + \text{Q2}$

The  $^{27}\text{Al}$  MAS NMR diagrams of carbonated Portland cement pastes are shown in Fig. 6-18. The aluminium signals were located at around 50ppm, indicating that aluminium was tetrahedrally coordinated. The aluminium resonance at this position not only differed from the hydrated Portland cement pastes, but also differed from the position of octahedral aluminium in calcium aluminosilicate and tetrahedral aluminium in  $\text{C}_3\text{A}$  in raw Portland cement (Table 6-4). These  $^{27}\text{Al}$  MAS/NMR signals of tetrahedrally coordinated aluminium atoms were not caused by anhydrous  $\text{C}_3\text{A}$  clinker or  $\text{C}_2\text{AH}_8$ , as no X-ray reflection peaks of  $\text{C}_2\text{AH}_8$  and  $\text{C}_3\text{A}$  in the diffractograms of one year old carbonated Portland cement pastes were found (Fig. 6-12). It is certain that these aluminium signals at this position were caused by aluminium incorporated in bridging site of C-S-H gel, i.e.  $\text{AlQ}_4(4\text{Si})$  (see Table 6-6). There were no notable differences among the control cement paste and heavy metal -doped pastes. All aluminium entered C-S-H gel or silica gel in all carbonated Portland cement pastes.

Tetrahedrally co-ordinated aluminium with respect to oxygen creates a negative charge imbalance. The presence of cations is essential to maintain electric neutrality in the matrix, which renders the sorption of heavy metal ions into structure of C-S-A-H gel in addition to other surface phenomena (Iler, 1982).

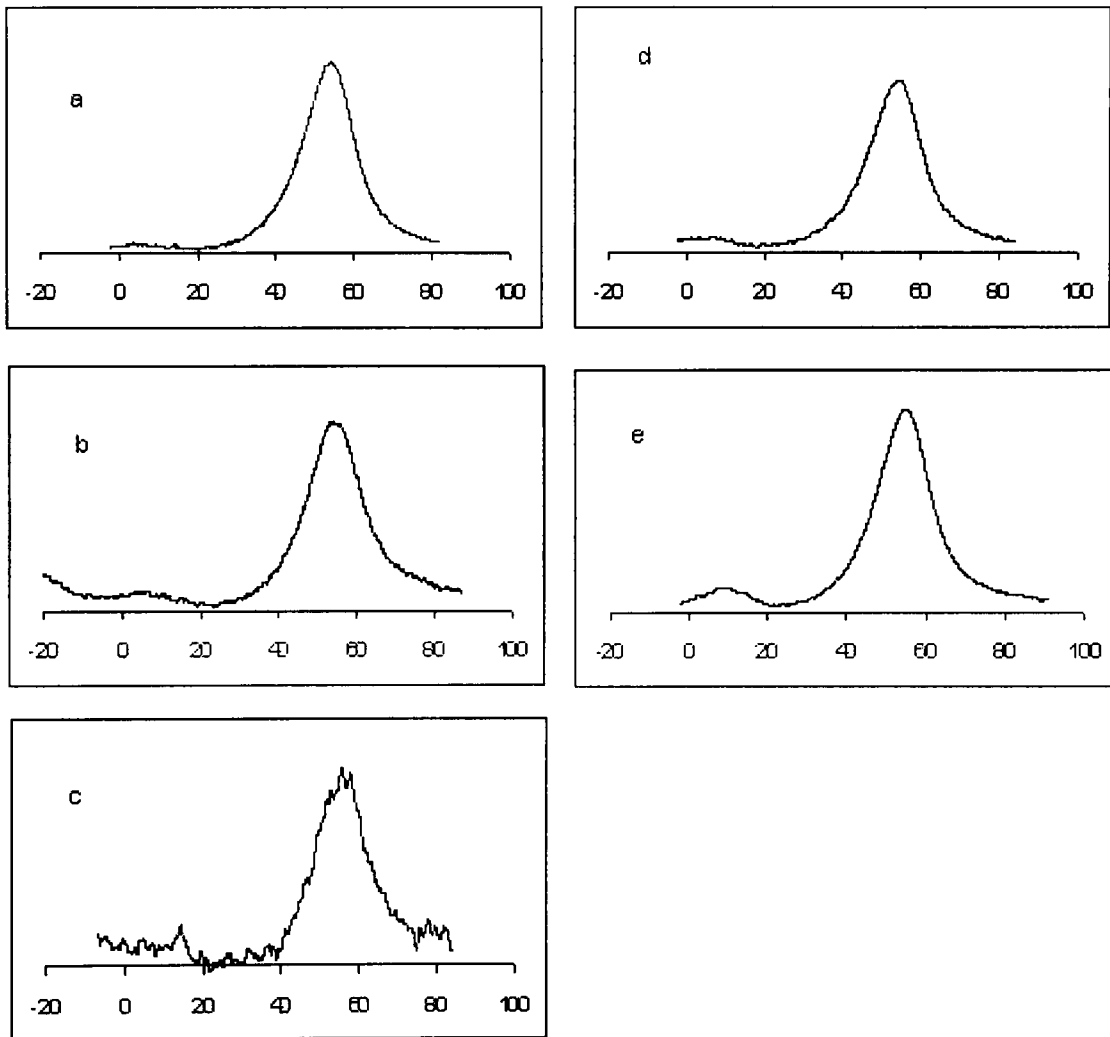
Table 6-6. The chemical shift of aluminium associated with silicon

Chemical environment	tetrahedra				octahedra
	Al (0Si)	Al (1-2 Si)	Al (3Si)	Al (4Si)	
Chemical shift, ppm	80	75-70	65	55	0-15

Aluminium incorporation in C-S-H gel increased its polymerisation and caused the chemical shift of  $^{29}\text{Si}$  NMR. Fig. 6-19 presents the  $^{29}\text{Si}$  MAS NMR spectra of carbonated Portland cement pastes. The very broad resonance from -85ppm to -120ppm was detected. Q0 and Q1 species in all carbonated cement pastes were not detected, unlike the hydrated Portland cement pastes, indicating carbonation was complete again.

Chemical shift changes are indicators to changes in chemical environments and structural parameters such as bond angles and bond lengths in the 1<sup>st</sup> and 2<sup>nd</sup> co-ordination sphere of the probe nuclei. The line width of the peak indicates the distribution in bond parameters of the specific Qn species. The broad peak of  $^{29}\text{Si}$  NMR in the carbonated

cement pastes demonstrated that C-S-H gel was highly disordered and may contain impurities. The introduction of cations with different ionic radii such as aluminium and heavy metals distorted structures by creating a greater range of bond angles and bond lengths in the network.



Chemical shift from  $\text{Al}^{3+}(\text{H}_2\text{O})$ , ppm

Fig. 6-18.  $^{27}\text{Al}$  NMR spectra of carbonated cement pastes (a, b, c, d and e stand for the control,  $\text{Cr}^{3+}$ ,  $\text{Cu}^{2+}$ ,  $\text{Pb}^{2+}$ , and  $\text{Zn}^{2+}$ -doped Portland cement pastes, respectively)

In general principle, by assuming a Gaussian line shape for the resonance, broad peaks of each individual Qn species are deconvoluted using an appropriate number of overlapping Gaussians, where the line width, line position and amplitude of each Gaussian are

varied in order to find the best fit. This method, however, is not suitable for this study, because the entry of aluminium resulted in the shift Qn species of  $^{29}\text{Si}$  NMR data. Lippman (1982) has found Q4 species of aluminosilicate can be arranged from -110ppm to -83.1ppm, depending on the how many aluminium atoms connect directly to silicon tetrahedra and metal cations in the aluminosilicate. On consideration of the entry of aluminium into C-S-H gel,  $^{29}\text{Si}$  NMR resonance from -85ppm to -120ppm can be assigned to any species of silicon other than Q0 and Q1 for the spectra obtained in this work.

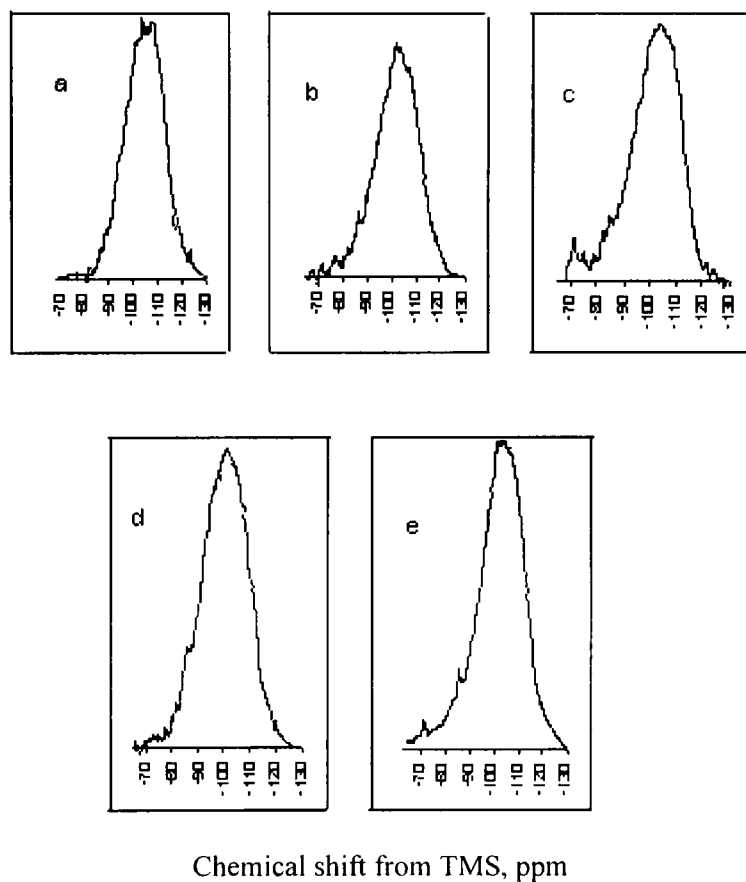


Fig. 6-19.  $^{29}\text{Si}$  NMR spectra of carbonated cement pastes

(a, b, c, d and e stand for  $\text{Cr}^{3+}$ ,  $\text{Cu}^{2+}$ ,  $\text{Pb}^{2+}$ , and  $\text{Zn}^{2+}$ -doped and the control Portland cement pastes, respectively)

To solve this problem, tricalcium silicate, which contained no aluminium, was used and compared with Portland cement. It was found that only branching sites (Q3 species, -90 to -100ppm) and three-dimensional frameworks (Q4 species, -100 to -120ppm) existed in the fully carbonated  $\text{C}_3\text{S}$  pastes (see Chapter 4). Likewise, the resonance found for

disordered  $^{29}\text{Si}$  in carbonated Portland cement pastes from  $-85\text{ppm}$  to  $-120\text{ppm}$  in this work can be assigned to  $\text{SiQ3(1Al)}$ ,  $\text{SiQ3}$ ,  $\text{SiQ4(4Al)}$ ,  $\text{SiQ4(3Al)}$ ,  $\text{SiQ4(2Al)}$ ,  $\text{SiQ4(1Al)}$  and  $\text{SiQ4(0Al)}$ , respectively, as shown in Table 6-7. It can be concluded that carbonation of cement resulted in condensation of silicate from isolated tetrahedra to branching sites and the three-dimensional frameworks. Again,  $^{29}\text{Si}$  NMR showed that heavy metals had no obvious difference in affecting the carbonation of cement.

Table 6-7.  $^{29}\text{Si}$  NMR data of carbonated cement pastes (species proportion, %)

Species	Control	Cr	Cu	Pb	Zn
Q4(4Al), Q3 (1Al), 85ppm	7.07	0	3.39	6.76	8.51
Q4(3Al), Q3, 90ppm	10.1	3.51	10.17	9.46	12.77
Q4(2Al), Q3, 95ppm	18.18	17.54	20.34	18.92	23.4
Q4(1Al), Q3, 100ppm	29.29	35.09	33.9	29.73	31.91
Q4(0Al), 110ppm	25.25	31.58	23.73	24.32	17.02
Q4, 115ppm	10.1	12.28	6.78	10.81	6.38
Central position of peak, ppm	104	106	105	103	102
FWHM*, ppm	19	20.5	20	20	20

Note: FWHM means full width at half maximum

A broad resonance of  $^{29}\text{Si}$  NMR from  $-85\text{ppm}$  to  $-120\text{ppm}$  is generally found in zeolitic gel, i.e. 3D framework share tetrahedral corner oxygen atoms of silicon or aluminium tetrahedra (network formers), before crystallisation of the zeolites occurs (Wang and Scrivener, 2003). The carbonation of cement with or without heavy metals gave a similar structure to zeolitic gel. It lacked the periodic order of a crystal with calcium as a network modifier and heavy metals as modifiers or as network intermediates. This is because carbonation of cement occurred fairly quickly in cement pastes, where species had limited mobility and without enough time for the orientation and alignment to form a proper crystal structure. An amorphous structure of C-S-A-H gel with very low  $\text{Ca}/(\text{Si}+\text{Al})$  ratio or silica gel with aluminium provided a strong heavy metal binding capability.

#### 6.3.4 Additional discussion

The forgoing examination of phases demonstrates that heavy metals formed double hydroxides in hydrated Portland cement pastes. In addition, the sorption of heavy metals in cement matrices resulted in the differences in the quantity, polymorphism, and decomposition temperature of hydration products of cement.

Unlike hydrated Portland cement/heavy metal systems, no heavy metal compounds were detected in the carbonated Portland cement suspensions or pastes doped with heavy metals by XRD and DTA/TG techniques. Isomorphous replacement of calcium by heavy metals in the crystalline lattice of calcium carbonate is an important incorporation mechanism of heavy metals in carbonated cement-base s/s systems (Glasser, 1997). It was noted that there was no noticeable angular position shifts related to calcium carbonate in the diffractograms of carbonated cement pastes in this work. The amount of substitution of heavy metal for calcium in calcium carbonate may be limited, as the radii of heavy metal ions are very different from calcium ions.

Nevertheless, heavy metals influenced the polymorphs of calcium carbonate and decomposition temperature of calcium carbonate. These results strongly indicate that heavy metal ions could be absorbed in calcium carbonate. The sorption of heavy metals on the C-S-A-H gel or silica gel with aluminium could also be an important immobilisation mechanism, because carbonated cement pastes were normally dominated by low Ca/Si ratio of calcium silicate (aluminate) hydrate gel (around 40% by mass, see Table 6-4) in addition to calcium carbonate.

C-S-H gel is a typical amorphous nano-scale interpenetrating network of a variety of morphologies and chemical compositions, surrounding more-or-less gel pores (Escalante-Garcia *et al.*, 1999). These gel pores and thermodynamic metastability of C-S-H gel give a high specific surface area (200-300m<sup>2</sup>/g) and chemical activity as well as high binding capacity for various heavy metal ions (Escalante-Garcia and Sharp, 1999; Jennings *et al.*, 1981; Juenger and Jennings, 2001; Jennings, 2000). Some metals such as Ni<sup>2+</sup> and Co<sup>2+</sup> are immobilised by sorption or co-precipitation onto C-S-H (Richardson and Groves, 1993; 1997).

## 6.4 Summary

Portland cement pastes containing heavy metals were largely devoid of crystalline phases apart from portlandite or calcium carbonate and appeared to be dominated by amorphous calcium silicate hydrate gel. Thermal analysis demonstrated to be helpful in characterisation of C-S-H gel. In addition,  $^{29}\text{Si}$  and  $^{27}\text{Al}$  solid state magic angle spinning/nuclear magnetic resonance (NMR) techniques obtained considerable information about the connectivity of Si and Al atoms in this work.

Of the metals investigated,  $\text{Zn}^{2+}$  inhibited the early hydration of Portland cement, whereas other metals promoted hydration. At a later age, all metals appeared to promote hydration of Portland cement. XRD and DTA/TG results indicated that heavy metals inhibited the precipitation of portlandite.

Thermal analysis (DTA/TG) and XRD examinations demonstrated that Cu and Cr in hydrated Portland cement pastes reacted with calcium and formed double hydroxides ( $\text{Ca}_2\text{Cr}(\text{OH})_7\cdot 3\text{H}_2\text{O}$ ,  $\text{Ca}_2(\text{OH})_4\cdot \text{Cu}(\text{OH})_2\cdot m\text{H}_2\text{O}$ ). These compounds were crystalline in the hydrated Portland cement suspensions. Pb and Zn appeared to be absorbed in hydrated cement matrices, although calcium zincate was detected in Portland cement suspension doped with zinc at early age by XRD.

Hydration resulted in end groups (Q1) and Q2 species. The average length of calcium silicate hydrate gel (Psi) was around 3.03-3.79 and the estimated average Ca/Si ratio of C-S-H gel was in the range of 1.53-1.74.

Complete carbonation of Portland cement was difficult to obtain in the laboratory. Using gaseous  $\text{CO}_2$ , up to 8 cycles of crushing and grinding and repeated exposure to this gas was required before anhydrous cement phases were no longer present in the carbonated Portland cement pastes or suspensions.

The carbonation of previously hydrated pastes was much easier to achieve, as it took only 5 cycles to obtain an anhydrous-phase free product, which indicated that hydration products of Portland cement were liable to undergo carbonation.

Heavy metals had little effect on the progress of carbonation of Portland cement and this has implications for the applications of accelerated carbonation technology in waste management.

During carbonation, isolated tetrahedra of silicates (alite and belite) condensed to branching sites (Q3) and to the three-dimensional cross-linked framework (Q4). This study revealed that accelerated carbonation of cement resulted in the formation of silica gel and low ratio Ca/Si C-S-H gel, which incorporated aluminium and had a greater range of bond angles and bond lengths. Four coordinated aluminium created a negative charge imbalance and therefore favoured the immobilisation of heavy metal cations to maintain electric neutrality in the matrix. The estimated average Ca/Si ratios in the C-S-H gel in the carbonated Portland cement pastes varied from 0.29 to 0.77, depending on the heavy metals.

Although no heavy metal compounds were found in the carbonated Portland cement pastes doped with heavy metals, heavy metals influenced the polymorphism of calcium carbonate, shifted the decomposition temperature of calcium carbonate and affected the Ca/Si ratio of C-S-A-H gel. Heavy metals could be incorporated in calcium carbonate and C-S-A-H gel due to sorption.

## Chapter 7

### Morphology and microanalysis of heavy metal-doped Portland cement pastes

#### 7.1 Background

As stated earlier, wastes and contaminated soil containing heavy metal are treated by cement-based solidification/stabilisation technology to reduce their relative toxicity and facilitate handling prior to landfill disposal of these wastes. Cement hydration is sometimes retarded by heavy metals due to precipitation of low solubility reaction products on the cement grain surfaces, for example, calcium zincate identified by XRD in Chapters 4 and 6. Accelerated carbonation has been used to overcome these deleterious waste-binder interactions (Bukowski and Berger, 1979; Berger and Banwart, 2000). This work confirmed that heavy metals had little deleterious effect on the carbonation of Portland cement (see Chapter 6).

The further development of solidification/stabilisation is dependent on the detailed understanding of the immobilisation mechanisms of heavy metals (Kantro, 1975; Kinniburgh *et al.*, 1976; Mollah *et al.*, 1995; 1998). Previous chapters in this thesis discussed the interactions of heavy metals and Portland cement and put forward the mechanisms of heavy metal fixation.

In the hydration of cement, sorption is likely to be effective in the low concentration ranges of heavy metals (Cheng and Bishop, 1992; Zhang *et al.*, 2000). Precipitation may occur when a solution is over-saturated with respect to a particular phase. The initial precipitation often yields X-ray amorphous products in the hydrated cement pastes (Faucon *et al.*, 1997; Price, 1995; Gatty *et al.*, 2001). In this study, thermal analyses confirmed the presence of amorphous double hydroxides of calcium and heavy metal in the hydrated heavy metal -doped cement pastes (see chapter 6).

In the completely carbonated Portland cement pastes or suspensions doped with heavy metals, no heavy metal compounds were detected by XRD or thermal analysis techniques. Sorption was most likely to be a dominated mechanism of heavy metal

fixation over a wide range of concentrations, presumably due to the high sorption capacity of carbonated cement matrices (James, 1996; Thomas and Jennings, 1998).

This chapter applies scanning electron microscopy (SEM) to observe the microstructure of cement pastes containing heavy metals ( $\text{Pb}^{2+}$ ,  $\text{Zn}^{2+}$ ,  $\text{Cr}^{3+}$  and  $\text{Cu}^{2+}$ ). Microanalysis data obtained with energy dispersive X-ray spectroscopy (EDS) in this work were used to investigate the correlation of heavy metals and cement components and to elucidate the incorporation mechanisms of heavy metals.

## ***7.2 Experimental***

### **7.2.1 Materials**

Portland cement was supplied by Blue Circle Ltd (UK). The major component phases expressed as Bogue compositions are: alite 56%, belite 20%, aluminate 9% and ferrite 7%.  $\text{Cu}^{2+}$ ,  $\text{Cr}^{3+}$ ,  $\text{Pb}^{2+}$  and  $\text{Zn}^{2+}$  nitrate salts from their respective standard reagents were used in all experiments.

### **7.2.2 Methods**

#### **7.2.2.1 Hydration**

Hydrated pastes were prepared by mixing the metal nitrate solutions with Portland cement (see Chapter 2). Morphology observations and EDS microanalyses were made on 6 month-old cement pastes. Fracture specimens were gold coated for high quality images. For energy disperse X-ray analysis, polished specimens were mounted on stubs using two-part epoxy resin and coated with carbon to ensure a good electrical conductivity.

#### **7.2.2.2 Carbonation**

Cement/heavy metal mixtures for accelerated carbonation, prepared at the same time and under the same condition as for the hydration studies, were exposed to 100%  $\text{CO}_2$  in a

reaction chamber for a period of 30 minutes. Following this, samples were removed and ground to <0.03mm with a pestle and mortar and placed back in the chamber for another 30 minutes. This procedure was repeated 5 times. By adding water or heavy metal nitrate solutions into above samples (cement/liquid ratio: 10:1), the cement pastes were exposed to CO<sub>2</sub> in the chamber for 3 weeks and then stored until 6 months.

### **7.2.2.3 Scanning electron microscopy and energy dispersive X-ray spectroscopy**

Morphology studies and microanalyses were conducted using a JEOL JSM-640 SEM equipped with an energy dispersive X-ray spectrometer (LINK ANINCA, LINK ISIS 300) with an accelerating voltage of 15kV to provide qualitative and semi-quantitative information on the elemental composition in the bulk of the matrix. The target area is typically 1 micrometer in diameter. Efforts were made to centre the beam of electrons in the middle of a cluster of particles so that the characteristic X-ray was generated solely from the same phase of cement pastes. In this work about 80 images were used for statistical accuracy.

Since light elements cannot be detected by this method, the compositional totals are lower than 100%. Micro-porosity could lower the totals due to the retardation of incident electrons by fields resulting from internal charging on the surfaces of pores (Jawed *et al.*, 1983, Jun *et al.*, 1997). For convenient comparison, the most data obtained were normalised. In addition, the microanalysis results were plotted as molar ratios and not as percentages of individual elements to eliminate the effects of micro porosity, carbon dioxide and water content.

## **7.3 Results and discussion**

### **7.3.1 Anhydrous particles and reaction products of cement**

In the back-scattered image, residual cement grains appeared brightest followed by the hydration products such as calcium hydroxide, calcium carbonate, calcium-silicate-hydrate and darkest regions being the epoxy-filled pore spaces.

Microanalyses demonstrated that anhydrous particles in cement pastes were mostly calcium silicates and solid solutions of calcium aluminate, calcium silico-aluminate and calcium ferrite, as shown in Table 7-1. After normalisation, the compositions of the former were CaO 72-74%, SiO<sub>2</sub> 24-25%; whilst those of the latter were Al<sub>2</sub>O<sub>3</sub> 19-29%, SiO<sub>2</sub> 5-9%, CaO 45-53% and Fe<sub>2</sub>O<sub>3</sub> 14-21%.

Table 7-1. The compositions of some residuals of hydrated cement pastes (%)

Spots	Compositions (%)					Phases, Ca/Si
	Al <sub>2</sub> O <sub>3</sub>	SiO <sub>2</sub>	CaO	Fe <sub>2</sub> O <sub>3</sub>	Total	
1	22.25	4.63	49.96	13.15	89.99	CASF
2	20.1	5.84	47.5	18.61	92.05	CASF
3	27.4	8.25	48.05	13.73	97.43	CASF
4	25.04	5.21	51.77	13.16	95.18	CASF
5	16.62	14.01	45.31	12.09	88.03	CASF
6	1.53	23.44	64.39	0.85	90.21	C <sub>3</sub> S, 2.94
7	0.71	24.51	65.69	0.41	91.32	C <sub>3</sub> S, 2.88
8	0.6	24.26	65.81	0.43	91.1	C <sub>3</sub> S, 2.91
9	1.53	24.69	69.09	0.8	96.11	C <sub>3</sub> S, 2.99
10	1.17	24.66	68.56	0.81	95.2	C <sub>3</sub> S, 2.98
11	1.01	24.76	68.25	0.44	94.46	C <sub>3</sub> S, 2.96
12	0.98	24.78	67.98	0.59	94.33	C <sub>3</sub> S, 2.94

Taylor (1997) claimed that the existence of silico-aluminates in the hydration products of Portland cement is evidence for some reaction between the individual phases. According to this work, however, calcium silico-aluminates were anhydrous phases of Portland cement.

Comparing cement pastes in the presence of heavy metals with the control cement paste, there were no differences in the residual compositions of cement, but there were differences in the quantity of residuals. Generally speaking, anhydrous cement clinkers in the hydrated heavy metal -doped cement pastes were less than in the hydrated control cement paste. According to the SEM observation, there appeared to be more anhydrous particles in the hydrated cement pastes than in carbonated cement pastes, consistent with

the diffractograms. As anhydrous particles do not have the ability to trap heavy metals, a high reaction degree is essential to use cement efficiently in cement-based s/s. From this standpoint, accelerated carbonation has advantages over hydration.

Fracture SEM images of hydrated pastes with or without heavy metals are shown in Fig. 7-1. There were significant morphological differences among the hydrated pastes. In the control cement paste (Fig. 7-1a), C-S-H gel was seen as a fibrous material, the fibres being up to around 2 microns long. This type of C-S-H gel was the outer product, forming in the space with physical constraint. SEM images indicate that heavy metals inhibited the formation and growth of fibrous C-S-H gel. As shown in Fig. 7-1, in heavy metal -doped pastes, tightly packed equant grains and honeycomb C-S-H gel were observed. This can be classified as the inner hydration product, which had a compact and fine-scale morphology.

In all hydrated cement pastes, the presence of very thin hydration rims of different brightness around the cement grains was observed, exhibiting two, three or even four distinct grey levels. The outermost shell was grey, and the outer rim was darker than the interior one adjacent to the anhydrous cement core. The compositional differences in different brightness are shown in Table 7-2. According to the ratio of Ca/Si, the outer and outmost layers contained the portlandite. Some hollow shells were also observed where the cement grains totally reacted leaving a darker inner C-S-H core surrounded by the lighter outer C-S-H rims. In general, the brighter C-S-H gel has higher Ca/Si ratio, although the incorporation of heavy metals and other substances can affect the brightness.

Table 7-2, The compositions of C-S-H gel in different brightness around the clinker of cement (%)

Position, brightness	Al <sub>2</sub> O <sub>3</sub>	SiO <sub>2</sub>	SO <sub>3</sub>	CaO	Ca/Si	remarks
Core, brightest	1.7	25.27	1.16	68.41	2.89	anhydrous
Inner, grey	2.69	44.32	1.08	44.68	1.01	C-S-H(1)
Outer, dark	1.99	26.65	3.09	64.43	2.42	C-S-H(2)
Outermost, grey	1.54	18.67	3.73	72.24	3.87	C-S-H (containing portlandite)

The C-S-H compositions in different areas of the control hydrated cement paste are presented in Table 7-3. Ca/Si ratios were in the range of 2-3. Although effort has been made to focus the target in 1 micrometer in diameter, the analysed spots could contain information from other phases.

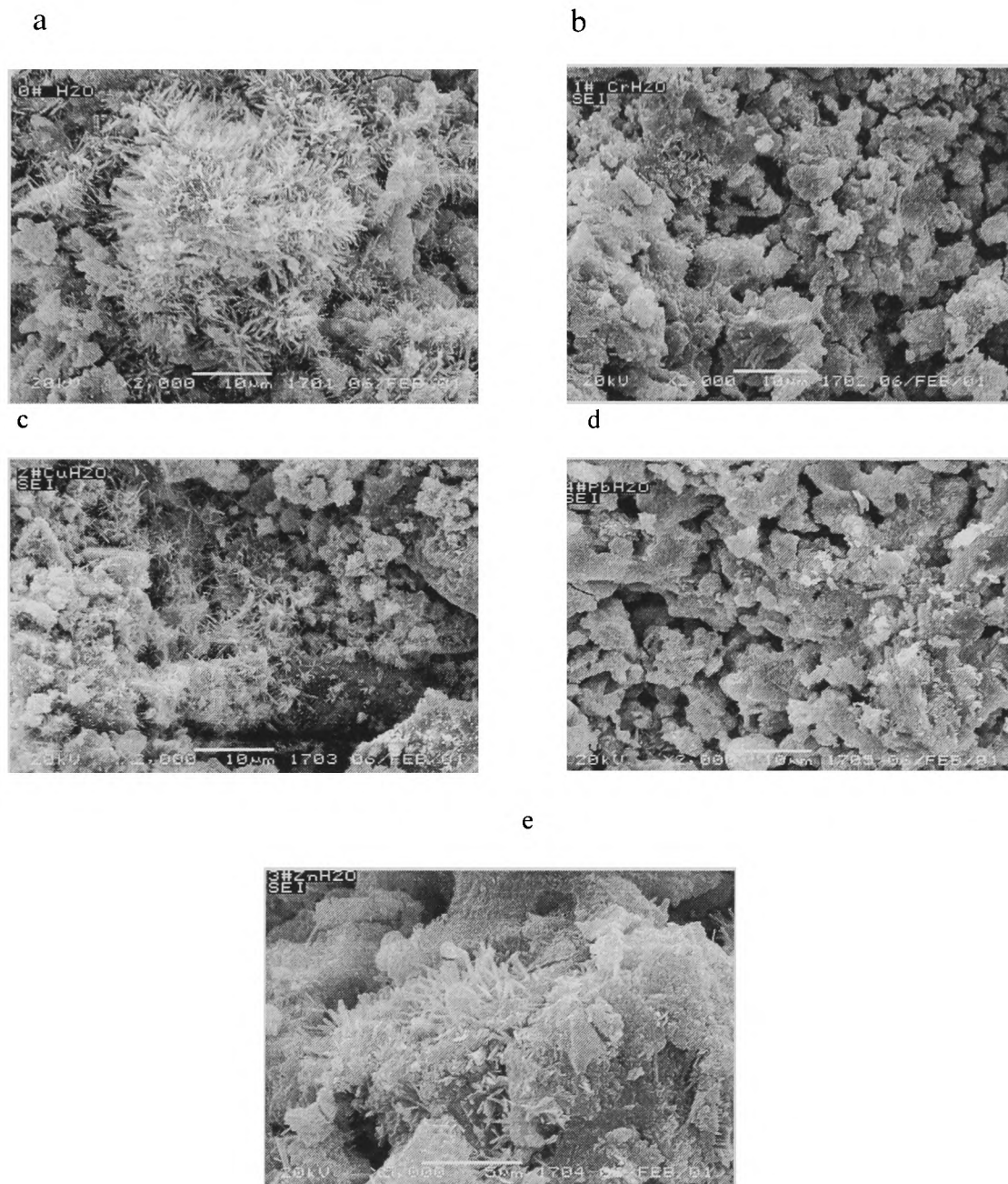


Fig. 7-1. SEM images of fracture surface of hydrated cement pastes (a, b, c, d and e stand for control,  $\text{Cr}^{3+}$  -,  $\text{Cu}^{2+}$  -,  $\text{Pb}^{2+}$  - and  $\text{Zn}^{2+}$  -doped cement pastes)

The accicular habit of ettringite was observed in the control cement paste and in the  $\text{Cu}^{2+}$  and  $\text{Zn}^{2+}$  -doped hydrated cement pastes, and was dispersed throughout the microstructure. Compared with the control paste, the tabular crystals of calcium hydroxide were very rare in the heavy metal -doped pastes, confirming that heavy metals inhibited the formation of portlandite again, which is consistent with the XRD examinations.

Table 7-3. The compositions of C-S-H gel in the control hydrated cement paste (%)

Analysis Spot	$\text{Al}_2\text{O}_3$	$\text{SiO}_2$	$\text{SO}_3$	$\text{CaO}$	$\text{Fe}_2\text{O}_3$	Ca/Si
1	1.77	32.41	1.11	62.26	1.02	2.06
2	2.46	30.84	4.58	60.09	0.59	2.08
3	3.15	29.07	5.85	57.81	1.51	2.13
4	4.73	27.76	4.6	59.73	1.12	2.3
5	1.76	29.46	2.3	63.83	0.79	2.31
6	1.47	29.55	2.48	64.21	0.76	2.33
7	3.58	27.44	5.46	60.05	1.67	2.34
8	2.3	28.06	4.79	62.06	0.77	2.36
9	3.17	27.46	5.47	60.76	0.9	2.37
10	1.91	28.63	3.46	63.56	0.83	2.38
11	4.07	26.17	6.58	58.22	1.37	2.48
12	1.47	28.26	2.38	65.5	0.74	2.51
13	1.75	27.59	2.84	64.96	1.08	2.53
14	1.83	27.4	3.42	64.74	0.82	2.53
15	2.65	26.52	5.44	62.8	0.74	2.59
16	2.41	25.72	4.34	62.29	1.53	2.59
17	2.4	26.8	4.29	64.94	0.67	2.59
18	1.63	27.09	2.86	65.67	0.97	2.59
19	1.99	26.39	2.27	65.22	0.67	2.59
Average	2.45	28.03	3.92	62.56	0.98	2.4
Standard deviations	0.92	1.67	1.5	2.5	0.32	0.17

SEM images of carbonated cement pastes with or without heavy metals are presented in Fig. 7-2. In the control carbonated paste and the  $\text{Cr}^{3+}$  -doped carbonated paste the fibres

are attributed to calcium tricarboaluminate ( $C_3A_3CaCO_3 \cdot 27H_2O$ ), because of its high aluminium content.

The C-S-H gel and silica gel appeared as tightly packed equant grains in all carbonated pastes. The C-S-H grain size was smallest in the Cu-doped paste. The compositions of some C-S-H gel in carbonated pastes are shown in Table 7-4. EDS microanalyses show that carbonated pastes exhibited low Ca/Si ratio C-S-H gel for example, Ca/Si around 0.07. This is consistent with results based on TG analysis and NMR examination (see Chapter 6).

Table 7-4. The compositions of C-S-H in the carbonated cement pastes

Analysis spot	Al <sub>2</sub> O <sub>3</sub>	SiO <sub>2</sub>	SO <sub>3</sub>	CaO	Ca/Si
1	1.58	94.01	0.05	4.35	0.07
2	4.06	77.19	0.49	13.36	0.19
3	3.84	73.45	0.7	16.88	0.25
4	3.95	73.3	0.85	17.06	0.25
5	3.85	71.99	0.7	17.93	0.27
6	3.61	70.47	0.74	19.78	0.3
7	4.32	68.96	1.07	20.29	0.31
8	4.22	68.03	1.05	21.62	0.34
9	4.01	67.71	1.05	22.21	0.35
10	4.28	65.23	1.24	23.11	0.38
11	4.78	65.16	1.53	23.12	0.38
12	4.27	63.61	1.26	25.43	0.42
13	3.86	59.86	0.92	30.12	0.53
14	5.57	55.65	0.68	30.75	0.59
15	2.79	52.84	1.36	37.09	0.75
16	4.03	50.57	1.35	36.34	0.76
17	2.81	49.33	1.32	40.74	0.88
18	2.58	48.98	1.08	41.72	0.91
19	3.54	47.48	1.87	42.44	0.96
20	2.2	47.55	0.98	43.99	0.99
Average	3.71	63.57	1.01	26.42	0.50
Standard deviations	0.92	12.11	0.4	11.01	0.28

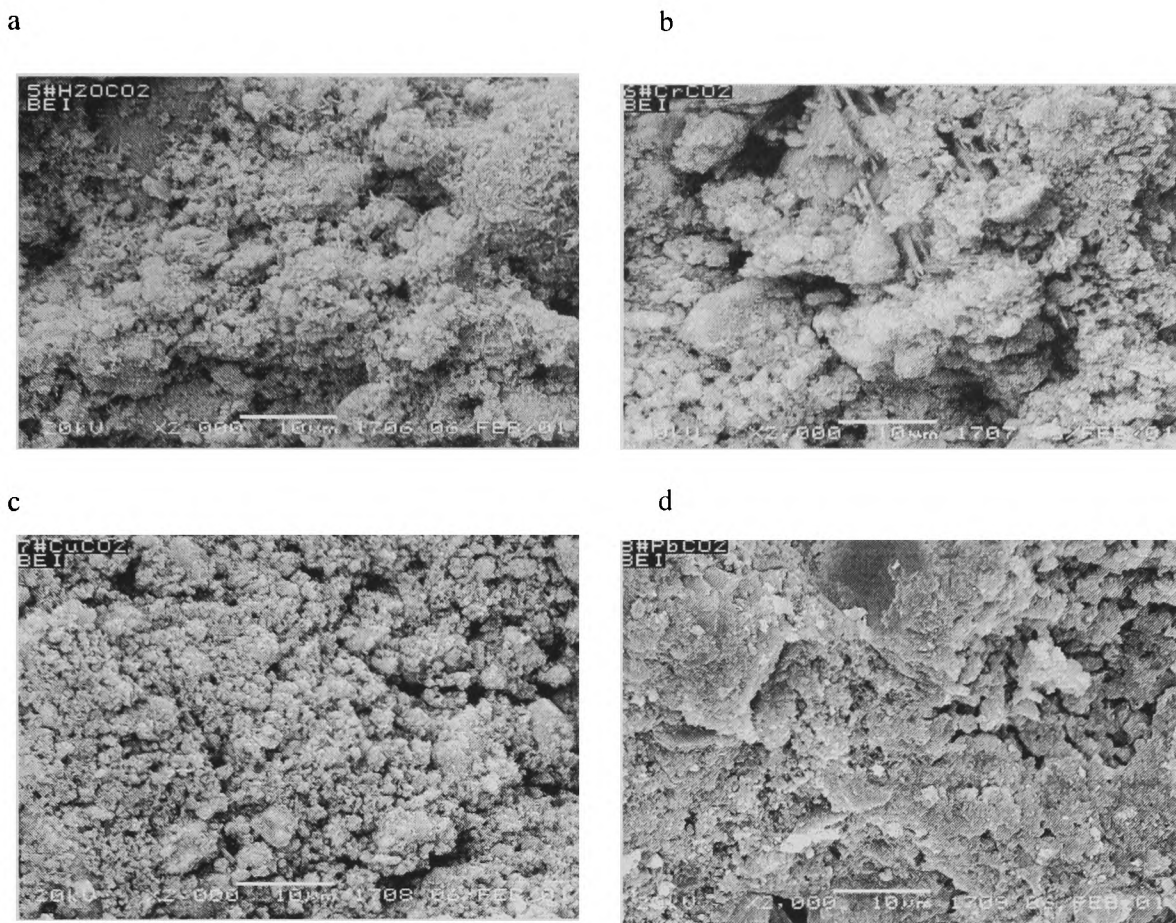


Fig. 7-2. SEM images of fracture surface of carbonated cement pastes. (a, b, c and d stand for control,  $\text{Cr}^{3+}$ -,  $\text{Cu}^{2+}$ -and  $\text{Pb}^{2+}$ -doped cement pastes)

When the microanalysis results of hydrated pastes were compared with those of carbonated pastes, another noted difference was the correlation of silicon and aluminium. The atom ratio plots of Al/S versus Si/S in the control hydrated paste and control carbonated paste are shown in Fig. 7-3 and Fig. 7-4, respectively. Sulphur was chosen as a reference, because it co-existed with aluminium. In all carbonated pastes, silicon and aluminium correlate positively with each other, indicating that aluminium was incorporated in the C-S-H gel or silica gel. In contrast, poor correlation between aluminium and silicon can be seen in the hydrated cement pastes, suggesting that aluminium did not coexist with C-S-H gel. These results are consistent with results of  $^{29}\text{Si}$  and  $^{27}\text{Al}$  solid-state NMR techniques, which have been applied to probe chemical changes taking place in both hydration and carbonation of cement in the presence of heavy metals. Four co-ordinated aluminium respective to oxygen are expected to create a negative charge imbalance and facilitate the incorporation of heavy metals in C-S-A-H gel or S-A-H gel to maintain electric neutrality in the matrix (Williams *et al.*, 2002).

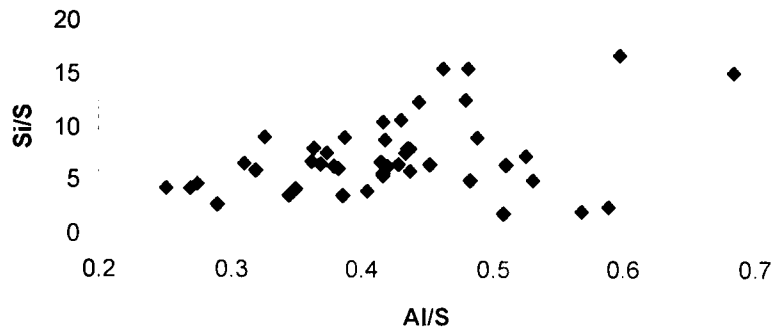


Fig. 7-3. Atom ratio plots of Al/S versus Si/S in the hydrated cement pastes

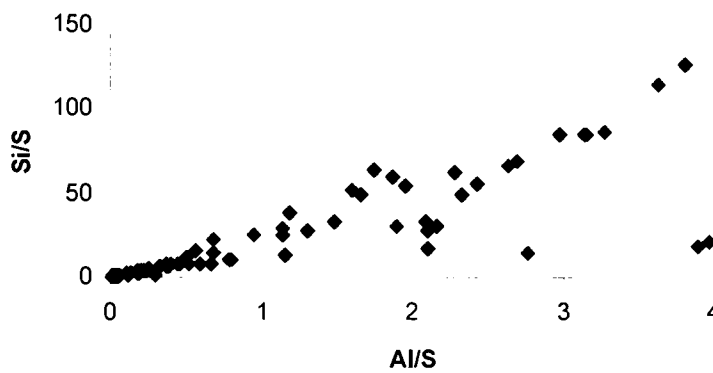


Fig. 7-4. Atom ratio plots of Al/S versus Si/S in the carbonated cement pastes

### 7.3.2 Incorporation of heavy metal in the cement matrix

In heavy metal -doped cement pastes, the heavy metal distributions varied from place to place, for example, CuO contents varied from 0% to 25.49%w/w in the Cu -doped hydrated cement paste. The odd distribution of heavy metals in the pastes indicated that heavy metals could form heavy metal compounds or adsorb on the surfaces of some phases preferably. From the mean oxide compositions (Table 7-5 and Table 7-6), each heavy metal existed in the area with lower silicon contents and higher Ca/Si ratios compared to the control paste or the areas without heavy metal, indicating that heavy metals were incorporated in the reaction products such as calcium carbonate, C-S-H gel and portlandite.

Interpretation of data, however, is not straightforward because most microanalyses are of mixtures of many phases (Harrisson and de Mora, 1996; Grutzeck *et al.*, 1999). In this

work, the microanalysis data were analysed using statistical methods to provide information on the compositions of residual clinkers, reaction products in cement pastes and heavy metal incorporation. In addition, the microanalysis results were plotted as atom ratios and not as percentages of individual elements to eliminate the effects of micro porosity, carbon dioxide and water content.

The atom ratio plots of M/Al (M stands for Cr, Cu, Pb and Zn) versus Ca/Al or Si/Al in the hydrated cement pastes are shown from Fig.7-5 to Fig. 7-8. Statistical analysis results of the SEM/EDS microanalyses of hydrated heavy metal-doped cement pastes are compared in Table 7-7.

Table 7-5. Average compositions of microanalyses of the hydrated cement pastes (%)

Samples	Analysed spots	Al <sub>2</sub> O <sub>3</sub>	SiO <sub>2</sub>	SO <sub>3</sub>	CaO	Ca/Si	MO*
Control	100	3.73	20.52	3.47	68.78	3.59	0
Cr	80	2.26	8.12	2.83	77.43	10.21	2.61
Cu	80	2.82	10.56	4.19	68.85	6.99	2.58
Pb	80	2.63	17.24	4.44	67.09	4.17	1.37
Zn	80	4.48	17.28	4.12	63.77	3.95	1.16

Note: MO stands for Cr<sub>2</sub>O<sub>3</sub>, CuO, PbO and ZnO, respectively.

In the Cr<sup>3+</sup>-doped hydrated cement paste, the correlation coefficients of Cr/Al-Ca/Al, Si/Al-Cr/Al and Cr/Al-S/Al were very high, indicating that chromium may react with calcium hydroxide to form double hydroxide of calcium and chromium, *i.e.* Ca<sub>2</sub>Cr(OH)<sub>7</sub>.3H<sub>2</sub>O. The microanalysis results support the conclusion obtained from XRD and DTA/TG studies. In addition to encapsulation in ettringite, chromium could also be incorporated in C-S-H gel based on the results of statistical analysis in this work, primarily substituting for both calcium and silicon in C-S-H and affecting the polymerisation of silicates.

In the Pb<sup>2+</sup>-doped hydrated cement paste, lead demonstrated a strong correlation with silicon. The results of microanalyses suggested that lead was bound into C-S-H gel in the hydrated Portland cement paste. Microanalysis confirmed that the coexistence of Pb(OH)<sub>2</sub> with portlandite was likely based on the correlation coefficients of Pb/Al-Ca/Al. This agrees with the investigations made by Thomas *et al.*(1981) and Ortego *et al.*(1989).

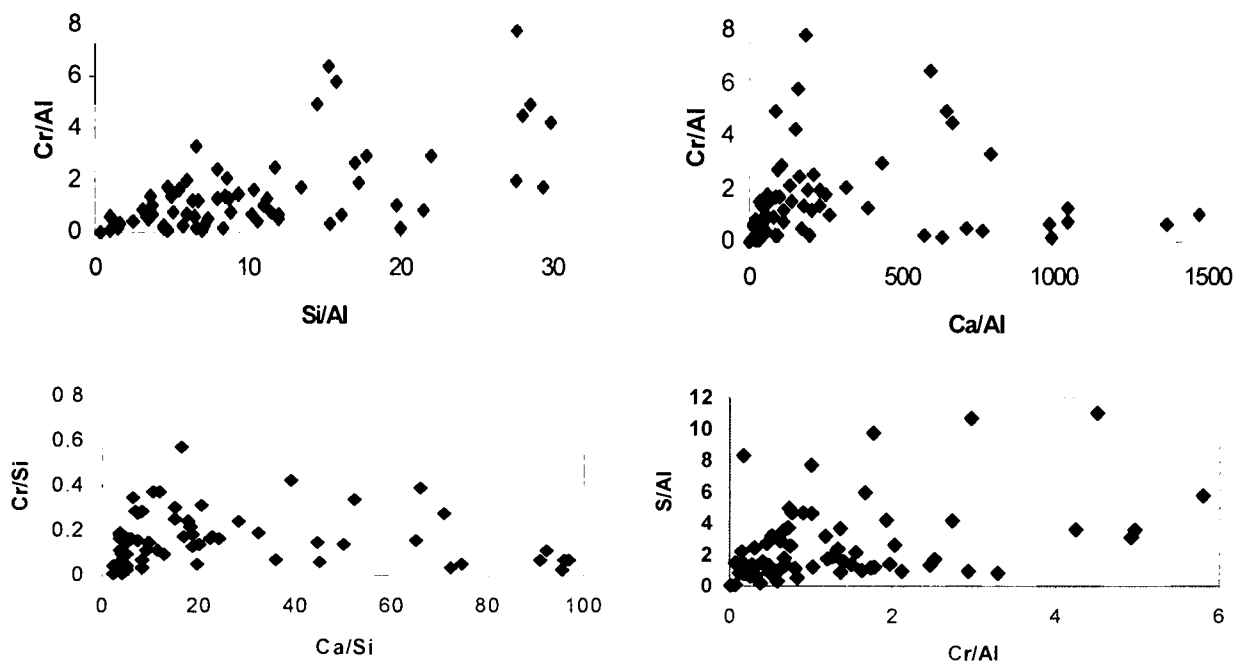


Fig. 7-5. Atom ratio plots of chromium with cement components in the Cr<sup>3+</sup>-doped hydrated cement paste

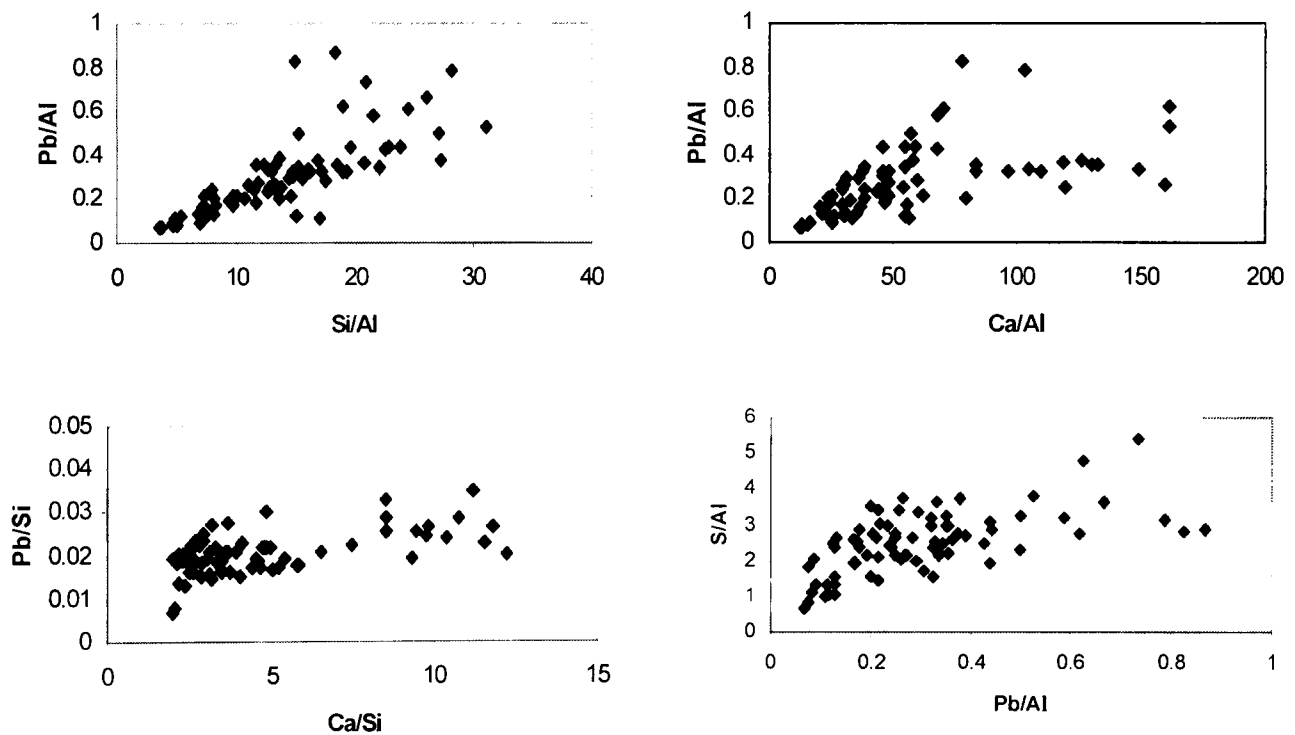


Fig. 7-6. Atom ratio plots of lead with cement components in the Pb<sup>2+</sup>-doped hydrated cement paste

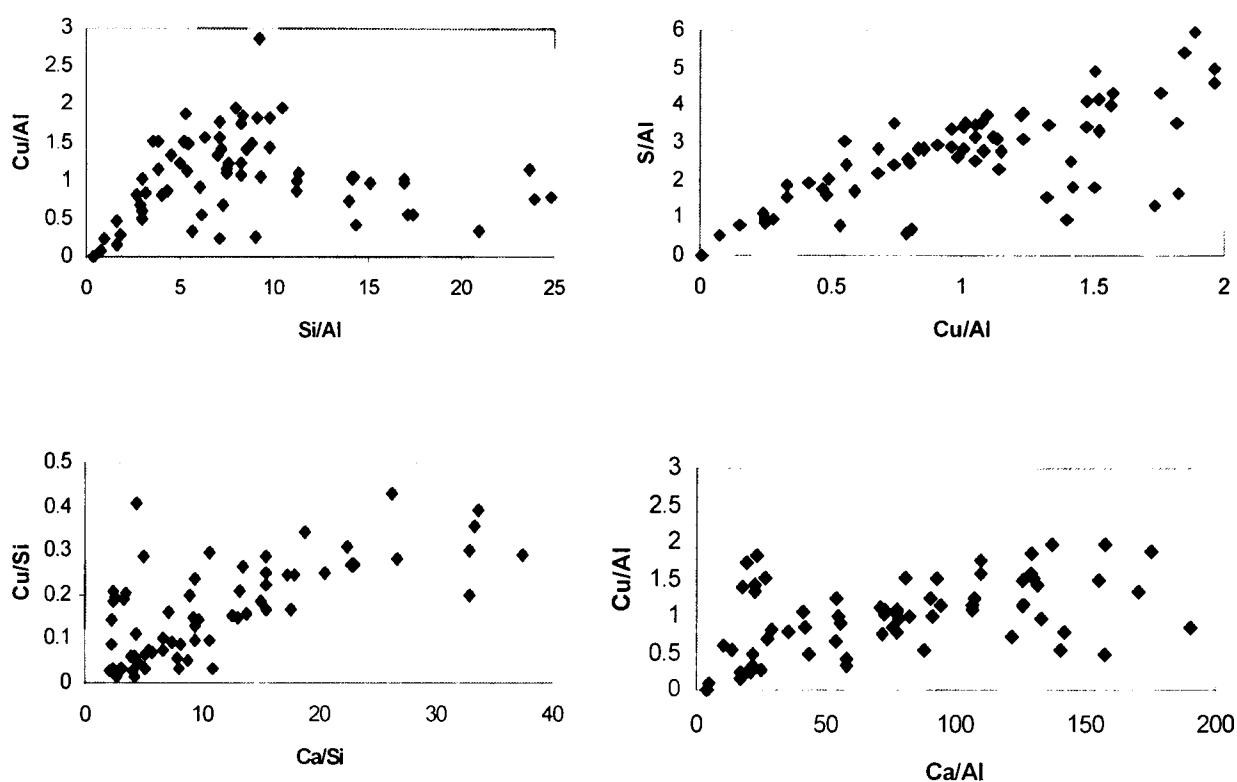


Fig. 7-7. Atom ratio plots of copper with cement components in the  $\text{Cu}^{2+}$ -doped hydrated cement paste

Table 7-6. Average compositions of microanalyses of the carbonated cement pastes (%)

Samples	Analysed spot numbers	$\text{Al}_2\text{O}_3$	$\text{SiO}_2$	$\text{SO}_3$	CaO	Ca/Si	MO*
Control	100	3.58	26.09	2.75	63.21	2.60	0
Cr	80	2.00	16.66	3.90	63.56	4.09	1.57
Cu	80	1.94	10.05	3.23	66.07	7.04	1.15
Pb	80	1.85	16.64	3.72	64.98	4.18	1.69

Note: MO stands for  $\text{Cr}_2\text{O}_3$ ,  $\text{CuO}$ ,  $\text{PbO}$  and  $\text{ZnO}$ , respectively.

Copper behaved very differently from other heavy metals in the hydrated Portland cement paste. There was no obvious correlation among copper and components of cement, suggesting copper could form a copper hydroxide. The copper hydroxide may co-precipitate with calcium hydroxide to form double hydroxide of copper and calcium or physically incorporated in cement matrices (see Fig. 7-7).

The high correlation coefficients of Zn/Al-Ca/Al supports the proposition that the formation of calcium zincate ( $\text{CaZn}_2(\text{OH})_6 \cdot 2\text{H}_2\text{O}$ ). This work confirmed that zinc retarded the early hydration of cement by the surface precipitation of an amorphous or crystalline layer of calcium zincate on the anhydrous clinker grains (see Chapters 4 and 6). It is also noted that zinc had a strong positive correlation with silicon, suggesting that zinc ions also adsorbed onto the surface of C-S-H gel, as shown in Fig. 7-8. In addition, zinc exhibited a positive correlation with sulphur, suggesting that some zinc ions were incorporated in ettringite, which is in accordance with the XRD examinations.

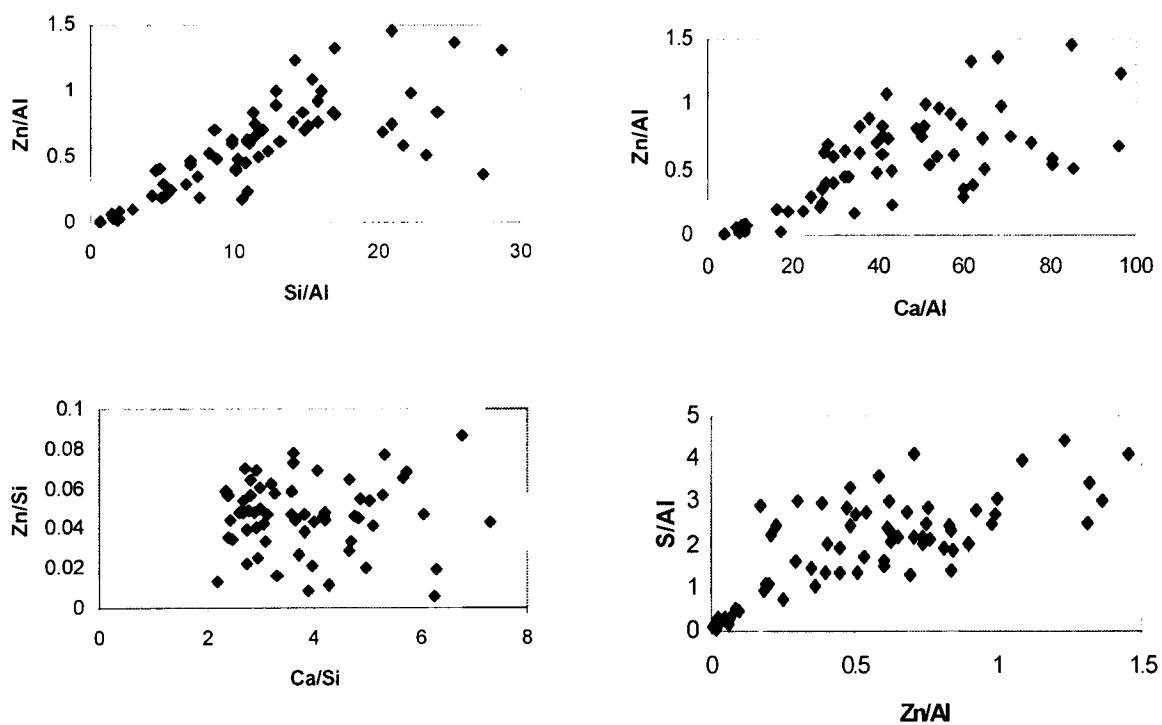


Fig. 7- 8. Atom ratio plots of zinc with cement components in the  $\text{Zn}^{2+}$ -doped hydrated cement paste

The atom ratio plots of M/Al (M stands for Cr, Cu and Pb) versus Ca/Al or Si/Al in the carbonated cement pastes are shown from Figs. 7-9 to Fig. 7-11. The statistical interpretation of these results is shown in Table 7-8. In the carbonated cement pastes heavy metals had a very strong positive correlation with calcium. According to this, it is reasoned that heavy metals investigated could coexist with calcium as complex carbonates or adsorption on the surface of calcium carbonate. It is worth noting that in the carbonated cement pastes heavy metals had a positive correlation with  $\text{SO}_3$ , again, indicating that heavy metals could have a close relation with sulphur compounds, presumably ettringite.

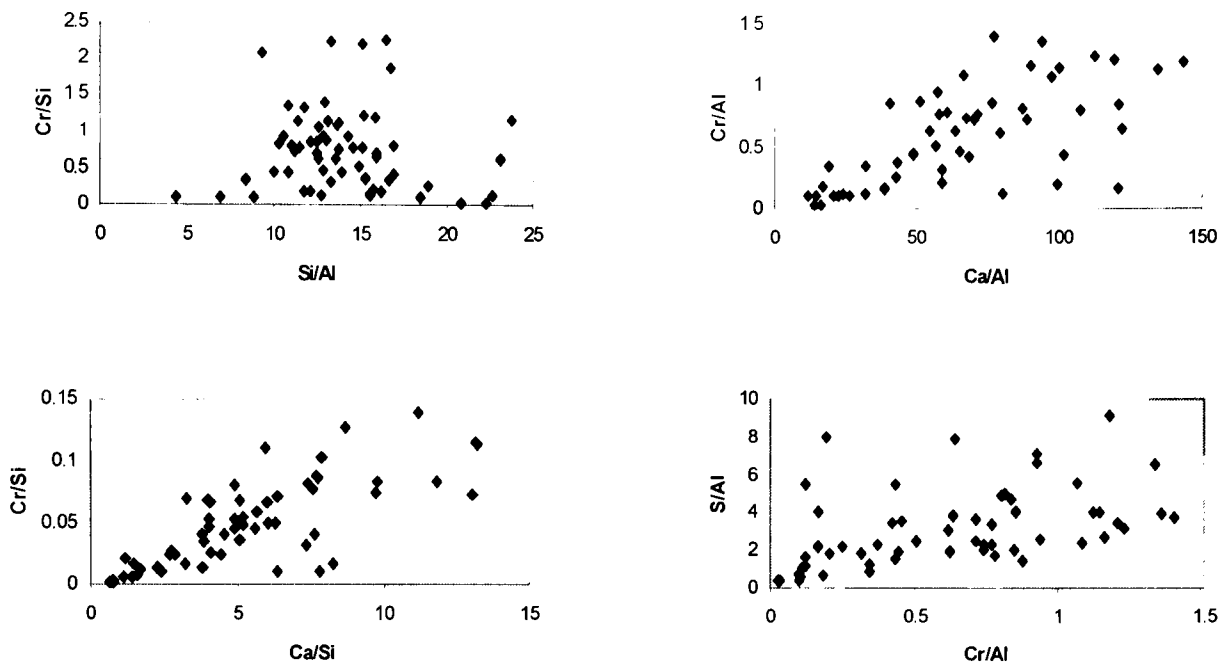


Fig. 7-9. Atom ratio plots of chromium with cement components in the  $\text{Cr}^{3+}$ -doped carbonated cement paste

Table 7-8. The correlation coefficients of atom ratio in the carbonated cement pastes\*

Samples	Si/Al- Ca/Al	M/Al- Ca/Al	Si/Al- M/Al	M/Al- S/Al	M/Si- Ca/Si	M/S- Al/S	Si/S- Al/S
Control	0.45						0.58
Cr	-0.12	0.81	0.09	0.61	0.84	-0.03	0.88
Cu	0.65	0.84	0.44	0.80	0.69	0.48	0.75
Pb	0.10	0.80	0.07	0.68	0.83	0.21	0.64

Note: M stands for Cr, Cu, Pb and Zn, respectively.

Table 7-7. The correlation coefficients of atom ratio in the hydrated cement pastes\*

Samples	Si/Al- Ca/Al	M/Al- Ca/Al	Si/Al- M/Al	M/Al- S/Al	M/Si- Ca/Si	M/S- Al/S	Si/S- Al/S
Control	0.44						0.14
Cr	0.80	0.74	0.82	0.84	-0.05	0.03	0.18
Cu	0.16	0.12	0.06	0.29	0.16	-0.03	0.14
Pb	0.37	0.55	0.88	0.55	0.44	-0.22	0.28
Zn	0.52	0.64	0.61	0.62	0.36	-0.17	0.53

Note: M stands for Cr, Cu, Pb and Zn, respectively.

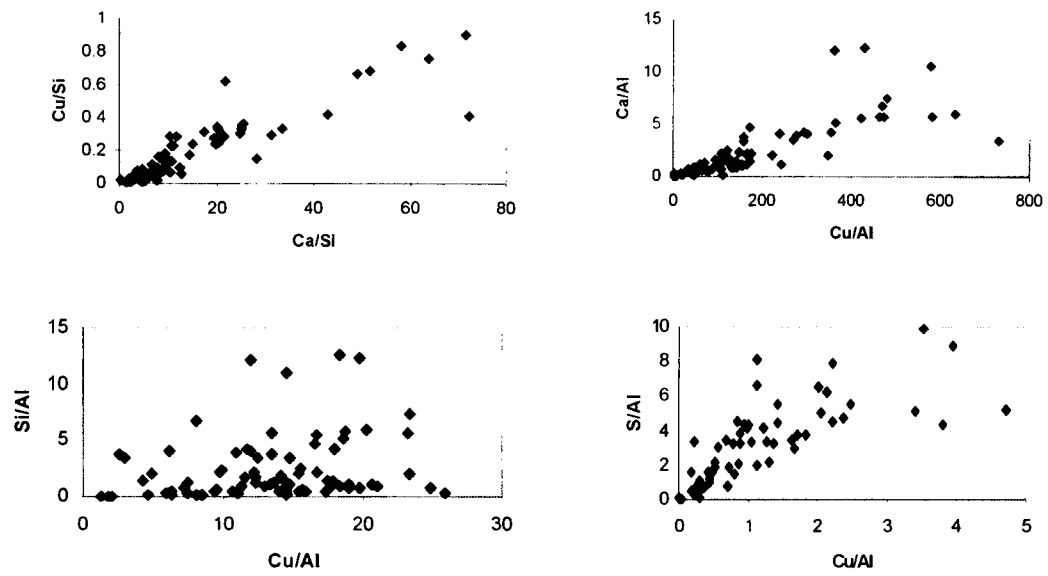


Fig. 7-10. Atom ratio plots of copper with cement components in the  $\text{Cu}^{2+}$ -doped carbonated cement paste

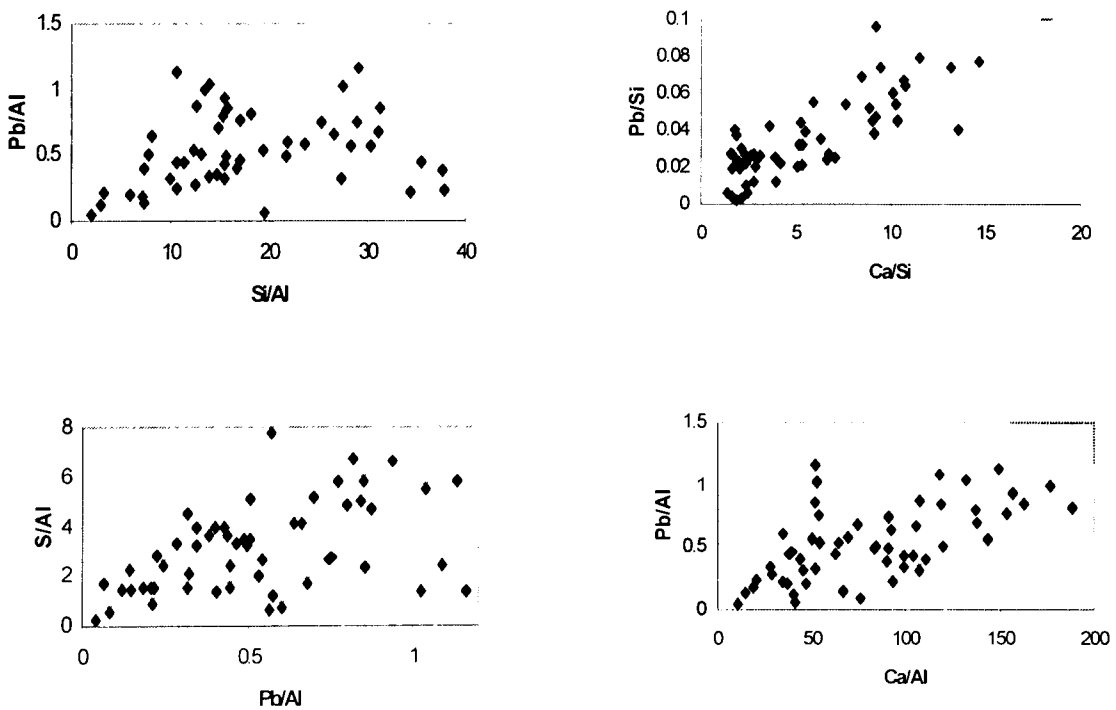


Fig. 7-11. Atom ratio plots of lead with cement components in the  $\text{Pb}^{2+}$ -doped carbonated cement paste

#### *7.4 Summary*

The hydrated and carbonated Portland cement pastes doped with heavy metals were studied using SEM/EDS. The main findings are summarised as follows:

Anhydrous clinker did not have the capacity of trapping heavy metals. The remainders of cement clinker in the hydrated cement pastes were much more numerous than in the carbonated cement pastes, which could be one of main advantages of the accelerated carbonation process in cement-based solidification/stabilisation of wastes. This work revealed that the accelerated carbonation of cement may use cement clinkers more efficiently than the conventional hydration of cement.

From statistical results (correlation coefficients of heavy metals and components of cements) and atom ratio plots, SEM/EDS microanalyses supported the examination relevant to the incorporation mechanism of heavy metals in cement pastes using XRD and DTA/TG techniques. Heavy metals could form precipitants of double hydroxides in the hydrated Portland cement pastes, in addition to absorbing in C-S-H gel.

The existence of very low Ca/Si ratio C-S-H gel and nearly pure silica gel was confirmed with SEM/EDS in the carbonated cement pastes, in agreement with estimated results based on thermal analyses. Unlike in the hydrated cement pastes, aluminium entered C-S-H gel (low Ca/Si ratio) or silica gel and favoured the incorporation of heavy metals in the carbonated cement pastes.

The fixation of heavy metals in the carbonated Portland cement pastes was found to be associated with calcium carbonate and C-S-H gel, supporting the findings based on XRD, DTA/TG and NMR techniques.

## Chapter 8

# Thermodynamic modelling of heavy metal-cement systems using PHREEQC

### 8.1 Background

Most research conducted to date on solidification/stabilisation (s/s) of wastes has been acquired through chemical, physical and leaching tests of treated wastes from laboratory, treatability studies and technology demonstrations (Price, 1995). Despite the increasing uses of cement-based s/s technologies for contaminated soils, sewage sludge and other industrial wastes prior to landfill or other disposal alternatives, the mechanisms involved, durability and performance of stabilised waste forms over time are not fully understood (Berger *et al.*, 1972; Slegers and Rouxhet, 1976; Redmond *et al.*, 2002a; 2002b). Knowledge of the dissolution/precipitation of various phases, the interaction of the aqueous species, and interaction of aqueous species with anhydrous cement phases is a key to the understanding and, in some cases, control of these processes (Meima and Comans, 1997; Zhang *et al.*, 1993).

As is well known, thermodynamic modelling can be very useful for understanding dissolution and precipitation, oxidation and reduction, acid-base and co-ordinative interactions (Stronach and Glasser, 1997; Berner, 1992; Bennett, 1992). It has been applied to the study of the hydration of cement (Atkins *et al.*, 1992; Atkins and Bennett, 1992; 1993; Damidot and Glasser, 1992; 1993a; 1993b; 1995). Typically, the thermodynamic modelling requires the computation of equilibrium compositions for systems containing an aqueous phase and solid phases (Thomas and Jennings, 1998; Van Eijik and Brouwers, 2001).

For modelling the behaviour of hydrated and carbonated cement and cement-based s/s systems a good database is essential (Harris *et al.*, 2002; Harrison and de Mora, 1996). The good database should contain all the possible compounds for a given set of components. In addition, we need to compile model parameters for the prediction of the

behaviour of compounds formed in cement matrices relevant to a wider range of conditions (Klich *et al.*, 1999; Sugama *et al.*, 1996; Atkins and Macphee, 1991).

In this chapter, thermodynamic modelling with a geochemical code, PHREEQC, was used as a tool to identify stable phases and phase assemblages in cement –based s/s systems and the phases most likely to control the heavy metal release. It was also used to predict the solubility change of these phases as a function of pH in cement matrices.

## **8.2 Databases**

The thermodynamic data are typically stored in stand-alone databases or integrated within specific computer codes. The former can be accessed by some specialised computer programs for thermodynamic modelling (Damidot *et al.*, 1994). Thermodynamic databases can be broadly separated into three groups:

- Pure substance databases;
- Databases for modelling solid solution phases relevant to metal-metal, metal-oxide and oxide-oxide systems;
- Databases for modelling aqueous systems for aqueous species and substances.

It is well known that the shortage of suitable thermodynamic data limits the reliability of thermodynamic modelling, as calculations with missing compounds could obtain misleading results (Saetta *et al.*, 1993; 1995; Vander Lee, 1998). The use of estimated data is one of amendments if no thermodynamic data are available (Thomas and Jennings, 1998; Saetta *et al.*, 1993; 1995). It must be, however, recognised that the estimated data have a degree of uncertainty. When editing a database for special calculations from different databases and estimated data, we also must pay much attention to the data consistency (Hudales, 1994).

## **8.2 Geochemical modelling codes**

The main geochemical codes available for thermodynamic modelling are summarised in appendix C. The latest version of PHREEQC is designed to perform a wider variety of

aqueous geochemical calculations. It eliminates many of the deficiencies and limitations of the former PHREEQE versions (Parkhurst, 1995; Parkhurst *et al.*, 1999; Parkhurst and Appelo, 2001). Based on an ion–association aqueous model, it uses an iterative solubility product approach to calculate the equilibrium solution composition and solid phase assemblage. PHREEQC has capabilities for:

- speciation and saturation index calculations.
- reaction path and advective-transport calculations involving specified irreversible reactions, mixing of solutions, mineral and gas equilibrium, surface–complexation reaction, and
- inverse modelling, which finds sets of mineral and gas mole transfers.

#### ***8.4 Modelling strategy of this work***

According to some theories of crystallisation, the rate of crystal nucleation and growth depends on the super-saturation level of the solution. The greater the super-saturation level of the solution, the greater the rate of crystal nucleation and growth. In thermodynamic modelling, saturation index (SI) is used to describe the apparent closeness to equilibrium between a solid phase and aqueous solution. SI value of zero indicates that the solution is saturated with respect to a particular solid and a value larger than zero means it is over-saturated and a precipitate will form (Boerjesson and Emreen, 1998; Park and Batchelor, 1999). If SI is less than zero, the solid will dissolve.

The key problems in thermodynamic modelling are to decide the parameters and reaction conditions, which reflect the real situation in cement-based s/s systems (Tyrer, 2001; Berger and Banwart, 2000). The treatment systems in this work involved the pure cement phases (C<sub>3</sub>S, C<sub>3</sub>A and C<sub>4</sub>AF) and Portland cement as chemical immobilisation matrices. The systems chosen for thermodynamic modelling included CaO-SiO<sub>2</sub>-Al<sub>2</sub>O<sub>3</sub>-M(NO<sub>3</sub>)<sub>x</sub>-H<sub>2</sub>O, CaO-SiO<sub>2</sub>-Al<sub>2</sub>O<sub>3</sub>-M(NO<sub>3</sub>)<sub>x</sub>-H<sub>2</sub>O-CO<sub>2</sub>(g) at different pH values, where the M represents heavy metals including Zn, Pb, Cu and Cr; x is 2 or 3. In this work, all calculations were performed at a constant temperature of 25°C.

Based on suspension pH measurements, thermodynamics modelling with the geochemical code PHREEQC and the edited database from LLNL (Lawrence Livermore National Laboratory) (Wolery, 1990) and the HATCHES (AEA Technology/Nirex, see Cross *et al.*, 1987) was used to model likely compounds by calculating the saturation index and solubility of precipitates associated with heavy metals in cement-based s/s systems. In other words, PHREEQC was used to calculate aqueous species distributions, dissolution and precipitation, aqueous compositions and pH changes before and after reactions in various cement-heavy metal-water systems in different conditions.

## 8.5 Results and discussion

### 8.5.1 pH values of cement suspensions

On the first contact of cement with water, the phases of cement decompose and hydrate rapidly. Calcium and silica pass into solution due to small grain size and instability of cement clinker phases with water. In the absence of admixtures, the amount of calcium that goes into solution and the resulting hydrolysis are the most important factors affecting the pH. The higher calcium content of cement phases, the higher pH of suspensions of cement phases (as shown in Table 8-1). In the presence of heavy metals, the equilibrium pH was dependent on the hydration of all substances present (Table 8-2). The hydrolysis of heavy metals lowered the suspension pH and inhibited the precipitation of portlandite (see Chapters 3, 4 and 6).

Table 8-1. The suspension pH of pure cement phases and cement

Phase	C <sub>3</sub> S	C <sub>2</sub> S	C <sub>3</sub> A	CA	C <sub>4</sub> AF	C <sub>12</sub> A <sub>7</sub>	Portland cement
pH	12.4	12.3	12.4	11.5	12.4	11.8	12.4

The carbonation reactions of cement are much more complex than its hydration reactions. The pH values of the carbonated suspensions decreased with the increasing number of carbonation cycles (see Chapters 4 and 6). If cement carbonation was complete, the suspension pH of cement became high alkalinity upon removal from contact with CO<sub>2</sub> due to the hydration of cement phases. After the 8<sup>th</sup> carbonation cycle (see Chapter 2 for

carbonation procedures), the pH values of cement suspensions with heavy metals were around pH 10 at 28 days of age.

Table 8-2. The pH of hydrated and carbonated cement suspensions with heavy metals

Suspensions	Pb	Cr	Zn	Cu	Control
Carbonation	10.3	10.2	9.9	9.9	10.4
Hydration	12.4	12.4	12.0	12.2	12.4

### 8.5.2 Thermodynamic modelling of phases in cement pastes

Assumed that cement phases dissolve congruently in water, the aqueous solution compositions of cement phases and Portland cement were calculated using PREEQC (Table 8-3). The phases formed during hydration and carbonation of cement –based systems are shown in Table 8-3 and Table 8-4. For the sake of comparison, the major reaction products identified by XRD and NMR are also presented in these tables. The modelling results are consistent with the laboratory examinations.

At the normal hydration pH, i.e. around 12.5, calcium silicate hydrate gel (CSH (Ca/Si: 1.8), CSH (Ca/Si: 1.1) and CSH (Ca/Si: 0.8)) and portlandite are over-saturated. According to the calculations of saturation indices, portlandite is under-saturated, when the pH <12.5; the reduction of pH will result in the decalcification of C-S-H gel. At pH 11, the predominant products could be CSH (Ca/Si: 1.1) instead of CSH (Ca/Si: 1.8). Furthermore, at pH 10, CSH (Ca/Si: 1.8) is under-saturated and CSH (Ca/Si: 0.8) is predominant product instead of CSH (Ca/Si: 1.1).

The presence of heavy metals will result in the reduction of pH in cement hydration and consequently inhibit the formation of portlandite, which was observed in the heavy metal -doped suspensions and pastes of C<sub>3</sub>S and Portland cement. The decalcification phenomenon of C-S-H gel due to the presence of heavy metals was also observed in C<sub>3</sub>S pastes (see Chapter 4).

The hydration products of calcium aluminate in the absence of gypsum are C-A-H phases. The solubility of these phases is in the order according to the calculations in this work (Table 8-5):

Table 8-3. The decomposition of cement phases and precipitates

Systems	Calculated aqueous compositions (mmole/l)					Oversaturated phases according to modelling	Main hydration products identified in experiments
	Ca	Si	Al	Fe	SO <sub>4</sub> <sup>2-</sup>		
C <sub>3</sub> S + water	21	8.4				C-S-H (Ca/Si: 1.8, 1.1, 0.8), Ca(OH) <sub>2</sub>	C-S-H (Ca/Si around 1.5), Ca(OH) <sub>2</sub>
C <sub>2</sub> S + water	14	2				C-S-H (Ca/Si: 1.1, 1.8, 0.8), Ca(OH) <sub>2</sub>	
C <sub>3</sub> A + water	58		39			C-A-H, gibbsite, boehmite, diaspore	C <sub>3</sub> AH <sub>6</sub> , C <sub>4</sub> AH <sub>19</sub> , C <sub>2</sub> AH <sub>8</sub> , gibbsite
C <sub>4</sub> AF + water	22		11	11		C-(A, F)-H, gibbsite, boehmite, diaspore, goethite, Fe(OH) <sub>3</sub>	C <sub>2</sub> (A,F)H <sub>8</sub>
C <sub>3</sub> A + gypsum + water	58		39		24	AFm-SO <sub>4</sub> <sup>2-</sup> , ettringite	ettringite
Portland cement + water	58	8.4	39	11	24	C-S-H (Ca/Si: 1.8, 1.1, 0.8), C-A-H, AFm-SO <sub>4</sub> <sup>2-</sup> , ettringite, gibbsite, boehmite, diaspore, goethite, Fe(OH) <sub>3</sub> , Ca(OH) <sub>2</sub>	C-S-H (Ca/Si: around 1.6), ettringite, Ca(OH) <sub>2</sub>



The above sequence confirms the tendency of conversion of C-A-H into hydrogarnet and is in agreement with experimental observations (see Chapter 5).

In the presence of gypsum, the main hydration product of calcium aluminate is ettringite or monosulfate. Since the solubility of ettringite is much lower than that of monosulfate (Table 8-5), it is not possible that ettringite converts to monosulfate if the gypsum content is sufficient for reaction with aluminate. Otherwise, ettringite reacts with C-A-H and the formation of monosulfate occurs, because the solubility of C-A-H is higher than that of monosulfate (Table 8-5).

The natural carbonation of cement can also be thought of as a process of pH reduction, in which portlandite will convert into  $\text{CaCO}_3$  (calcite, aragonite and vaterite). Additionally, higher ratio of C-S-H gel changes into lower ratio C-S-H gel and results in the gradual formation of more calcium carbonate and silica gel. If the pH is less than pH 8 in the carbonated cement paste, the Ca/Si ratio of C-S-H gel is less than 0.8, because CSH (0.8) is under-saturated, not to say CSH (1.1) and CSH (1.8); if pH is less than 5, only silica gel can exist in cement-based systems. Thus, the appropriate degree of carbonation needs to be controlled according to properties of wastes and cements carefully to achieve optimum immobilisation of wastes in cement-based s/s.

For the natural carbonation of calcium aluminate, with the increase of the degree of carbonation (using pH as an indicator), saturation indices of C-A-H, calcium monocarboaluminate and calcium tricarboaluminate decrease and become negative correspondingly. According to the order of saturation index reaching zero, the instability of C-A-H in the presence of  $\text{CO}_2$  will result in the formation of calcium carboaluminate, and then calcium carboaluminate changes into hydrous alumina and calcite.

During the accelerated carbonation of cement, the decomposition products of cement phases will react with dissolved  $\text{CO}_2$  to form calcium carbonate, silica gel, calcium carboaluminum and hydrous alumina. When the pH is less than 7.5, calcium carboaluminum will eventually change into  $\text{CaCO}_3$  and gibbsite. This is in agreement with the XRD examinations (see Chapter 6).

The amount of dissolution is associated with the instability of the hydration and carbonation products of cement in water. The aqueous compositions of major reaction products of cement are presented in Table 8-5 and Table 8-6.

Table 8-4. The major phases of carbonated cement

Systems	Gas in equilibrium (0.3MPa)	Oversaturated phases according to modelling	Main carbonation products identified in experiments
C <sub>3</sub> S + water	CO <sub>2</sub>	SiO <sub>2</sub> , CaCO <sub>3</sub>	C-S-H (Ca/Si around 0.1), CaCO <sub>3</sub>
C <sub>2</sub> S + water	CO <sub>2</sub>	SiO <sub>2</sub> , CaCO <sub>3</sub>	
C <sub>3</sub> A + water	CO <sub>2</sub>	gibbsite, boehmite, diaspore, CaCO <sub>3</sub>	C <sub>3</sub> A(CaCO <sub>3</sub> ) <sub>0.5</sub> H <sub>12</sub> , C <sub>3</sub> A(CaCO <sub>3</sub> )H <sub>11</sub> , gibbsite, CaCO <sub>3</sub>
C <sub>4</sub> AF + water	CO <sub>2</sub>	gibbsite, boehmite, diaspore, goethite, Fe(OH) <sub>3</sub> , CaCO <sub>3</sub>	gibbsite, CaCO <sub>3</sub>
C <sub>3</sub> A + gypsum + water	CO <sub>2</sub>	gibbsite, boehmite, diaspore, CaCO <sub>3</sub>	gibbsite, gypsum, CaCO <sub>3</sub>
Portland cement +water	CO <sub>2</sub>	boehmite, diaspore, goethite, Fe(OH) <sub>3</sub> , SiO <sub>2</sub> , CaCO <sub>3</sub>	C-S-H (Ca/Si: 0.07-0.77), gypsum, CaCO <sub>3</sub>

Based on the total calcium concentrations, the stability of reaction products can be arranged in the following order:

Calcite > C-S-H > AFt-CO<sub>3</sub> > AFt-SO<sub>4</sub> > AFm-CO<sub>3</sub> > AFm-SO<sub>4</sub> > CH > C-A-H

The above sequence indicates that the carbonation products of cement are less soluble than the hydration products of cement. This could be one of the most important advantages of carbonation over hydration in cement-based s/s of wastes.

The assemblage of some phases will influence the dissolution of the phases present (Table 8-7). In the presence of portlandite the total Si concentrations in C-S-H gel solutions will reduce dramatically (about 3 orders of magnitude) due to the increase of total Ca concentration ( $1.5E-2$  mole/l, dominated by the dissolution of portlandite). It is inferred that the presence of portlandite can stabilise the C-S-H gel due to the reduction of calcium and silicon dissolution from C-S-H gel, especially higher Ca/Si ratio C-S-H gel (see Table 8-5, Table 8-6 and Table 8-7).

Table 8-5. The calculated aqueous solution compositions of major reaction products of cement (mmole/l, pH 12.5)

Phases	Ca	Si	Al	SO <sub>4</sub> <sup>2-</sup>
C-S-H	0.24-0.74	0.21-0.41		
Ca(OH) <sub>2</sub>	5.75			
AFt	1.5		0.5	0.28
AFm	2.9		1.43	0.21
Calcite	0.12			
Calcium monocarboaluminate	2.0			
Calcium tricarboaluminate	0.77			
C-A-H	24-15		4.3-1.6	

Table 8-6. The comparison of calculated solubility of C-S-H, portlandite and calcite at different pH values (mole/l)

pH		CaCO <sub>3</sub>	Ca(OH) <sub>2</sub>	CSH(1.8)	CSH(1.1)	CSH(0.8)	SiO <sub>2</sub> gel
8	Ca	1.01E-03			6.01E-01	7.02E-01	
	Si				5.52E-01	8.41E-01	1.82E-03
11	Ca	7.50E-05	5.0E-01	5.00E-02	7.88E-04	1.05E-03	
	Si			4.42E-01	1.32E-03	1.84E-03	1.30E-01
12	Ca	8.60E-05	6.9E-02	1.45E-03	3.35E-04	5.15E-04	
	Si			8.06E-04	3.05E-03	1.32E-03	1.10E-01
13	Ca	1.70E-04	1.36E-03	4.90E-04	2.46E-04	6.53E-04	
	Si			2.73E-04	2.23E-03	8.16E-04	1.02

The equilibrium pH of C-S-H with or without portlandite is presented in Fig. 8-1. The modelling results are in agreement with experimental examinations conducted by Klich *et al.* (1990; 1999) and Harris *et al.* (2002).

Table 8-7. The aqueous solution compositions of cement phase assemblages (mole/l)

Solids in equilibrium	Ca	Si	Al	SO <sub>4</sub> <sup>2-</sup>	pH
C-S-H + CH	1.50E-2	3.75E-6			12.37
C-S-H + ettringite	1.64E-3	5.46E-4	3.47E-4	5.21E-4	
C-S-H + CH +ettringite	1.50E-2	3.75E-6	6.99E-6	1.05E-5	12.37
C-S-H + CaCO <sub>3</sub>	1.05E-3	9.40E-4			11.06
C-S-H + SiO <sub>2</sub> gel	1.55E-3	4.87E-3			10.11
C-S-H + SiO <sub>2</sub> gel + CaCO <sub>3</sub>	2.22E-3	6.25E-3			10.24
SiO <sub>2</sub> gel + CaCO <sub>3</sub>	2.77E-4	2.05E-3			9.06

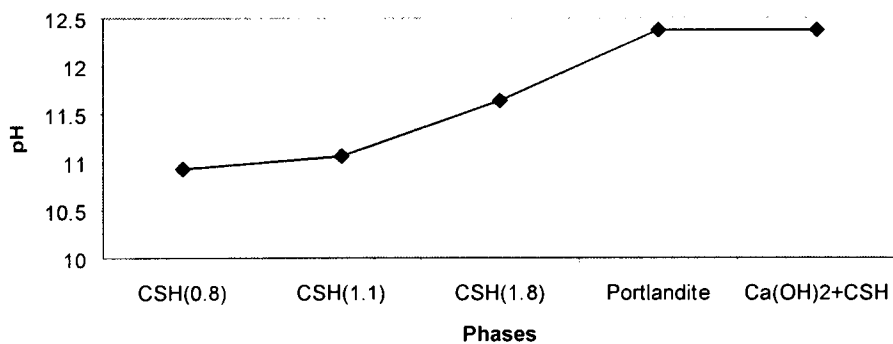


Fig. 8-1. The equilibrium pH of hydration products of calcium silicate

It is worth pointing out that in a real cement paste, it is likely that a continuous compositional range for C-S-H may exist, which can not be subdivided into CSH (1.8), CSH (1.1) and CSH (0.8) or C-S-H (1) and C-S-H (2) types (Kantro, 1975; Spence and Cook, 1983; Glasser, 1997). There may be the most frequent ratio of Ca/Si ratio of C-S-H gel in a cement paste, depending on pH values caused by admixtures such as CO<sub>2</sub> and

heavy metals (Viehlend *et al.*, 1996; 1997; Grutzeck *et al.*, 1999). At the present time, the data concerning  $K_{sp}$  of C-S-H with continuous Ca/Si ratio and incongruent dissolution are not available.

### 8.5.3 Thermodynamic modelling of heavy metal precipitates in cement systems

In cement-based *s/s* systems various reactions probably occurred in the near surface or surface of cement phase grains, where cement component concentrations may be very different from the bulk solution of cement due to diffusion rate control. To model the heavy metal compounds in cement pastes, essential parameters such as pH and concentrations of various components need to be chosen wisely.

The concentrations of Ca, S, Al, Si, and Fe depend on dissolution of cement phases and hydration or carbonation products of cement. As described earlier, PHREEQC was used to calculate the solubility of cement phases and reaction products, as shown in Table 8-3 and Table 8-5. These results are in good agreement with pore solutions of cement pastes measured by some researchers including Abderlaxig *et al.* (1999), Asavapisit *et al.* (1997) and Rogers and Aldridge (1977). For simplicity, we assume that reactions of heavy metals with cement occur in the pore solution of cement pastes in modelling.

According to the solubility calculations of hydration or carbonation products of cement phases and anhydrous cement phases (Table 8-5 and Table 8-3), the concentrations are chosen as (mmole/l): Ca 15.7; Si 1.9; S 15.7; Al 0.5 and Fe 0.3 to model the heavy metal precipitates in cement systems. In modelling, the effects of concentrations of cement components were investigated by magnifying or reducing 10-100 times. The concentrations of heavy metals were adopted on a concentration range of 10-1000 mmole/l, even though in reaction places (the surface or near surface of cement phase grains) the concentrations of heavy metals may be a bit lower than the bulk solution.

According to calculations, the variation of cement component concentrations such as calcium and silicon has less effect on the saturation indices of heavy metal compounds compared to the variation of heavy metal concentrations. Although the change of

concentration of any component can change the saturation indices of heavy metal compounds, it does not alter the sequence of the saturation indices reaching zero.

It must be remembered that thermodynamic calculations did not consider double hydroxides except for calcium zincate and solid solutions because of the shortage of reliable data concerning  $K_{sp}$  at the present time.

### 8.5.3.1 Hydrated cement systems

The various systems presented in Table 8-8 were calculated to model the heavy metal compounds in hydrated cement pastes. Modelling predicts that the oversaturated copper compounds in the Cu –doped cement paste are  $Cu_x(OH)_ySO_4$ ,  $CuO$ ,  $Cu(OH)_2$  and  $CuSiO_3$ . The saturation indices of copper sulphates such as antlerite, posnjakite and brochatite, are sensitive to the pH, especially at hyper-alkaline levels. It is inferred, therefore, that reduction of gypsum in cement will improve the resistance of solidified waste forms to environmental attack.

Modelling lead compounds in hydrated cement-based s/s system are,  $Pb_x(OH)_ySO_4$ ,  $PbO$ ,  $Pb(OH)_2$  and  $Pb_2SiO_4$ . Again, the saturation indices of lead sulphates are sensitive to the pH, which changes significantly when pH is changed a little, especially in high and low pH levels. In order to avoid the formation of lead sulphates, the gypsum content of cement should be as low as possible.

The zinc compounds to form in hydrated cement-bases s/s system are ferrite-Zn, zincite,  $Zn(OH)_2$ ,  $ZnSiO_3$ ,  $Zn_2SiO_4$  and calcium zincate  $(CaZn_2(OH)_6 \cdot 2H_2O)$ . The saturation indices of zinc sulphates are negative, indicating that they are under-saturated.

The heavy metal compounds in Table 8-8 were added, one by one, to the phase assemblage of CSH (0.8), CSH (1.1), CSH (1.8), ettringite, portlandite and hydrotalcite or to the phase assemblage of CSH (0.8), CSH (1.1), CSH (1.8), AFm- $SO_4$ , portlandite, C-A-H and hydrotalcite. Through iterative calculations in equilibrium with water, we can determine the sequence of the heavy metal compound precipitating, according to aqueous solution compositions and saturation index. This sequence reflects the tendency of formation of heavy metal compounds. As shown in Table 8-9, the most likely compounds formed in

cement pastes are  $\text{Cu}(\text{OH})_2$ ,  $\text{Pb}(\text{OH})_2$  and calcium zincate, respectively. These compounds were observed in heavy metal -doped  $\text{C}_3\text{S}$  suspensions, in addition to calcium copper hydroxide and calcium chromium hydroxide, which were not calculated because of the shortage of  $K_{sp}$  data.

Table 8-8. Modelling heavy metal compounds in hydrated cement pastes

Mineral assemblage	Initial aqueous solution (mmole/l)	Oversaturated compounds of heavy metals
CSH (0.8) CSH (1.1) CSH (1.8) ettringite portlandite hydrotalcite or CSH (0.8) CSH (1.1) CSH (1.8)	Ca15.7; Si 1.9; S 15.7; Al 0.5, Fe 0.3, Cu 10	antlerite, brochantite, chrysocolla, delafossite, diopside, ferrite-Cu, tenorite,
ettringite portlandite hydrotalcite or CSH (0.8) CSH (1.1) CSH (1.8)	Ca15.7; Si 1.9; S 15.7; Al 0.5, Fe 0.3, Pb 10	alamosite, lanarkite, litharge, massicot, minium, $\text{PbSiO}_3$ , $\text{Pb}_2\text{SiO}_4$ , $\text{Pb}_3\text{SO}_6$ , $\text{Pb}_4\text{SO}_7$
CSH (0.8) CSH (1.1) CSH (1.8)	Ca15.7; Si 1.9; S 15.7; Al 0.5, Fe 0.3, Zn 10	ferrite-Zn, zincite, calcium zincate, $\text{Zn}(\text{OH})_2$ , $\text{ZnSiO}_3$ , $\text{Zn}_2\text{SiO}_4$
C-A-H AFm- $\text{SO}_4$ portlandite hydrotalcite	Ca15.7; Si 1.9; S 15.7; Al 0.5, Fe 0.3, Cr 10	$\text{Cr}_2\text{O}_3$ , $\text{Cr}(\text{OH})_3$ ,

Table 8-9. Simulation of heavy metal compounds precipitating in hydrated cement pastes

Metals	The sequence of reaching over saturation
Cu	chrysocolla < diopside < antlerite < brochantite < tenorite < $\text{Cu}(\text{OH})_2$
Pb	alamosite < lanarkite < $\text{PbSiO}_3$ < $\text{Pb}_2\text{SiO}_4$ < $\text{Pb}_4\text{SO}_7$ < massicot < litharge < $\text{Pb}(\text{OH})_2$
Zn	$\text{Zn}(\text{OH})_2$ < zincite < $\text{ZnSiO}_3$ < $\text{Zn}_2\text{SiO}_4$ < calcium zincate

### 8.5.3.2 Carbonated cement systems

To model heavy metal compounds of heavy metals in carbonated cement pastes, the systems presented in Table 8-10 were calculated. The phase assemblage of calcite, SiO<sub>2</sub>, gibbsite and gypsum with heavy metal compounds was used to simulate the precipitation of heavy metal compounds in carbonated according to aqueous solution compositions and saturation index. The modelling results are presented in Table 8-11.

Table 8-10. Modelling heavy metal compounds in carbonated cement pastes

Mineral assemblage	Gas (0.3MPa)	Initial aqueous solution (mmole/l)	Oversaturated compounds of heavy metals
Calcite SiO <sub>2</sub> Gibbsite Gypsum	CO <sub>2</sub>	Ca15.7; Si 1.9; S 15.7 Al 0.5, Fe 0.3, Cu 10	antlerite, azurite, brochantite, chrysocolla, delafossite, diopside, ferrite-Cu, malachite, tenorite,
		Ca15.7; Si 1.9; S 15.7 Al 0.5, Fe 0.3, Pb 10	alamosite, anglesite, cerussite, hydrocerussite, lanarkite, minium, PbSiO <sub>3</sub> , Pb <sub>2</sub> SiO <sub>4</sub> , Pb <sub>2</sub> SO <sub>5</sub> , Pb <sub>4</sub> SO <sub>7</sub> , PbCO <sub>3</sub> PbO
		Ca15.7; Si 1.9; S 15.7 Al 0.5, Fe 0.3, Zn 10	ferrite-Zn, zincite, smithsonite, Zn(OH) <sub>2</sub> , Zn <sub>2</sub> SiO <sub>4</sub> , ZnSiO <sub>3</sub> , hydrozincite, ZnCO <sub>3</sub> H <sub>2</sub> O, Zn <sub>2</sub> SO <sub>4</sub> (OH) <sub>2</sub>
		Ca15.7; Si 1.9; S 15.7 Al 0.5, Fe 0.3, Cr 10	Cr <sub>2</sub> O <sub>3</sub> , Cr(OH) <sub>3</sub> ,

In the carbonated cement paste doped with copper, predicted copper compound is malachite (Cu<sub>2</sub>(OH)<sub>2</sub>CO<sub>3</sub>). The likely lead compounds in carbonated cement systems are hydrocerussite (Pb(OH)<sub>2</sub>.2PbCO<sub>3</sub>) and cerussite (PbCO<sub>3</sub>). The likely zinc compounds in the carbonated cement paste doped with zinc are ZnCO<sub>3</sub> and ZnCO<sub>3</sub>H<sub>2</sub>O. It should be pointed out that these compounds were not detected by XRD and DTA/TG in the carbonated suspensions or pastes of C<sub>3</sub>S and Portland cement doped with heavy metals due to the strong heavy metal binding capacity of cement carbonation products.

Table 8-11. Simulation of heavy metal compounds precipitating in carbonated cement pastes

Metals	The sequence of reaching over saturation
Cu	chrysocolla < azurite < tenorite < antlerite < brochantite < malachite
Pb	PbO < PbSiO <sub>3</sub> < Pb <sub>2</sub> SiO <sub>4</sub> < alamosite < anglesite < PbCO <sub>3</sub> PbO < Pb <sub>4</sub> SO <sub>7</sub> < PbOPbSO <sub>4</sub> < hydrocerussite < cerussite
Zn	calcium zincate < Zn(OH) <sub>2</sub> < zincite < hydrozincite < ZnSiO <sub>3</sub> < Zn <sub>2</sub> SiO <sub>4</sub> < simthsonite < ZnCO <sub>3</sub> H <sub>2</sub> O

#### 8.5.4 Solubility control compounds of heavy metals in cement systems

Using PHREEQC the aqueous solubility of heavy metal compounds with mineral assemblage shown in Table 8-12 was calculated. The calculation results at pH 12.5 are presented in Table 8-13, and Figs. 8-2, 8-3 and 8-4. The prediction of heavy metal releases from cement pastes to water are summarised in Table 8-14.

According to the solubility calculations of Cu<sub>x</sub>(OH)<sub>y</sub>SO<sub>4</sub>, CuO, Cu(OH)<sub>2</sub> and CuSiO<sub>3</sub>, tenorite (CuO) has the lowest solubility (Fig. 8-2). The compounds Cu<sub>x</sub>(OH)<sub>y</sub>SO<sub>4</sub>, Cu(OH)<sub>2</sub> and CuSiO<sub>3</sub> could convert into tenorite in cement-based s/s systems in the long term. Malmstrom *et al.* (2000) and Meima and Comans (1997) reported such conversion in precipitation of wastewater in the presence of sulphate in high alkaline media. But at an early age, Cu(OH)<sub>2</sub> is the most likely solubility control compound in hydrated cement pastes. In carbonated cement systems, from the solubility sequence of copper compounds in Table 8-13, Cu<sub>2</sub>CO<sub>3</sub>(OH)<sub>2</sub> is a likely solubility control compound. It is predicted that a carbonated cement –based s/s system could improve the effectiveness retaining copper (see Table 8-14).

As shown in Fig. 8-3 and Table 8-13, the most likely solubility control compound in both hydrated and carbonated cement-based s/s systems is Pb(OH)<sub>2</sub>, which was readily detected by XRD in the lead -doped C<sub>3</sub>S suspensions (see Chapter 4). Based on solubility calculations of lead compounds, carbonation can reduce the release of lead to the environments due to the pH reduction, compared to the hydrated cement system (Table 8-14).

Table 8-12. The phase assemblage in the calculations of aqueous solubility of heavy metal compounds

Systems	Mineral assemblage
Hydration	CSH (0.8), CSH (1.1), CSH (1.8), ettringite, portlandite and hydrotalcite with heavy metal compounds, or CSH (0.8), CSH (1.1), CSH (1.8), AFm-SO <sub>4</sub> , hydrogarnet, portlandite and hydrotalcite with heavy metal compounds
Carbonation	Calcite, SiO <sub>2</sub> , gibbsite and gypsum with heavy metal compounds

Table 8-13. Comparison of the modelled aqueous solubility of heavy metal compounds in cement pastes

Metals	pH	The sequence of modelled aqueous solubility
Copper	>12	CuSiO <sub>3</sub> > Cu <sub>x</sub> (OH) <sub>y</sub> (SO <sub>4</sub> ) <sub>z</sub> > Cu <sub>2</sub> CO <sub>3</sub> (OH) <sub>2</sub> > Cu(OH) <sub>2</sub> > CuO
	<9	CuSiO <sub>3</sub> > Cu <sub>x</sub> (OH) <sub>y</sub> (SO <sub>4</sub> ) <sub>z</sub> > Cu(OH) <sub>2</sub> > Cu <sub>2</sub> CO <sub>3</sub> (OH) <sub>2</sub> > CuO
Lead	>12	PbO > Pb <sub>3</sub> (CO <sub>3</sub> ) <sub>2</sub> (OH) <sub>2</sub> > PbCO <sub>3</sub> > Pb <sub>x</sub> (OH) <sub>y</sub> (SO <sub>4</sub> ) <sub>z</sub> > PbSiO <sub>3</sub> > Pb(OH) <sub>2</sub>
	<9	PbO > Pb <sub>x</sub> (OH) <sub>y</sub> (SO <sub>4</sub> ) <sub>z</sub> > PbSiO <sub>3</sub> > PbCO <sub>3</sub> > Pb <sub>3</sub> (CO <sub>3</sub> ) <sub>2</sub> (OH) <sub>2</sub> > Pb(OH) <sub>2</sub>
Zinc	>12	Zn <sub>x</sub> (OH) <sub>y</sub> (SO <sub>4</sub> ) <sub>z</sub> > ZnCO <sub>3</sub> > Zn(OH) <sub>2</sub> > CaZn <sub>2</sub> (OH) <sub>6</sub> 2H <sub>2</sub> O > ZnO > Zn <sub>5</sub> (OH) <sub>6</sub> (CO <sub>3</sub> ) <sub>2</sub> > ZnCO <sub>3</sub> > Zn <sub>2</sub> SiO <sub>4</sub> > ZnSiO <sub>3</sub>
	<9	Zn <sub>x</sub> (OH) <sub>y</sub> (SO <sub>4</sub> ) <sub>z</sub> > Zn(OH) <sub>2</sub> > CaZn <sub>2</sub> (OH) <sub>6</sub> 2H <sub>2</sub> O > ZnO > Zn <sub>5</sub> (OH) <sub>6</sub> (CO <sub>3</sub> ) <sub>2</sub> > ZnCO <sub>3</sub> > ZnSiO <sub>3</sub> > Zn <sub>2</sub> SiO <sub>4</sub>

It is noted that the solubility of zinc hydroxide is higher than that of calcium zinc double hydroxide (calcium zincate) in the high pH (e.g.12.5), but lower than that of calcium zincate in the low pH (e.g. pH < 11). According to modelling (Fig. 8-4), it is predicted that the zinc silicates are likely solubility control compounds in both hydrated and carbonated cement pastes. The carbonated system has a better performance than hydrated cement due to the lower solubility of ZnSiO<sub>3</sub> in the pH range 7-10 than that of Zn<sub>2</sub>SiO<sub>4</sub> at pH >12 (see Table 8-14).

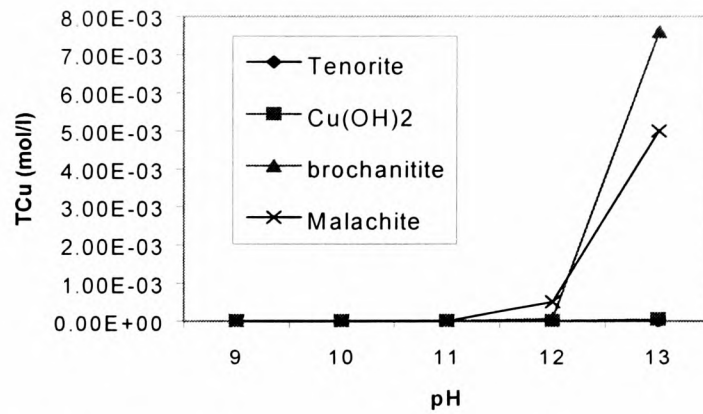
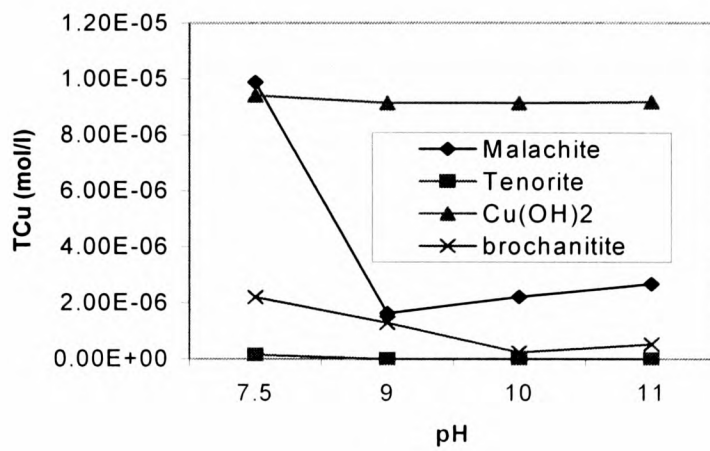


Fig. 8-2. The modelled aqueous solubility of copper compounds with pH

Table 8-14. The prediction of heavy metal releases from hydrated or carbonated cement pastes

metals	hydration		carbonation		effect of carbonation
	SCC*	leachate TM** (mol/l)	SCC*	leachate TM** (mol/l)	
copper	Cu(OH) <sub>2</sub>	9.86E-06	Cu <sub>2</sub> CO <sub>3</sub> (OH) <sub>2</sub>	1.64E-06	improvement
lead	Pb(OH) <sub>2</sub>	5.29E-08	Pb(OH) <sub>2</sub>	3.99E-09	improvement
zinc	ZnSiO <sub>3</sub>	2.23E-06	Zn <sub>2</sub> SiO <sub>4</sub>	1.20E-07	improvement
chromium	Cr(OH) <sub>3</sub>	5.59E-08	Cr(OH) <sub>3</sub>	1.38E-08	deterioration

Note: \* SCC—solubility control compound,

\*\*T means total, M = Cu, Cr, Pb, and Zn, respectively

The solubility control compound of chromium in cement paste is probably  $\text{Cr}(\text{OH})_3$ . Carbonation increase the release of chromium, suggesting that carbonation should be avoided for chromium immobilisation unless other pre-treatments are used.

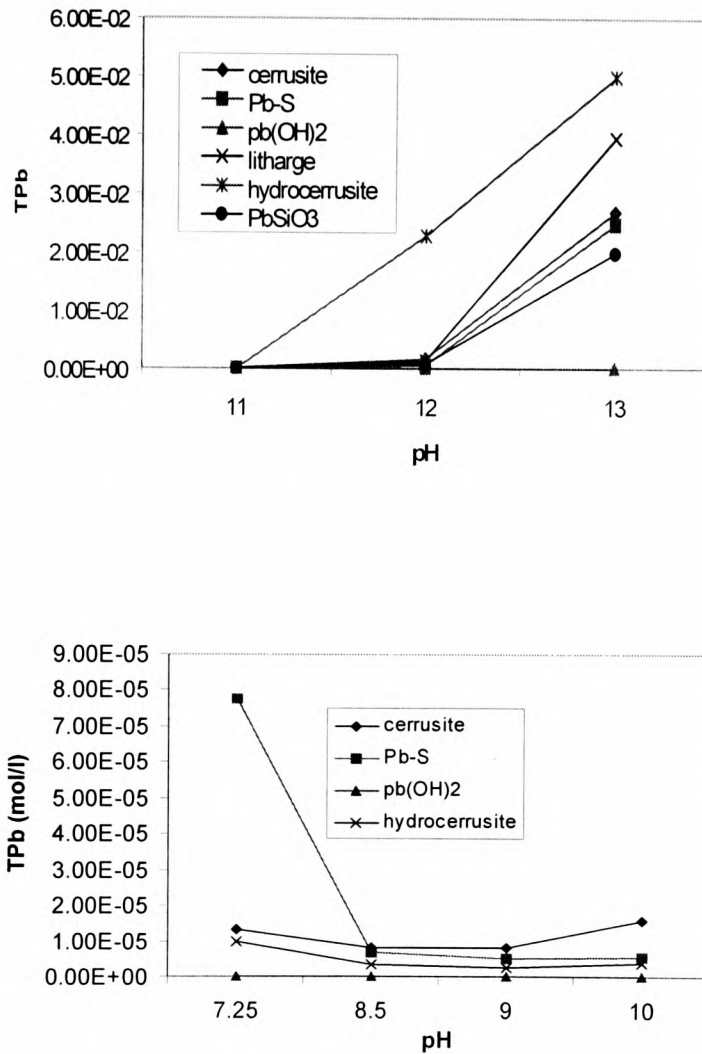


Fig. 8-3. The modelled aqueous solubility of lead compounds with pH

### 8.6 Shortcoming of the thermodynamic modelling

Carbonation can influence the retention of waste species within a solidified product and alter the rate at which some hazardous components leach from industrial wastes and Portland cement-based solidified/stabilised waste streams (Walton *et al.*, 1997; Lange *et al.*, 1996; Wang and Vipulanandan, 2000). The thermodynamic modelling in this work demonstrates that carbonation can improve the immobilisation of some heavy metals during cement-based s/s. In practice, the effects of carbonation are very different,

depending on the metal studied, waste features, leaching methods and curing conditions of solidified wastes (Montgomery *et al.*, 1988; 1991a; 1991b).

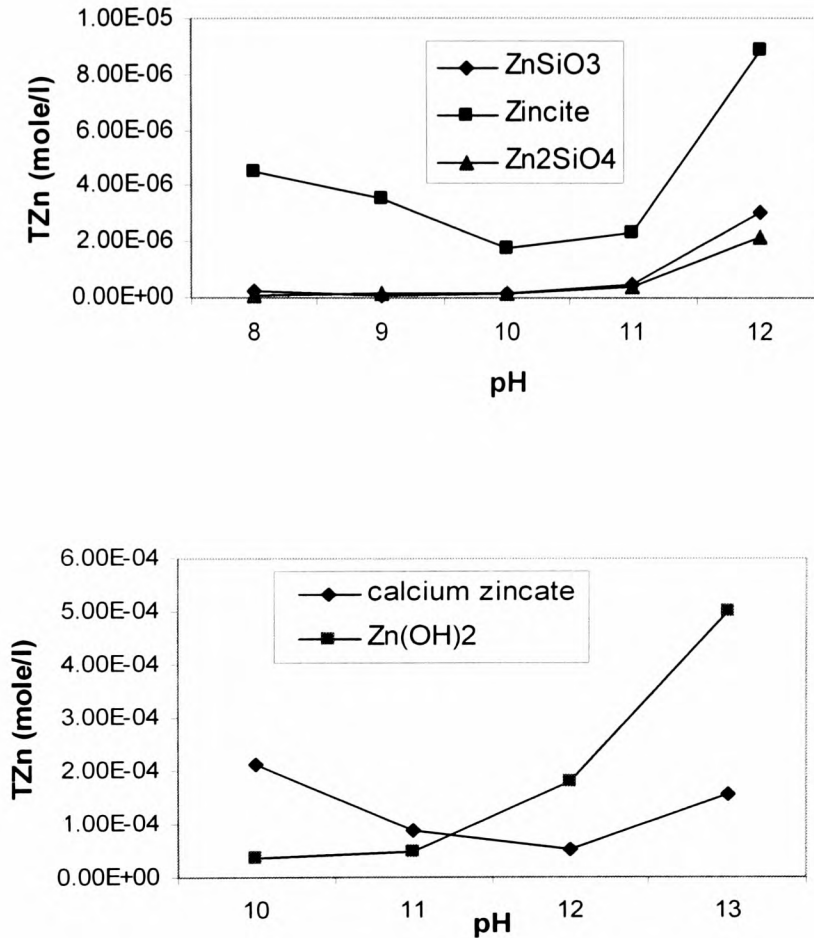


Fig. 8-4. The modelled aqueous solubility of zinc compounds with pH

Sweeney *et al.* (1998) reported the accelerated carbonation of Portland cement -based s/s of heavy metal bearing wastes. In their leaching experiments, carbonated samples demonstrated higher concentrations of Zn at low acid addition and comparable concentrations at higher acid additions compared to non-carbonated sample leachates. In contrast, Cr concentrations in non-carbonated samples were generally higher than their carbonated analogues, although the magnitude of Cr release was the lowest of all the detectable metals. Cu leachate concentrations were similar for both carbonated and non-carbonated samples.

Walton *et al.* (1997) demonstrated that some radionuclides formed solid solutions with calcite and this led to significantly lower release rates for Sr and Co in carbonated solidified waste forms. They also conducted dynamic leaching tests using water and 0.5N acetic acid, and found that calcium, cadmium, lead and cobalt experienced higher leaching rates from carbonated waste compared with non-carbonated analogues. They concluded that carbonation caused heavy metals such as nickel, cadmium, mercury to be mobilised.

In the calculations of this work, we considered only pure minerals, dissolving congruently according to their stoichiometry. In reality, however, co-precipitation or solid solution often controls the solubility and many solid solutions dissolve incongruently. In addition, omission of solids from the database (for example, double hydroxides of calcium and heavy metals), can also lead to unrealistic predictions or misleading modelling results. Moreover, the adsorption of heavy metal ions on the surface of cement hydrates or carbonation products has not been modelled due to the shortage of thermodynamic data for these materials. This should be taken into account in the further work on thermodynamic modelling.

The precipitation of heavy metal compounds in cement pastes depends on the concentration, temperature and reaction time. Kinetics should also be taken into account. Equilibrium may not be established between the solid and the soluble phases within the time span of treatment process. Some compounds rarely exist in s/s system (for example, zinc silicates), because of kinetic constrains. These departures from thermodynamic equilibrium impose further difficulties on the applications of models developed for equilibrium predictions.

## **8.7 Summary**

Using the experimental results reported earlier in this thesis, thermodynamic modelling with PHREEQC was carried out to investigate the phase development during the hydration and carbonation of cement. Heavy metal precipitates in these systems were calculated and compared. The main findings of this work are summarised as follows:

- The Ca/Si ratio of C-S-H gel depends on the pH of systems. The pH reduction due to carbonation or heavy metal hydrolysis results in decalcification of C-S-H

gel. Low Ca/Si ratio C-S-H gel is more resistant to solution pH changes than high Ca/Si ratio C-S-H gel.

- In cement-based s/s systems, the most likely precipitates of heavy metals are predicted as hydroxides and silicates. The modelling is useful in explaining experimental results.
- The modelling results indicate that carbonation products of cement are less soluble than hydration products of cement. It is predicted that carbonation can reduce the release of some heavy metals to the environment.

## Chapter 9

### General discussion

#### *9.1 Background*

The previous chapters have focused upon the laboratory examination and thermodynamic modelling of the mineralogical changes induced by hydration and carbonation of calcium oxide, pure cement phases and Portland cement in the presence or absence of heavy metals. The reaction products of these systems have been studied by XRD, DTA/TG, SEM/EDS and NMR techniques and interpreted by thermodynamic modelling. In addition, the procedures leading to the accelerated carbonation and the incorporation of heavy metals in cement-based systems were examined. For the convenience of further discussion, the major points are summarised as follows:

Chapter 3 described the interactions of heavy metals with calcium oxide and calcium hydroxide. The reaction products, including double hydroxides containing heavy metal and calcium, portlandite and calcium carbonate, were characterised by XRD and DTA/TG techniques.

In chapter 4, the effects of heavy metals on both the hydration and carbonation reactions of  $C_3S$  were examined by XRD, DTA/TG and  $^{29}Si$  MAS/NMR.  $Pb^{2+}$ ,  $Cu^{2+}$  and  $Cr^{3+}$  accelerated the hydration of  $C_3S$ , whereas  $Zn^{2+}$  retarded the early hydration of  $C_3S$ . All the metals influenced the polymorphism of calcium carbonate and the polymerisation of C-S-H gel.

In Chapter 5, the carbonation products of pure cement phases containing aluminium ( $C_3A$ ,  $C_4AF$ ,  $C_{12}A_7$  and  $CA$ ) were examined by XRD and compared to the hydrated samples. Changes induced by the presence of  $Zn^{2+}$ ,  $Pb^{2+}$ ,  $Cu^{2+}$  and  $Cr^{3+}$  on the reaction products of those phases were discussed.

In chapter 6, the reaction products of Portland cement were identified and characterised using XRD, DTA/TG, and  $^{29}Si$  and  $^{27}Al$  MAS/NMR. An important insight regarding the

connectivity of Si and Al atoms in the cement pastes was obtained. In carbonated Portland cement, aluminium was associated with calcium silicate hydrate gel and favoured the immobilisation of heavy metal ions to maintain electric neutrality in the matrix.

In Chapter 7, the hydrated and carbonated Portland cement pastes doped with heavy metals were studied using SEM/EDS to obtain heavy metal fixation data. Statistical analyses of microanalysis data supported the conclusions that heavy metals formed amorphous precipitates of double hydroxides or co-existed with C-S-A-H gel, portlandite and calcium carbonate in Portland cement pastes. SEM/EDS microanalyses confirmed the formation of very low Ca/Si ratio C-S-H gel in carbonated pastes.

Chapter 8 presented the thermodynamic modelling results of aqueous reaction processes of cement and the most likely compounds of heavy metals using the geochemical code PHREEQC and the LLNL database. Some of the predicted compounds, however, rarely exist in cement-based s/s systems due to kinetic constraints. The lack of thermodynamic data for some compounds for cement-base solidification/stabilisation is another problem.

This chapter discusses the interaction mechanisms of heavy metals with cement and the likely fixation mechanisms of heavy metals in hydrated and carbonated cement pastes further. The original contributions of this thesis and the recommendations for further work are also given in this chapter.

## ***9.2 Interaction mechanisms of heavy metals and cement***

It has shown that cement hydration involves a self-inhibiting series of reactions, which are probably largely controlled by the permeability and cohesion of protective colloidal coatings around reacting cement grains (Kantro, 1975; Kielsen, 1996). Both hydration and carbonation reactions of cement can be modified by heavy metals due to the modification to coating around cement grains, which have been supported by a number of laboratory studies (Tashiro *et al.*, 1977; 1979; Hudales, 1994). Three-dimensional structures up to 100-300nm thick containing heavy metal can form coatings around cement grains have been as observed by Cannell *et al.* (2000).

According to Poon *et al.* (1985; 1986), metals that form the least soluble hydroxides retard hydration reactions; those that form more soluble hydroxides exhibit only a slight degree of retardation; and metals forming soluble hydroxides behave as accelerators of cement hydration. Retardation has been attributed to the reduction in permeability cause by these reaction products (Tashiro and Oba, 1980). It is, however, difficult to apply these rules to explain the acceleration effects of heavy metals such as  $\text{Cr}^{3+}$  and  $\text{Cu}^{2+}$  on tricalcium silicate and Portland cement hydration. As described in Chapter 4 and 6,  $\text{Zn}^{2+}$  retarded the early hydration of both  $\text{C}_3\text{S}$  and Portland cement, although  $\text{Cu}(\text{OH})_2$  and  $\text{Cr}(\text{OH})_3$  are relatively insoluble in comparison to  $\text{Zn}(\text{OH})_2$  and  $\text{Ca}(\text{OH})_2$  (Table 9-1).

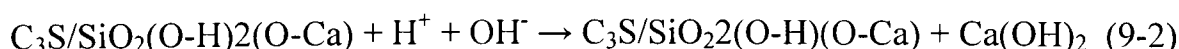
As the performance of Portland cement is dominated by  $\text{C}_3\text{S}$ , for the simplicity, we use  $\text{C}_3\text{S}$  as a representative to discuss the interactions of heavy metals with cement.

Table 9-1. The solubility and suspension pH of metal compounds (mg/l)

Metals	pH	Hydroxides	Carbonates
Ca	12.5	1300	2.76E-03
Cr	6.7	8.4E-04	
Cu	7.7	2.2E-02	1.01E-03
Pb	5.5	2.1	8.0E-05
Zn	6.7	1.1	2.52E-04

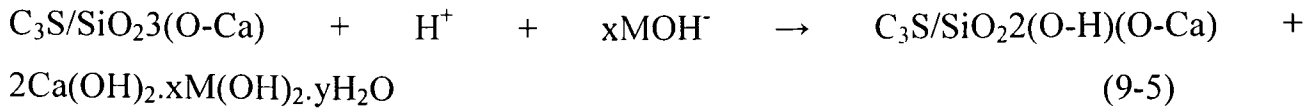
### 9.2.1 Hydration of $\text{C}_3\text{S}$

The hydration of  $\text{C}_3\text{S}$  is expressed as follows:

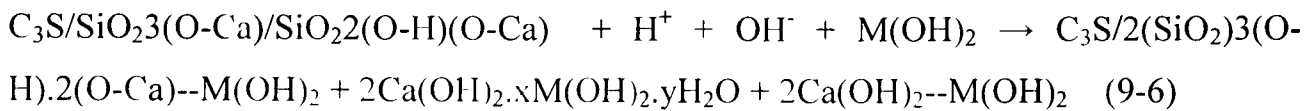


In the presence of heavy metals (M), the hydration of  $\text{C}_3\text{S}$  can be:





As hydration progresses, more and more hydrogen ions are consumed and pH approaches to the pH of saturated solution of portlandite (12.5) and then, portlandite precipitates from solutions.

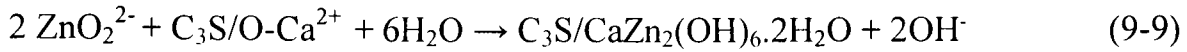


The formation of double hydroxides ( $\text{Ca(OH)}_2.\text{xM(OH)}_2.\text{yH}_2\text{O}$ ) or hydroxide did not inhibit the hydration of  $\text{C}_3\text{S}$  with the exception of calcium zincate, which forms on the surface of  $\text{C}_3\text{S}$ . The promoting effect of  $\text{Cu}^{2+}$ ,  $\text{Pb}^{2+}$  and  $\text{Cr}^{3+}$  on the hydration of  $\text{C}_3\text{S}$  could have been attributed to:

- the attack of  $\text{H}^+$  resulting from hydrolysis of heavy metals, supporting the theory of Taylor (1997), and
- the formation of double hydroxides, which consumes calcium ions and facilitates the decomposition of  $\text{C}_3\text{S}$

It should be noted that in the presence of heavy metals the hydration of  $\text{C}_3\text{S}$  or cement does not necessarily result in the precipitation of portlandite, according to this research (see Chapters 4 and 6). In literature, for example, Byfors *et al.* (1986) and Cartledge *et al.* (1990), however, heavy metals were taken as inhibitors of  $\text{C}_3\text{S}$  or cement hydration based on the observation of setting, strength development, portlandite precipitation or heat evolution, which is dependent on the formation of hydration products such as portlandite and ettringite.

$\text{Zn}^{2+}$  retarded the early hydration of  $\text{C}_3\text{S}$ , and this could arise from the formation of  $\text{CaZn}_2(\text{OH})_6.2\text{H}_2\text{O}$  on  $\text{C}_3\text{S}$  surfaces (see the following chemical equations) and prevent material transport that is necessary for hydration to continue. As a result, the pH of suspensions of  $\text{C}_3\text{S}$  and Portland cement doped with  $\text{Zn}^{2+}$  was below 12 and portlandite did precipitate even in 3 months of hydration (see Chapter 4 and Chapter 6).



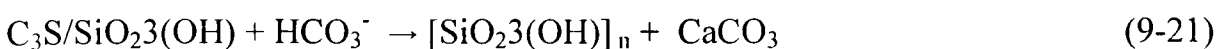
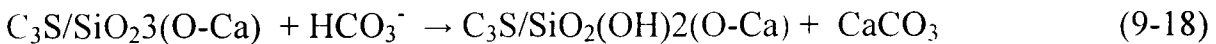
In longer term, pH will reach 12.5 with hydration of cement phases and calcium zincate will dissolve. Consequently, the degree of hydration will increase dramatically.

### 9.2.2 Carbonation of C<sub>3</sub>S

The natural carbonation of C<sub>3</sub>S can be expressed in the following chemical reactions:



The accelerated carbonation of C<sub>3</sub>S can be expressed in the following chemical reactions:



Compared to cement hydration, cement carbonation occurred more rapidly and reaction degree was higher, because the solubility of calcium carbonate is much lower than that of portlandite, which facilitates the dissolution of cement phases in carbonation process of cement.

In the presence of heavy metals (M), the natural carbonation and accelerated carbonation of C<sub>3</sub>S can be expressed as:

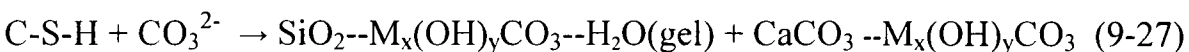
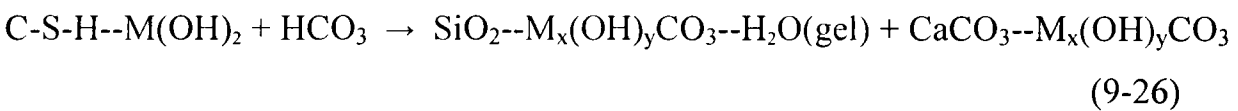
Hydration of heavy metals:



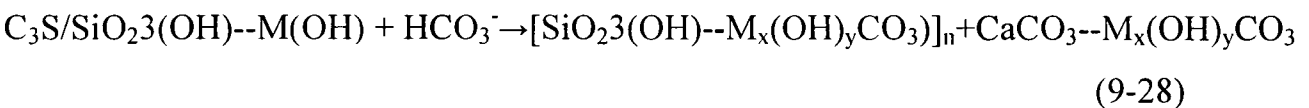
Carbonation of heavy metals:



Natural carbonation of cement:



Accelerated carbonation of cement:



Hydrolysis of heavy metal ions resulted in the reduction of solution pH and promoted the carbonation of C<sub>3</sub>S and Portland cement. In the carbonation processes, heavy metal ions were largely incorporated in calcium carbonate and C-S-H gel (low Ca/Si ratio). Consequently, heavy metals influence the polymorphism and conversion of calcium carbonate as well as the polymerisation of C-S-H gel (see Chapter 4 and Chapter 6).

### 9.3 Heavy metal incorporation in cement matrices

As described earlier, heavy metals affected the reaction rates of cement, the precipitation of portlandite, polymorphism of calcium carbonate, formation of C-A-H phases and polymerisation of C-S-H gel. This indicates that heavy metals co-existed with such phases and influenced their transformations. X-ray diffractometry failed to find heavy metal compounds in the hydrated and carbonated cement pastes directly, because the precipitated heavy metal compounds in hydrated cement pastes are amorphous and very small in size (nanoscale). In the carbonated cement pastes doped with heavy metals, no heavy metal compounds precipitated.

Many factors affect the crystallisation of heavy metal compounds. In cement pastes the saturation indices of heavy metal compounds are very high and the homogeneous or spontaneous nucleation of these compounds occurs very quickly. If heterogeneous nucleation and second nucleation are taken into account in the cement pastes, the nucleation time could be even shorter (Cannell *et al.*, 2000; Salhan *et al.*, 2003). As the nucleation and aggregation of heavy metal compounds occur too quickly and species may not have sufficient mobility or enough time to undergo adequate orientation and alignment before bonding into a highly ordered structure, heavy metal compounds are inclined to form amorphous structures in cement pastes. High temperature or high pressure is needed for the formation of some highly crystalline phases in cement pastes (Mullin, 1972; De Ceukelair and Van Nieuwenburg, 1993).

In order to create a favourable environment for the crystallisation of heavy metal compounds, the suspensions of calcium oxide, calcium hydroxide, C<sub>3</sub>S and Portland cement in the presence of heavy metals over different reaction times were studied. In these suspensions all the species had high mobility and enough time to orientated and align before bonding into ordered structures.

Consequently, in the hydrated heavy metal –doped suspensions of calcium oxide, calcium hydroxide, C<sub>3</sub>S and Portland cement, layered double hydroxides of calcium and copper, chromium or zinc such as Ca<sub>2</sub>Cr(OH)<sub>7</sub>.3H<sub>2</sub>O, Ca<sub>2</sub>(OH)<sub>4</sub>xCu(OH)<sub>2</sub>.mH<sub>2</sub>O and CaZn<sub>2</sub>(OH)<sub>6</sub>.2H<sub>2</sub>O were detected by XRD. In the Cu<sup>2+</sup>, Zn<sup>2+</sup> and Pb<sup>2+</sup> -doped suspensions, Cu(OH)<sub>2</sub>, Zn(OH)<sub>2</sub> and Pb(OH)<sub>2</sub> were also detected.

Based on the above studies, the presence of these double hydroxides as an amorphous structure in the hydrated heavy metal –doped pastes of calcium oxide, calcium hydroxide, C<sub>3</sub>S and Portland cement were confirmed by DTA/TG analyses. In addition, SEM/EDS microanalyses demonstrated that there was a strong correlation between heavy metals and calcium in cement matrices. The uneven distribution of heavy metals associated with calcium also supports that heavy metals formed double hydroxides with calcium. It was noted that these compounds were stable in hydrated cement-based systems during the case of this study.

In the hydrated C<sub>3</sub>A suspensions and pastes doped with heavy metals, no heavy metal compounds were detected. This suggests that C-A-H phases and other products formed in the hydration of C<sub>3</sub>A had stronger capacity for absorbing heavy metal than the hydration products of C<sub>3</sub>S, *i.e.* portlandite and C-S-H gel (Ca/Si around 1.6).

The fixation mechanism of heavy metals in the carbonated cement-based systems was different from that in the hydrated systems. The double hydroxides of calcium and heavy metals, in addition to calcium carbonate, were detected in the early carbonation of calcium oxide or calcium hydroxide suspensions with heavy metals. As time progressed, however, some double hydroxides disappeared. In carbonated suspensions and pastes of C<sub>3</sub>S and Portland cement in the presence of heavy metals, no heavy metal compounds were detected at any age of carbonation.

Heavy metal compounds precipitate on the surface of solid more likely than from bulk solution (James and Healy, 1972; Elliott *et al.*, 1986; Kulik and Kersten, 2001). For example, as shown in Table 9-2, K<sub>sp</sub> of metal hydroxides in bulk solution is less than on the surface of silica (Elliott *et al.*, 1986). According to Hughes (1976), James (1996), Hong and Glasser (2002) and Glasser (1997), calcium carbonate and C-S-H gel have a strong capacity of binding metals. Owing to the high binding capability of fresh calcium carbonate and gel phases (low Ca/Si ratio C-S-H gel and C-S-A-H gel), the heavy metals were completely incorporated in these phases.

In the precipitation of calcium carbonate and C-S-A-H gel, heavy metal ions could be adsorbed on their surfaces and then enter the lattice to form a solid solution, altering the structure (crystallinity, crystal defects, particle size) and solubility of products (Kitamura *et al.*, 2002). As a result, heavy metals influenced the conversion of polymorphs of

calcium carbonate and polymerisation of C-S-H gel. If the amount of heavy metal is sufficient, co-precipitation results in the formation of three-dimensional structures, which usually exist as amorphous forms or intermediate between amorphous and crystalline structures (Kinniburgh *et al.*, 1976; Tamas *et al.*, 1992). This is consistent with Ostwald's rule: the structure with highest entropy develops first and then transforms to more stable crystalline phases successively.

Table 9-2. The solubility products of metal hydroxides on the surface of silica and in bulk solution (after James and Healy, 1972; Elliott *et al.*, 1986)

Metal ions	lg Ksp (in the solution)	lgKsp (on the surface of silica)
Ca <sup>2+</sup>	-5.19	-6.67
Mg <sup>2+</sup>	-11.15	-12.75
Cu <sup>2+</sup>	-19.32	-20.91
Pb <sup>2+</sup>	-15.1	-16.52
Zn <sup>2+</sup>	-16.6	-18.17
Cr <sup>3+</sup>	-29.8	-32.19
Al <sup>3+</sup>	-33.5	-35.97
Fe <sup>3+</sup>	-38.8	-41.2

According to the mineralogy, zinc or magnesium can substitute for calcium in calcite (Deer *et al.*, 1982; Komilis and Hand, 1999; Kulik and Kersten, 2001). It has been shown that almost all of calcium in tobermorite (C<sub>5</sub>S<sub>6</sub>H<sub>5</sub>) and xonotlite (C<sub>6</sub>S<sub>6</sub>H) (natural crystalline phases of calcium silicate hydrate) can be replaced with either cobalt or nickel (Komarneni *et al.*, 1988). Isomorphous replacement by heavy metals in the crystalline lattice of calcium carbonate or portlandite and the amorphous structure of C-S-H gel, therefore, is probable, according to Matsuyama and Yong (2000) and Kirkpatrick *et al.* (1997). If heavy metal ions enter the lattice of portlandite or calcium carbonate, the cell dimensions would be expected to change and result in a shift in the peak positions. It is noted, however, that no observable or minor angular position changes occurred in the X-ray diffraction patterns of portlandite, calcite, aragonite or vaterite. Thus it is inferred that the amount of heavy metals that enter the lattices of these minerals was limited. The sorption of heavy metals on the C-S-H gel and calcium carbonate could be a more important mechanism according to Kwan *et al.* (1996) and Lo *et al.* (2000).

The SEM/EDS microanalyses demonstrated that there was the strong correlation among heavy metals and calcium and silicon of the carbonated cement matrices. This supports that heavy metals examined were incorporated in calcium carbonate and C-S-H gel.

#### ***9.4 Aspects relevant to the practical applications of accelerated carbonation***

Throughout this work, to effect accelerated carbonation, the samples were exposed to CO<sub>2</sub> immediately after mixing with water or heavy metal solutions. The complete carbonation of these samples required 8 sequential cycles of crushing, grinding and exposure to CO<sub>2</sub>. This work also found that carbonation of hydrated cement pastes only required 5 cycles to complete the carbonation, which was much easier than accelerated carbonation of anhydrous cement.

A comparison of hydrated and carbonated cement with heavy metals suggests that the significant advantages of accelerated carbonation cement-based s/s over traditional cement-based s/s could result from:

- The precipitation of fresh calcium carbonate, which incorporates heavy metal ions
- The higher polymerisation of silicate phases and their higher sorption capacity for heavy metal ions due to lower Ca/Si ratio and the presence of aluminium, compared to C-S-H gel produced in the hydration of cement
- Mild pH, which reduces the release of heavy metals
- Carbonation products of cement are more stable than hydration products of cement
- Less deleterious effect of heavy metals on cement carbonation than on cement hydration
- The higher reaction degrees of cement in carbonation than in hydration, using cement clinkers more efficiently.

In practice, accelerated carbonation could be applied in two different modes, in-situ and ex-situ. The former means that the treatments are conducted where the wastes are to be

disposed. The latter means the treatment is carried out away from the site at a designated treatment facility. The degree of carbonation may vary and be very limited due to the control process of CO<sub>2</sub> diffusion and limited contacting time with CO<sub>2</sub> in both in-situ or ex-situ carbonation processes. Thus, any benefits and advantages of carbonation may not be realised (Loo *et al.*, 1994; McWhinney and Cocks, 1993).

Carbonation reduces the pH from around 12.5 to 9, at which many heavy metal compounds have their lowest solubility. This could reduce the release of heavy metals to the environment but also lower the pH buffering capacity of cement when it is attacked by acid, so the carbonation technology has both positive and negative effects and is not suitable for use in acidic environments (Redmond *et al.*, 2002a; 2002b). In addition, according to the present work, over carbonation (pH less than 7) also results in the dissolution of heavy metal compounds and cement matrices and increases the release of heavy metals. The optimum degree of carbonation, therefore, needs to be carefully controlled.

### ***9.5 Major contributions of this work***

This work involves the study of pastes and suspensions of calcium oxide, calcium hydroxide, pure cement phases and Portland cement using a wide range of analytical approaches. It provides further insight into hydration and carbonation of cement as well as encapsulation of heavy metals in cement matrices. The research findings extend knowledge of how accelerated carbonation may influence the release of heavy metals to the environment from waste forms. This work made the following contributions to cement-based solidification/stabilisation and cement chemistry:

- Through an analysis of phase development during hydration and carbonation of cementitious materials in the presence of heavy metals: This work examined the reaction products and their conversions of various systems including suspensions and pastes of calcium oxide, tricalcium silicate, aluminate and Portland cement.
- By a characterisation of C-S-H gel in hydrated and carbonated C<sub>3</sub>S and Portland cement pastes: Based on the detailed examinations of silicates, the structural

models of C-S-H gel and chemical mechanisms on the interactions of  $C_3S$  with heavy metals in both hydration and carbonation processes were put forward.

- Providing a clarification of heavy metal effects on the hydration of cement: Heavy metals such as  $Cu^{2+}$ ,  $Pb^{2+}$  and  $Cr^{3+}$  promoted the hydration of  $C_3S$  and Portland cement, but inhibited the precipitation of portlandite due to hydrolysis. This research revealed that the hydration of cement in the presence of heavy metals resulted in the formation of double hydroxides ( $Ca_2Cr(OH)_7 \cdot 3H_2O$ ,  $Ca_2(OH)_4xCu(OH)_2 \cdot mH_2O$  and  $CaZn_2(OH)_6 \cdot 2H_2O$ ). The chemical mechanism relevant to promoting effect was found to be the precipitation of double hydroxide and  $H^+$  attacks on cement phases.
- By an examination of chemical mechanisms of heavy metal fixation in hydrated and carbonated cement pastes: This work found the hard evidence that most of heavy metal ions were chemically incorporated in C-S-H gel and calcium carbonate in the carbonated cement pastes and co-precipitated with portlandite (double hydroxides) in the hydrated cement pastes.
- Providing the elucidation of the benefits of accelerated carbonation of cement: This work demonstrated that accelerated carbonation of cement in the presence of heavy metals had many advantages over traditional hydration of cement regarding cement-based solidification/stabilisation technology in waste management.
- With thermodynamic modelling: Simple systems were adopted during this study, modelling results are in good agreement with laboratory examinations and are helpful in understanding chemical mechanism occurring in cement systems.

### ***9.6 Recommendations for further work***

The recommendations for further work fall into three separate areas for research and under each the general objectives are outlined:

- Industrial wastes are very complex variable materials and have different ability to influence reactions of cement and the effectiveness of cement-based s/s. Better

understandings of the kinetics of carbonation and an appropriate carbonation degree to achieve the maximum benefits are needed to study for specific wastes. The effects of carbonation on the porosity and permeability of solidified wastes are not known at the present time and require study (Conner and Lear, 1991; Speiser *et al.*, 2000). The long-term effects of carbonation on the release of heavy metals to environments and database for the prediction of heavy metal leaching need further work.

- The retention and immobilisation of organic compound with carbonation of cement could be the subject of the further investigation. Some organic compounds severely inhibit the hydration of cement, for example, sugars (Caldewell and Cote, 1990; Montgomery *et al.*, 1991a; 1991b). As a result, the conventional cement-based s/s is sometimes paralysed in the management of wastes containing organic matter (Soundarajan *et al.*, 1990). Accelerated carbonation could be an effective alternative method for the disposal of waste containing organic matters. The fundamental chemistry of cement carbonation in the presence of organic matters is not clear at the present time and needs to study further (Glasser, 1997).
- According to the characteristics of waste, there is a need to develop the design and diagnostic methods for managing different wastes based on accelerated carbonation of cementitious materials (Tashrio and Oba, 1979; Valls and Vazquez, 2000). The results of this work will have a practical application by enabling process operators to adjust the process parameters.

## Chapter 10

### Conclusions

The overall objective of this research was to investigate the phase development of cement carbonation in the presence of heavy metals, compared with the control samples as well as hydrated analogues. To this end, experimental analysis approaches (XRD, DTA/TG, SEM/EDS and NMR) and thermodynamic modelling with a geochemical code, PHREEQC, were employed to study the crystalline and amorphous phases in a variety of systems designed. The main research findings are summarised as follows:

- Studies into the hydrated pastes and suspensions of C<sub>3</sub>S and Portland cement in the presence of heavy metals revealed that Cr<sup>3+</sup>, Cu<sup>2+</sup> and Pb<sup>2+</sup> accelerated the hydration of C<sub>3</sub>S and Portland cement, whereas Zn<sup>2+</sup> retarded early-age hydration of C<sub>3</sub>S and Portland cement. For one year old pastes, all heavy metals investigated slightly increased the degree of hydration of C<sub>3</sub>S and Portland cement.
- In the hydrated pastes and suspensions of calcium oxide, C<sub>3</sub>S and Portland cement with heavy metals (Cr<sup>3+</sup>, Cu<sup>2+</sup>, Pb<sup>2+</sup> or Zn<sup>2+</sup>), double hydroxides of calcium and heavy metals, Ca<sub>2</sub>Cr(OH)<sub>7</sub>·3H<sub>2</sub>O, Ca<sub>2</sub>(OH)<sub>4</sub>xCu(OH)<sub>2</sub>·mH<sub>2</sub>O and CaZn<sub>2</sub>(OH)<sub>6</sub>·2H<sub>2</sub>O, were detected and characterised by powder X-ray diffraction and DTA/TG techniques.
- At an early hydration period heavy metals showed retarding effect on the precipitation of portlandite due to hydrolysis of heavy metals. The major early-hydration products of C<sub>3</sub>S and Portland cement were C-S-H gel and double hydroxides.
- In the control and Cr<sup>3+</sup>-, Pb<sup>2+</sup>-doped hydrated C<sub>3</sub>S pastes, Q1 species were dominant; whereas in Cu<sup>2+</sup>- and Zn<sup>2+</sup>-doped hydrated C<sub>3</sub>S pastes, Q2 groups were dominant. The lengths of C-S-H in the control and Cr<sup>3+</sup>, Cu<sup>2+</sup>, Pb<sup>2+</sup> and Zn<sup>2+</sup>-doped hydrated pastes of C<sub>3</sub>S were 3.62, 3.66, 5.11, 3.52 and 5.86 respectively. Heavy metals slightly lowered the Ca/Si ratio of C-S-H gel in hydrated C<sub>3</sub>S pastes.

- In all hydrated Portland cement pastes, Q1 species were more than Q2 species, although heavy metals influenced the proportion of species. The lengths of C-S-H in the control and  $\text{Cr}^{3+}$ ,  $\text{Cu}^{2+}$ ,  $\text{Pb}^{2+}$  and  $\text{Zn}^{2+}$  -doped hydrated Portland cement pastes were 3.27, 3.03, 3.79, 3.20 and 3.11, respectively. Heavy metals affected the Ca/Si ratio of C-S-H gel in hydrated Portland cement pastes. The Ca/Si ratios were in the range of 1.53--1.74.
- In the carbonated pastes of  $\text{C}_3\text{S}$  and Portland cement, calcium carbonate including calcite, aragonite and vaterite, and low Ca/Si ratio C-S-H gel were detected. According to NMR results, only Q4 groups and Q3 species existed in carbonated pastes of  $\text{C}_3\text{S}$  and Portland cement. DTA/TG, NMR and SEM/EDS confirmed the presence of very low Ca/Si ratio C-S-H gel (e.g. Ca/Si: 0.07).
- None of heavy metal compounds formed in the carbonated pastes and suspensions of  $\text{C}_3\text{S}$  and Portland cement doped with heavy metals. The polymerisation of C-S-H gel and the polymorphism and decomposition temperature of calcium carbonate were influenced by heavy metals present, indicating that heavy metals were incorporated in these phases.
- Double hydroxides of heavy metal and calcium,  $\text{Ca}_2\text{Cr}(\text{OH})_7 \cdot 3\text{H}_2\text{O}$ ,  $\text{Ca}_2(\text{OH})_4\text{xCu}(\text{OH})_2 \cdot \text{mH}_2\text{O}$  and  $\text{CaZn}_2(\text{OH})_6 \cdot 2\text{H}_2\text{O}$ . and  $\text{PbCO}_3$  were identified in the carbonated suspensions of calcium oxide and calcium hydroxide at the early stage of carbonation. The comparisons of these systems and carbonated suspensions of  $\text{C}_3\text{S}$  and Portland cement as well as the hydrated analogous at the same level of heavy metal contamination indicated that low Ca/Si ratio C-S-H gel had a strong capacity of binding heavy metal. The lower Ca/Si ratio of C-S-H gel, the stronger heavy metal - binding capacity of C-S-H gel.
- In hydrated Portland cement pastes, aluminium existed as ettringite or monocarbonate, but in cement carbonation, aluminate phases were in tetrahedral forms, forming a mixed  $\text{AlO}_4/\text{SiO}_4$  three-dimensional network. The incorporation of aluminium in C-S-H gel created a negative charge imbalance and therefore favoured heavy metal binding to maintain electric neutrality in the matrix.
- In the absence of gypsum the products of  $\text{C}_3\text{A}$  hydration were primarily hydrogarnet, gehlenite hydrate,  $\text{C}_4\text{AH}_x$  and calcium carboaluminate (due to the presence of very

little CO<sub>2</sub>). Heavy metals, especially Zn<sup>2+</sup>, showed the capacity of inhibiting the formation of hydrogarnet. In the presence of gypsum, ettringite was main hydration product of C<sub>3</sub>A.

- In the absence of gypsum, the hydration products of pure cement phases containing aluminium were readily susceptible to carbonation. Carbonation involved conversion of hydrogarnet and other C-A-H phases to calcium monocarboaluminate, tricarboaluminate and calcium carbonate. This transformation process was promoted by heavy metals. In the presence of gypsum, during carbonation process of aluminate CO<sub>3</sub><sup>2-</sup> substituted for SO<sub>4</sub><sup>2-</sup> in ettringite and formed calcium tricarboaluminate, which eventually transformed into calcium carbonate and gibbsite. The conversion of calcium carbonate polymorphs through Ostwald ripening occurred very slowly.
- The reactivity of C<sub>3</sub>A, C<sub>12</sub>A<sub>7</sub>, CA and C<sub>4</sub>AF in carbonation was much lower than in hydration. The higher calcium oxide content of cement phases, the higher reactivity of cement phases. Unlike CA and C<sub>4</sub>AF, the hydration and carbonation of C<sub>3</sub>A or C<sub>12</sub>A<sub>7</sub> increased obviously with time.
- Heavy metals were completely incorporated in the hydrated and carbonated suspensions or pastes of aluminium –bearing pure cement phases. Heavy metals influenced the crystal polymorphism of calcium carbonate and the formation of C-A-H, ettringite and calcium carboaluminates.
- Heavy metals had less effect on the carbonation of C<sub>3</sub>S and Portland cement than on the hydration of C<sub>3</sub>S and Portland cement. This could be one obvious advantage to applying an accelerated carbonation process in waste treatment. The reactivity of C<sub>3</sub>S and Portland cement was greater during carbonation than during hydration. This could be another main advantage of accelerated carbonation, because it can use cement clinker more efficiently than conventional hydration in cement-based s/s.
- The complete carbonation of Portland cement and pure cement phases was difficult to achieve. Using gaseous CO<sub>2</sub>, up to 8 cycles of crushing, grinding and exposure to this gas was required. The carbonation of previously hydrated pastes was much easier, as it took 5 cycles of the above carbonation procedure to effect complete carbonation.
- According to thermodynamic modelling with PHREEQC and LLNL database, heavy metals could form precipitates of hydroxides, sulphate, carbonates, silicates and

---

hydroxyl carbonates in cement-based *s/s* systems. The most likely heavy metal compounds are hydroxides in hydrated cement –based systems. This agrees with experimental examinations in this work.

- The modelling results indicate that carbonation products of cement are less soluble than hydration products of cement. It is predicted that carbonation can reduce the release of some heavy metals to the environment in cement –based *s/s*.
- Compared to calcium oxide or pure cement phase systems, the carbonation products of cement, for example, C-S-A-H gel, demonstrated the stronger capacity of absorbing heavy metals. It is proposed that composite cementitious materials could improve the effectiveness of *s/s* of heavy metal –bearing wastes and contaminated soil.
- Based on the structural models of C-S-H gel put forward in this work, the incorporation of heavy metals in C-S-H gel or C-S-A-H gel or aluminium –bearing silica gel was inferred to be similar to that seen in glass. Heavy metals acted as network modifiers or network intermediates.

## References

- Abderlaxig, B. E. I., Bonner, D. G., Nowell, D. V., Dransfield, J. M. and Egan, P. J. (1999) The solution chemistry and early hydration of OPC pastes with or without admixture. *Therochimica Acta*, 340-341: 417-430.
- Akhter, H., Cartledge, F. K., Roy, A. and Tittlebaum, M. E. (1997) Solidification/stabilisation of arsenic salts: effects of long cure times, *Journal of Hazardous Materials*, 52: 247-264.
- Albino, V., Cioffi, R., Marroccoli, M. and Santoro, L. (1996) Potential application of ettringite generating systems for hazardous waste stabilisation, *Journal of Hazardous Materials*, 51: 241-252.
- Alunno, R.V. and Medici, F. (1995) Immobilisation of toxic metals in cement matrices, *Cement and Concrete Research*, 25: 1147-1152.
- Andersen, M. D., Jakobsen, H. J. and Skibsted, J. (2003) Incorporation of aluminium in the calcium silicate hydrate (C-S-H) of hydrated Portland cements: A high-field  $^{27}\text{Al}$  and  $^{29}\text{Si}$  MAS NMR Investigation, *Inorg. Chem.*, 42 (7): 2280-2287.
- Arafat, H. A. and Hebatpuria, V. M. (1999) Immobilization of phenol in cement-based solidified/stabilized hazardous wastes using regenerated activated carbon: role of carbon, *Journal of Hazardous Materials*, 70(3): 139-156.
- Asavapisit, S., Fowler, G. and Cheeseman, C. R. (1997) Solution chemistry during cement hydration in the presence of metal hydroxide wastes, *Cement and Concrete Research*, 27: 1249-1260.
- Atkins, M. and Bennett, D. G. (1992) A thermodynamic model for blended cements, *Cement and Concrete Research*, 22: 497-502.
- Atkins, M., Glasser, F. P. and Kindness, A. (1992) Cement hydrated phases: solubility at 25°C, *Cement and Concrete Research*, 22: 241-246.

- Atkins, M. and Macphee, A. (1991) Solubility properties of ternary compounds in the CaO-Al<sub>2</sub>O<sub>3</sub>-SO<sub>3</sub>-H<sub>2</sub>O system, *Cement and Concrete Research*, 21: 991-998.
- Banfill, P. F. G. and Saunders, D. C. (1986) The relationship between the sorption of organic-compounds on cement and the retardation of hydration, *Cement and Concrete Research*, 16(3): 399-410.
- Benjamin, M. M. and Leckie, J. O. (1981) Multiple site adsorption of Cd, Zn and Pb on amorphous iron oxyhydroxide, *Journal of Colloid and Interface Science*, 79: 209-221.
- Bennett, D. G. (1992) A thermodynamic model for blended cements, *Journal of Nuclear Materials*, 190: 315-325.
- Berger, P. L., Young J. F. and Leung, K. (1972) Acceleration of hydration of calcium silicates by carbon dioxide treatment, *Nature Physical Science*, 240: 16-18.
- Berger, A. and Banwart, S. A. (2000) Carbon dioxide mediated dissolution of Ca-feldspar: implications for silicate weathering, *Chemical Geology*, 163: 25-42.
- Berner, U. R. (1992) Thermodynamic modelling of cement degradation, *Cement and Concrete Research*, 22: 465-475.
- Biddappa, C. C., Chino, M. and Kumazawa, K. (1981) Adsorption, desorption, potential and selective distribution of heavy metals in selected soils of Japan, *Journal of Environmental Science and Health, part B*, 156: 511-528.
- Boerjesson, S. and Emreen, A. (1998) A program for solubility calculations involving complex solids, *Computer and Geoscience*, 24: 839-846.
- Bonen, D. and Sarkar, S. L. (1995) The effects of simulated environmental attack on immobilisation of heavy metals doped in cement-based materials, *Journal of Hazardous Materials*, 40: 321-335.
- Boynton, R. S. (1980) *The chemistry and technology of lime and limestone*, Wiley Interscience, New York.

- Bozkurt, S., Moreno, L. and Neretnieks, I. (2000) Long term processes in waste deposits, *The Science of Total Environment*, 250: 101-121.
- Brady, N. C. and Weil, R. R. (1996) *The nature and properties of soils*, 11<sup>th</sup> edition, Prentice Hall International, London.
- Breysse, D. and Gerard, B. (1997) Modelling of permeability in cement-based materials: Part 1-uncracked medium, *Cement and Concrete Research*, 27, 5: 761-769.
- Brindle, T. R., Cote, P. L., Constable, T. W. and Fraser, J. L. (1987) Evaluation of heavy metal leachability from solid wastes, *Water Science and Technology*, 19: 1029-1036.
- Brough, A. R., Dobson, C. M. and Richardson, I. G. (1996) Alkali activation of reactive silicas in cements: In situ <sup>29</sup>Si MAS NMR studies of the kinetics of silicate polymerization, *J. Mater Sci.*, 31 (13): 3365-3373.
- Bukowski, J. M. and Berger, R. L. (1979) Reactivity and strength development of CO<sub>2</sub> activated non-hydraulic calcium silicates, *Cement and Concrete Research*, 9(1): 57-68.
- Byfors, K., Hansson, C. M. and Tritthart, J. (1986) Pore solution expression as a method to determine the influence of mineral additives on chloride binding, *Cement and Concrete Research*, 16(5): 760-770.
- Caldewell, R. J. and Cote, P. L. (1990) Investigation of solidification for the immobilization of trace organic contaminants, *Hazardous Waste & Hazardous Materials* 7(3): 273-282.
- Cannell, B. S., Eghmy, T. T., Krzow, J. E., Eusden, J. D., Show, E. L. and Francis, C. A. (2000) Heavy metal stabilisation in municipal solid waste combustion bottom ash using soluble phosphate, *Waste Management*, 20: 135-148.
- Cartledge, F. K., Butler, L. D., Chaslani, D., Eaton, H. C., Frey, F. P., Herrera, E., Tittlebaum, M. E. and Yang, S. L. (1990) Immobilisation mechanisms in stabilisation/solidification of Cd and Pb salts using Portland cement fixing agents, *Environmental Science and Technology*, 24: 867 –873.

- Chandra, S. (1997) 10<sup>th</sup> international congress on the cement chemistry of cement, *Cement and Concrete Research*, 27: 1613-1617.
- Cheeseman, C. R., Butcher, E. J., Sollars, C. J. and Perry, R. (1993) Heavy metal leaching from hydroxide, sulfide and silicate stabilised/solidified wastes, *Waste Management*, 13: 545-552.
- Chen, W. W. J. and Wu, C. M. L. (2000) Durability of concrete with high cement replacement, *Cement and Concrete Research*, 30: 865-879.
- Cheng, K.Y. and Bishop, P. L. (1992) Sorption, Important in stabilised/solidified waste forms, *Hazardous Waste and Hazardous Materials*, 9: 289-296.
- Chimenos, J. M., Fernandez, A. I., Nadal, R. and Espiell, F. (2000) Short-term natural weathering of MSWI bottom ash, *Journal of Hazardous Materials*, B79: 287-299.
- Clark, B. A. and Brown, P. W. (1999) Phases formed from the hydration of tetracalcium aluminoferrite and magnesium sulfate, *Adv. Cem. Res.*, 11 (3): 133-137.
- Cocke, D. L., Ortego, J. D., McWhinney, H., Lee, K. and Shukla, S. A. (1989) A model for lead retardation of cement setting. *Cement and Concrete Research*, 19: 156-159.
- Cong, X. D. and Kirkpatrick, R. J. (1996) <sup>29</sup>Si MAS NMR study of the structure of calcium silicate hydrate, *Adv. Cem. Based Mater.*, 3 (3-4): 144-156.
- Conner, J. R. (1990) *Chemical fixation and solidification of hazardous waste*, Van Nostrand Reinhold, New York.
- Conner, J. R. and Hoeffner, S. L. (1998) The history of stabilisation/solidification technology, *Critical reviews in Environmental Science and Technology*, 28: 325-396.
- Conner, J. R. and Lear, P. R. (1991) Immobilisation of low level organic compounds in hazardous waste, *Proc. Air and Waste Management*, 84<sup>th</sup> Annual Meeting, Vancouver, BC.

- Cross, J. E., Ewart, F. T. and Tweed, C. J. (1987, Revised 1991) Thermodynamic modelling with application to nuclear waste processing and disposal, HATCHES (HARwell/nirex Thermodynamic database for CHEMical Equilibrium Studies).
- Cullity, B. D. (1978) Elements of X-ray diffraction, Addison Wesley Publishing Company, Reading.
- Damidot, D. and Glasser, F. P. (1992) Thermodynamic investigation of CaO-Al<sub>2</sub>O<sub>3</sub> system at 50°C, Cement and Concrete Research, 22: 1179-1191.
- Damidot, D. and Glasser, F. P. (1993a) Thermodynamic investigation of the CaO-Al<sub>2</sub>O<sub>3</sub>-CaSO<sub>4</sub>-H<sub>2</sub>O system at 25°C and the influence of Na<sub>2</sub>O, Cement and Concrete Research, 23: 221-238.
- Damidot, D. and Glasser, F. P. (1993b) Thermodynamic investigation of the CaO-Al<sub>2</sub>O<sub>3</sub>-CaSO<sub>4</sub>-K<sub>2</sub>O-H<sub>2</sub>O system at 25°C and the influence of Na<sub>2</sub>O, Cement and Concrete Research, 23: 1195-1204.
- Damidot, D., Stronach, S., Kindness, A., Atkins, M. and Glasser, F. P. (1994) Thermodynamic investigation of the CaO-Al<sub>2</sub>O<sub>3</sub>-CaCO<sub>3</sub>-H<sub>2</sub>O closed system at 25°C and the influence of Na<sub>2</sub>O, Cement and Concrete Research, 24: 563-572.
- Damidot, D. and Glasser, F. P. (1995) Investigation of the CaO-Al<sub>2</sub>O<sub>3</sub>-SiO<sub>2</sub>-H<sub>2</sub>O system at 25°C by thermodynamic calculations. Cement and Concrete Research, 25: 22-28.
- De Ceukelaire, L. and Van Nieuwenburg, D. (1993) Accelerated carbonation of blast-furnace cement concrete, Cement and Concrete Research, 23: 442-452.
- Deer W. A., Howie, R. A. and Zussman, J. (1982) An introduction to the rock forming minerals, Longman Group Limited, London.
- Dias, W. P. S. (2000) Reduction of concrete sorptivity with age through carbonation, Cement and Concrete Research, 30: 1255-1261.
- Dweck, O. and Buchler, P. M. (2000) Hydration of Portland cement blended with calcium carbonate, Thermochemica Acta, 346: 105-113.

- Dweck, J., Buchler, P. M. and Kartledge, F. K. (2001) The Effect of bentonites on cement hydration during solidification/stabilisation of tannery wastes, *Journal of Thermal Analysis and Calorimetry*, 64: 1011-1016.
- Dweck, J., da Silva, P. E. F. and Aderne R. S. (2003) Evaluating cement hydration by non-conventional DTA - An application to waste solidification, *J Therm. Anal. Calorim.*, 71 (3): 821-827.
- Elliott, H. A., Liberati, M. R. and Huang, C.P. (1986) Competitive adsorption of heavy metals by soils, *Journal of Environmental Quality*, 15: 214-219.
- Engelhardt, G. and Michel, D. (1987) High resolution solid state NMR of silicates and zeolites, John Wiley & Sons, Chichester.
- Environmental data services Ltd., (2003) Directory 2003, 10<sup>th</sup> edition, London.
- Escalante-Garcia, J. I. and Sharp, J. H. (1998a) Effect of temperature on the hydration of the main clinker phases in Portland cements: Part I, neat cements, *Cement and Concrete Research*, 28 (9): 1245-1257.
- Escalante-Garcia, J. I. and Sharp, J. H. (1998b) Effect of temperature on the hydration of the main clinker phases in Portland cements: Part II, blended cements, *Cement and Concrete Research*, 28 (9): 1259-1274.
- Escalante-Garcia, J. I., Mendoza, G. and Sharp, J. H. (1999) Indirect determination of the Ca/Si ratio of the C-S-H gel in Portland cements, *Cement and Concrete Research*, 29 (12): 1999-2003.
- Escalante-Garcia, J. I. and Sharp, J. H. (1999) Variation in the composition of C-S-H gel in Portland cement pastes cured at various temperatures, *Journal of the American Ceramic Society*, 82 (11): 3237-3241.
- Famy, C. Taylor, H. F. W. (2001) Ettringite in hydration of Portland cement concrete and its occurrence in mature concretes, *Mater. J.*, 98 (4): 350-356.

- Famy, C. Scrivener, K. L. and Crumbie, A. K. (2002a) What causes differences of C-S-H gel grey levels in backscattered electron images?, *Cement and Concrete Research*, 32 (9): 1465-1471.
- Famy, C., Scrivener, K. L. and Atkinson, A. (2002b) Effects of an early or a late heat treatment on the microstructure and composition of inner C-S-H products of Portland cement mortars, *Cement and Concrete Research*, 32 (2): 269-278.
- Faucon, P., Delaye, J. M., Virlet, J., *et al.*, (1997) Study of the structural properties of the C-S-H(I) by molecular dynamics simulation, *Cement and Concrete Research*, 27 (10): 1581-1590.
- Frey, H. C., Herrera, E., Tittlebaum, M. E. and Yang, S. L. (1990) Immobilisation mechanisms in solidification/stabilisation of Cd and Pb salts using Portland cement, *Environmental Science and Technology*, 24: 867-873.
- Gatty, L., Bonnamy, S., Feylessoufi, A., *et al.*, (2001) A transmission electron microscopy study of interfaces and matrix homogeneity in ultra-high-performance cement-based materials, *J Mater. Sci.*, 36 (16): 4013-4026.
- Giles, D. E., Ritchie, I. M. and Xu, B. A. (1993) The kinetics of dissolution of slaked lime, *Hydrometallurgy*, 32: 119-1228.
- Glasser F. P. (1992) Application of cements to the treatment and conditioning of toxic wastes, In: *Proceedings of 9<sup>th</sup> International Congress on the Chemistry of Cement*, Dehli, India.
- Glasser F. P. (1997) Fundamental aspect of cement solidification and stabilisation, *Journal of Hazardous Material*, 52: 151-170.
- Glasser F. P., Kindness, A. and Stronach, S. A. (1999) Stability and solubility relationships in AFm phases, *Cement and Concrete Research*, 29: 861-866.
- Glasson, D. R. (1961) Reactivity of lime and related oxides: crystal changes in hydrated lime at different temperature, *J. Appl. Chem.*, 11: 24-27.

- Goodbrake, C. J., Young, J. F. and Berger, R. L. (1979) Reaction of C<sub>2</sub>S and C<sub>3</sub>S with CO<sub>2</sub> and water vapour, *Journal of the American Ceramic Society*, 62(3-4): 168-171.
- Goto, S., Suenaga, K. and Kado, T. (1995) Calcium silicate carbonation products, *Journal of the American Ceramic Society*, 78(11): 2867-2872.
- Gougar, M. L. D., Scheetz, B. E. and Roy, D. M. (1996) Ettringite and C-S-H Portland cement phases for waste ion immobilization: A review, *Waste Management*, 16 (4): 295-303.
- Griffin, R. A. and Shimp, N. F. (1976) Effect of pH on exchange-adsorption or precipitation of lead from landfill leachates by clay minerals, *Environmental Science and Technology*, 10 (13): 1256-1261.
- Grutzeck, M. W., Kwan, S., Thompson, J. L., *et al.* (1999) A sorosilicate model for calcium silicate hydrate (C-S-H), *J. Mater. Sci. Lett.*, 18 (3): 217-220.
- Harris, A. W., Manning, M. C., Tearle, W. M. and Tweed, C. J. (2002) Testing models of the dissolution of cements and leaching of synthetic C-S-H gels, *Cement and Concrete Research*, 32: 731-746.
- Harrison, R. M. and de Mora, F. (1996) *Introductory chemistry for the environmental sciences*, Cambridge University Press, Cambridge.
- Hebatpuria, V. A. and Arafat, H. A. (1999a) Leaching behaviour of selected aromatics in cement-based solidification/stabilization under different leaching tests, *Environmental Engineering Science*, 16(6): 451-463.
- Hebatpuria, V. A. and Arafat, H. A. (1999b) Immobilization of phenol in cement-based solidified/stabilized hazardous wastes using regenerated activated carbon: leaching studies, *Journal of Hazardous Materials* 70(3): 117-138.
- Hill, J. and Sharp, J. H. (2002) The mineralogy and microstructure of three composite cements with high replacement levels, *Cement and Concrete composite*, 24 (2): 191-199.

- Hills, C. D. (1992) The hydration of ordinary Portland cement during cement-based solidification of toxic wastes, PhD thesis, University of London.
- Hills, C. D., Sollars, C. J. and Perry, R. (1994) A calorimetric and micro-structural study of solidified toxic wastes - Part 2: A model for poisoning of OPC hydration, *Waste Management*, 14(7): 601-612.
- Hills, C. D. and Sollars, C. J. (1995) A calorimetric study of the effect of organic-compounds on the initial behaviour of cement-based solidified wastes, *Waste Management & Research*, 13(1): 21-36.
- Hills, C. D. and Pollard, S. J. T. (1997) The influence of interference effects on the mechanical, microstructural and fixation characteristics of cement-solidified waste forms, *Journal of Hazardous Materials*, 52: 171-191.
- Hills, C. D., Jones, H. M., Bone, B., Carey, P. J., Barnard, L. H., Boardman, D. I., and Macleod, C. L. (2003) Validation of Remedial Performance of Stabilisation/Solidification, Draft Report for the Environment Agency (II).
- Holt, C. C. and Freer-hewish, R. J. (1996) Lime treatment of capping layers in accordance with the current specification for highway works, In: Rogers, C. D. F.(Ed), *Lime stabilisation*, Thomas Telford, London, 51-61.
- Hong, S. Y. and Glasser, F. P. (2002) Alkali sorption by C-S-H and C-A-S-H gels - Part II. Role of alumina, *Cement and Concrete Research*, 32 (7): 1101-1111.
- Hudales, J. M. B. (1994) The Use of M.I.W fly ash in asphalt for road construction in: Goumans, J., Van der Sloot, H. A., Aalbers T. G. (Eds.) *Environmental aspects of construction with waste materials*, Elsevier Science, 227-232.
- Hughes. F. (1976) Attenuation of pollutants in municipal landfill leachate by passage through clay, *Environmental Science and Technology*, 10 (13): 1262-1267.
- Iler, R. K., (1982) *The chemistry of silica*, A Wiley-Interscience Publication, John Wiley & Sons, New York.

- Isenburg, J. and Moore, M. (1992) Generalized acid neutralization capacity test, stabilisation and solidification of hazardous, radioactive, and mixed waste, 2nd Volume, T. M. Gilliam and C. C. Wiles, (Eds.) American Society for Testing and Materials, Philadelphia, 361-377.
- Isoo, T., Takahashi, I. T., Okamoto, N. and Fukuhara, M. (2000) Development of large steelmaking slag blocks using a new carbonation process, *Advances in Cement Research*, 12(3): 97-101.
- Ivey, D. B., Heinmann, R. B., Neuwirth, M., Shumborski, D., Mikula, R. J. and Lam, W.W. (1990) Electron microscopy of heavy metal waste in cement matrices, *Journal Materials Science Letters*, 25: 5055-5062.
- James, B. R. (1996) The challenge of remediating chromium-contaminated soil, *Environ. Sci. Technol*, 30: 248A-251A.
- James, R. O and Healy, T. W . J. (1972) Adsorption and precipitation of metals on the surface of silica, *Colloid Inter. Sci.*, 40: 42-52.
- Jawed, I., Skalnery, J. and Yong, J. F. (1983) *Structure and performance of concretes*, Applied Science Publishers, London.
- Jeffrey, J. (1996) Effect of carbonation on the nitrogen BET surface area of hardened Portland cement paste, *Advn. Cem. Based Mat.*, 3: 76-80.
- Jennings, H. M., Dalgeish, B. J. and Pratt, P. L. (1981) Morphological development of hydrates of tricalcium silicate as examined by electron microscopic techniques, *Journal of American Ceramic Society*, 64: 567-571.
- Jennings, H. M. and Pratt, P. L. (1978) On the hydration of Portland cement, *Proc. British Ceramic Society*: 28-32.
- Jennings, H. M. (2000) A model for the microstructure of calcium silicate hydrate in cement paste, *Cement and Concrete Research*, 30 (1): 101-116.
- Johannesson, B. and Utgenannt, P. (2001) Microstructural changes caused by carbonation of cement mortar, *Cement and Concrete Research*, 31: 925-931.

- Johnson, D. C., Macleod, C. L. and Hills, C. D, (2001) Comparison of the accelerated carbonation of slag, deinking ash and Portland cement, Centre for contaminated land remediation, the University of Greenwich, Chatham Maritime.
- Juenger, M. C. G. and Jennings, H. M. (2001) The use of nitrogen adsorption to assess the microstructure of cement paste, *Cement and Concrete Research*, 31 (6): 883-892.
- Jun, K. S., Shin, H. S. and Paik, B. C. (1997) Microstructural analysis of OPC/silica fume/Na-bentonite interactions in cement based solidification or organic contaminated hazardous waste, *Journal of Environmental Science and Health*, A32 (4): 913-928.
- Kang, S. H., Lee, S. G., Jung, W. M. *et al.*, (2003) Effect of Taylor vortices on calcium carbonate crystallisation by gas-liquid reaction, *Journal of Crystal Growth*, 254: 196-205.
- Kantro, D. L. (1975) Tricalcium silicate hydration in the presence of various salts, *Journal of Testing and Evaluation*, 3: 312-321.
- Kiellsen, K. O. (1996) Heat curing and post-heat curing regimes of high-performance concrete: Influence on microstructure and C-S-H composition, *Cement and Concrete Research*, 26 (2): 295-307.
- Kinniburgh, D. G., Jackson, M. L. and Syers, J. K. (1976) Adsorption of alkaline earth, transition and heavy metal cations by hydrous oxide gels of iron and aluminium, *Journal of the Soil Science Society of America*, 40: 796-799.
- Kirkpatrick, R. J., Yarger, J. L., McMillan, P. F., *et al.* (1997) Raman spectroscopy of C-S-H, tobermorite, and jennite, *Adv. Cem. Based Mater.*, 5 (3-4): 93-99.
- Kitamura, M., Konno, H., Yasui, A. and Masuoka, H. (2002) Controlling factors and mechanism of reactive crystallisation of calcium carbonate polymorphs from calcium hydroxide suspensions, *Journal of Crystal Growth*, 236: 323-332.

- Klich, I, Batchelor, B., Wilding, L. P. and Drees, L. R. (1990) Mineralogical alterations that affect the durability and metals containment of aged solidified and stabilized wastes, *Cement and Concrete Research*, 29: 1433-1440.
- Klich, I., Wilding, L.P. Drees, L.R. and Landa, E.R. (1999) Importance of microscopy in durability studies of solidified and stabilized contaminated soils, *Soil Science Society of America Journal*, 63: 1274-1283.
- Komarneni, S. Breval, E. and Roy, R. (1988) Reactions of some calcium silicates with metal cations, *Cement and Concrete Research*, 18: 204-220.
- Komilis, D. P. and Han, R. K. (1999) The effect of MSW pre-treatment on landfill behaviour, *Waste Manage Res.*, 17: 10-19.
- Kulik, D. A. and Kersten, M. (2001) Aqueous solubility diagrams for cementitious waste stabilization systems: II, end-member stoichiometries of ideal calcium silicate hydrate solid solutions, *Journal of the American Ceramic Society*, 84 (12): 3017-3026.
- Kwan, S., Thompson, J. and Grutzeck, M. W. (1996) Structures and phase relations of aluminum-substituted calcium silicate hydrate, *Journal of the American Ceramic Society*, 79 (4): 967-971.
- Lange, L. C., Hills, C. D. and Poole, A. B. (1996) The effect of accelerated carbonation on the properties of cement solidified waste forms, *Waste Management*, 16: 757-763.
- Lea, F. M. (1970) *The chemistry of cement and concrete*, Edwards Arnold, London.
- Li, X. D., Poon C. S., Sun, H., Lo, I. M. C. and Kirk, D. W. (2001) Heavy metal speciation and leaching behaviour in cement based solidified/stabilized waste materials, *Journal of Hazardous Materials*, A82: 215-230.
- Lin, T. T., Lin, C. F., Wei, W. C. and Lo, S. I. (1993) Mechanisms of metal stabilisation in cementitious matrices: Interactions of tricalcium aluminate and copper oxide/hydroxide, *Environmental Science and Technology*, 28: 1312-1318.

- Lin, C. K., Chen, J. N. and Li, C. C. (1997) NMR, XRD and EDS study of solidification/stabilisation of chromium with Portland cement and  $C_3S$ , *Journal of Hazardous Materials*, 56: 21-34.
- Lippmaa, E., Magi, M., Samoson, A., Engelhardt, G and Grimmer, A. R. (1980) Structural studies of silicates by solid-state high resolution  $^{29}Si$  NMR, *J. Am Chem. Soc.*, 102: 4889-4893.
- Lippmaa, E., Magi, M. and Tarmak, M. (1982) A high resolution  $^{29}Si$  NMR study of the hydration of tricalcium silicate, *Cement and Concrete Research*, 12: 597-602.
- Lo, I. M. C. (1996) Solidification/stabilization of phenolic waste using organic-clay complex. *Journal of Environmental Engineering*, 27: 850-855.
- Lo, I. M. C., Tang, S. I., Li, K. D. and Poon, C. S. (2000) Leaching and microstructural analysis of cement-based solid waste, *Environmental Science and Technology*, 34: 5038-5042.
- Loo, Y. H., Chin, M. S., Tam, C. T. and Ong, K. C. G. (1994) A carbonation prediction model for accelerated carbonation testing of concrete, *Magazine of Concrete Research*, 46: 191-200.
- Macias, A. (1997) Impact of carbon dioxide on the immobilisation of cement waste chromium, *Cement and Concrete Research*, 27: 215-225.
- Maries, A. (1992) Utilisation of carbon dioxide in concrete construction, *Proceedings of Sustainable Development of the Cement and Concrete Industry*, Ottawa.
- Macphee, D. E., Luke, K., Glasser, F. P. and Lachowski, E. E. (1989) Solubility and ageing of calcium silicate hydrates in alkaline solution at 25°C, *Journal of the American Ceramic Society*, 72 (4): 646-654.
- Malmstrom, M. E., Destouni, G., Banwart, S. A. and Stromberg, B. H. E. (2000) Resolving the scale-dependence of mineral weathering rates, *Environmental Science and Technaolgy*, 34 (7): 1375-1378.

- Matsuyama, H. and Young, J. F. (2000) Effects of pH on precipitation of quasi-crystalline calcium silicate hydrate in aqueous solution, *Adv Cem. Res.*, 12 (1): 29-33.
- McConnell, J. D. C. (1955) The Hydration of larnite ( $\beta$ -Ca<sub>2</sub>SiO<sub>4</sub>) and bredigite ( $\alpha$ -Ca<sub>2</sub>SiO<sub>4</sub>) and the properties of the resulting gelatinous plombierite, *Mineral Magazine*, 30: 672-680.
- McWhinney, H. G., Cocke, D. L., Balke, K. and Ortego, J. D. (1990a) An investigation of mercury solidification and stabilisation in Portland cement using X-ray photoelectron spectroscopy and energy dispersive spectroscopy, *Cement and Concrete Research*, 20: 79-91.
- McWhinney, H. G., Rowe, M. W., Cocke, D. L., Ortego, J. D. and Yu, G. S. (1990b) X-ray photoelectron and FTIR spectroscopic investigation of cement doped with barium nitrate, *Journal of Environmental Science and Health*, A25: 463-477.
- McWhinney, H. G. and Cocke, D. L. (1993) A surface study of the chemistry of zinc, cadmium and mercury in Portland cement, *Waste Management*, 13: 117-123.
- McKinley, J. D., Thomas, H. R., Williams, K. P. and Reid, J. M. (2001) Chemical analysis of contaminated soil strengthened by the addition of lime, *Engineering Geology*, 60: 181-192.
- Meima, J. A. and Comans, R. N. J. (1997) Geochemical modelling of weathering reactions in municipal solid waste incinerator bottom ash, *Environmental Science and Technology*, 31(5): 1269-1276.
- Mollah, Y. M., Vempati, R. K., Lin, T. C. and Cocke, D. L. (1995) The interfacial chemistry of solidification/stabilisation of metals in cement and pozzolanic material systems, *Waste Management*, 15: 137-148.
- Mollah, M. Y., Lu, F. and Cocke, D. L. (1998) An X-ray diffraction (XRD) and Fourier transform infrared spectroscopic (FT-IR) characterisation of speciation of arsenic (V) in Portland cement type-V. *The Science of the Total Environment*, 224: 57-68.

- Montgomery, D. M., Sollars, C. J. and Perry, R. (1988) Cement-based solidification for the safe disposal of heavy metal contaminated sewage sludge, *Waste Management and Research*, 6: 217-226.
- Montgomery, D. M., Sollars, C. J. and Perry, R. (1991a) Optimization of cement-based stabilization/solidification of organic-containing industrial wastes using organophilic clays, *Waste Management and Research*, 9: 21-34.
- Montgomery, D. M., Sollars, C. J. and Perry, R. (1991b) Treatment of organic-contaminated industrial wastes using cement-based s/s, *Waste Management and Research*, 9: 103-111.
- Moore, A. E. and Taylor, H. F. W. (1968) Crystal structure of ettringite, *Nature*, 218: 1048-1049.
- Moore, A. E. and Taylor, H. F. W. (1970) Crystal structure of ettringite, *Acta Cryst*, B26: 386-393.
- Morse, J. W., and Mackenzie, F. T. (1990) *Geochemistry of sedimentary carbonates*, Elsevier, Amsterdam.
- Mullin, J. W. (1972) *Crystallisation*, Butterworth & Co. Ltd, London.
- Murat, M. and Sorrentino, F. (1996) Effect of large addition of Cd, Pb, Cr, Zn to cement raw meal on the composition and the properties of the clinker and the cement, *Cement and Concrete Research*, 26: 377-385.
- Neville, P. (1995) *Properties of concrete*, Longman, Edinburgh.
- Ngala, V. T. and Page, C. L. (1997) Effects of carbonation on pore structure and diffusion properties of hydrated cement pastes, *Cement and Concrete Research*, 27: 995-1007.
- NocunWczelik, W. (1997) Effect of some inorganic admixtures on the formation and properties of calcium silicate hydrates produced in hydrothermal conditions, *Cement and Concrete Research*, 27 (1): 83-92.

- Nonat, A. (1997) Physico-chemical parameters determine hydration and particle interactions during the setting of silicate cements, *Solid State Ionic*, 101-103: 923-930
- Nugent, M. A., Brantley, S. L., Pantano, C. G., and Maurice, P. A. (1998) The influence of natural mineral coatings on feldspar weathering, *Nature*, 395: 588-591.
- Oates, J. A. H. and Joseph, A. H. (1998) *Lime and limestone: chemistry and technology, production and uses*. Weinheim. Chichester.
- Omotoso, O. E., Ivey, D. G. and Mikula, R. (1998) Hexavalent chromium in tricalcium silicate - Part II Effects of Cr-VI on the hydration of tricalcium silicate, *J. Mater Sci.*, 33 (2): 515-522.
- Ortego, J. D., Jackson, S., Yu, G. S., McWhinney, H. G. and Cocke, D. L. (1989) Solidification of hazardous substances – a TGA and FTIR study of Portland cement containing metal nitrates, *Journal of Environmental Science and Health*, A24: 589-602.
- Ortego, J. D. and Barroeta, Y. (1991) Leaching effects on silicate polymerisation, *Environ. Sci. Technol.*, 25: 1171-1174.
- Osborne, G. J. (1999) Durability of Portland blast-furnace slag cement concrete, *Cement and Concrete Composites*, 21: 11-21.
- Papadakis, V. G., Vayenas, C. G. and Fardis, M. N. (1989) A reaction engineering approach to the problem of concrete carbonation, *Journal of the American Institute of Chemical Engineers*, 35 (10): 1639-1650.
- Papadakis, V. G., Vayenas, C. G. and Fardis, M. N. (1991) Fundamental modelling and experimental investigation of concrete carbonation, *Materials Journal*, 88 (4): 363-373.
- Park, J. Y. and Batchelor, B. (1999) Prediction of chemical speciation in stabilised/solidified wastes using a general chemical equilibrium model: Part 1 chemical representation of cementitious binders, *Cement and Concrete Research*, 29: 361-368.

- Parkhurst, D. L., Thorstenson, D. C. and Plummer, L. N., (1980) PHREEQE- a computer program for geochemical calculations, U.S. Geological Survey, Dever.
- Parkhurst, D. L. and Appelo, C. A. J. (1999) PHREEQC2, a computer program for speciation, batch reaction, one dimensional transport, and inverse geochemical calculation, US Geological Survey, Dever.
- Parkhurst, D. L. and Appelo, C. A. J. (2001) User's guide to PHREEQC, US Geological Survey, Dever.
- Perkins, D. (1998) Mineralogy, Prentice-Hall Inc., New Jersey.
- Phair, J. W., van Deventer J. S. J. and J. D. Smith, (2004) Effect of Al source and alkali activation on Pb and Cu immobilisation in fly-ash based "geopolymers". Applied Geochemistry, 19: 423-434.
- Poellmann, H., Kuzel, St. A., Kuzel, H. J. and Wenda, R. (1993) Solid solution in ettringites, Part II: incorporation of  $B(OH)_4^-$  and  $Cr_2O_4^{2-}$  in  $CaO.Al_2O_3.3CaSO_4.32H_2O$ , Cement and Concrete Research, 23: 422-430.
- Poon, C. S., Peters, D. J., Perry, R., Barnes, P. and Barker, A. P. (1985) Mechanisms of metal stabilisation in cement based fixation processes. Science of the Total Environment, 41: 55-63.
- Poon, C. S., Clark, A. I. and Perry, R. (1986) Permeability study of the cement based solidification process for the disposal of hazardous wastes, Cement and Concrete Research, 16: 161-172.
- Price, D. G. (1995) Weathering and weathering processes. Quarterly Journal of Engineering Geology, 28: 243-252.
- Puls, R. W. and Bohn, H. L. (1988) Sorption of cadmium, nickel, and zinc by kaolinite and montmorillonite suspensions, Journal of the Soil Science Society of America, 52: 1289-1292.



- Redmond, S., Pimienta, P. and Bentz, D. P. (2002a) Effects of incorporation of municipal solid waste incineration fly ash in cement pastes and mortars: experimental study, *Cement and Concrete Research*, 32: 301-311.
- Redmond, S., Pimienta, P. and Bentz, D. P. (2002b) Effects of incorporation of municipal solid waste incineration fly Ash in cement pastes and mortars: modelling, *Cement and Concrete Research*, 32: 565-576.
- Richardson, I. G. and Groves, G. W. (1993) The incorporation of minor trace elements into calcium silicate hydrate gel in hardened cement pastes, *Cement and Concrete Research*, 23: 131-138.
- Richardson, I. G. and Groves, G. W. (1997) The structure of the calcium silicate hydrate phases present in hardened pastes of white Portland cement blast-furnace slag blends, *J. Mater. Sci.*, 32 (18): 4793-4802.
- Richardson, I. G. (1999) The nature of C-S-H in hardened cements, *Cement and Concrete Research*, 29 (8): 1131-1147.
- Richardson, I. G. (2000) The nature of the hydration products in hardened cement pastes, *Cement Concrete Composite*, 22 (2): 97-113.
- Richardson, J. M., Biernacki, J. J., Stutzman, P. E., *et al.*, (2002) Stoichiometry of slag hydration with calcium hydroxide, *Journal of the American Ceramic Society*, 85 (4): 947-953.
- Rinehart, T. L., Sculze, D. G., Bricka, R. M., Bajt, S. and Blatchley, E. R. (1997) Chromium leaching vs. oxidation state for a contaminated solidified/stabilised soil. *Journal of Hazardous Materials*, 52: 213-221.
- Ritchie, I. M. and Xu, B. A. (1990) The kinetics of lime slaking, *Hydrometallurgy*, 32: 119-128.
- Rixom, M. R. and Mailvaganam, N. P. (1986) *Chemical admixtures for concrete*, 2<sup>nd</sup> ed, E and F. N. Spon, London.

- Rogers, D. E. and Aldridge, L. P. (1977) Hydrates of calcium ferrite and calcium aluminoferrites, *Cement and Concrete Research*, 7: 399-410.
- Roy, S. K., Poh, K. B. and Northwood, D. O. (1999) Durability of concrete – accelerated carbonation and weathering studies, *Building and Environment*, 34: 597-606.
- Saetta, A. V., Schrefler, B. A. and Vitaliani, R. V. (1993) The carbonation of concrete and the mechanism of moisture, heat and carbon dioxide flow through porous materials, *Cement and Concrete Research*, 23: 761-772.
- Saetta, A. V., Schrefler, B. A. and Vitaliani, R. V. (1995) 2-D model for carbonation and moisture/heat flow in porous materials, *Cement and Concrete Research*, 25 (8): 1703-1712.
- Salhan, A., Billingham, J. and King, A. C. (2003) The effect of a retarder on the early stages of the hydration of tricalcium silicate, *J Eng. Math.*, 45 (3-4): 367-377.
- Sauman, Z. (1971) Carbonization of porous concrete and its main binding components, *Cement and Concrete Research*, 1: 645-662.
- Scrivener, K. L., Damidot, D. and Famy, C. (1999) Possible mechanisms of expansion of concrete exposed to elevated temperatures during curing (also known as DEF) and implications for avoidance of field problems, *Cement and Concrete Aggregate*, 21 (1): 93-101.
- Sersale, R. (1983) Aspects of the chemistry of additions, In: *Advance in cement technology*, (Ed) Ghosh, S. N., Pergamon, Oxford.
- Shimaoka, T. and Hanashima, M. (1996) Behaviour of stabilized fly ashes in solid waste landfills, *Waste Management*, 16: 545-554.
- Skalny, J. and Young, J. F. (1980) Mechanisms of Portland cement hydration, *Proc. 7<sup>th</sup> Int. Cong. Chem. Cem.*, 2: 113-119, Paris.
- Slegers, P. and Rouxhet, P. (1976) Carbonation of hydration products of tricalcium silicate, *Cement and Concrete Research*, 6: 381-388.

- Smith, R. W., Gutierrez, N. and Tarquin, A. (1997) Role of carbonation in the transient leaching of cementitious waste forms, *Environmental Science and Technology*, 31: 2345-2349.
- Soundarajan, R., Barth, E. F. and Gibbones, J. J. (1990) Using an organophilic clay to chemically stabilize waste containing organic compounds, *Hazard. Mater. Control*, 3: 42-45.
- Speiser, C., Baumann, T. and Niessner, R. (2000) Morphological and chemical characterisation of calcium-hydrate phases formed in alteration processes of deposited municipal solid waste incinerator bottom ash, *Environmental Science and Technology*, 34 (23): 5030-5037.
- Spence, R. J. S. and Cook, D. J. (1983) *Building materials in developing countries*, John Wiley & Sons, Chichester.
- Stegemann, J. A. and Cote, P. L. (1990) Summary of an investigation of test methods for solidified waste evaluation, *Waste management*, 10: 41-52.
- Stein, H. N. and Stevels, J. M. (1964) Influence of silica on the hydration of  $C_3S$ . *J. Appl. Chem.*, 14: 338-345.
- Stephan, D., Maleki, H. and Knoefel, D. (1999) Influence of Cr, Ni, and Zn on the properties of pure clinker phases, Part 1.  $C_3S$ . *Cement and Concrete Research*, 29: 545-552.
- Stronach, S. A. and Glasser, F. P. (1997) Modelling the impact of abundant geochemical components on phase stability and solubility of the CaO-SiO<sub>2</sub>-H<sub>2</sub>O system at 25°C: Na<sup>+</sup>, K<sup>+</sup>, SO<sub>4</sub><sup>2-</sup>, Cl<sup>-</sup> and CO<sub>3</sub><sup>2-</sup>, *Adv. Cem. Res.*, 9 (36): 167-181.
- Stumm, W. and Morgan, J. J. (1970) *Aquatic chemistry: an introduction emphasising chemical equilibria in natural waters*, Wiley, New York.
- Sun, G. K., Brough, A. R. and Young, J. F. (1999) <sup>29</sup>Si NMR study of the hydration of Ca<sub>3</sub>SiO<sub>5</sub> and Ca<sub>2</sub>SiO<sub>4</sub> in the presence of silica fume, *Journal of the American Ceramic Society*, 82 (11): 3225-3230.

- Suzuki, K. (1985) Formation and carbonation of C-S-H in water, *Cement and Concrete Research*, 15: 213-224.
- Sweeney, R. E. H., Hills, C. D. and Buenfeld, N. R. (1998) Investigation into the carbonation of stabilised/solidified synthetic waste, *Environmental Technology*, 19: 893-905.
- Tamas, F. D., Csetenyi, L. and Tritthart, E. (1992) Effect of adsorbent on the leachability of cement bonded electroplating wastes, *Cement and Concrete Research*, 22: 399-404.
- Tashiro, C., Takahashi, H., Kanaya, M., Hirakida, I. and Yoshida, R. (1977) Hardening properties of cement mortar adding heavy metal compounds and solubility of heavy metal hardened mortar, *Cement and Concrete Research*, 7: 283-290.
- Tashiro, C., Oba, J. and Akama, K. (1979) The Effect of metal oxides on the formation of ettringite and the microstructure of hardened ettringite, *Cement and Concrete Research*, 9: 303-308.
- Tashiro, C. and Oba, J. (1979) The Effect of  $\text{Cr}_2\text{O}_3$ ,  $\text{Cu}(\text{OH})_2$ ,  $\text{ZnO}$  and  $\text{PbO}$  on the compressive strength and hydrates of hardened  $\text{C}_3\text{A}$  paste. *Cement and Concrete Research*, 9, 253-258.
- Tashiro, C. and Oba, J. (1980) The Effect of  $\text{Cu}(\text{OH})_2$  on the hydration of  $\text{C}_3\text{A}$  in: *Proceedings of the Seventh International Congress of Cement Chemistry*, 2(2): 59-63, Paris.
- Tessier, A., Campbell, P. G. C. and Bisson, M. (1979) Sequential extraction procedure for the speciation of particulate trace metals, *Analytical Chemistry*, 51: 844 –850.
- Taylor, H. F. W. (1986) Proposed structure for calcium silicate hydrated gel, *J Am. Ceram. Soc.*, 69 (6): 464-467.
- Taylor, H. F. W. (1990) *Cement chemistry*, Academic Press Limited, London.
- Taylor, H. F. W., Famy, C. and Scrivener, K. L. (2001) Delayed ettringite formation, *Cement and Concrete Research*, 31 (5): 683-693.

- Taylor, H. F. W. (1993) Nanostructure of C-S-H: current status, *Adv. Cem. Basic Mat.*, 1: 38-46.
- Taylor, H. F. W. (1997) *Cement chemistry*, (2<sup>nd</sup> Edition), Thomas Telford Press, London.
- Thomas, D. A., Jameson, D. A. and Double, D. D. (1981) The effect of lead nitrite on the early hydration of Portland cement, *Cement and Concrete Research*, 11: 143-153.
- Thomas, J. J. and Jennings, H. M. (1998) Free-energy-based model of chemical equilibria in the CaO-SiO<sub>2</sub>-H<sub>2</sub>O system, *J Am. Ceram. Soc.*, 81 (3): 606-612.
- Trussel, S. S. and Spence, R. D. (1994) A review of stabilisation/solidification interferes, *Waste Management*, 14: 507-519.
- Tseng D.H. (1988) Solidification/stabilisation of hazardous sulphates with Portland cement, *J. of the Chinese Institute of Engineering*, 11: 219-225.
- Tyrer, M. (1990) PhD thesis, Aston University, Birmingham.
- Tyrer, M. and Yunus, I. (1995) Assessment of the geochemical impact of emplacing a Concrete Service Road in a Granite Tunnel c-in-c report to SKB, Sweden.
- Tyrer, M. (1994) Modelling the interaction of blended cements with natural ground waters Rep DoE/HMIP/TR-WSA-53.
- Tyrer, M. (2001) *Thermodynamic modelling, an introduction for earth scientist, material scientist and chemists*, The University of Greenwich, Chatham Maritime.
- Valls, S. and Vazquez, E. (2000) Stabilisation and solidification of sewage sludge with Portland Cement, *Cement and Concrete Research*, 30: 1671-1678.
- Van Eijk, R. J. and Brouwers, H. J. H. (2001) Modelling the effects of waste components on cement hydration, *Waste Management* 21: 279-284.
- Van Herck, P. and Vandecasteele, C. (2001) Evaluation of the use of sequential extraction procedure for the characterisation and treatment of metal containing solid waste, *Waste Management*, 21: 685 –694.

- Vander Lee, (1998) Thermodynamic and mathematical concept of CHESS, Paris.
- Viehland, D., Li, J. F., Yuan, L. J., *et al.* (1996) Mesostructure of calcium silicate hydrate (C-S-H) gels in Portland cement paste: Short-range ordering, nanocrystallinity, and local compositional order, *Journal of the American Ceramic Society*, 79 (7): 1731-1741.
- Viehland, D., Yuan, L. J., Xu, Z., *et al.*, (1997) Structural studies of jennite and 1.4 nm tobermorite: Disordered layering along the [100] of jennite, *Journal of the American Ceramic Society*, 80 (12): 3021-3028.
- Wang, C. H. and Huang, C. P. (1994) Treatment of metal industrial wastewater by fly ash and cement fixation, *Journal of Environmental Engineering*, 120 (6): 1470-1487.
- Wang, S. D. and Scrivener, K. L. (2003)  $^{29}\text{Si}$  and  $^{27}\text{Al}$  NMR study of alkali-activated slag, *Cement and Concrete Research*, 33 (5): 769-774.
- Wang, S. and Vipulanandan, C. K. (2000) S/S of Cr with cement leachability and XRD analyses, *Cement and Concrete Research*, 30: 385-389.
- Walton, J. C., Bin-Shafique, S. and Vipulanandan, C.K. (1995) Effect of clays and cement on the solidification/stabilisation of phenol-compounds soils, *Waste Management*, 15: 399-406
- Walton, J. C., Bin-Shafique, S., Smith, R.W., Gutierrez, N. and Tarquinn, A.T. (1997) The role of carbonation in transient leaching of cementitious waste forms, *Environmental Science and Technology*, 31: 2345-2349.
- Wiles, C. C. (1987) A review of solidification/stabilisation technology, *Journal of Hazardous Material*, 14: 5-21.
- Williams, P. J., Biernacki, J. J., Walker, L. R., *et al.* (2002) Microanalysis of alkali-activated fly ash-CH pastes, *Cement and Concrete Research*, 32 (6): 963-972.
- Wolery, T. (1992) EQ3/6: a software package for geochemical modelling of aqueous systems, Lawrence Livermore National laboratory.

- Xu, B. A., Giles, D. E. and Ritchie, I. M. (1997) Reaction of lime with aluminate-containing solutions, *Hydrometallurgy*, 44: 231-244.
- Xu, B. A., Giles, D.E. and Ritchie, I. M. (1998) Reactions of lime with carbonate-containing solutions, *Hydrometallurgy*, 48: 205-224.
- Xu, Z. and Viehland, D. (1996) Observation of a mesostructure in calcium silicate hydrate gels of Portland cement, *Phys. Rev. Lett.*, 77 (5): 952-955.
- Young, J. F., Berger, R. L. and Breese, J. (1974) Accelerated curing of compacted Ca silicate mortars on exposure to CO<sub>2</sub>, *Journal of the American Ceramic Society*, 57 (9): 394-397.
- Yousuf, M. and Mollah, A. (1995) The interfacial chemistry of solidification/stabilisation of metals in cement and pozzolanic material systems, *Waste Management*, 15: 137-148.
- Zhang X. Z., Chang, W. Y., Zhang, T. J., *et al.*, (2000) Nanostructure of calcium silicate hydrate gels in cement paste, *Journal of the American Ceramic Society*, 83 (10): 2600-2604.
- Zhang, Z. Z., Sparks, D. L. and Scrivner, N. C. (1993) Sorption and desorption of quaternary amine cations on clays, *Environmental Science and Technology*, 27: 1625-1631.
- Zhang, H. and Odler, D. (1996) Investigations of high SO<sub>3</sub> Portland clinkers and cements, *Cement and Concrete Research*, 26: 1315-1324.

## Appendix A

### Syntheses of cement pure phases

Synthesis of  $C_3S$ : grind a 3:1 molar ratio mixture of  $CaCO_3$  and  $SiO_2$  to a fine powder in a ceramic ball mill and then pelletise and sinter in air at  $1500^\circ C$  for 2 hours. Repeat these cycles until no free  $CaO$  is detected by XRD.

Synthesis of  $C_3A$ : mixtures of stoichiometric amounts of  $CaCO_3$  and  $Al_2O_3$  were fired at  $800^\circ C$  for 1 hour,  $1000^\circ C$  for 4 hours and ignite at  $1425^\circ C$ . Repeat the procedures of crushing, pelletising and firing until pure product was obtained.

Synthesis of  $CA$ : mixtures of stoichiometric amounts of  $CaCO_3$  and  $Al_2O_3$  were fired at  $1425^\circ C$  for 6 hours. Repeat the procedures of crushing, pelletising and firing until pure product was obtained.

Synthesis of  $C_{12}A_7$ : mixtures of stoichiometric amounts of  $CaCO_3$  and  $Al_2O_3$  were fired at  $1350^\circ C$  for 6 hours. Repeat the procedures of crushing, pelletising and firing until pure phase was obtained.

Synthesis of  $C_4AF$ : a mixture of  $CaCO_3$ ,  $Al_2O_3$  and  $Fe_2O_3$  in a 4:1:1 molar ratio was pelletised and sintered in air at  $1370^\circ C$  for 90 minutes. This procedure of crushing, pelletising and sintering was repeated until pure product was obtained.

### Syntheses of heavy metal compounds

Hydroxides of heavy metals were prepared by the slow addition of 10M NaOH solution to the solutions of heavy metal nitrates until a pH 8-9 was achieved and hydroxides were precipitated. The hydroxide slurry was allowed to settle for 1 hour and was then filtered through a  $0.45\mu m$  membrane filter. The filter-cake was then dried in a drying vessel to constant weight and ground to less than  $100\mu m$  using a mortar and pestle. Dried, ground hydroxide salts were sealed in plastic bottles for subsequent use.

The preparation of metal carbonate salts involved placing freshly prepared hydroxide filter-cake in a carbon dioxide chamber (see section 2.3.3) at a pressure of 0.3MPa for 3 days. Following carbonation the salts were dried and ground as described above.



## Appendix B

### Diffractograms of pastes of $C_{12}A_7$ , CA and $C_4AF$

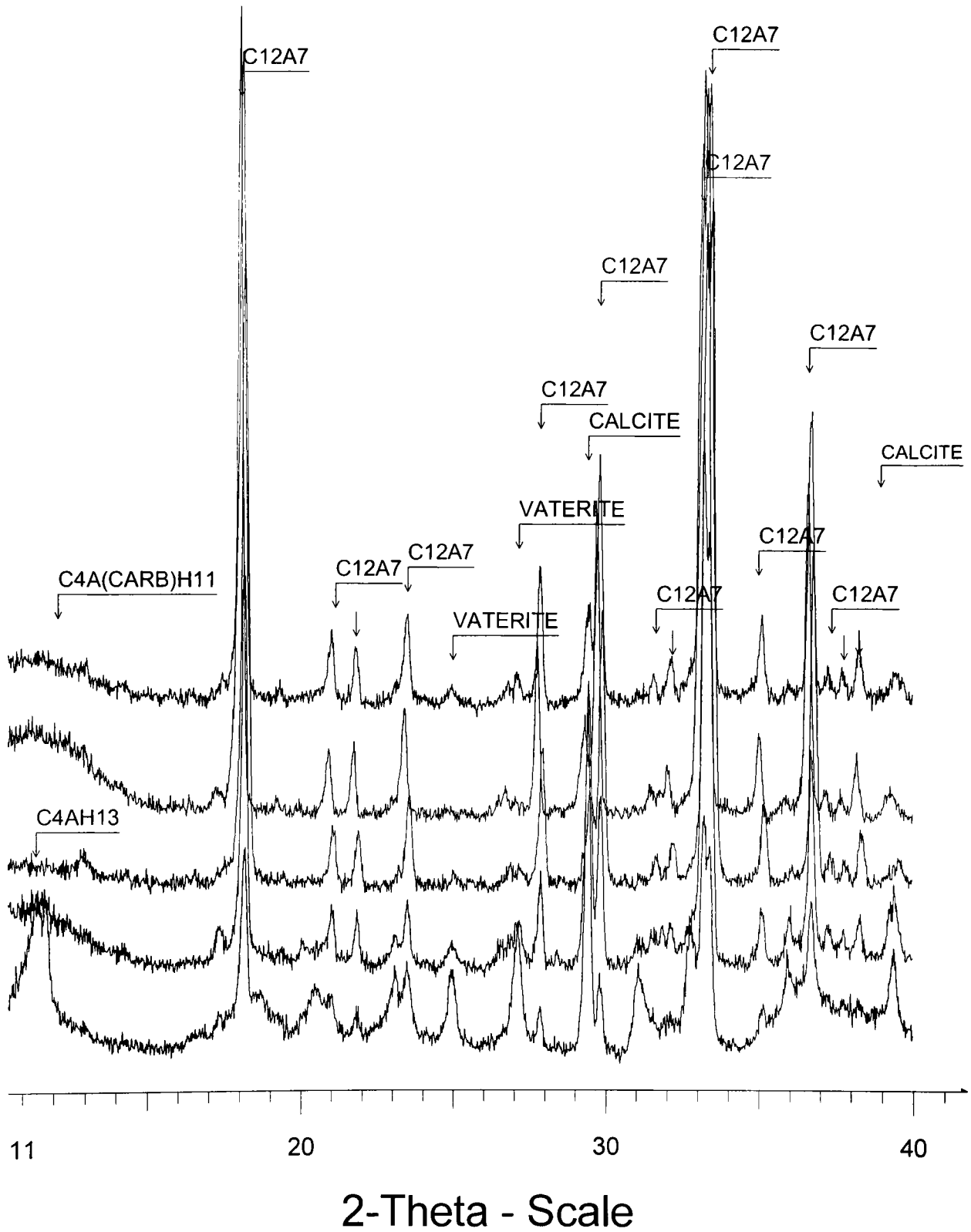


Fig. 1. Diffractograms of the hydrated  $C_{12}A_7$  pastes aged 28-days  
(From bottom to top are control,  $Cr^{3+}$ ,  $Cu^{2+}$ ,  $Pb^{2+}$ , and  $Zn^{2+}$ -doped pastes, respectively)

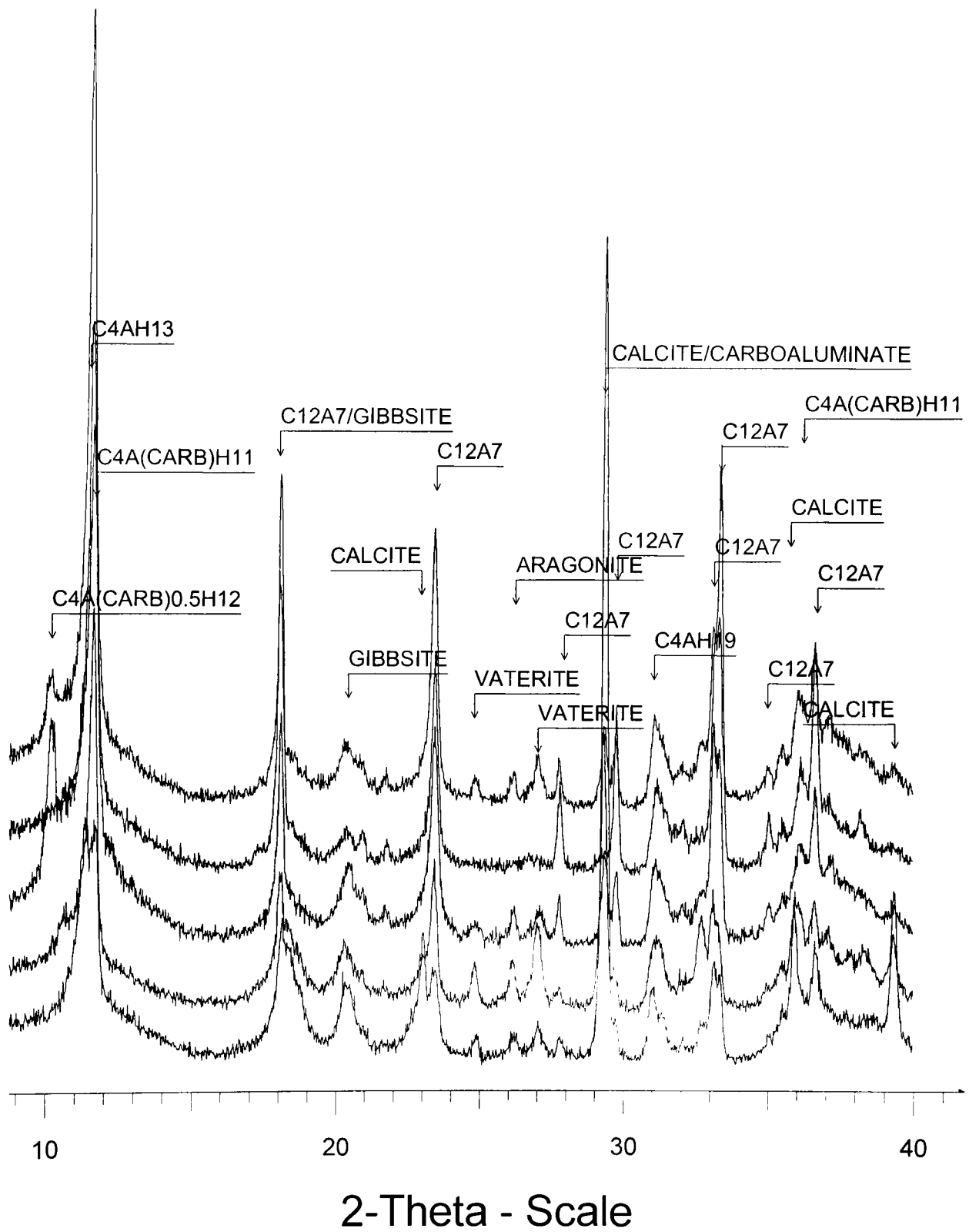


Fig. 2. Diffractograms of the hydrated  $C_{12}A_7$  pastes aged one year (From bottom to top are control,  $Cr^{3+}$ ,  $Cu^{2+}$ ,  $Pb^{2+}$ , and  $Zn^{2+}$ -doped pastes, respectively)

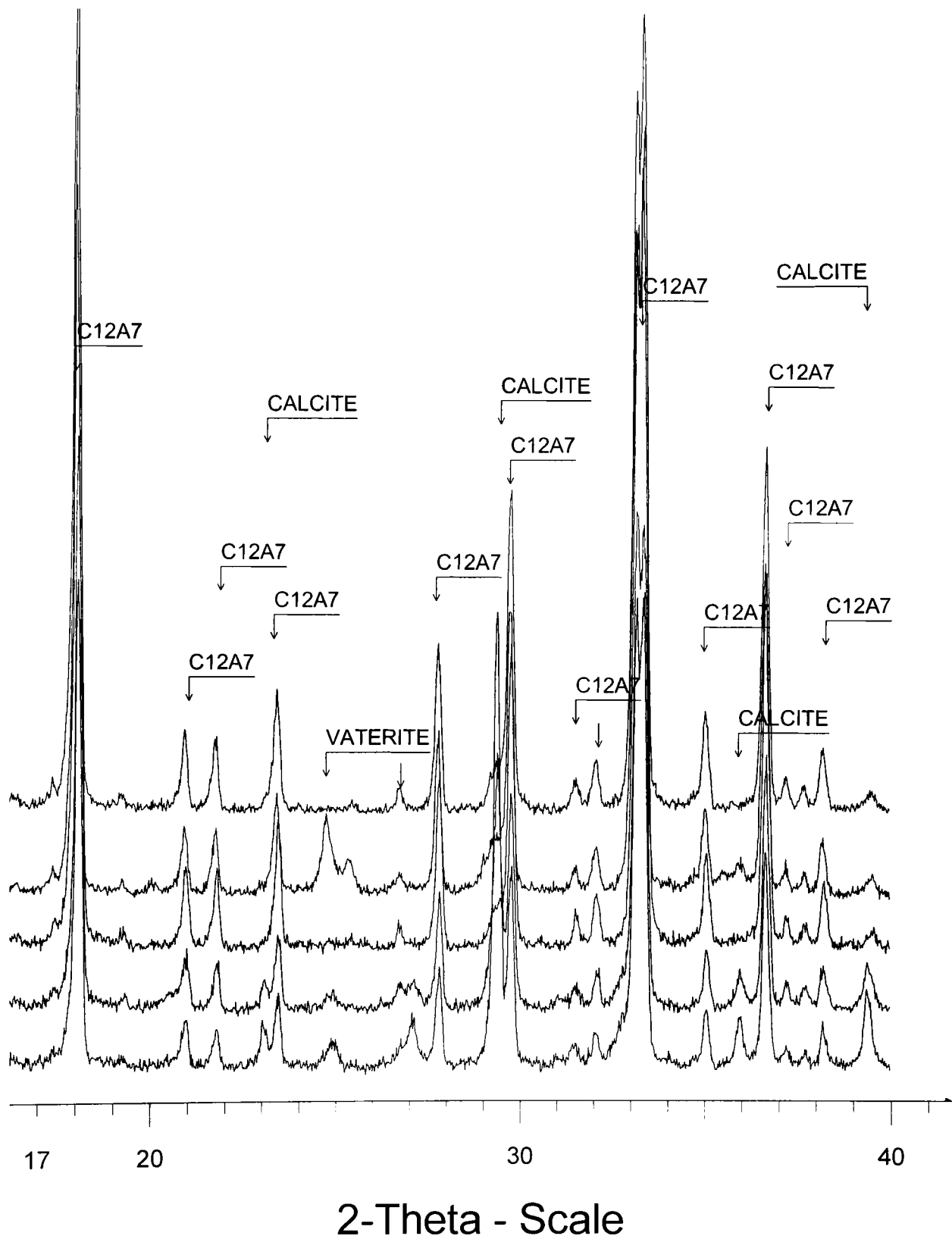


Fig. 3. Diffractograms of the carbonated C<sub>12</sub>A<sub>7</sub> pastes at 28-days  
 (From bottom to top are control, Cr<sup>3+</sup>, Cu<sup>2+</sup>, Pb<sup>2+</sup>, and Zn<sup>2+</sup>-doped pastes, respectively)

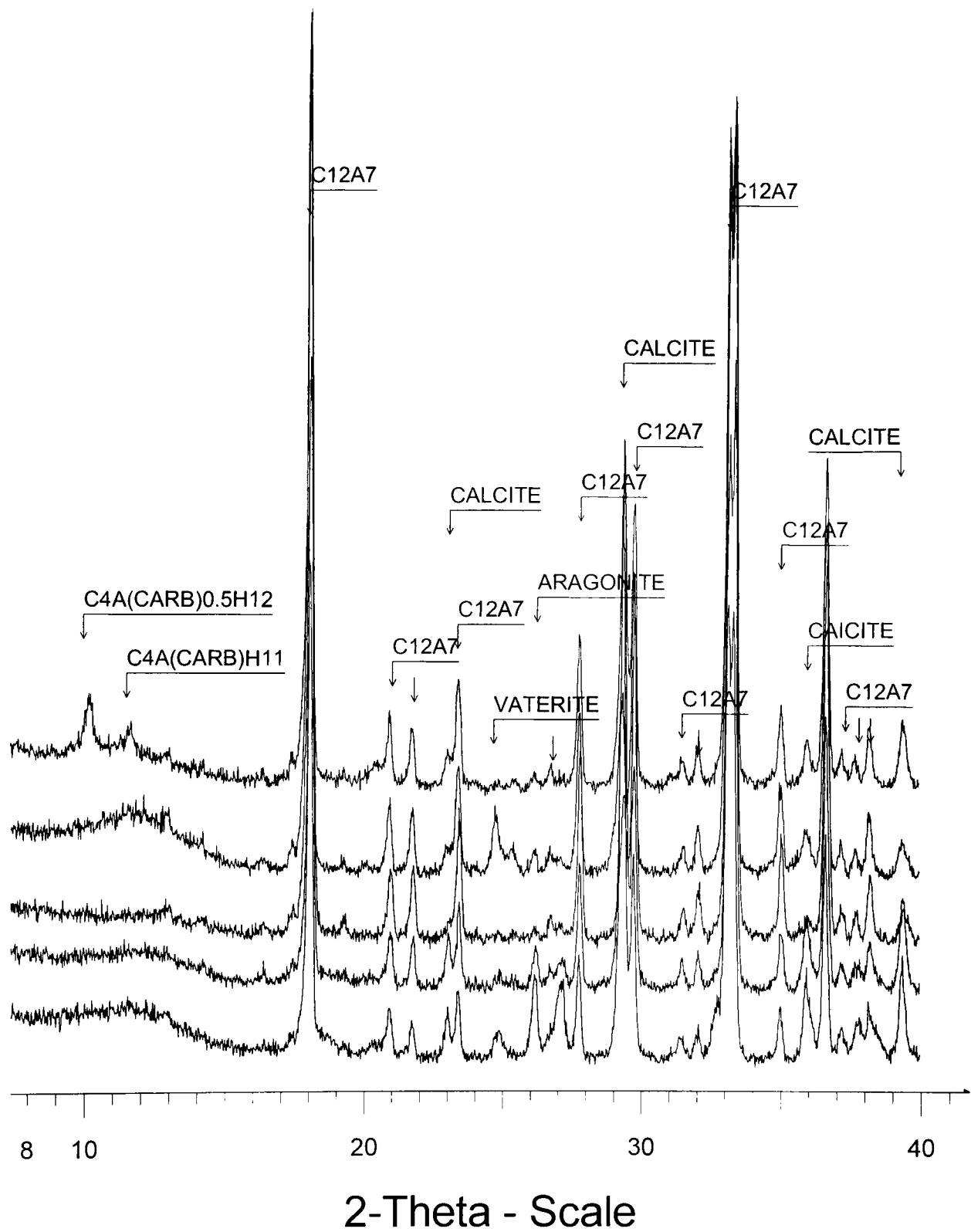


Fig. 4. Diffractograms of the carbonated  $C_{12}A_7$  pastes at one year  
 (From bottom to top are control,  $Cr^{3+}$ ,  $Cu^{2+}$ ,  $Pb^{2+}$ , and  $Zn^{2+}$ -doped pastes, respectively)

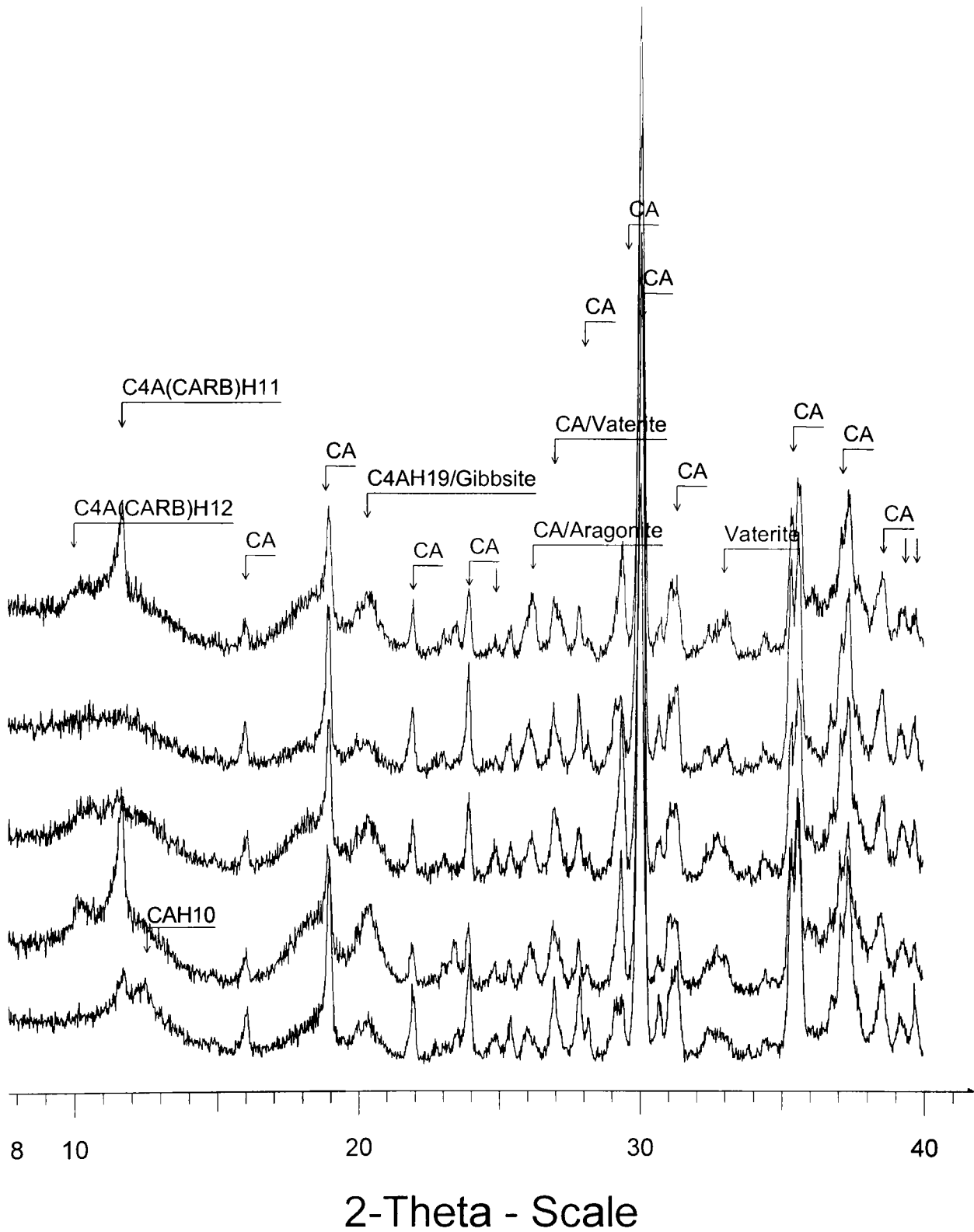


Fig. 5. Diffractograms of the hydrated CA pastes aged 28-days  
 (From bottom to top are control, Cr<sup>3+</sup>, Cu<sup>2+</sup>, Pb<sup>2+</sup>, and Zn<sup>2+</sup>-doped pastes, respectively)

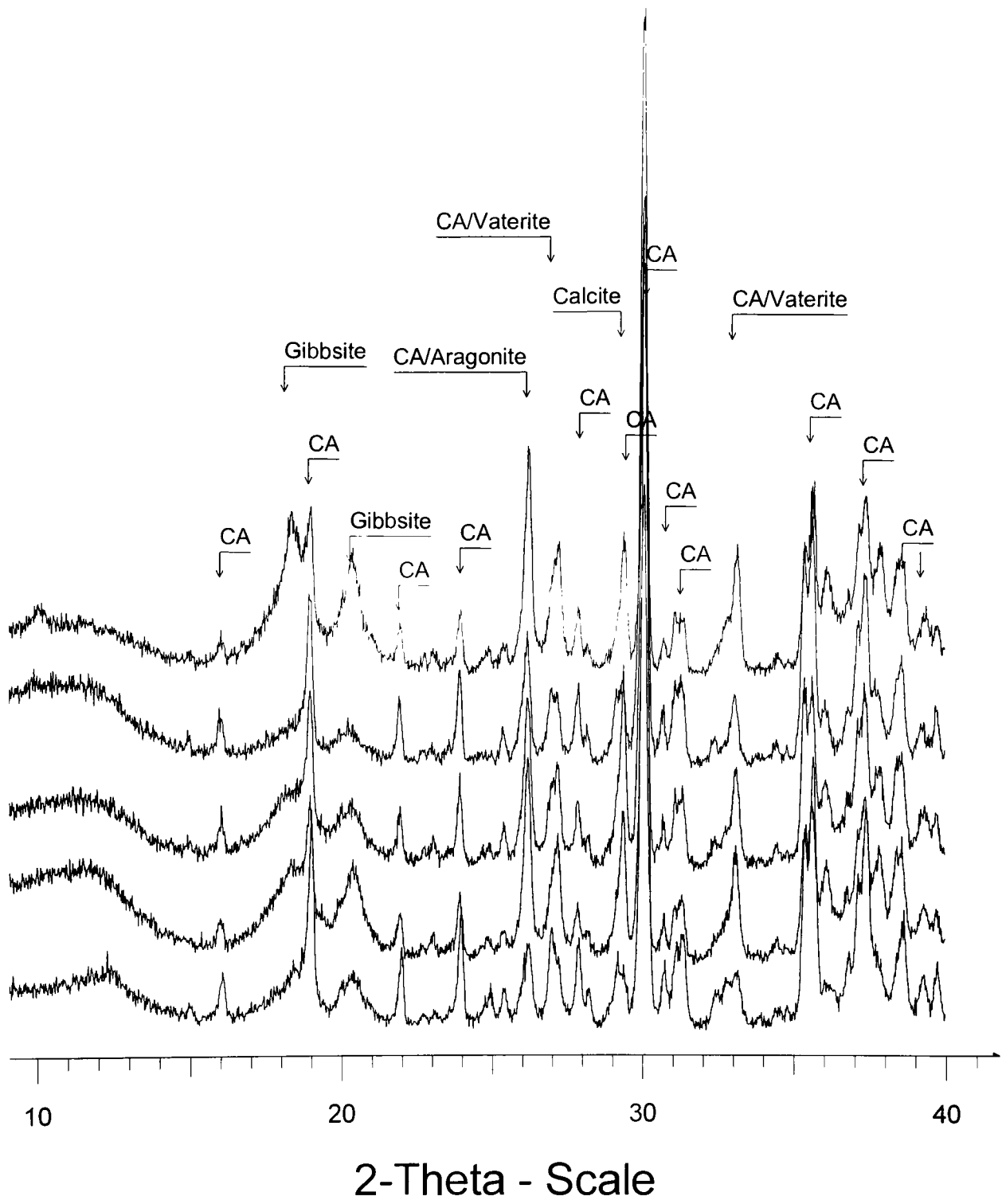


Fig. 6. Diffractograms of the hydrated CA pastes aged one year  
 (From bottom to top are control, Cr<sup>3+</sup>, Cu<sup>2+</sup>, Pb<sup>2+</sup>, and Zn<sup>2+</sup>-doped pastes, respectively)

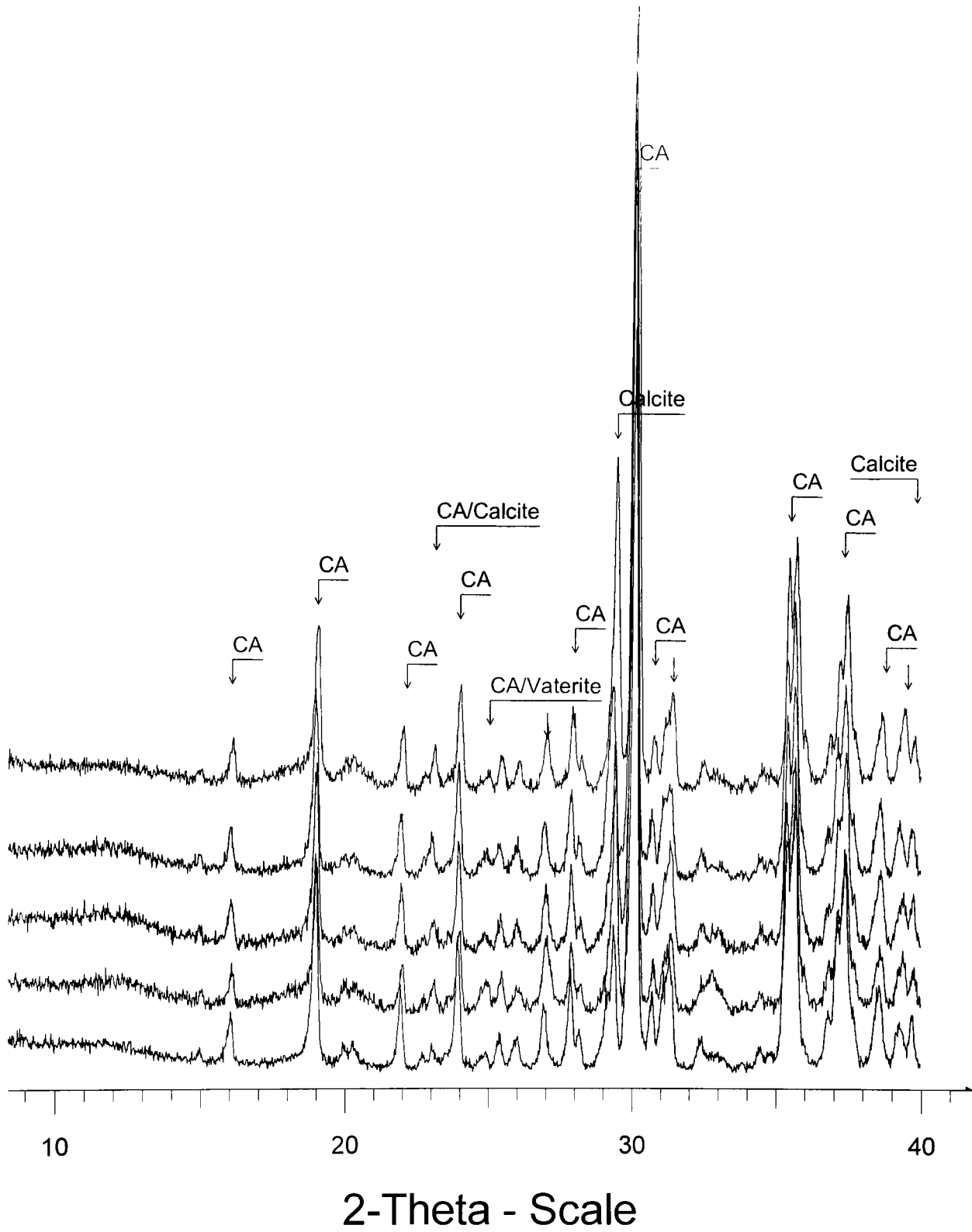


Fig. 7. Diffractograms of carbonated CA pastes at 28-days  
 (From bottom to top are control, Cr<sup>3+</sup>, Cu<sup>2+</sup>, Pb<sup>2+</sup>, and Zn<sup>2+</sup>-doped pastes, respectively)

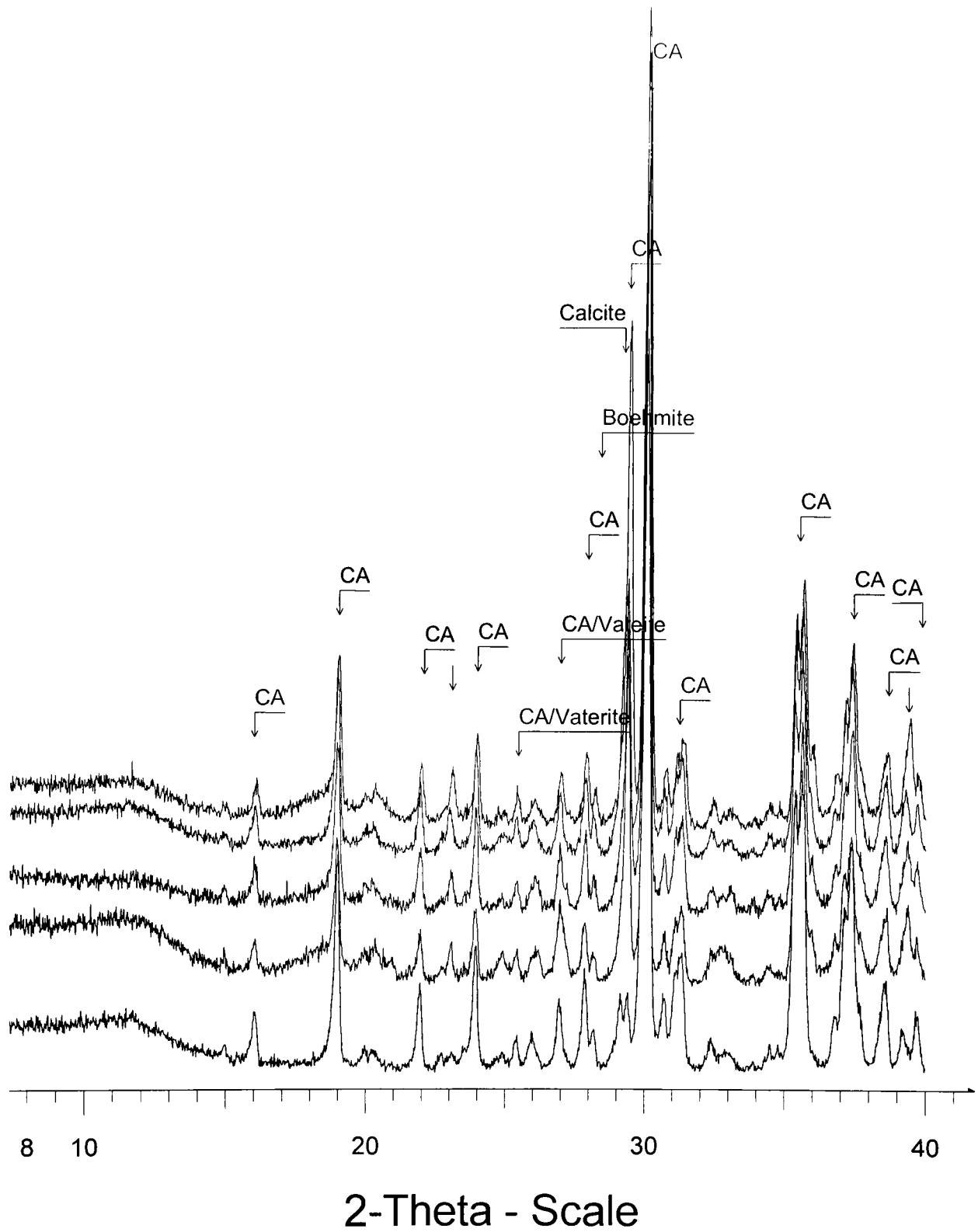


Fig. 8. Diffractograms of carbonated CA pastes at one year  
 (From bottom to top are control, Cr<sup>3+</sup>, Cu<sup>2+</sup>, Pb<sup>2+</sup>, and Zn<sup>2+</sup>-doped pastes, respectively)

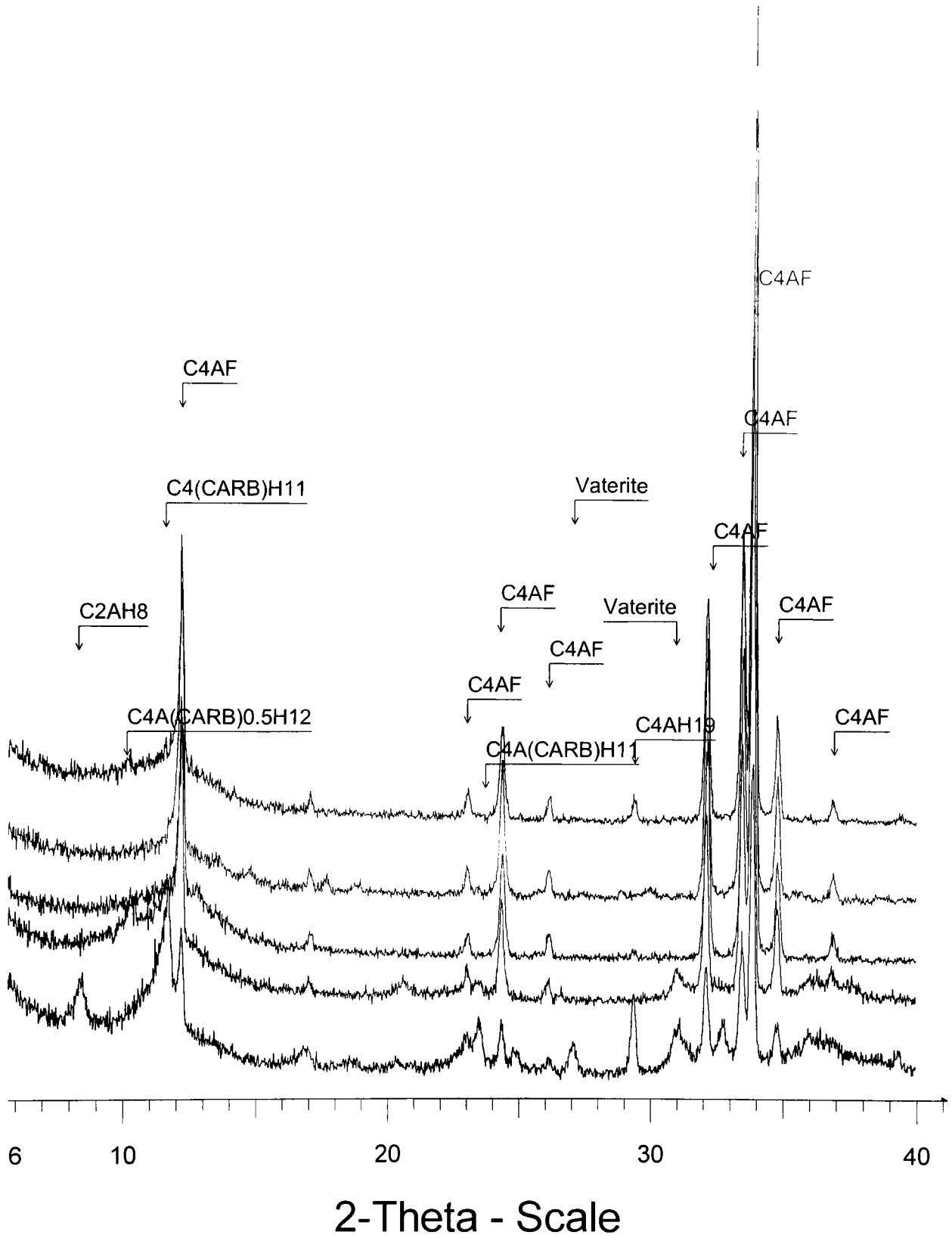


Fig. 9. Diffractograms of the hydrated  $C_4AF$  pastes aged 28-days  
 (From bottom to top are control,  $Cr^{3+}$ ,  $Cu^{2+}$ ,  $Pb^{2+}$ , and  $Zn^{2+}$ -doped pastes, respectively)



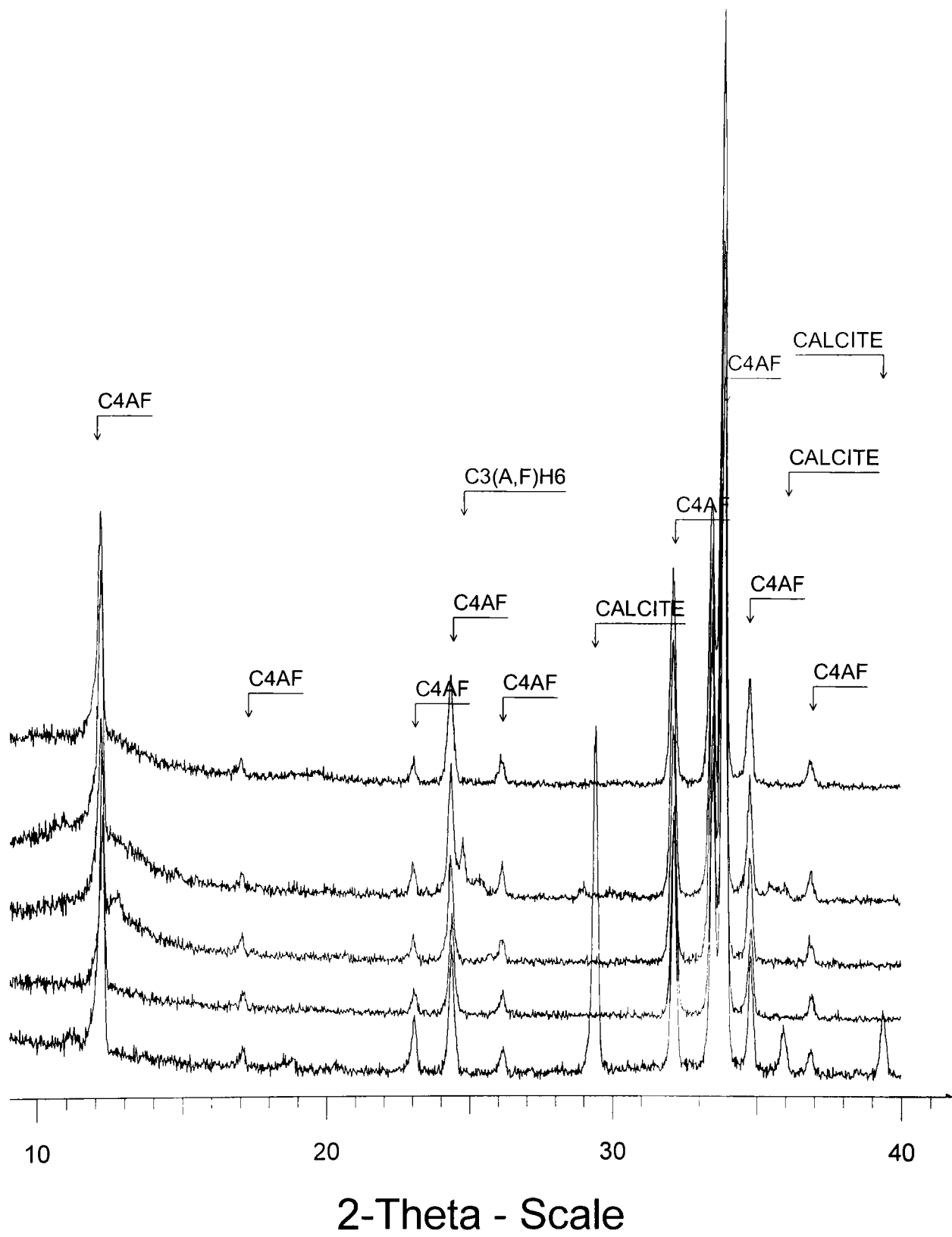


Fig. 11. Diffractograms of the carbonated  $C_4AF$  pastes at 28-days  
 (From bottom to top are control,  $Cr^{3+}$ ,  $Cu^{2+}$ ,  $Pb^{2+}$ , and  $Zn^{2+}$ -doped pastes, respectively)

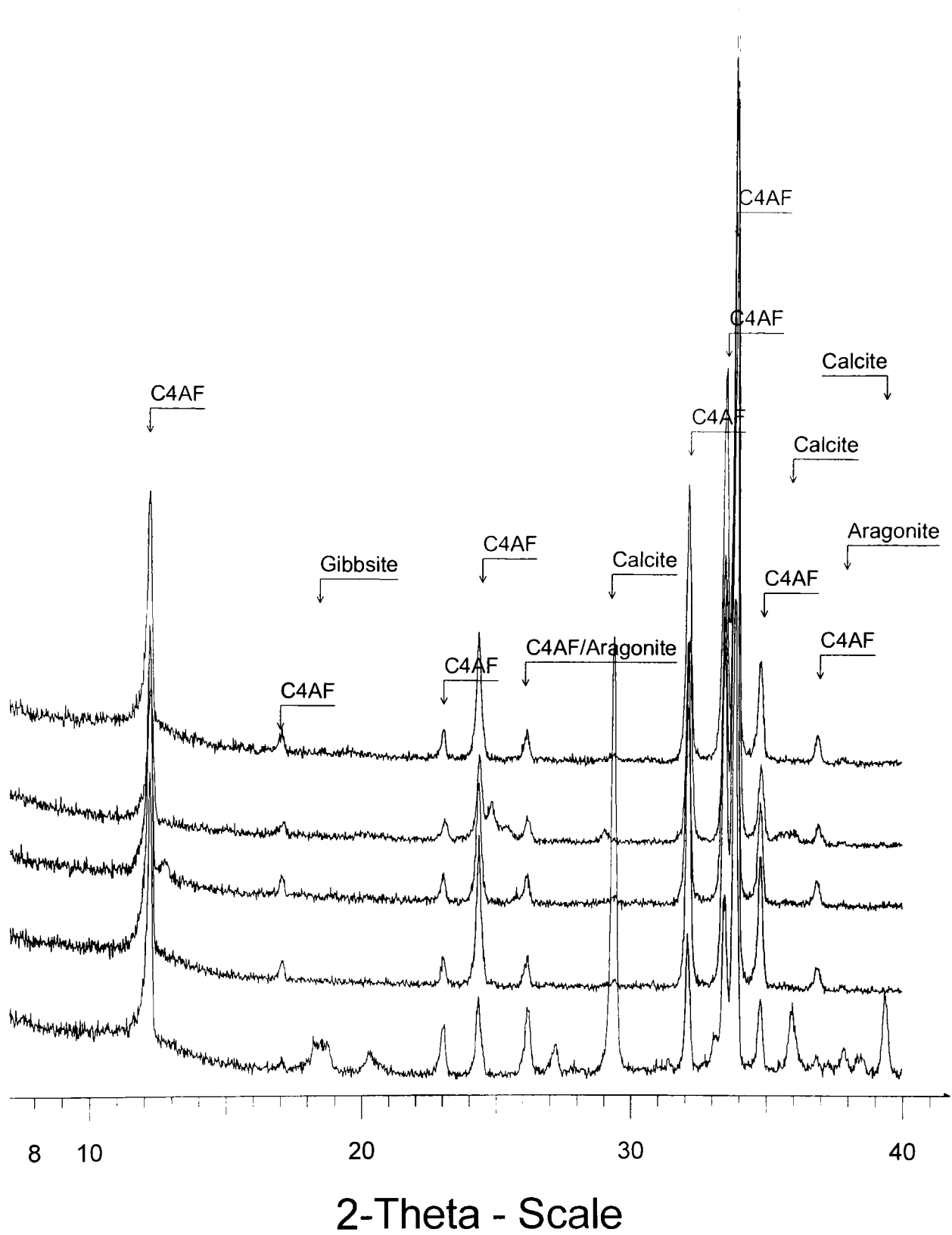


Fig. 12. Diffractograms of the carbonated  $C_4AF$  pastes at one year (From bottom to top are control,  $Cr^{3+}$ ,  $Cu^{2+}$ ,  $Pb^{2+}$ , and  $Zn^{2+}$ -doped pastes, respectively)

## Appendix C

### Main aqueous databases and geochemical codes

#### 1 Stand-alone aqueous databases

- The CHEMVAL database covers the majority of elements thought to have radiological significance and groundwater speciation. The latest version of the database (Version 6) contains ~650 aqueous species and ~350 pure solid species with particular emphasis on actinide chemistry and heavy metal chemistry in natural solutions (Atkins and Bennett, 1992). The database can be used with codes such as PHREEQE, MINEQL and EQ3/6.
- HATCHES (AEA Technology/Nirex) database has been compiled for the use in radiochemical modelling work in conjunction with the codes PHREEQE and EQ3/6 (Cross *et al.*, 1991). The database includes data for the actinides U, Th, Pu, Np, Am and Cm and for several fission products including Cs, Ru, Tc and Sr; in total there are 1176 aqueous species and 772 solid phases. Each entry includes a full description of the source of the data, any comments concerning the validity of the data, together with details of any calculations that have been performed on the data.
- NAGRA Thermochemical Database (National Co-operative for the Disposal of Radioactive Waste) includes core data and supplemental data. The core data are well-characterised aqueous species, minerals and gases of elements commonly found in significant quantities in natural waters. The supplemental data are for elements that are found in natural waters, but not as major components or those that are of interest principally for the safety assessment of nuclear waste facilities. The core substances include the common aqueous species and minerals of fluoride, chloride, bromide, iodide, sulphate, bisulphide, nitrate, ammonia, phosphate, As(III), carbonate, borate, magnesium, calcium, strontium, barium, lithium, sodium and potassium. The supplemental components include those for silica, iron, manganese, uranium, palladium, nickel, selenium and some organic complexes (Benner, 1992; Park and Batchelor, 1999).

## 2 Aqueous databases integrated within computer codes

- The EQ3/6 software packages were developed by Lawrence Livermore National Laboratory (Wolery, 1992) and are for computing chemical equilibrium problems in aqueous geochemistry. EQ3 can calculate the distribution of chemical species (ions, neutral species, ion-pairs, and complexes) in an aqueous solution and the saturation-state of the fluid with respect to all relevant mineral phases in the database. The calculation predicts the changes in fluid composition and precipitation/dissolution of minerals. The program uses the Newton-Raphson method and convergence is aided by optimising starting estimates. The aqueous solution model calculated by EQ3 is used as a starting point for mass transfer computations by EQ6, which can compute several kinds of mass transfer models.
- MINEQL/PSI (Paul Scherrer Institute, Switzerland) was adapted and extended to assess the solubility and speciation of radioactive waste nuclides in ground waters under conditions which are expected to exist in the surroundings of planned underground repositories (Berner, 1992). It includes data for 1807 aqueous species/complexes, 415 solid phase pure compounds and 7 gases with particular emphasis in the areas of radionuclide chemistry and organic complexation (Berger and Banwart, 2000). With the use of an additional database that includes standard reaction enthalpies and heat capacities at 25°C, the relevant equilibrium constants at 25°C can be converted to other temperatures using Ulich's formulae. The activity coefficients for dissolved species are modelled with a temperature dependent function of the Davies approximation type. The database is compatible for use with the codes MINEQL and PHREEQE.
- The original version of PHREEQE can handle a database of a maximum of 27 elements, 250 species and 40 minerals. A preliminary thermodynamic database is provided with the code, derived from the WATEQ2 database, and includes 120 aqueous species for 19 elements and 24 mineral species.

## 3. Main geochemical codes

- PHREEQE was originally written to model the interactions of natural waters with mineral phases and simulate the chemical speciation of the aqueous solution. The

program calculates the equilibrium water chemistry for a particular chemical inventory and associated minerals, and draws on a database of thermodynamic data (Parkhurst *et al.*, 1980; 1990). The chemical system to be equilibrated by PHREEQE is defined using analytical data for its chemical composition, pH, redox potential (Eh) and temperature. Two main options are available in the original PHREEQE code for the activity coefficient expressions of the ionic species: the Debye-Hückel correction and the Davies correction. The latter formulation is preferred but is only accurate up to a maximum ionic strength of 0.5M.

- The software PHREEQC (Parkhurst, 1995; Parkhurst *et al.*, 1999; Parkhurst and Appelo, 2001) is designed to perform a wider variety of aqueous geochemical calculations, which eliminates many of the deficiencies and limitations of the former PHREEQE versions.
- CHESS, a versatile geochemical modelling tool for hydrologists, geochemists, engineers and others working in environmental science (Vander Lee, 1998). CHESS comes with a user-friendly graphical interface.
- WATEQ4F (US Geological Survey) is a chemical speciation code for natural water which also includes a self contained database. The code uses measurements of temperature, pH, Eh, dissolved oxygen and alkalinity and the chemical analysis of a water sample as input and calculates the distribution of aqueous species, ion activities and mineral saturation indices. WATEQ4F solves a set of non-linear mass action and mass balance equations using the mathematical method known as the continued fraction method. The Davies equation is used in most cases to calculate individual ion activity coefficients for the solute species. The temperature range over which WATEQ4F can be used is 0 to 100°C but uncertainties increase considerably when there are large departures from 25°C.
- Geochemist's Workbench, is a set of software tools for manipulating chemical reactions, calculating stability diagrams and the equilibrium states of natural waters, tracing reaction processes, and plotting the results of these calculations ([www.rochware.com](http://www.rochware.com)).

- JESS, The Joint Expert Speciation System (JESS) is a powerful research tool for modelling chemical speciation in complex aqueous environments. It was designed to solve problems requiring expert knowledge of solution chemistry (see [www.nea.fr](http://www.nea.fr)).
- MINEQL+, a complete chemical equilibrium modelling system for water chemistry calculations, titration curves, and much more. The '+' of MINEQL+ stands for a graphical interface, which makes MINEQL easier to use ([www.nea.fr](http://www.nea.fr)).
- MINTEQA2, is U.S. EPA geochemical equilibrium speciation model capable of computing equilibria among the dissolved, adsorbed, solid and gas phases in an environmental setting. MINTEQA2 includes an extensive database of reliable thermodynamic data that is accessible to PRODEFA2, an interactive program designed to be executed prior to MINTEQA2 for the purpose of creating the required MINTEQA2 input file ([//les.web.psi.ch](http://les.web.psi.ch)).
- PASSIPHIC is used to simulate reactions of non-ideal solid solution phases, which calculate the equilibrium for an aqueous phase in contact with a complex solid, for example, cement (Boerjesson and Emreen, 1998). It has been used to simulate leaching of cement with non-saline groundwater and the result is compared to experimental data. The agreement between experimental and calculation has been found to be good.
- SOLTEQ have been also applied to predict the chemical speciation of compounds in various waste/binder systems. Based on MINTEQA2, SOLTEQ can calculate activity coefficients for high ionic strength solutions occurring in the s/s waste forms (Park and Batchelor, 1999).

## Appendix D

### Glossary

#### A

Accelerator - A compound which is used to increase the rate at which a gel or final set is formed

Aalamosite  $\text{PbSiO}_3$

AFm - Calcium aluminium/iron mono (1 counter ion) of the general formula  $\text{Cm}(\text{A/F})\text{Z}_1\text{Hn}$ .

AFt - Calcium aluminium/iron tri (3 counter ions), of the general formula  $\text{Cm}(\text{A/F})\text{Z}_3\text{Hn}$ .

$\text{Al}(\text{OH})_3$  - Aluminium hydroxide

Alite -  $\text{C}_3\text{S}$ , tricalcium silicate.

Antlerite -  $\text{Cu}_3(\text{SO}_4)(\text{OH})_4$

Argillaceous - Material containing  $\text{SiO}_2$ ,  $\text{Al}_2\text{O}_3$  and  $\text{Fe}_2\text{O}_3$  in a useable form for cement manufacture.

Azurite -  $\text{Cu}_3(\text{CO}_3)_2(\text{OH})_2$

#### B

Belite -  $\text{C}_2\text{S}$ , dicalcium silicate

Brochantite -  $\text{Cu}_4(\text{SO}_4)(\text{OH})_6$

#### C

$\text{C}_{12}\text{A}_7$  - Mayernite, a highly reactive phase found in cements.

$\text{C}_2\text{AS}$  - Gehlenite, a poorly hydrating phase found in HAC made with high silica bauxite.

$\text{C}_3\text{A}$  - Tricalcium aluminate, a reactive phase found in cements.

$\text{C}_3\text{AH}_6$  - HAC hydration product after conversion from  $\text{CAH}_{10}$ , the cause of reduction in physical performance and dimensional stability in HAC concretes.

$\text{C}_4\text{AF}$  - Brownmillerite, a reactive phase found in cements.

CA - Mono calcium aluminate, a reactive phase found in cements.

C-A-H - Calcium aluminate hydrate, Secondary amorphous hydration product of cement.

$\text{CAH}_{10}$  - Initial structural hydration product of HAC.

Calcareous Material containing  $\text{CaCO}_3$  used in cement manufacture.

Calcium zincate -  $\text{CaZn}(\text{OH})_6\text{2H}_2\text{O}$

Cement - A material which can be used to bind unconsolidated materials.

Cerrussite -  $\text{PbCO}_3$

Chrysocolla -  $\text{CuSiO}_3 \cdot 2\text{H}_2\text{O}$

CH - Calcium Hydroxide, also used to indicate the early amorphous calcium hydroxide hydration product of cement.

Clinker - The fused calcination products of cement formation.

Concrete - Concretes contain coarse and fine aggregates, cement, water and hydration modifiers

CSA - Calcium sulpho aluminate, mainly  $\text{C}_4\text{A}_3$ .

C-S-H - Calcium silicate hydrate, final amorphous hydration product of cement.

D

Delafossite -  $\text{CuFeO}_2$

Dioptase -  $\text{CuSiO}_2(\text{HO})_2$

E

Ettringite -  $\text{Ca}_6\text{A}_{12}(\text{SO}_4)_3(\text{OH})_{12} \cdot 26\text{H}_2\text{O}$  (or  $\text{C}_6\text{A}_3\text{H}_{32}$  in cement notation) is a naturally occurring mineral which forms hexagonal crystal structures.

F

Ferrite-Cu -  $\text{CuFe}_2\text{O}_4$

Ferrite-Zn -  $\text{ZnFe}_2\text{O}_4$

Flux - Material which either lowers the melting point or acts as a transport assistant in clinker formation.

Free Lime - Calcium oxide which remains uncombined within the clinker

G

Gel A stage of hydration at which cementitious mixtures retain their supported shape. The gel can be broken using mechanical means without a large effect on the final physical characteristics of the cured mixture.

H

HAC - High alumina cement.

Hydrocerussite -  $\text{Pb}_3(\text{CO}_3)_2(\text{OH})_2$

Hydrozincite -  $\text{Zn}_5(\text{CO}_3)_2(\text{OH})_6$

Hydration - The reaction with water of anhydrous materials.

L

Lanarkite -  $\text{Pb}_2(\text{SO}_4)\text{O}$

Litharge - PbO

M

Mayenite  $C_{12}A_7$

Massicot - PbO

Minium -  $Pb_3O_4$

P

PC - Portland cement, named after the visual similarity between the set material and Portland stone.

R

Raw meal - Total ground raw materials of cement production prior to calcination.

Retarder - A compound which can delay the onset of a gel or final set, many retarders increase the final physical performance of the mortar or concrete

S

Strätlingite -  $C_2ASH_8$ , crystalline hydration product of cement.

T

Thaumasite -  $Ca_3Si(OH)_3SO_4CO_3 \cdot 24H_2O$  ( $C_3SH_{27}$ ), a naturally occurring material easily confused by XRPD with Ettringite.

Z

Zincite, ZnO